

JAMES COOK UNIVERSITY

SCHOOL OF ENGINEERING

AN INSIGHT INTO TIME RATE OF
CONSOLIDATION

Julie Lovisa

Thesis submitted to the School of Engineering and Physical Sciences in partial fulfilment of the requirements for the degree of

Doctor of Philosophy
(Geotechnical Engineering)

July, 10th 2012

STATEMENT OF ACCESS

I, the undersigned, the author of this thesis, understand that James Cook University will make it available for use within the University Library and, by microfilm or other means, allow access to users in approved libraries.

All users consulting in this thesis will have to sign the following statement:

In consulting this thesis, I agree not to copy or closely paraphrase it in whole or in part without the written consent of the author; and to make proper public written acknowledgement for any assistance which I have obtained from it.

Beyond this, I do not wish to place any restriction on access to this thesis.



.....
Signature

10 July 2012
.....
Date

STATEMENT OF SOURCES

DECLARATION

I declare that this thesis is my own work and has not been submitted in any form for another degree or diploma at any university or other institution of tertiary education. Information derived from the published or unpublished work of others has been acknowledged in the text and a list of references is given.



.....
Signature

10 July 2012
.....

Date

DECLARATION – ELECTRONIC COPY

I, the undersigned, the author of this work, declare that to the best of my knowledge, the electronic copy of this thesis submitted to the library at James Cook University is an accurate copy of the printed thesis submitted.



.....
Signature

10 July 2012
.....

Date

ACKNOWLEDGEMENTS

The financial support provided by the Australian Research Council, Coffey Geotechnics and the Port of Brisbane Corporation is gratefully acknowledged.

This research project would not have been possible without the help and support of the kind people around me, some of whom I would like to give particular mention to here. I wish to express my deepest gratitude to my supervisor, Associate Professor Sivakugan, who has been abundantly helpful and offered invaluable advice, support and guidance. I would also like to thank my associate supervisor, Associate Professor Wayne Read, whose mathematical expertise is unparalleled. I am also eternally grateful to Mr. Warren O'Donnell, for his constant support and assistance in the laboratory.

Special thanks also to my family, especially Mum and Dad, who have been, and will probably always remain, my biggest supporters. Above all, I would like to thank my partner, Chris Ryan. It is to him I dedicate this thesis.

Abstract

Terzaghi's elegant theory of one-dimensional consolidation is dependent upon a number of assumptions which can, at times, severely limit the predictive capabilities of the resulting analytical model. Although other more complex models exist, Terzaghi's one-dimensional model remains popular amongst practicing engineers due to its inherent simplicity and notoriety. The purposes of this study have been to explore key aspects of Terzaghi's consolidation theory, and extend the analytical solution to incorporate a variety of loading scenarios that may give rise to non-uniform distributions of excess pore water pressure. To do this, Terzaghi's consolidation equation was solved within the program MATLAB using a collocation approach to solve for series coefficients, instead of the more traditional orthogonality approach. A novel truncation technique was also employed in cases where discontinuities were present in the initial condition, which would have otherwise elicited Gibbs phenomena, an undesirable trait of series solutions.

By varying the initial condition in the MATLAB program, the consolidation behaviour of a soil subjected to a variety of different initial excess pore water pressure (u_i) distributions was analysed in terms of excess pore water pressure decay and percentage consolidation settlement. These simulations were conducted for both singly and doubly drained soil layers. In many singly drained cases, the excess pore water pressure within the soil layer decayed in a peculiar fashion, where a 'redistribution' of pore pressure occurred during the early stages of consolidation.

When viewing consolidation behaviour in terms of percentage consolidation (U), it was easily shown that any reference to drainage path length (H_{dr}) should be avoided. In fact, continuing to use the traditional expression for time factor (T) in terms of H_{dr} can actually complicate analyses. Instead, T should be expressed in terms of layer thickness (H) only. By adopting this alternative time factor expression, a relationship between the consolidation behaviour due to uniform and non-uniform u_i -distributions was developed. This relationship utilised the knowledge that after some short time during consolidation, any skewness attributed to the non-uniform u_i -distribution will disappear, and the decay of excess pore water pressure with depth will revert to a sinusoidal or half-sinusoidal shape, for doubly or singly drained cases, respectively. Correction factors were then developed so that the widely

available $U - T$ values can be easily adjusted to account for any non-uniform u_i -distribution.

Currently, some form of Terzaghi's consolidation theory is also used to analyse laboratory time-settlement data so that important consolidation properties such as the coefficient of consolidation (c_v) can be back-calculated. The efficacy of some of the more popular curve-fitting techniques when applied to different soil types was assessed using a new c_v -calculation procedure which steers away from traditional curve-fitting procedures and instead takes advantage of the matrix manipulation capabilities of MATLAB. It was found that this proposed method and Taylor's square-root of time method yielded the most accurate values of c_v . Previously restricted to data obtained from a uniform u_i -distribution, the Taylor and Casagrande curve-fitting techniques were also generalised to account for a variety of non-uniform u_i -distributions. Two of these modified procedures (a singly/doubly drained layer subjected to a sinusoidal u_i -distribution) were also experimentally verified.

It was also shown that the traditional restrictions associated with consolidation oedometers are not as inflexible as previously assumed. Currently, standard practice requires the height to diameter ratio of a consolidating sample to remain less than 0.4 to avoid any effect of wall friction. However, results suggest that data obtained from a 'tall' oedometer with a height as much as twice its diameter can still be analysed using conventional curve-fitting techniques.

Finally, the effects of time-dependent loading were investigated using two approaches; a constant-rate loading approach, and a discretised loading approach, which more closely models the stepped nature of fill application in the field. It was found that for T increments less than 0.0143, the discretised loading approach effectively became a constant-rate loading problem, an inference that was also experimentally verified.

List of Publications

Journals

	Status
Lovisa, J., Read, W. W., and Sivakugan, N. (2010). “Consolidation behavior of soils subjected to asymmetric initial excess pore pressure distributions.” <i>International Journal of Geomechanics ASCE</i> , 10(5), 181-189.	Accepted and published
Lovisa, J., Read, W. W. and Sivakugan, N. (2011). “Consolidation behavior of soils subjected to asymmetric initial excess pore pressure distributions with one-way drainage.” <i>International Journal of Geomechanics ASCE</i> , 12(3), 318-322.	Accepted and published
Lovisa, J., Read, W. W. and Sivakugan, N. (2011). “A critical reappraisal of the average degree of consolidation.” <i>Geotechnical and Geological Engineering</i> , 29(5), 873-879.	Accepted and published
Lovisa. J., Read, W. W. and Sivakugan, N. (2012). “Calculating c_v based on non-uniform initial excess pore pressure.” <i>Geotechnique</i> 62(8), 741-748.	Accepted and published
Hanna, D., Sivakugan, N. and Lovisa, J. (2013). “A simple approach to consolidation due to constant rate loading in clays.” <i>International Journal of Geomechanics ASCE</i> (submitted June 2011).	Accepted and in production
Lovisa, J., Read, W. W. and Sivakugan, N. (2013a). “Time factor in consolidation -A critical review.” <i>International Journal of Geomechanics ASCE</i> (in production).	Accepted and in production
Lovisa, J., Sivkugan, N., and Read, W. (2013b). “Calculating c_v using modified Taylor and Casagrande curve-fitting methods.” <i>ASTM Geotechnical Testing Journal</i> (submitted December 2012).	Under review
Lovisa, J. and Sivakugan, N. (2013a). “An in-depth comparison of c_v values determined using common curve-fitting techniques.” <i>ASTM Geotechnical Testing Journal</i> (submitted April 2012).	Accepted and in production
Lovisa, J., and Sivakugan, N. (2013b). “Tall oedometer testing: A method to account for wall friction.” <i>ASTM Geotechnical Testing Journal</i> (submitted)	Under review

April 2012).

Sivakugan, N., Lovisa, J., and Ameratunga, J. (2013). "Consolidation settlements due to ramp loading." *Engineering Geology* (submitted January 2012).

Under review

Refereed Conference Proceedings

Status
Accepted and presented
Accepted and presented
Accepted and presented

Lovisa, J., Read, W., and Sivakugan, N. (2011). "Degree of consolidation - peaked initial excess pore water pressure distributions." *13th International Conference of the IACMAG*, Melbourne, 9-11 May.

Lovisa, J., Arulrajah, A., Ameratunga, J., Boyle, P., Read, W. W. and Sivakugan, N. (2011). "Consolidation behavior of dredged slurry and marine clay." *14th Asian Regional Conference on Soil Mechanics and Geotechnical Engineering*, Hong Kong, 23-27 May

Lovisa, J., Sivakugan, N., and Read, W. (2012). "Discretisation of constant rate loading." *11th Australia New Zealand Conference on Geomechanics*, Melbourne, 15-18 July.

Table of Contents

Chapter 1: Introduction	1
1.1 General	1
1.2 Problem Definition	1
1.3 Scope of research.....	2
1.4 Thesis overview.....	3
Chapter 2: Analytical solution	5
2.1 General	5
2.2 Terzaghi's consolidation equation.....	5
2.2.1. Derivation	7
2.2.2. Initial and boundary Conditions	10
2.3 Mathematical solution for the consolidation equation.....	11
2.3.1. Limitations of the traditional solution process	15
2.3.2. Proposed method	17
2.4 Assumption 8 – Initial excess pore water pressure distribution	19
Incorporation of non-uniform u_i into proposed method	22
2.5 Summary.....	23
Chapter 3: Quantifying consolidation behaviour	24
3.1 General	24
3.2 Local measures of the rate of consolidation	24
3.2.1. Degree of consolidation isochrones.....	24
3.2.2. Excess pore water pressure isochrones.....	25
3.2.3. Doubly drained soil layer	26
3.2.4. Singly drained soil layer	32
3.3 Average degree of consolidation	37
3.3.1. Derivation	37
Traditional method	38
Discharge method.....	40
3.3.2. Time factor review	42
3.3.3. Percentage consolidation of non-uniform u_i -distributions.....	47
Comparison with reported values	51
3.3.4. The relevance of drainage path length.....	52
History of H_{dr}	52
H_{dr} Definition A.....	52
H_{dr} Definition B.....	55
Comparison of drainage conditions.....	59
3.3.5. Adjusting uniform results to account for non-uniform u_i -distributions.....	61
Justification.....	61
Proposed method for determining U - T curves	63
3.4 Summary.....	72
Chapter 4: Coefficient of consolidation.....	73
4.1 General	73
4.2 Current methods for determining c_v	73
4.2.1. Validation of c_v values.....	74
4.2.2. Limitations of current methods.....	76
4.2.3. Evaluation of c_v reliability	79
4.2.4. Automation of curve-fitting methods	80
Calculate mode	80
Analyse mode	89
4.2.5. Comparison between experimental and theoretical results	90

4.3	Tall oedometer.....	98
4.3.1.	Background.....	98
4.3.2.	Development of analytical solution.....	99
	Effect of varying height to diameter ratio	105
	Applied pressure vs. self-weight	107
4.3.3.	Experimental Investigation.....	109
	Apparatus and testing procedure	110
	Sensitivity analysis with regards to effective friction angle.....	112
	Sensitivity analysis with regards to interface friction angle.....	113
	Results	115
4.4	Calculating c_v from data due to non-uniform u_i -distributions	116
4.4.1.	Development of approximate solutions.....	117
	Non-linear least squares method.....	118
	$U-T$ approximations for non-uniform u_i -distributions	120
4.4.2.	Generalisation of curve-fitting procedures	124
	Log-time method	124
	Time exponent method	126
4.4.3.	Evaluation of adjustment factors	127
4.5	Summary.....	129
Chapter 5: Experimental validation of pore pressure redistribution and curve-fitting procedures.....		130
5.1	General	130
5.2	Pore pressure redistribution.....	130
5.2.1.	'Arched' u_i -distribution with one-way drainage.....	131
5.2.2.	Sinusoidal u_i -distribution with one-way drainage	132
5.3	Generalised curve-fitting procedures.....	137
5.3.1.	Singly drained layer subjected to a sinusoidal u_i -distribution	137
	Experimental Strategy	137
	Results – Doubly-to-singly drained consolidation process (1 to 4).....	143
	Results – Singly drained consolidation process (2 to 4).....	141
5.3.2.	Doubly drained layer subjected to a sinusoidal u_i -distribution.....	146
	Experimental Strategy	147
	Results	148
5.3.3.	Practical Implications	155
5.4	Summary.....	157
Chapter 6: Time-dependent loading		158
6.1	General	158
6.2	Ramp loading.....	158
6.2.1.	Approximations for ramp loading	164
6.3	Discretised loading	165
6.4	Experimental investigation	167
6.4.1.	Discretised approaching constant rate loading	167
6.4.2.	Construction settlements	168
6.5	Summary.....	170
Chapter 7: Summary, conclusions and recommendations		172
7.1	Summary.....	172
7.2	Conclusions	173
7.2.1.	Excess pore water pressure dissipation	173
7.2.2.	Average degree of consolidation	174
7.2.3.	Coefficient of consolidation – uniform initial excess pore water pressure distributions	174
7.2.4.	Tall oedometer.....	175

7.2.5.	Coefficient of consolidation – non-uniform initial excess pore water pressure distributions	176
	One-way drainage.....	176
	Two-way drainage.....	177
7.2.6.	Time-dependent loading.....	177
7.3	Recommendations for future research.....	178
7.3.1.	Partial drainage boundaries	178
7.3.2.	Soil properties that vary with depth.....	178
7.3.3.	2D and 3D effects.....	179
7.4	Final comments	179
	References	180

List of Figures

Figure 2.1 – Components of discharge velocity at six faces of a soil element	7
Figure 2.2 – Example of Gibbs phenomenon	16
Figure 2.3 – Example of Gibbs phenomenon when the number of terms is increased	16
Figure 2.4 – Collocation and truncation example	18
Figure 2.5 - Example of non-linear u_i -distribution.....	20
Figure 2.6 - MATLAB solution procedure	23
Figure 3.1 – Isochrones for a uniform u_i -distribution with two-way drainage.....	26
Figure 3.2 – Isochrones for a linearly increasing u_i -distribution with two-way drainage	27
Figure 3.3 – Isochrones for a linearly decreasing u_i -distribution with two-way drainage	27
Figure 3.4 – Isochrones for a sinusoidal u_i -distribution with two-way drainage	28
Figure 3.5 – Isochrones for a triangular u_i -distribution with two-way drainage	29
Figure 3.6 – Isochrones for linearly increasing u_i -distributions with two-way drainage, where the value at $z/H = 0$ varies from 0.2 to 0	29
Figure 3.7 – Isochrones for an asymmetric u_i -distribution with two-way drainage, where $b = 2$	31
Figure 3.8 – Isochrones for an asymmetric u_i -distribution with two-way drainage, where $b = 12$	32
Figure 3.9 – Isochrones for a uniform u_i -distribution with one-way drainage.....	33
Figure 3.10 – Isochrones for a linearly increasing u_i -distribution with one-way drainage.....	34
Figure 3.11 – Isochrones for a linearly decreasing u_i -distribution with one-way drainage	35
Figure 3.12 – Isochrones for a sinusoidal u_i -distribution with one-way drainage.....	35
Figure 3.13 – Isochrones for skewed u_i -distributions with one-way drainage, where the maximum initial pressure occurs at (a) $Z = 0.2$, (b) $Z = 0.5$ and (c) $Z = 0.8$ for a spread of $b = 2$	36
Figure 3.14 – Isochrones for skewed u_i -distributions with one-way drainage, where the maximum initial pressure occurs at (a) $Z = 0.2$, (b) $Z = 0.5$ and (c) $Z = 0.8$ for a spread of $b = 12$	37
Figure 3.15 – Traditional settlement method: (a) doubly drained layer, (b) u_i -distribution, and (c) pore pressure dissipation.....	39
Figure 3.16 - Excess pore water pressure isochrones for a uniform u_i -distribution	42
Figure 3.17 – Average degree of consolidation curves for singly and doubly drained layers	43
Figure 3.18 – Excess pore water pressure isochrones for a uniform u_i -distribution using the traditional expression for time factor (in terms of drainage path length)	44
Figure 3.19 – Average degree of consolidation curves for singly and doubly drained layers in terms of the traditional time factor	45
Figure 3.20 – Comparing settlements for different drainage configurations using (a) traditional method, and (b) proposed method.....	46
Figure 3.21 – U_z and P_z isochrones for a singly drained layer subjected to a sinusoidal u_i -distribution determined using (a) singly drained solution, and (b) reflection method.....	47

Figure 3.22 – U - T curves for a singly or doubly drained soil layer subjected to different u_r -distributions	49
Figure 3.23 – U - $\log T$ curves for a singly or doubly drained soil layer subjected to different u_r -distributions	50
Figure 3.24 – $\log U$ - $\log T$ curves for a singly or doubly drained soil layer subjected to different u_r -distributions	50
Figure 3.25 – U - T curves for series solution results compared with Terzaghi and Frohlich (1936) tabulated values	51
Figure 3.26 – Effective drainage path factor as a function of U for key u_r -distributions.....	54
Figure 3.27 – Determination of maximum drainage path length for select isochrones for (a) doubly drained; or (b) singly drained consolidating layer	57
Figure 3.28 – Variation of maximum drainage path length with time for a doubly drained clay layer subjected to key u_r -distributions	58
Figure 3.29 – Variation of maximum drainage path length with time for a singly drained clay layer subjected to key u_r -distributions	59
Figure 3.30 – A comparison between singly and doubly drained clay layers subjected to key u_r -distributions	60
Figure 3.31 – Comparison between U values for non-uniform and uniform u_r -distributions with one-way drainage	62
Figure 3.32 – Comparison between U values for non-uniform and uniform u_r -distributions with two-way drainage	63
Figure 3.33 – Excess pore water pressure to decay for (a) uniform and (b) linearly increasing u_r -distributions with two-way drainage.....	64
Figure 3.34 – Excess pore water pressure to decay for non-uniform u_r -distributions normalised by corresponding decay for a uniform u_r -distribution (one-way drainage)	66
Figure 3.35 – Excess pore water pressure to decay for non-uniform u_r -distributions normalised by corresponding decay for a uniform u_r -distribution (two-way drainage)	66
Figure 3.36 – Values of U calculated using the asymptotic values of R_a in Eq. (3.40) compared with exact values of U for sinusoidal and half-sinusoidal u_r -distributions.....	68
Figure 3.37 – Values of U calculated using the asymptotic values of R_a in Eq. (3.40) compared with exact values of U for linearly increasing and decreasing u_r -distributions with one-way drainage	69
Figure 3.38 – Excess pore pressure to decay for linear u_r -distributions normalised by corresponding decay for a uniform u_r -distribution (one-way drainage)	70
Figure 3.39 – Adjustment factors for using linear u_r -distributions.....	71
Figure 4.1 – Comparison between experimental and theoretical results using values of c_v calculated from (a) Casagrande and (b) Taylor curve-fitting methods	77

Figure 4.2 – Comparison between key curve-fitting values derived using Taylor and Casagrande's curve-fitting methods; (a) d_0 and (b) d_{100}	77
Figure 4.3 – Proportion of total settlement over a 24 hr period attributed to primary consolidation by each curve-fitting method	78
Figure 4.4 – Type of fit associated with RMS errors of (a) 0.166, (b) 0.04, and (c) 0.016	79
Figure 4.5 – Program used to analyse consolidation data	82
Figure 4.6 – Example analysis using Casagrande's log-time method	82
Figure 4.7 – Example analysis using Taylor's root-time method.....	83
Figure 4.8 – Example analysis using the Asaoka method.....	84
Figure 4.9 – Example analysis using Cour's inflection point method	85
Figure 4.10 – Schematic representation of Step 2; Calculating U_{Exp} using values of $d_{100,n}$	87
Figure 4.11 – Schematic representation of Step 3; Calculating d_{100} using the variance method.....	88
Figure 4.12 – Example analysis using the variance (or Lovisa) method	89
Figure 4.13 – Example fit between theoretical and experimental results	90
Figure 4.14 – Settlement-time curves for different soil types when consolidated under an applied stress of 28 kPa.....	91
Figure 4.15 – Comparison between Taylor and Casagrande d_0 values for the three soils.....	92
Figure 4.16 – Comparison between Taylor/Cour/Lovisa and Casagrande d_{100} values for the three soils tested (for stress range of 7 kPa to 888 kPa).....	92
Figure 4.17 – Comparison between Taylor/Cour/Lovisa and Casagrande c_v values for the three soils tested (for stress range of 7 kPa to 888 kPa).....	93
Figure 4.18 – Variation in predicted c_v values with applied stress and corresponding RMS error for K_{50} soil	94
Figure 4.19 – Variation in predicted c_v values with applied stress and corresponding RMS error for K_{60} soil	95
Figure 4.20 – Variation in predicted c_v values with applied stress and corresponding RMS error for DM soil.....	96
Figure 4.21 – Schematic diagram of tall oedometer	100
Figure 4.22 – Variation in effective stress with depth and increasing diameter for an applied pressure of 80 kPa	103
Figure 4.23 – Variation in u_i with z/H and increasing H/D for a diameter of 0.5 m (Legend – see Figure 4.22).....	104
Figure 4.24 – Variation in u_i with z/H , assuming $q/\gamma D > 10$ (i.e. neglecting the self-weight component)	105
Figure 4.25 – Average degree of consolidation behaviour due to initial excess pore pressure distributions resulting from H/D ratios of 0.17, 0.4, 1, 2, 3, 4, 5 for both singly and doubly drained cases.....	106
Figure 4.26 – Variation in u_i with z/H and $H/D = 3$ and 5 for $q/\gamma D = 1, 2$ and 5	107

Figure 4.27 – Average degree of consolidation behaviour due to initial excess pore pressure distributions resulting from u_i -distributions where $q/\gamma D = 1$ and 5 and $H/D = 3$ and 5, and 0.5 and 5 for both doubly and singly drained cases, respectively.....	109
Figure 4.28 – Schematic of tall oedometer apparatus.....	111
Figure 4.29 – Effect of friction angle on u_i -distribution where $H/D = 2.1$	112
Figure 4.30 – Average degree of consolidation behaviour due to u_i -distributions resulting from ϕ' values of 15° , 20° , 25° , 30° and 35° for both singly and doubly drained cases, where $H/D = 2.1$	113
Figure 4.31 – Initial excess pore water pressure distributions resulting from δ/ϕ' values of 0 to 11.....	114
Figure 4.32 – Average degree of consolidation behaviour due to u_i -distributions resulting from δ/ϕ' values of 0, 0.25, 0.5, 0.75 and 1 for both singly and doubly drained cases, where $H/D = 2.1$ and $\phi' = 25^\circ$	115
Figure 4.33 – Variation in c_v values determined using data obtained from tall and standard oedometer tests	116
Figure 4.34 – RMS error for (a) uniform u_i -distribution, and (b) a linearly decreasing u_i -distribution (singly drained).....	119
Figure 4.35 – $U-T$ approximation curves for a uniform u_i -distribution with one- or two-way drainage	122
Figure 4.36 – $U-T$ approximation curves for a linearly increasing u_i -distribution with one- or two-way drainage.....	122
Figure 4.37 – $U-T$ approximation curves for a linearly decreasing u_i -distribution with one- or two-way drainage.....	123
Figure 4.38 – $U-T$ approximation curves for a sinusoidal u_i -distribution with one- or two-way drainage	123
Figure 4.39 – Evaluation of c_v using log-time method.....	125
Figure 4.40 – Evaluation of c_v using time-exponent method	127
Figure 5.1 – Consolidation behaviour due to an arched u_i -distribution in terms of (a) pore pressure isochrones for $T = 0.02, 0.06, 0.1, 0.2 \dots 1.0$, and (b) variation in pore pressure at $z = H$ with T	131
Figure 5.2 – Pore water pressure isochrones due to an arched u_i -distribution with accompanying sinusoidal approximations.....	133
Figure 5.3 – Tendency of pore water pressure isochrones to become sinusoidal in shape for different H/D values, under doubly drained conditions.....	134
Figure 5.4 – Consolidation behaviour due to a sinusoidal u_i -distribution in terms of (a) pore pressure isochrones for $T = 0.02, 0.06, 0.1, 0.2 \dots 1.0$, and (b) variation in pore pressure at $z = H$ with T	135
Figure 5.5 – Variation in experimental and theoretical base pore water pressure with time for a sinusoidal u_i -distribution with one-way drainage	136

Figure 5.6 – Average degree of consolidation curves translating a doubly drained layer to a singly drained layer subjected to a sinusoidal u_i -distribution	138
Figure 5.7 – Excess pore water pressure isochrones due to an arched u_i -distribution with two-way drainage.....	140
Figure 5.8 – Average degree of consolidation curves using $T_{block} = 0.01$ and 0.04 isochrones of an arched u_i -distribution as ‘initial’ u_i -distributions with subsequent one-way drainage	141
Figure 5.9 – Modified Casagrande curve-fitting procedure for a singly drained layer subjected to a sinusoidal u_i -distribution	142
Figure 5.10 – Modified Taylor curve-fitting procedure for a singly drained layer subjected to a sinusoidal u_i -distribution	142
Figure 5.11 – Example analysis using (a) modified Casagrande curve-fitting technique, and (b) modified Taylor curve-fitting technique.....	143
Figure 5.12 – Comparison between values of c_v obtained using trial and error versus modified curve-fitting technique (sample of 141 mm height subjected to an applied load of 160 kPa)	145
Figure 5.13 – Comparison between values of c_v obtained using trial and error versus modified curve-fitting technique (sample of 100 mm height subjected to an applied load of 160 kPa)	145
Figure 5.14 – Average degree of consolidation curves translating a doubly drained layer subjected to uniform or sinusoidal u_i -distributions	147
Figure 5.15 – Modified Casagrande curve-fitting procedure for a doubly drained layer subjected to a sinusoidal u_i -distribution	149
Figure 5.16 – Modified Taylor curve-fitting procedure for a doubly drained layer subjected to a sinusoidal u_i -distribution	150
Figure 5.17 – Analysis of data set 1 using traditional and modified Casagrande curve-fitting techniques	151
Figure 5.18 – Analysis of data set 2 using traditional and modified Casagrande curve-fitting techniques	151
Figure 5.19 – Analysis of data set 1 using traditional and modified Taylor curve-fitting techniques ..	152
Figure 5.20 – Analysis of data set 2 using traditional and modified Taylor curve-fitting techniques ..	153
Figure 5.21 – Experimental vs theory using (a) $c_{v,Cas}$ and (b) $c_{v,Tay}$ for data set 1	155
Figure 5.22 – Experimental vs theory using (a) $c_{v,Cas}$ and (b) $c_{v,Tay}$ for data set 2	155
Figure 6.1 – Approximating actual loading rate with constant rate loading.....	159
Figure 6.2 – Infinitesimal pressure increments applied during loading	159
Figure 6.3 – During and post-construction consolidation settlement for various construction times (T_L) with one-way drainage permitted	163
Figure 6.4 – Approximation constants	164
Figure 6.5 – Effect of varying number of loading steps within construction period of T_L for a doubly drained layer.....	166
Figure 6.6 – Pore pressure isochrones as they become sinusoidal.....	167

Figure 6.7 – Experimental vs. theoretical time-dependent loading.....	168
Figure 6.8 – Theoretical and experimental construction settlements normalised by constant rate loading parameters	169

List of Tables

Table 2.1 – Assumptions applicable to Terzaghi's consolidation theory	6
Table 2.2 – Initial and boundary conditions.....	11
Table 2.3 – Possible u_i -distributions.....	21
Table 3.1 - Example of traditional consolidation analysis	46
Table 3.2 – Graphical example illustrating Terzaghi's average degree of consolidation at $T = 0.1$	65
Table 3.3 – Adjustment factors for key non-uniform u_i -distributions.....	67
Table 4.1 – Soil properties.....	78
Table 4.2 – Limiting values of H/D for $q/\gamma D$ values where the average degree of consolidation resembles the uniform u_i case.....	108
Table 4.3 – Modified sample dimensions.....	110
Table 4.4 – $U-T$ approximations for two-way drainage.....	120
Table 4.5 – $U-T$ approximations for one-way drainage.....	121
Table 4.6 – f_c and f_T curve-fitting factors for two-way drainage	128
Table 4.7 – f_c and f_T curve-fitting factors for one-way drainage	128
Table 5.1 – Details of doubly drained to singly drained testing	139
Table 5.2– Results from Tests 1 and 2 obtained using (a) MATLAB trial-and-error, and (b) modified curve-fitting techniques	146
Table 5.3– Details of doubly drained testing	148
Table 5.4 – Results obtained using traditional and modified curve-fitting techniques to analyse data sets 1 and 2.....	154
Table 6.1 – Consolidation parameters	167

Chapter 1: Introduction

1.1 General

Possibly the most significant contribution to geotechnical engineering was Karl Terzaghi's theory of consolidation, which properly identified and quantified the underlying physical processes of consolidation by utilizing the principle of effective stress. Upon application of a load to a fully saturated layer of soil, an increase in pore water pressures throughout the layer will occur. Once these generated pore water pressures have dissipated to zero, primary consolidation can be considered complete. Terzaghi's one-dimensional consolidation theory mathematically describes this process.

All soils undergo consolidation in response to an increase in excess pore water pressure. However, for granular soils such as sands, the permeability is relatively high so that the excess pore water pressures dissipate virtually instantaneously. In direct contrast, fine-grained soil such as clays have generally very low permeability and therefore the dissipation is a much slower process. In many cases, an engineering structure or embankment will continue to undergo settlement for many years after construction is complete. Thus, whilst consolidation applies to all soils, it is the fine-grained soils that are of particular concern.

1.2 Problem Definition

The consolidation of fine-grained soils is actually rather more complicated than the process described by Terzaghi. In fact, the settlement a saturated layer of fine soil undergoes in response to an externally applied load is due to a combination of processes; immediate compression, primary consolidation, and secondary consolidation. Immediate settlement, also known as elastic settlement, can be considered to occur almost instantaneously when an external load is applied. The settlement that occurs due to secondary consolidation (or creep) is often considered to occur after primary consolidation is complete, but in actual fact, occurs simultaneously behind the scenes of primary consolidation. The very existence of these discrepancies between definitions of the onset of secondary consolidation is evidence of the controversial and still widely perplexing nature of the creep process. Further compounding the limitations of Terzaghi's one-dimensional consolidation theory are the assumptions upon which this theory is based, some of which are considered more realistic than others.

Despite these limitations, Terzaghi's one-dimensional consolidation theory is still widely used to evaluate soil compressibility, and has permeated virtually all aspects of geotechnical engineering. Whilst other more complex models exist which account for factors such as secondary consolidation, finite strains, three-dimensional consolidation etc., many

geotechnical engineers still revert back to Terzaghi's basic theory due to its inherent simplicity. Thus, the main objective of this project is to present a critical review of this one-dimensional theory of consolidation, along with possible refinements that do not severely compromise the simplicity of the overall model.

1.3 Scope of research

In instances where consolidation is expected to take a prolonged period of time, the following predictions are often required;

- a) the ultimate settlement of the structure/embankment, and
- b) the rate at which the settlement will occur.

The primary objective of this project is to systematically explore all aspects of Terzaghi's theory that apply to (b), the *rate* at which consolidation settlement occurs.

The scope of this project comprises the following sub-objectives:

- i. Mathematically refine the series solution to Terzaghi's consolidation equation so that a variety of non-uniform initial excess pore water pressure distributions can be investigated without incurring Gibbs phenomenon.
- ii. Study the effect of non-uniform initial excess pore water pressure distributions on the dissipation of excess pore water pressure during consolidation.
- iii. Study the effect of non-uniform initial excess pore water pressure distributions on the percentage consolidation of a soil layer during consolidation.
- iv. Critically analyse the effectiveness of popular curve-fitting techniques in accurately predicting the coefficient of consolidation using data obtained from different soil types.
- v. Modify current curve-fitting methods that fit experimental data to theory to predict consolidation properties so that they can account for a variety of non-uniform initial excess pore water pressure distributions.
- vi. Carry out laboratory tests to simulate non-uniform initial excess pore water pressure distributions and verify theoretical findings such as pore pressure redistribution.

- vii. Investigate the effect of time-dependent loading on percentage settlement when the external load is applied at either a constant rate or at discrete time intervals.

1.4 Thesis overview

Chapter 1 introduces Terzaghi's theory of consolidation in relation to its prevalence within geotechnical society. It also alludes to the limitations of this theory and how these limitations might affect the accuracy of any subsequent consolidation predictions made using this theory. Finally, a brief overview of the thesis is presented in this section.

In Chapter 2, Terzaghi's fundamental one-dimensional consolidation equation is derived from first principles, with separate solutions provided for one- and two-way drainage cases. The drawbacks associated with current techniques for solving the series coefficients are discussed, and an alternative method has been proposed to negate these shortcomings. This proposed method was developed with the potential to cater for any initial condition (i.e. initial excess pore water pressure distribution), not just the uniform case commonly assumed in consolidation analyses.

In Chapter 3, the solution procedure developed in Chapter 2 is used to investigate the effects of various non-uniform initial excess pore water pressure distributions on the consolidation behaviour of singly and doubly draining layers. Here, the consolidation behaviour is investigated in terms of excess pore pressure dissipation, degree of consolidation, and average degree of consolidation or percentage settlement. Using these results, the relevance of current time factor notation has also been assessed, with reference to the term maximum drainage path length. Finally, simple adjustment factors have been derived that can adjust the widely available average degree of consolidation values for a uniform case of initial excess pore pressure to account for a variety of non-uniform initial pore water pressure distributions.

The parameter, coefficient of consolidation, is discussed in relation to average degree of consolidation in Chapter 4. Popular curve-fitting techniques that fit experimental data to the theoretical average degree of consolidation curve in order to back-calculate consolidation parameters are critically reviewed using copious experimental data. A new oedometer apparatus is also discussed, where the effect of skin friction is incorporated into the initial excess pore water pressure distribution. Conclusions derived from this research are also experimentally verified using a tall oedometer. Finally, popular curve-fitting techniques (Taylor's square-root of time method, and Casagrande's logarithm-time method) are modified so that they can be applied to any set of settlement-time data, regardless of the initial excess pore water pressure distribution.

Results gathered in Chapter 3 regarding the dissipation of excess pore water pressure are experimentally verified in Chapter 5 by recreating a non-uniform initial excess pore water pressure distribution within a laboratory setting. This non-uniform initial excess pore water pressure distribution is also used to generate data that can be subsequently analysed using the modified curve-fitting techniques proposed in Chapter 4.

In Chapter 6, the effects of time-dependent loading on the consolidation behaviour of a soil layer are investigated. Two forms of time-dependent loading are studied; a constant rate or ramp loading, and a discretised loading approach. Results gathered from this study are also experimentally verified within this chapter.

Chapter 7 presents the summary and conclusions of this research, along with recommendations for future avenues of research.

Chapter 2: Analytical solution

2.1 General

A soil can be reduced to the following components; a skeleton of solid grains enclosing voids which may be filled with gas, with liquid, or with a combination of gas and liquid. If a stress is then externally applied to the soil in such a way that its volume is decreased, there are three factors to which this decrease may be attributed; a compression of the skeleton, a compression of water and air within the voids, and an escape of water and air from the voids. It is reasonable to assume that the soil grains and pore water are relatively incompressible. As a result, it follows that if the soil mass is completely saturated, any volume change can be attributed entirely to the escape of pore water from the voids.

Karl Terzaghi's most significant contribution to geotechnical engineering was his theory of consolidation (Terzaghi 1925), which properly identified and quantified the underlying physical processes associated with a saturated soil undergoing a volume change due to an externally applied load. During this time, Terzaghi identified the principle of effective stress, which provided the basis for understanding the process of consolidation.

2.2 Terzaghi's consolidation equation

The consolidation process begins when the placement of a fill or some other load generates an increase in the vertical total stress ($\Delta\sigma_v$) within the soil. Initially, the load is carried entirely by the pore water, which produces a net increase in the pore water pressure within the soil (which was previously operating under hydrostatic conditions). This increase in pore water pressure, termed excess pore water pressure (u), is generally assumed to equal the total applied stress, such that $u = \Delta\sigma_v$. Thus, the vertical effective stress (σ'_z) immediately after loading is unchanged from its initial value (σ'_{z_0}). The excess pore water pressure generates a localised increase in the total head, which subsequently induces a hydraulic gradient. As a result, some of the pore water begins to flow and the excess pore water pressure begins to dissipate, whilst the vertical effective stress simultaneously increases.

In addition to computing the magnitude of settlement that a consolidating soil layer will undergo, an estimate is also required of the *rate* at which the settlement occurs. When dealing with coarse-grained soils with inherently large values of permeability, it can often be assumed that the majority of settlement takes place approximately instantaneously. However, when dealing with fine-grained soils (which may be characterised by values of permeability

of the order 10^{-8} m/s), the time required for the final settlement to mature can take months, or even years (Lancellotta 2009).

The theory developed by Terzaghi to describe the transient coupled phenomenon of consolidation is reliant upon the assumptions listed in Table 2.1, some of which are more realistic than others.

Table 2.1 – Assumptions applicable to Terzaghi's consolidation theory

Assumption	Justification
1) The soil is fully saturated and homogenous.	Do not vary in any important degree from actual conditions.
2) Both the water and soil particles are incompressible.	
3) Darcy's law of water flow applies.	Completely valid.
4) The change in volume is one-dimensional and in the vertical direction (i.e. the direction of applied pressure).	One-dimensional conditions can be closely realised in laboratory tests. Select loading scenarios in the field can facilitate predominantly one-dimensional consolidation (elaborated upon later).
5) The coefficient of permeability (k_v) in the vertical direction remains constant.	Constant values for soil properties with depth can generally be assumed. In other cases, an 'equivalent' property may be required.
6) Deformations are infinitesimal.	Valid as long as strains are small in magnitude.
7) The change in volume directly corresponds to the change in void ratio (e) such that $\partial e / \partial \sigma'_v$ remains constant.	A greatly idealised assumption which has limited validity. However, a more correct relationship can severely complicate the analysis, which negates one of the primary goals of this study; to maintain the simplicity of Terzaghi's one-dimensional consolidation theory.
8) Immediately after loading, the excess pore water pressure (u) is constant with depth and equal to the applied pressure ($\Delta\sigma_v$).	This assumption is only applicable in cases where the loaded area is extensive (i.e. the area over which the applied pressure acts is <i>much</i> greater than the thickness of the soil layer). In many cases, this assumption is invalid.

2.2.1. Derivation

An analytical procedure for computing the rate of consolidation can thus be developed by revisiting the physical process of excess pore water dissipation and applying the assumptions shown in Table 2.1. First, consider the discharge velocity at the center of the soil element of thickness dz (and side lengths dy and dz) shown in Figure 2.1. This discharge velocity has components v_x , v_y , and v_z in the x -, y - and z -directions, respectively. At the center of the element, the rate of flow in the x -direction is $v_x dy dz$, where $dy dz$ is the area of the element perpendicular to the x -direction.

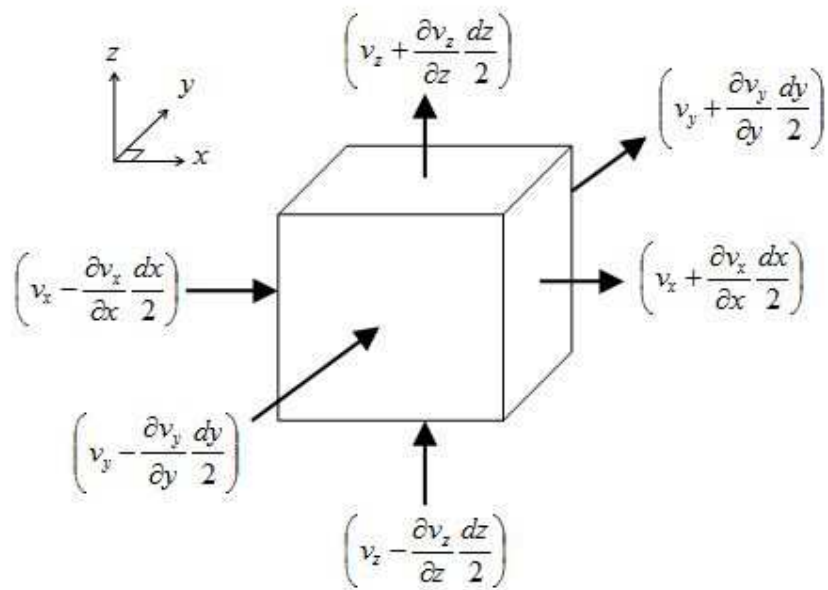


Figure 2.1 – Components of discharge velocity at six faces of a soil element

If dv_x/dx is the rate of change of v_x in the x -direction, and $(dv_x/dx)(dx/2)$ is the total change in v_x between the center and a face of the soil element, the rate of flow in the x -direction *into* the soil element ($q_{x,in}$) can be given by:

$$q_{x,in} = \left(v_x + \frac{\partial v_x}{\partial x} \frac{dx}{2} \right) dy dz \quad (2.1)$$

Similarly, the rate of flow in the x -direction *out of* the soil element ($q_{x,out}$) is:

$$q_{x,out} = \left(v_x - \frac{\partial v_x}{\partial x} \frac{dx}{2} \right) dy dz \quad (2.2)$$

Using Eqs. (2.1) and (2.2), the net flow into or out of the soil element in the x -direction (q_x) can then be calculated as:

$$q_x = \frac{\partial v_x}{\partial x} dx dy dz \quad (2.3)$$

This procedure can be repeated to determine q_y and q_z both into and out of the soil element in the y - and z -directions, respectively. Finally, the net volume of water flowing per unit of time (t) into or out of the soil element can be calculated as follows:

$$q = \left(\frac{\partial v_x}{\partial x} + \frac{\partial v_y}{\partial y} + \frac{\partial v_z}{\partial z} \right) dx dy dz \quad (2.4)$$

where q is essentially the change in volume of water in the soil element per unit of time. The continuity equation shown in Eq. (2.4) can be reduced further when only one-dimensional flow is considered, as per Assumption 4 to give:

$$q = \frac{\partial v_z}{\partial z} dx dy dz \quad (2.5)$$

By introducing the porosity (n), the volume of water in the element can be defined as $n dx dy dz$. Thus, the net change in volume of water in the soil element per unit time can also be given by:

$$q = -\frac{\partial}{\partial t} (n dx dy dz) \quad (2.6)$$

where the negative sign allows any reduction in volume to be viewed as positive. Eq. (2.6) can be also be rewritten in terms of void ratio (e) using the known relationship between n and e so that:

$$q = -\frac{\partial}{\partial t} \left(\left(\frac{e}{1+e} \right) dx dy dz \right) \quad (2.7)$$

Eqs. (2.5) and (2.7) can be equated to give the continuity equation, where flow takes place in the vertical direction only:

$$\frac{\partial v_z}{\partial z} dx dy dz = -\frac{\partial}{\partial t} \left(\left(\frac{e}{1+e} \right) dx dy dz \right) \quad (2.8)$$

Darcy's law (Assumption 3) can be expressed in terms of excess pore water pressure:

$$v_z = -\frac{k_v}{\gamma_w} \frac{\partial u}{\partial z} \quad (2.9)$$

where k_v = coefficient of permeability in the vertical direction which is assumed to be constant over the entire depth of the soil layer (as per Assumption 5), γ_w = the unit weight

of water, z = depth (measured downward from the surface of the soil layer), and u = the excess pore water pressure. Substituting Eq. (2.9) into (2.8) gives:

$$\frac{k_v}{\gamma_w} \frac{\partial^2 u}{\partial z^2} dx dy dz = \frac{\partial}{\partial t} \left(\left(\frac{e}{1+e} \right) dx dy dz \right) \quad (2.10)$$

Assuming that changes in void ratio during consolidation are small (as per Assumption 6), $(1+e)$ can be approximated by $(1+e_0)$, where e_0 is the initial void ratio of the soil element. This assumption considerably simplifies Eq. (2.10), as $(dx dy dz)/(1+e_0)$, which is the constant volume of solids, effectively remains independent of time. Thus, Eq. (2.10) can be simplified to give:

$$\frac{k_v}{\gamma_w} \frac{\partial^2 u}{\partial z^2} dx dy dz = \frac{\partial e}{\partial t} \frac{dx dy dz}{1+e} \quad (2.11)$$

or

$$\frac{k_v}{\gamma_w} \frac{\partial^2 u}{\partial z^2} = \frac{1}{1+e} \frac{\partial e}{\partial t} \quad (2.12)$$

The relationship between the coefficient of volume compressibility (m_v), void ratio and vertical effective stress can then be applied to Eq. (2.12) to give:

$$\frac{k_v}{\gamma_w} \frac{\partial^2 u}{\partial z^2} = -m_v \frac{\partial \sigma'_v}{\partial t} \quad (2.13)$$

where

$$m_v = -\frac{\partial e}{\partial \sigma'_v} \frac{1}{1+e} \quad (2.14)$$

and $\partial e / \partial \sigma'_v$ remains constant (as per Assumption 7). Any increase in vertical effective stress results in a simultaneous decrease in excess pore water pressure. This can be written as:

$$\frac{\partial \sigma'_v}{\partial t} = -\frac{\partial u}{\partial t} \quad (2.15)$$

Eq. (2.15) can then be substituted into Eq. (2.13) to give the basic differential equation of consolidation:

$$\frac{\partial u}{\partial t} = \frac{k_v}{m_v \gamma_w} \frac{\partial^2 u}{\partial z^2} \quad (2.16)$$

By introducing the coefficient of consolidation (c_v), which can be defined as

$$c_v = \frac{k_v}{m_v \gamma_w} \quad (2.17)$$

Eq. (2.16) becomes

$$\frac{\partial u}{\partial t} = c_v \frac{\partial^2 u}{\partial z^2} \quad (2.18)$$

This equation is the differential equation governing one-dimensional consolidation and the dissipation of excess pore water pressures, and is noticeably similar to Fick's law of thermal diffusion.

2.2.2. Initial and boundary Conditions

The consolidation equation in Eq. (2.18) expresses the dependent variable, excess pore water pressure (u), as a function of the independent variables, depth (z) and time (t). In this partial differential equation, u is differentiated once with respect to t , and twice with respect to z . Thus, two boundary conditions are required, which must provide information about the excess pore water pressure at two specific depths of the clay layer. It is here that the drainage conditions under which the soil layer consolidates become important, which can be directly expressed in terms of excess pore water pressure.

In a doubly drained soil stratum, pore water is expelled from the voids and drained out of the soil upwards and downwards through the top and bottom drainage boundaries. For example, a clay layer open to atmosphere and underlain by sand would be considered doubly drained. However, a condition may exist where only one face of the clay layer (top or bottom) allows pore water drainage. This condition is often referred to as single drainage or one-way drainage. An impervious boundary can be present in the form of very stiff clay of low permeability or bedrock, usually located beneath the consolidating layer. All singly drained analyses conducted throughout this investigation have the impermeable boundary located at the base of the soil layer.

A freely draining upper boundary exists at the top of the soil profile in the form of ground level exposed to atmospheric pressure, or at the bottom of a granular soil layer overlain by other soils. A freely draining boundary condition can also be assumed in cases involving a contiguous material of comparatively high permeability (e.g. sand seam). Depending upon the number of freely draining boundaries, the layer is said to be either singly or doubly drained.

In summary, the boundary conditions can comprise either one drainage boundary and one impermeable boundary, or two drainage boundaries. These drainage conditions must be expressed in terms of excess pore water pressure in order to be applied to Eq. (2.18). For example, at a freely draining boundary, $u = 0$ at this point at all times during consolidation. Conversely, if an impermeable boundary is present, (i.e. no flow is allowed through this point), $\partial u / \partial z = 0$.

An initial condition in terms of t is also required, and this is most easily gathered from knowledge of the distribution of excess pore water pressure with depth at the onset of consolidation ($t = 0$). As per Assumption 8, this initial excess pore water pressure distribution is constant with depth and equal to the applied pressure ($\Delta\sigma_v$).

These initial and boundary conditions are summarised in Table 2.2 in terms of the total thickness of the soil layer, H .

Table 2.2 – Initial and boundary conditions

Boundary Condition	Mathematical Expression
1) There is complete drainage at the top of the soil layer.	$u(0,t) = 0$
2a) There is complete drainage at the base of the soil layer.	$u(H,t) = 0$
2b) The base of the soil layer is impermeable.	$\frac{\partial u(H,t)}{\partial z} = 0$
3) The initial excess pore water pressure at the onset of consolidation is equal to the applied pressure.	$u(z,0) = \Delta\sigma_v$

2.3 Mathematical solution for the consolidation equation

Terzaghi's consolidation equation can be solved if a separable function of two variables (z and t) is adopted as an expression for the excess pore water pressure in Eq. (2.18). The solutions for the boundary conditions in Table 2.2 can then be obtained using Fourier series.

An expression for u can be obtained as a product of some function of z and some function of t as shown:

$$u = f(z) \cdot g(t) \quad (2.19)$$

Thus,

$$\frac{\partial u}{\partial t} = f \cdot \frac{\partial g}{\partial t} = f(z) \cdot g'(t) \quad (2.20)$$

and

$$\frac{\partial^2 u}{\partial z^2} = \frac{\partial^2 f}{\partial z^2} \cdot g = f''(z) \cdot g(t) \quad (2.21)$$

Substitution of Eqs. (2.20) and (2.21) into Eq. (2.18) gives:

$$f(z) \cdot g'(t) = c_v f''(z) \cdot g(t) \quad (2.22)$$

or

$$\frac{1}{c_v} \frac{g'(t)}{g(t)} = \frac{f''(z)}{f(z)} \quad (2.23)$$

The left-hand side of Eq. (2.23) is now independent of any changes in z , and the right-hand side is correspondingly independent of any changes in t . Thus, if Eq. (2.23) is valid for all values of z and t , then each side must be a constant which is assigned the variable $-\lambda^2$. Each side of Eq. (2.23) can then be rewritten as:

$$f''(z) + \lambda^2 f(z) = 0 \quad (2.24)$$

and

$$g'(t) + \lambda^2 c_v g(t) = 0 \quad (2.25)$$

The solutions to Eqs. (2.24) and (2.25) are shown in Eqs. (2.26) and (2.27), respectively:

$$f(z) = C_1 \sin(\lambda z) + C_2 \cos(\lambda z) \quad (2.26)$$

$$g(t) = C_3 \exp(-c_v \lambda^2 t) \quad (2.27)$$

where C_1 , C_2 and C_3 = arbitrary constants.

Eq. (2.19) then becomes

$$u = [C_4 \sin(\lambda z) + C_5 \cos(\lambda z)] \exp(-c_v \lambda^2 t) \quad (2.28)$$

where C_4 and C_5 = arbitrary constants.

It can be seen that boundary condition 1 is satisfied if $C_5 = 0$. This leaves

$$u = [C_4 \sin(\lambda z)] \exp(-c_v \lambda^2 t) \quad (2.29)$$

For a doubly drained layer, applying boundary condition 2a to Eq. (2.29) yields the following eigenvalues (λ_{DD}):

$$\lambda_{DD} = \frac{n\pi}{H} \quad (2.30)$$

which can be substituted back into Eq. (2.29) by means of a Fourier series to give:

$$u_{DD} = \sum_{n=1}^{\infty} A_{DD,n} \sin\left(\frac{n\pi z}{H}\right) \exp\left(-\frac{c_v n^2 \pi^2 t}{H^2}\right) \quad (2.31)$$

where u_{DD} = excess pore water pressure for a doubly drained case and $A_{DD,n}$ = series coefficients.

Similarly, for a singly drained layer, applying boundary condition 2b to Eq. (2.29) yields the following eigenvalues (λ_{SD}):

$$\lambda_{SD} = \frac{(2n-1)\pi}{2H} \quad (2.32)$$

which can be substituted back into Eq. (2.29) by means of a Fourier series to give:

$$u_{SD} = \sum_{n=1}^{\infty} A_{SD,n} \sin\left(\frac{(2n-1)n\pi z}{2H}\right) \exp\left(-\frac{c_v(2n-1)^2 \pi^2 t}{4H^2}\right) \quad (2.33)$$

where u_{SD} = excess pore water pressure for a doubly drained case and $A_{SD,n}$ = series coefficients.

Introducing the term time factor (T), which is a dimensionless variable that is a function of coefficient of consolidation (c_v), time (t), and total layer thickness (H), Eqs. (2.31) and (2.33) become:

$$u_{DD} = \sum_{n=1}^{\infty} A_{DD,n} \sin\left(\frac{n\pi z}{H}\right) \exp(-n^2 \pi^2 T) \quad (2.34)$$

$$u_{SD} = \sum_{n=1}^{\infty} A_{SD,n} \sin\left(\frac{(2n-1)n\pi z}{2H}\right) \exp\left(-\frac{(2n-1)^2 \pi^2 T}{4}\right) \quad (2.35)$$

In order to determine the series coefficients, the initial condition (boundary condition 3) must be applied to Eqs. (2.34) and (2.35). This boundary condition ($u(z,0) = \Delta\sigma_v$) will be fulfilled if the series coefficients in Eqs. (2.34) and (2.35) are determined so that:

$$\Delta\sigma_v = \sum_{n=1}^{\infty} A_{DD,n} \sin\left(\frac{n\pi z}{H}\right) \quad (2.36)$$

$$\Delta\sigma_v = \sum_{n=1}^{\infty} A_{SD,n} \sin\left(\frac{(2n-1)n\pi z}{2H}\right) \quad (2.37)$$

The series coefficients ($A_{DD,n}$ and $A_{SD,n}$) are traditionally determined using an orthogonality relationship. This procedure utilises definite integrals, which have been

provided in Eqs. (2.38) to (2.41) in terms of some iteration of the eigenvalues for each drainage case.

$$\int_0^{2H} \sin\left(\frac{m\pi z}{2H}\right) \sin\left(\frac{n\pi z}{2H}\right) dz = 0 \quad (2.38)$$

$$\int_0^H \sin\left(\frac{m\pi z}{H}\right) \sin\left(\frac{n\pi z}{H}\right) dz = 0 \quad (2.39)$$

$$\int_0^{2H} \sin^2\left(\frac{n\pi z}{2H}\right) dz = H \quad (2.40)$$

$$\int_0^H \sin^2\left(\frac{(2n-1)\pi z}{H}\right) dz = \frac{H}{2} \quad (2.41)$$

where m and n = unequal integers.

If both sides of Eq. (2.36) are multiplied by $\sin(n\pi z/2H)dz$ and integrated between 0 and $2H$, all terms in the series except the n th term will assume the form of Eq. (2.38) and disappear. The remaining n th term will resemble Eq. (2.40) and will have a definite value. This can be mathematically carried out as follows:

$$\begin{aligned} \Delta\sigma_v &= \sum_{n=1}^{\infty} A_{DD,n} \sin\left(\frac{n\pi z}{H}\right) \\ \int_0^{2H} \Delta\sigma_v \sin\left(\frac{n\pi z}{2H}\right) dz &= A_{DD,n} \int_0^{2H} \sin^2\left(\frac{n\pi z}{2H}\right) dz \\ \int_0^{2H} \Delta\sigma_v \sin\left(\frac{n\pi z}{2H}\right) dz &= A_{DD,n} H \\ A_{DD,n} &= \frac{1}{H} \int_0^{2H} \Delta\sigma_v \sin\left(\frac{n\pi z}{2H}\right) dz \end{aligned} \quad (2.42)$$

and can be repeated for the singly drained case using Eqs. (2.39) and (2.41) to give:

$$A_{SD,n} = \frac{2}{H} \int_0^H \Delta\sigma_v \sin\left(\frac{(2n-1)\pi z}{H}\right) dz \quad (2.43)$$

Since $\Delta\sigma_v$ is a constant, the integrals in Eqs. (2.42) and (2.43) can be evaluated and substituted back into Eqs. (2.34) and (2.35) to give the general equations for excess pore water pressure decay during consolidation if the layer is doubly or singly drained, respectively.

$$u_{DD} = \sum_{n=1}^{\infty} \left[\frac{2\Delta\sigma_v}{n\pi} \left(1 - (-1)^n \right) \sin\left(\frac{n\pi z}{H}\right) \right] \exp\left(-n^2\pi^2 T\right) \quad (2.44)$$

$$u_{SD} = \sum_{n=1}^{\infty} \left[\frac{4\Delta\sigma_v}{(2n-1)\pi} \sin\left(\frac{(2n-1)\pi z}{2H}\right) \right] \exp\left(\frac{-(2n-1)^2\pi^2 T}{4}\right) \quad (2.45)$$

2.3.1. Limitations of the traditional solution process

The mathematical series solutions shown in Eqs. (2.44) and (2.45) are analytical solutions that describe the decay of excess pore water pressure within a saturated soil layer subjected to an initial distribution of excess pore water pressure that is constant within the soil layer, usually assumed to equal the magnitude of externally applied pressure. However, these expressions can only be evaluated for a finite number of terms. If a discontinuity is present in the initial condition, this evaluation using a finite number of terms can introduce problems associated with Gibbs phenomenon.

This phenomenon refers to the erratic behaviour of the Fourier series of a piecewise continuously differentiable periodic function at a discontinuity (Carslaw 1930). Mathematically, Gibbs phenomenon manifests during the approximation of a discontinuous function by a finite series of continuous sine waves. That is, when the series approximation attempts to satisfy a discontinuity, the series solution oscillates rapidly about the true value as the discontinuities are approached, with the series solution over-shooting the correct value by up to 18% near the discontinuity (Arfken 1970). In this study, a discontinuity essentially refers to a non-zero value of excess pore water pressure at a drainage boundary. Clearly, if a uniform or constant value of initial excess pore water pressure is adopted as the initial condition, two discontinuities will be present in the doubly drained case, and one discontinuity will be present in the singly drained case.

This can be illustrated by simply evaluating the excess pore water pressure at $t = 0$ using Eqs. (2.44) or (2.45) and plotting this against depth (z) normalised by the layer thickness (H). The series coefficients were calculated using an orthogonality relationship to satisfy the initial condition. As a result, the excess pore water pressure at $t = 0$ evaluated using the series solution *should* be equal to the externally applied pressure (i.e. the initial condition). However, when this procedure is carried out for the doubly drained case (where a discontinuity is present at each drainage boundary) using 400 terms, the excess pore water pressure is not constant with depth, as shown in Figure 2.2. At each drainage boundary (i.e. at $z/H = 0$ and $z/H = 1$), the solution overshoots and undershoots the desired value ($u(z,0)/\Delta\sigma_v = 1$).

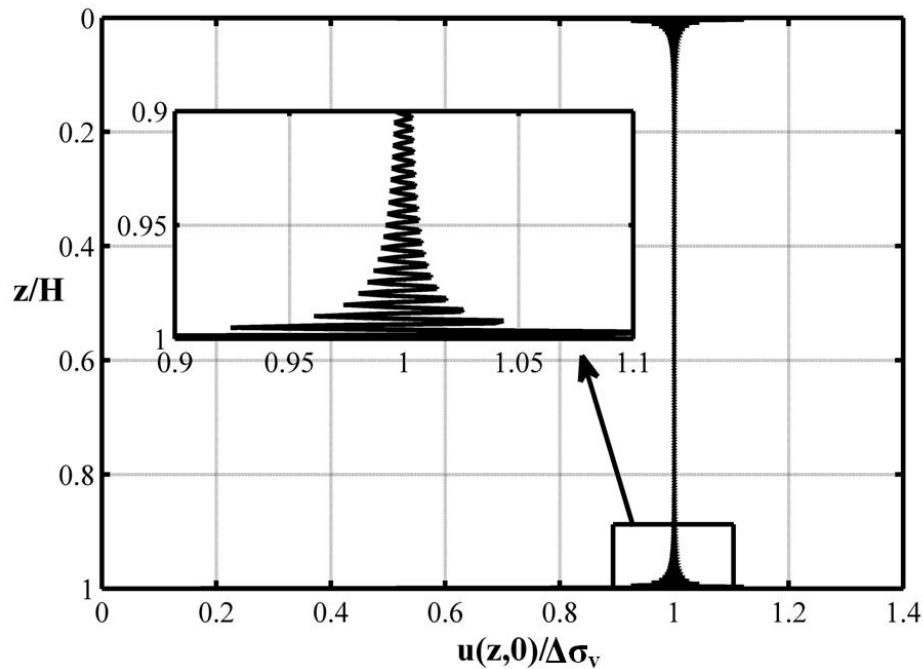


Figure 2.2 – Example of Gibbs phenomenon

If the number of terms is doubled, the error of the approximation is reduced in width and energy, as shown in Figure 2.3.

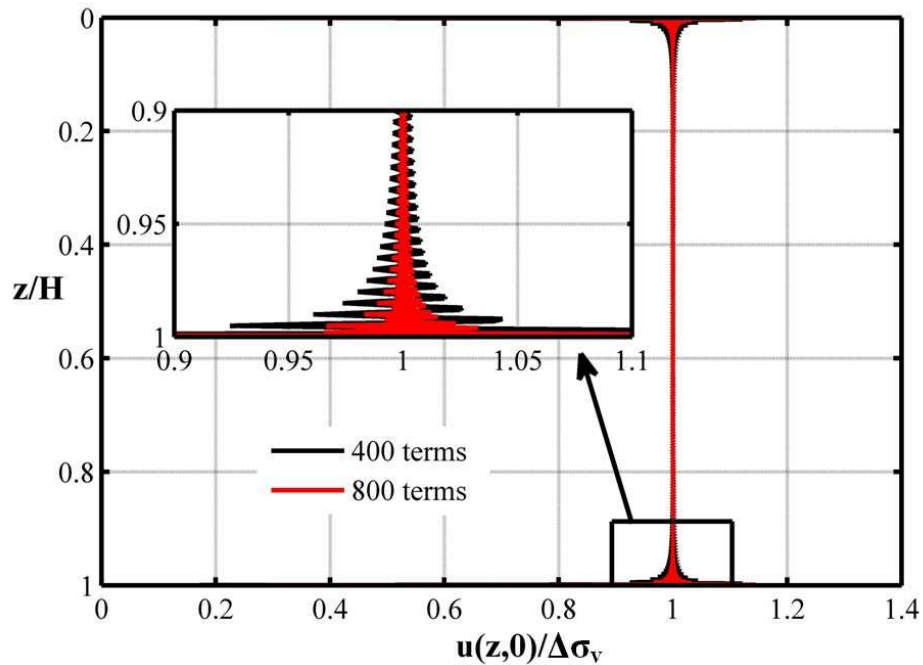


Figure 2.3 – Example of Gibbs phenomenon when the number of terms is increased

Increasing the number of terms does not remove this oscillatory effect, but merely moves it closer to the point of discontinuity. Further increases in the number of terms will not

eliminate the Gibbs phenomenon, but will simply result in oscillations that converge to a fixed height. Thus, when an orthogonality relationship is used to evaluate the series coefficients, it is impossible to eliminate errors associated with Gibbs phenomenon.

2.3.2. Proposed method

Using a novel method comprised of collocation coupled with select truncation, it is possible to develop an approximation to describe the decay of excess pore water pressure with time without incurring any degree of Gibbs phenomenon. Eqs. (2.36) and (2.37) were previously evaluated using an orthogonality relationship to solve for the series coefficients (Taylor 1948, Holtz and Kovacs 1981). However, a more efficient evaluation procedure consists of a pseudo-spectral or collocation approach, where the series is truncated after N terms and forced to satisfy the general solution at M ($= N$) collocation points. In practice, a value of M greater than N can be selected, which then reduces the collocation to discrete least squares. Values of M chosen in the range $2N$ to $3N$ work well, in practice. All analyses in this investigation were conducted using $M = 2N$. The collocation procedure was implemented in the program MATLAB, which is capable of complex matrix manipulations, thereby making it an ideal tool for this analysis.

If used to determine the series coefficients, a collocation approach would still result in a series approximation with Gibbs phenomenon occurring at the discontinuities. However, this can be avoided by introducing an extra step into the procedure, and herein lies the novelty of the proposed method. When a discontinuity is present, the collocation approach is modified by removing collocation points from the immediate vicinity of the discontinuity. In the doubly drained example used previously, the initial excess pore water pressure distribution contained two discontinuities; one at the surface of the soil layer ($z = 0$), and one at the base ($z = H$). Instead of choosing M collocation points from $(0, H)$ and conducting the subsequent analysis, the points are selected from the interval $(\Delta, H - \delta)$ instead, where Δ and δ are small non-zero increments. In effect, the position vector is marginally truncated at the points of discontinuity by Δ and δ . The steps taken to implement this process in the program MATLAB are outlined as follows.

First, a position vector is specified which encompasses the truncated thickness $(\Delta, H - \delta)$ of the soil layer being considered:

$$z_i = \Delta + \frac{i(H - \Delta - \delta)}{M + 1} \quad (2.46)$$

where $i = 1, \dots, M$. Using the position vector in Eq. (2.46), Eqs. (2.36) and (2.37) can be simplified and represented as:

$$\Delta\sigma_v = \sum_{n=1}^{\infty} A_j u_j(z_i) \quad (2.47)$$

where $u_j(z_i) = \sin(\lambda_j z_i)$, A_j are the series coefficients, λ_j are the eigenvalues, and $i = 1, \dots, N$. Eq. (2.47) can be easily presented for either a doubly or singly drained case by using the appropriate eigenvalues and series coefficients. The series coefficients can then be determined by solving Eq. (2.47) after multiplication by transpose of the coefficient matrix:

$$U^T \tilde{g} = U^T U \tilde{a} \quad (2.48)$$

where $[U]_{ij} = u_j(z_i)$; $[\tilde{g}]_i = \Delta\sigma_v$; and $[\tilde{a}]_u = A_j$. The corresponding vector of series coefficients can then be used to calculate the decay of excess pore water with time at any depth within the soil layer using Eqs. (2.34) and (2.35).

When the boundaries where a discontinuity occurred were truncated by 0.5% (i.e. $\Delta = \delta = 0.005H$), virtually all oscillatory effects of Gibbs phenomenon were eliminated, as demonstrated in Figure 2.4. The solution at $t = 0$ now equals the desired value (i.e. $u(z,0) = \Delta\sigma_v$).

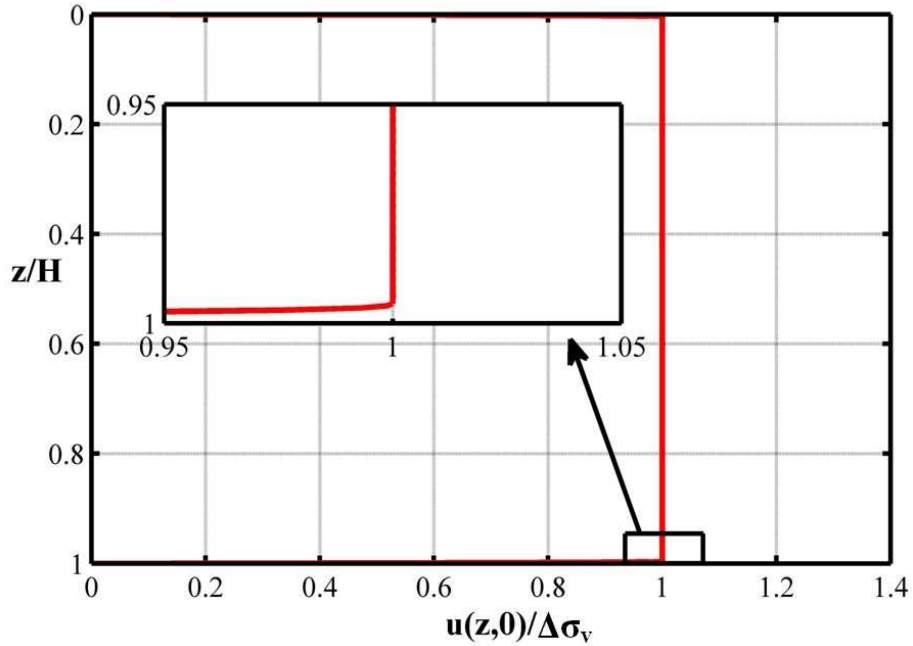


Figure 2.4 – Collocation and truncation example

The accuracy of the series approximation developed using M collocation points can be checked by evaluating the series at $T = 0$ and comparing this with the initial excess pore

water pressure with depth of the soil layer. To ensure confidence in results based on allocation of M and N number of points, the following root mean square (RMS) error was calculated:

$$\epsilon^2 = \frac{\int_{\Delta}^{H-\delta} \left(u(z,0) - \sum_{n=1}^N A_n u_n(z,0) \right)^2 dz}{\int_0^H dz} \quad (2.49)$$

When 400 terms was used ($N = 400$), the RMS error was of the order 10^{-4} . When the number of terms was increased to $N = 800$, the error correspondingly decreased to the order of 10^{-7} . Simulations took approximately two seconds to complete.

2.4 Assumption 8 – Initial excess pore water pressure distribution

Despite evidence to the contrary, many geotechnical analyses that utilise Terzaghi's consolidation theory still adopt a uniform initial excess pore water pressure distribution within the soil layer in response to an externally applied load. The assumption of a uniform initial excess pore water pressure distribution, herein termed u_i -distribution, is only valid for certain cases where an extensive loaded area is applied to a comparatively thin layer of clay. Here, the axial stress distribution can be assumed as constant throughout the thickness of the clay layer (Jumikis 1962). If the consolidating layer is comparatively thick with respect to the width of the loaded area, the u_i -distribution can be expected to decrease with depth.

In cases such as hydraulically placed fills, where self-weight consolidation takes place, a linearly increasing u_i -distribution can occur, where the pressure increases directly in proportion with depth, usually according to γz , where γ is the unit weight of the slurry. Thus, a linear u_i -distribution of the form $(\gamma - \gamma_w)z$ can be anticipated when considering the placement of hydraulic fill or slurry. Linearly increasing/decreasing u_i -distributions can also occur as a result of the sudden lowering of a groundwater table beneath a saturated stratum (Lambe and Whitman 1969).

Other more obscure u_i -distributions can exist, as acknowledged by Taylor (1962), who suggested that two or more of the traditionally accepted u_i -distributions be combined to approximate actual distributions, an example of which is shown in Figure 2.5. Chu and Wan (2005) suggested a method for estimating the average degree of consolidation based on the

pore water pressure distribution, and presented two case studies where pore water pressure dissipation was measured prior to and during vacuum preloading. Soil I consists of a 6 m very soft clay slurry which overlies Soil II, a 16 m soft silty clay. Pore water pressure transducers were used to evaluate the u_i -distribution shown in Figure 2.5, prior to vacuum loading. Here, excess pore water pressures were present as the subsoil was still undergoing consolidation.

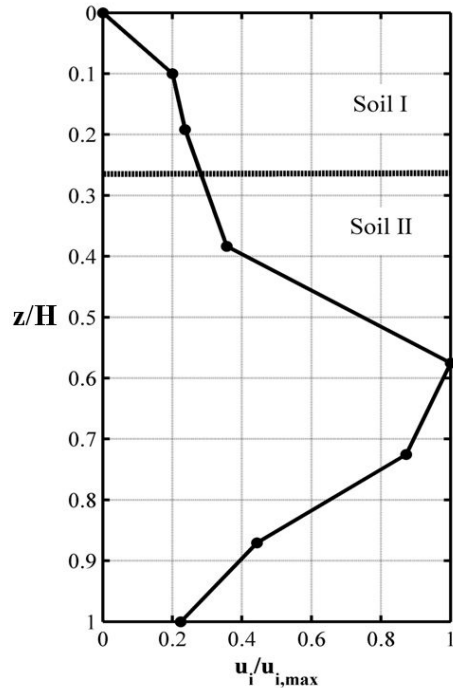
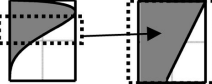


Figure 2.5 - Example of non-linear u_i -distribution

A constant or linear distribution of excess pore pressure is commonly adopted in most consolidation analyses. Janbu et al. (1956) analysed the average consolidation behaviour of a consolidating soil layer with a freely draining upper surface and impermeable base, for linearly increasing and decreasing initial excess pore pressure distributions. The assumption of uniform initial excess pore pressure was adopted by Mesri (1973) for calculations involving the settlement of a consolidating layer separated from freely draining upper and lower surfaces by incompressible layers of finite permeability. Kim et al. (2007) investigated the spatial distribution of excess pore-water pressure induced by piezocone penetration into over-consolidated clays. Simple equations for estimating the consolidation coefficient and final settlement based on any type of linear loading with one-way or two-way drainage have also been proposed by Singh (2008).

A summary of possible u_i -distributions is shown in Table 2.3, which encompass a wide range of loading scenarios, all of which have been considered in this investigation.

Table 2.3 – Possible u_i -distributions

Case	u_i-distribution	Loading scenario
I		A uniform distribution of u_i can be expected in situations where thin layers of clay are subjected to extensive loaded areas, such as foundations, mats etc. (e.g. standard oedometer tests)
II		A linearly increasing u_i -distribution can occur due to self-weight of the soil, or any instance where materials suspended in a liquid (e.g. hydraulic fills, sludge deposits etc.)
III		For thicker layers of clay and finite loaded areas, a linearly decreasing u_i -distribution can be used to approximate the decrease in vertical stresses that occur according to Boussinesq's pressure equations. Although this is approaching a two- or three-dimensional problem, one-dimensional consolidation analysis can still be used to determine the conservative case (i.e. a 1-D analysis will tell the user the slowest possible rate of consolidation).
IV		A trapezoidal u_i -distribution (with maximum pressure at the top of the clay layer) can be expected in cases where foundation loads are applied to clay layers interspersed with other layers of approximately infinite or zero permeability (i.e. can be treated as drainage boundaries). Here, the axial pressure from the foundation load is distributed on each layer approximately trapezoidally.
V		A trapezoidal u_i -distribution (with maximum pressure at the base of the clay layer) is possible when the self-weight of the soil (Case II) is added to the trapezoidal distribution resulting from a structurally imposed load (Case IV).
VI		Sinusoidal and half-sinusoidal u_i -distributions can be expected when some unknown degree of consolidation has taken place over some unknown timeframe. Here, the 'initial' distribution is taken to be sinusoidal or half-sinusoidal depending upon the existing drainage configuration.

Incorporation of non-uniform u_i into proposed method

The collocation procedure used to evaluate the series coefficients was generalized in terms of the u_i -distribution, which is a function of depth (z), now that non-uniform u_i -distributions are being considered. Eq. (2.47) can be rewritten to incorporate this u_i -distribution as follows:

$$g(z_i) = \sum_{n=1}^{\infty} A_n u_n(z_i) \quad (2.50)$$

where g is used to represent the u_i -distribution. The efficacy of this collocation method is evident upon further examination of Eq. (2.50) – the u_i -distribution can either be evaluated at each point within the position vector using a known function, or the u_i -distribution can be an array of points gathered from field data, and not necessarily a function at all. Either form of input will produce a realistic output of excess pore water pressure decay, unique to the relevant u_i -distribution.

The generalised procedure used to assess the consolidation behaviour due to each of the distributions shown in Table 2.3 is outlined in Figure 2.6, for a doubly drained layer. A similar procedure was followed for the singly drained cases. The collocation method outlined previously was used to solve for the series coefficients. In cases where a discontinuity was present in the u_i -distribution, the collocation points were truncated by a specific value (Δ for the upper boundary and δ for the lower), usually less than 0.5% of H , to avoid Gibbs phenomena.

Values of Δ and δ less than 0.5% of H , with $N = 1000$ to 1500 terms were found to be suitable for this analysis, and generated a corresponding RMS error of the order 10^{-8} to 10^{-12} in the truncated region. All oscillatory behaviour characteristic of Gibbs phenomena was removed, including any overshoot. When no discontinuities were present, $N = 400$ terms was generally sufficient to achieve the same accuracy.

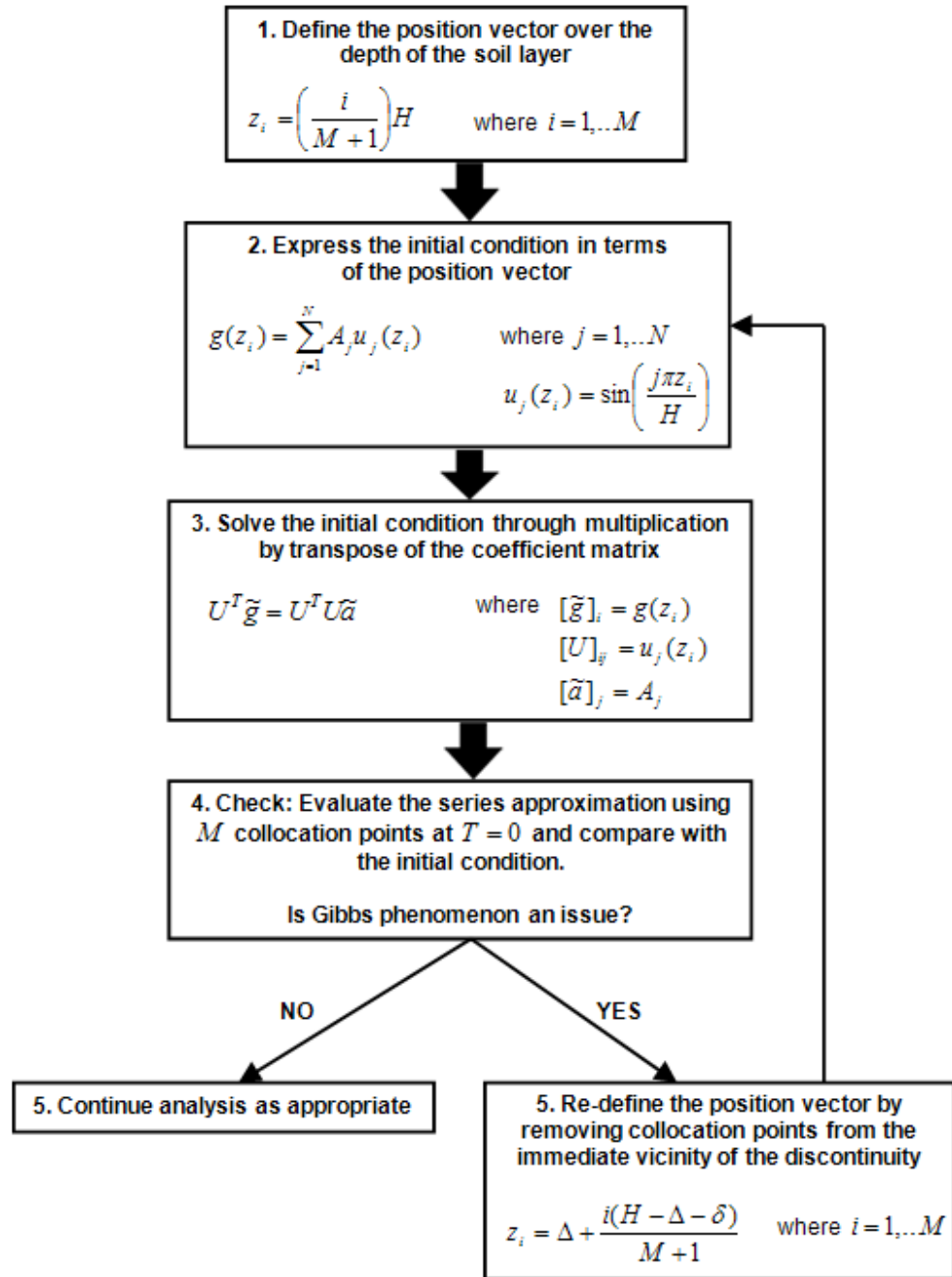


Figure 2.6 - MATLAB solution procedure

2.5 Summary

Using the solution process outlined in Figure 2.6, the consolidation behaviour in terms of both degree of consolidation isochrones and average degree of consolidation curves can be theoretically determined for a soil layer subjected to any number of non-uniform initial excess pore water pressure distributions. The results that were gathered after conducting these simulations are explained in further detail in Chapter 3.

Chapter 3: Quantifying consolidation behaviour

3.1 General

The consolidation behaviour of a soil stratum subjected to any u_i -distribution can be quantified using degree of consolidation (U_z), direct pore water pressure decay (P_z), or average degree of consolidation (U). Both U_z and P_z *locally* define the rate of consolidation (i.e. are dependent upon depth and time), which explains the inclusion of the subscript ‘ z ’. However, U is a *global* measure of the process (i.e. a function of time only) and can be shown to directly equal the percentage consolidation settlement.

3.2 Local measures of the rate of consolidation

The distribution of excess pore water pressure within a soil layer at any given time after consolidation has commenced can be represented by a line known as an isochrone. In one-dimensional consolidation, the excess pore water pressures vary with depth and time only – they do not vary over the cross-section of the loaded area. Each isochrone is essentially a graph of excess pore water pressure against depth at a fixed time. These isochrones are usually represented using normalised depth (z/H) and the dimensionless time factor (T) which can be described as follows:

$$T = \frac{c_v t}{H^2} \quad (3.1)$$

By providing a series of isochrones, the gradual decay of excess pore pressure and corresponding progression of degree of consolidation can be graphically depicted. As outlined in Section 2.3, the time factor values defined by Eq. (3.1) are dependent upon layer thickness and not drainage path length, which is contrary to traditional T notation. As a result, any references to T within this dissertation will be $\frac{1}{4}$ of the standard values of T , when dealing with a doubly drained layer.

3.2.1. Degree of consolidation isochrones

The degree of consolidation U_z is a measure of the degree to which consolidation has progressed at any depth within a consolidating soil stratum. The degree of consolidation can be expressed as

$$U_z = \frac{e_0 - e}{e_0 - e_p} \quad (3.2)$$

where e_0 = void ratio at the instant the external load is applied, and e_p = void ratio when the excess pore water pressure becomes zero. Since a linear relationship between void ratio and effective vertical stress is assumed (as per Assumption 7), the degree of consolidation defined by Eq. (3.2) is equal to the degree of excess pore water pressure dissipation. Thus,

$$U_z = \frac{u_i(z) - u(z,t)}{u_i(z)} \quad (3.3)$$

or

$$U_z = 1 - \frac{u(z,t)}{u_i(z)} \quad (3.4)$$

Values of U_z range from 0, indicating no consolidation has taken place, to 1 where the soil has completed consolidation under the applied load, which is technically only possible at $t = \infty$.

3.2.2. Excess pore water pressure isochrones

The isochrones produced by Eq. (3.4) do not adequately represent the pore pressure dissipation process when the initial excess pore pressure distribution is also a function of depth, as information is ‘lost’ during normalisation, where the denominator $u_i(z)$ varies with z . Thus, a supplementary expression is proposed in order to capture all information regarding excess pore pressure dissipation and consolidation progress:

$$P_z = \frac{u(z,t)}{u_{i,\max}} \quad (3.5)$$

Here, P_z = normalised excess pore pressure varying within the range of 0 to 1, and $u_{i,\max}$ = maximum value obtained from the initial excess pore pressure distribution due to the applied load.

Whilst the expressions in Eqs. (3.4) and (3.5) appear similar, it is important to note that the denominator in each has a significant influence upon the overall shape of isochrones when considering any non-uniform u_i -distribution. In Eq. (3.5), the denominator is essentially a constant, and the resulting isochrones directly depict the decay of excess pore water pressure. However, in Eq. (3.4) both the numerator and denominator are functions of depth, when considering non-uniform u_i -distributions. As a result, P_z and U_z isochrones can take quite different shapes.

3.2.3. Doubly drained soil layer

For a case of uniform initial excess pore water pressure, the excess pore water pressure (P_z) and degree of consolidation (U_z) isochrones depicting the progression of consolidation for $T = 0.025, 0.05, \dots, 0.25$ (i.e. time factor intervals of 0.025) are shown in Figure 3.1.

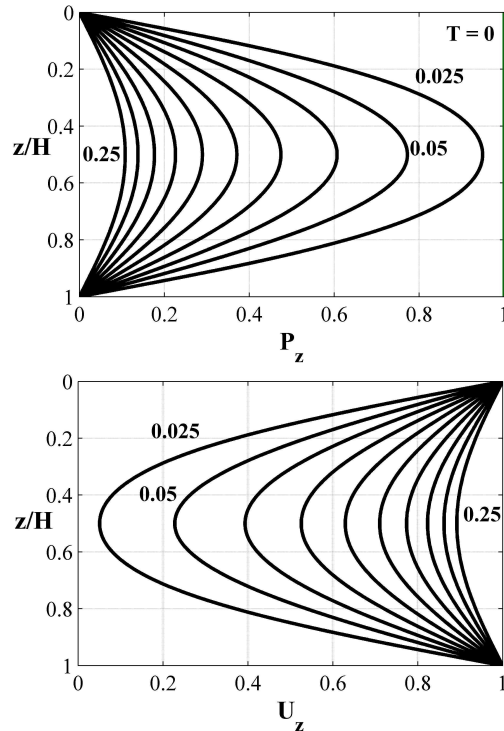


Figure 3.1 – Isochrones for a uniform u_i -distribution with two-way drainage

In this case, the degree of consolidation isochrones are simply a mirror image of the excess pore water pressure isochrones since the initial excess pore water pressure distribution is constant with depth. However, as shown in Figures 3.2 and 3.3, when the u_i -distribution is linear, the P_z -isochrones provide information regarding the skewed dissipation of excess pore pressure which is not clearly evident in the accompanying U_z -isochrones. In these figures, the u_i -distribution is indicated by the green line. Thus, in the case of non-uniform u_i -distributions, the term degree of consolidation is of little use. It simply states the percentage of initial pore pressure that has dissipated – a greater degree of consolidation does not always indicate higher pore water pressures. Therefore, it is more suitable to present U_z -isochrones in conjunction with P_z -isochrones for a comprehensive understanding of the pore pressure dissipation process.

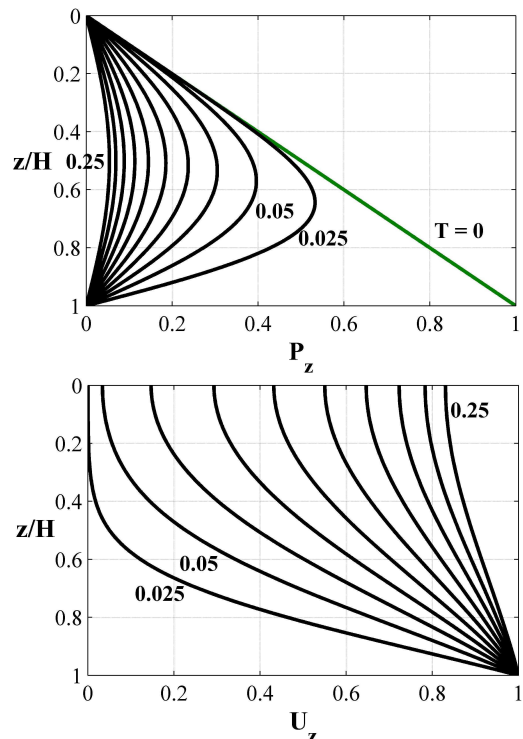


Figure 3.2 – Isochrones for a linearly increasing u_i -distribution with two-way drainage

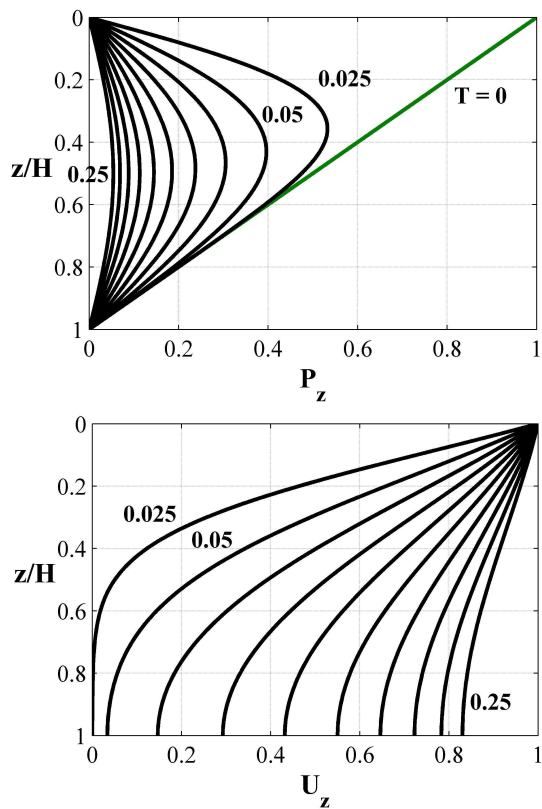


Figure 3.3 – Isochrones for a linearly decreasing u_i -distribution with two-way drainage

In reality, the consolidation behaviour of a soil layer will not always be analysed after immediate application of the design load. If analysis takes place after some unknown time has elapsed, the ‘new’ u_i -distribution will be sinusoidal (if the layer is doubly drained) and consolidation analysis would take place accordingly. Interestingly, the P_z -isochrones generated by a sinusoidal u_i -distribution are independent of depth, as shown in Figure 3.4. However, this is obvious upon re-examination of Eq. (3.4) – the sinusoidal component of the series solution in the numerator cancels with the sinusoidal component of the u_i -distribution, which is contained in the denominator. The remaining expression is a function of time only.

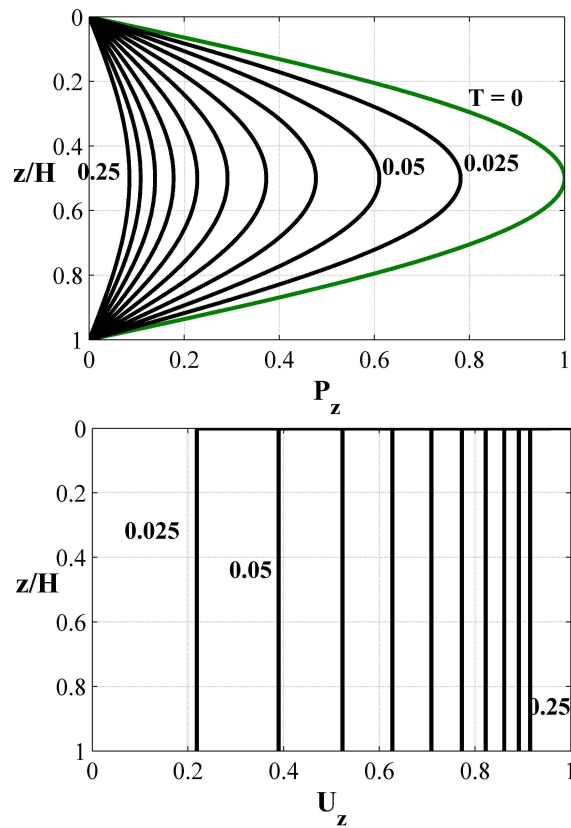


Figure 3.4 – Isochrones for a sinusoidal u_i -distribution with two-way drainage

The symmetrical triangular initial distribution highlighted in Figure 3.5 produces consolidation isochrones that indicate that consolidation proceeds fastest at the centre of the soil stratum. Although unclear near the top and bottom boundaries in Figure 3.5, the consolidation isochrones do comply with the initial boundary conditions that specify two drainage boundaries – each isochrone tends to 100% consolidation exactly at the top and bottom of the stratum. This immediate tendency toward 100% consolidation is observed in every case where the initial excess pore pressure is zero at a drainage boundary.

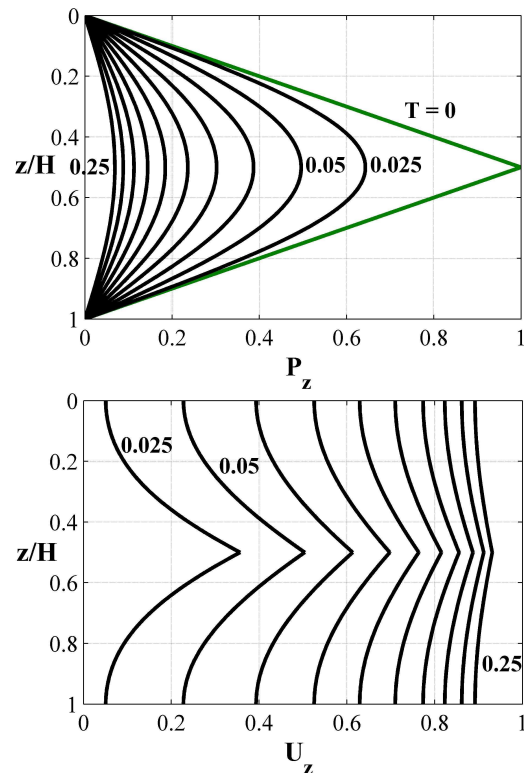


Figure 3.5 – Isochrones for a triangular u_i -distribution with two-way drainage

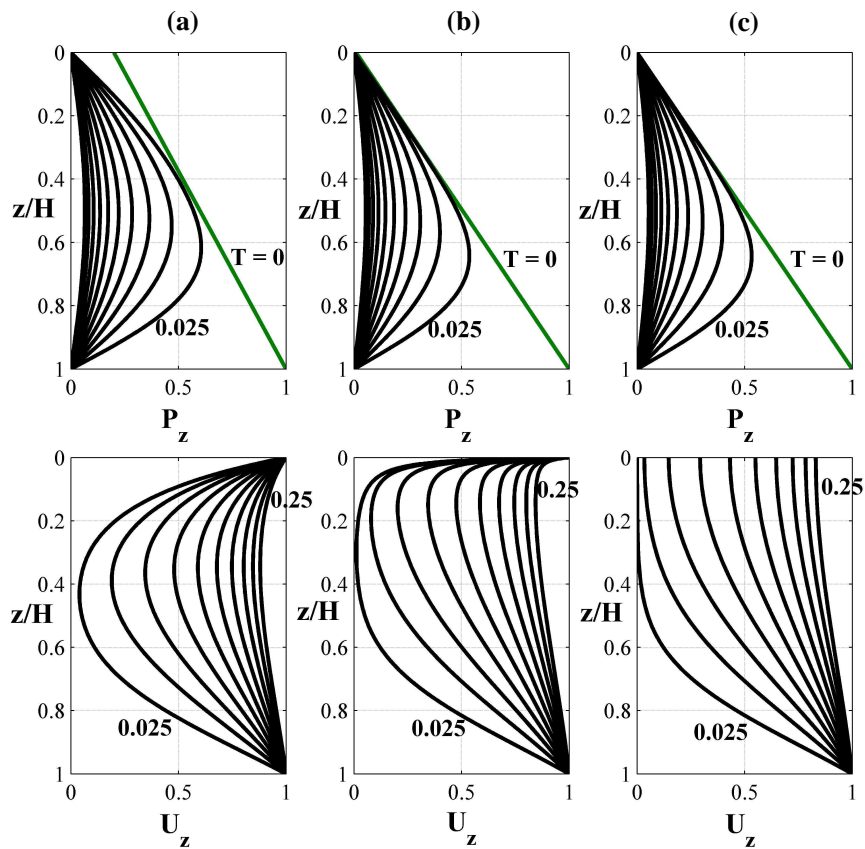


Figure 3.6 – Isochrones for linearly increasing u_i -distributions with two-way drainage, where the value at $z/H = 0$ varies from 0.2 to 0

This trend is further highlighted by results in Figure 3.6, where degree of consolidation isochrones are provided for three linearly increasing cases of initial excess pore water pressure. The linear distributions are adjusted to approach an origin boundary at the top of the soil stratum. Figure 3.6(a) shows a linearly increasing pore pressure distribution based on an initial normalised pore pressure value of 0.2 at $z/H = 0$, whilst Figure 3.6(b) demonstrates the skewed isochrones that result from a reduction in this value to 0.01. Based on Figure 3.6(b), it can be concluded that the isochrones in (c) each tend toward 100% consolidation exactly at the top stratum boundary.

The consolidation behaviour of soils is commonly analysed based upon symmetric initial excess pore pressure distributions, where the added advantage lies in the ability to analyse in terms of single or doubly drained strata, using the same graphs. However, the practical relevance of consolidation analysis in terms of asymmetrical excess pore pressure distributions must be considered.

The vertical stress increase beneath a loaded area generally peaks at some depth comparatively close to the soil surface, and subsequently decays with depth (Ranjan and Rao 1991). As a result, the excess pore pressure distribution with depth would resemble the shape shown in Case III, Table 2.3. This non-uniform u_i -distribution can be approximated using the following function, where the maximum initial pore water pressure of a unit value is forced to occur at the normalised depth of $z/H = 0.2$. The variation of u_i with depth is given by:

$$u_i(Z) = 10^{0.272b} Z^{0.25b} (1-Z)^b \quad (3.6)$$

where $Z = z/H$. The majority of excess pore water pressure is concentrated within a relatively narrow region from $z/H = 0.1$ to 0.4. The spread or skewness of this region is controlled by increasing/decreasing the variable b – a larger value of b will produce a more concentrated peak region in the u_i -distribution.

The pore pressure and degree of consolidation isochrones for a u_i -distribution where $b = 2$ are shown in Figure 3.7. Interestingly, a redistribution of excess pore pressure occurs toward the region of minimal initial excess pore pressure, which is a direct result of the concentrated nature of the initial excess pore pressures toward the surface drainage boundary. This phenomenon is briefly mentioned in Taylor (1962) for a decreasing linear u_i -distribution with an impermeable base layer – during the initial stages of consolidation, downward flow results in a transient increase in excess pore pressure near the impermeable base of the stratum. This increase was shown to gradually decay as the pore water eventually drains

through the top of the layer. However, the results in Figure 3.7 for bottom-skewed initial pore pressure distributions within a doubly drained layer demonstrate the prevalence of pore pressure redistribution for the majority of the consolidation process. This can introduce difficulties when it comes to analyzing the consolidation progress in terms of degree of consolidation.

As evidenced by Eq. (3.4), the degree of consolidation relationship is dependent upon a fundamental assumption that the initial excess pore pressure will always be greater than the corresponding pore pressure isochrones – a negative degree of consolidation is simply not feasible. As a result, the highlighted region shown in the $U_z - z/H$ plot in Figure 3.7 is not practically relevant, as negative values of degree of consolidation are present below $z/H \approx 0.6$. This is evident upon examination of the U_z -isochrone for $T = 0.025$ in Figure 3.7 which ‘becomes’ negative at values of $z/H > 0.6$. This highlighted area therefore directly indicates the region within the clay layer that undergoes pore pressure redistribution during consolidation.

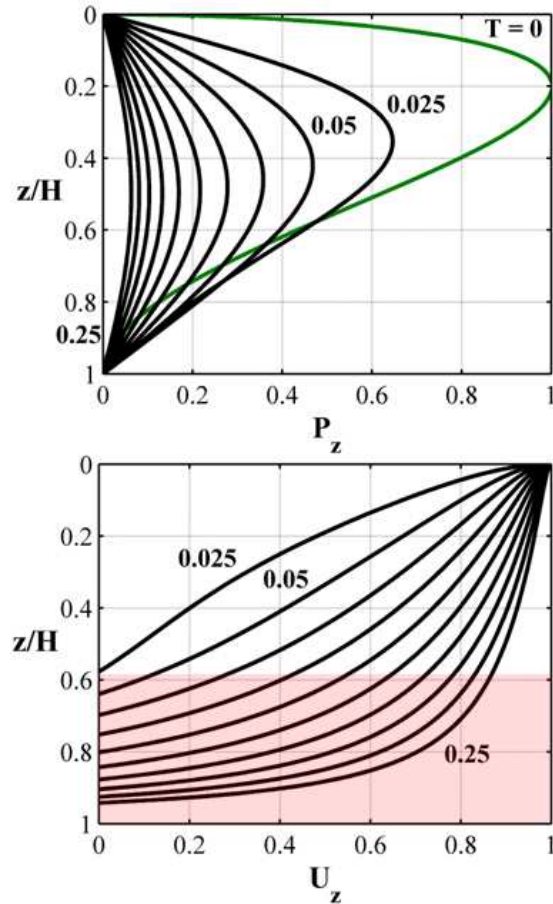


Figure 3.7 – Isochrones for an asymmetric u_i -distribution with two-way drainage, where $b = 2$

When the degree of spread is decreased (i.e. b is increased from 2 to 12), the phenomenon of pore pressure redistribution is observed at both the surface and base drainage boundaries, as shown in Figure 3.8. This greatly reduces the valid region of the $U_z - z/H$ plot, as highlighted.

It can thus be concluded that pore pressure redistribution is likely to occur in cases where the u_i -distribution contains a concentrated region of excess pore water pressure, with minimal pressures located elsewhere in the consolidating layer. Overall, the results indicate that the term degree of consolidation alone is inadequate in fully describing the consolidation process. Thus, for a complete description of consolidation behaviour, it is suggested that degree of consolidation isochrones be viewed in conjunction with pore pressure isochrones, both of which take quite different shapes.

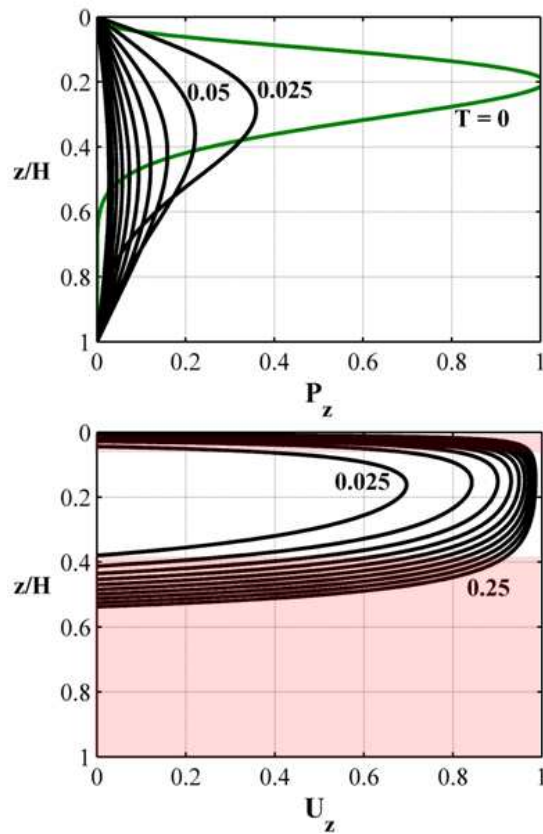


Figure 3.8 – Isochrones for an asymmetric u_i -distribution with two-way drainage, where $b = 12$

3.2.4. Singly drained soil layer

The u_i -distributions examined in Figures 3.1 to 3.4 were also studied for a singly drained soil layer, where the impermeable boundary was located at the base of the soil layer. For a

case of uniform initial excess pore water pressure, the excess pore water pressure (P_z) and degree of consolidation (U_z) isochrones depicting the progression of consolidation for $T = 0.1, 0.2, \dots, 1.0$ (i.e. at time factor intervals of 0.1) are shown in Figure 3.9. Again, the degree of consolidation isochrones are simply a mirror image of the excess pore water pressure isochrones since the initial excess pore water pressure distribution is constant with depth.

As with the doubly drained studies, little research has been conducted on the effect of non-uniform u_i -distributions on the consolidation behaviour of a singly drained soil layer. Singh and Swamee (2008) analysed linearly increasing and decreasing u_i -distributions to develop approximate simple invertible equations for consolidation curves in singly drained cases. Janbu et al. (1956) also analysed the average degree of consolidation of a consolidating soil layer with a freely drained upper surface and impermeable base, for linearly increasing and decreasing u_i -distributions.

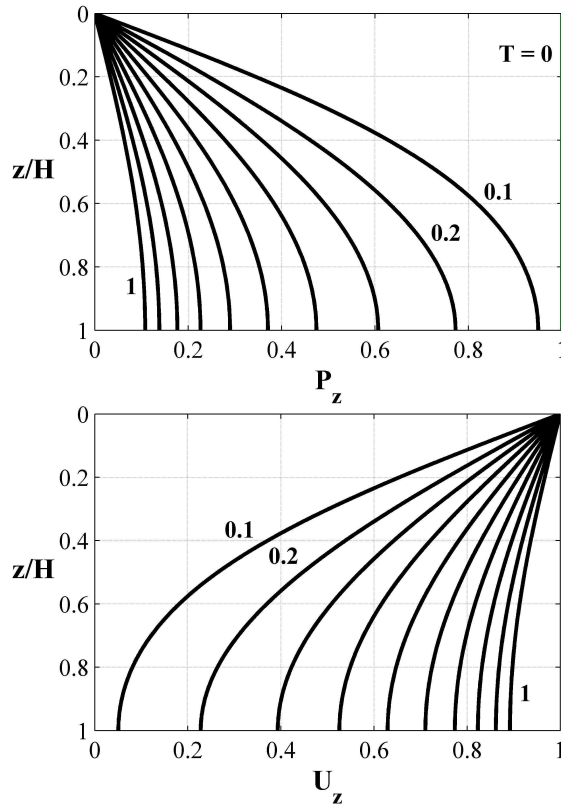


Figure 3.9 – Isochrones for a uniform u_i -distribution with one-way drainage

For a soil layer subjected to a linearly increasing u_i -distribution, the expected decay of excess pore water pressure and corresponding degree of consolidation is shown in Figure

3.10. No pore pressure redistribution is expected to take place during consolidation for this case, as the maximum initial excess pore pressure is greatest at the impermeable boundary.

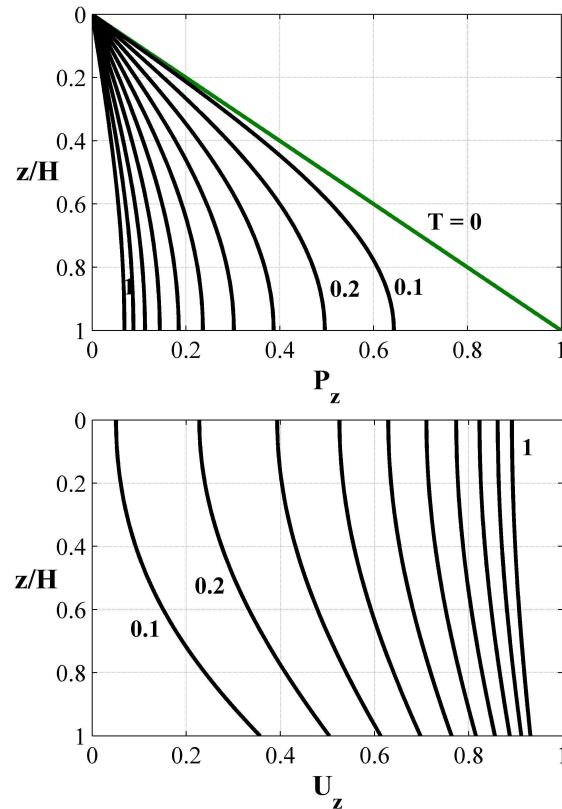


Figure 3.10 – Isochrones for a linearly u_i -distribution with one-way drainage

However, when a linearly *decreasing* u_i -distribution is instead analysed, where minimal initial pressures are located at the impermeable boundary, pore pressure redistribution occurs, which is evident in Figure 3.11. Additional isochrones have been included (highlighted in blue) for time factors of 0.02 and 0.06, since the initial stages of consolidation are critical when considering excess pore pressure redistribution. Again, due to this redistribution of pore pressure, it is only meaningful to view the upper half of the soil layer in terms of degree of consolidation.

Similarly, for a sinusoidal u_i -distribution, where minimal excess pore pressures exist near the impermeable boundary, pore pressure redistribution again occurs as demonstrated in Figure 3.12. However, in comparison with the linearly increasing u_i -distribution, a larger portion of the soil layer (approximately 80%) can be viewed in terms of degree of consolidation isochrones when the u_i -distribution is sinusoidal.

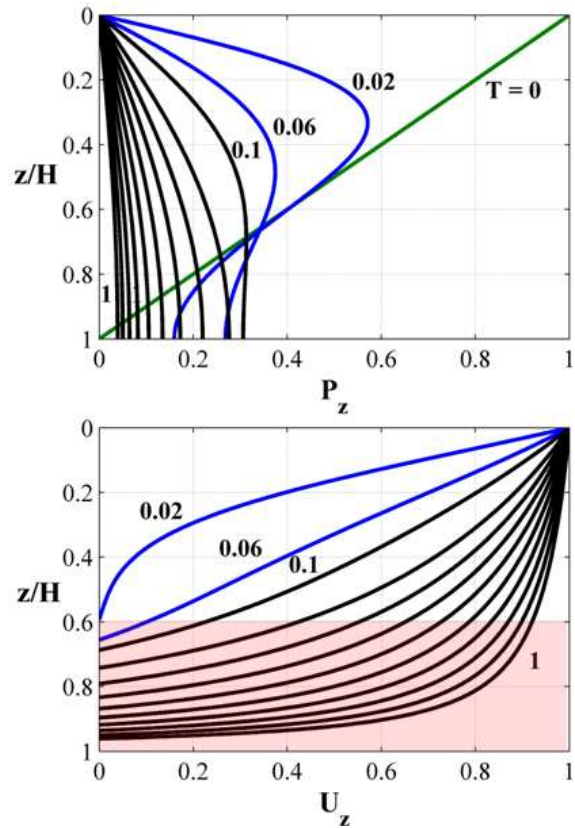


Figure 3.11 – Isochrones for a linearly decreasing u_i -distribution with one-way drainage

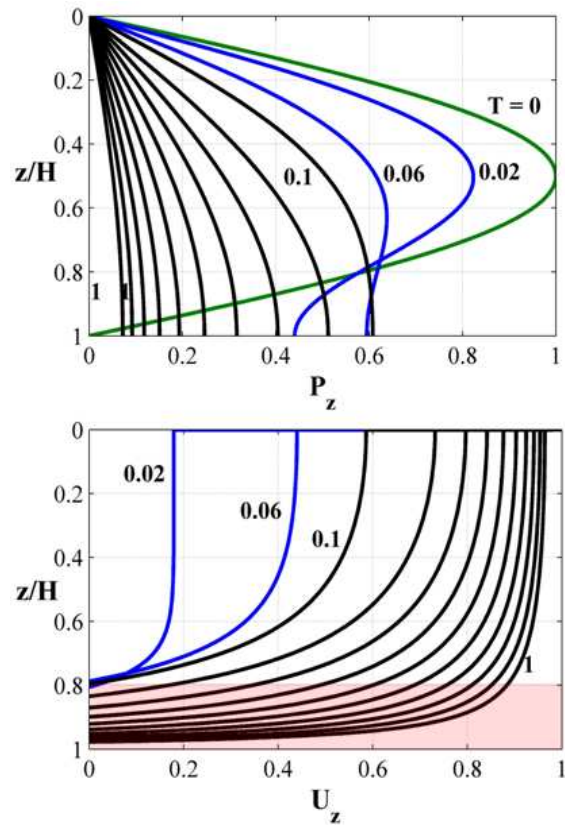


Figure 3.12 – Isochrones for a sinusoidal u_i -distribution with one-way drainage

Although the consolidation behaviour of a doubly drained layer subjected to asymmetric u_i -distributions has been analysed, it is important to assess the effect of introducing an impermeable boundary to the system. Since the following distributions contain regions of concentrated initial excess pore pressure, coupled with the introduced impermeable boundary, pore pressure redistribution can be expected to take place. The following equations have been used to describe the u_i -distributions in which the maximum initial excess pore water pressure was forced to occur near the top ($Z = 0.2$ – Case I), middle ($Z = 0.5$ – Case II), and bottom ($Z = 0.8$ – Case III) of the soil layer:

$$\text{Case I: } u_i(Z) = 10^{0.272b} Z^{0.25b} (1-Z)^b \quad (3.7)$$

$$\text{Case II: } u_i(Z) = 10^{0.602} Z^b (1-Z)^b \quad (3.8)$$

$$\text{Case III: } u_i(Z) = 10^{0.272b} Z^b (1-Z)^{0.25b} \quad (3.9)$$

The maximum initial excess pore pressure was held constant for all cases, so that $P_{Z,\max} = 1$. Furthermore, in each case, the point at which the maximum excess pore pressure occurred remained constant, so that the effect of varying the degree of spread (controlled by b) could be investigated.

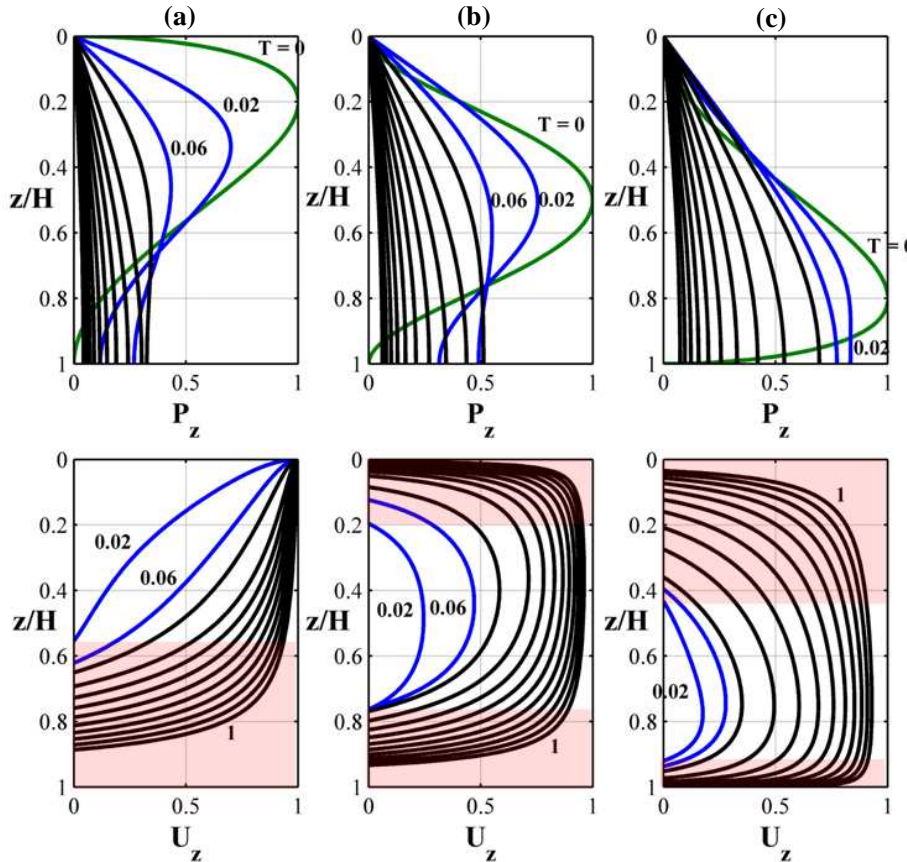


Figure 3.13 – Isochrones for skewed u_i -distributions with one-way drainage, where the maximum initial pressure occurs at (a) $Z = 0.2$, (b) $Z = 0.5$ and (c) $Z = 0.8$ for a spread of $b = 2$

For a large spread ($b = 2$), the isochronal decay of excess pore water pressure is shown in Figure 3.13, when the maximum initial value of pore water pressure is located at different points within the soil layer. The effect of reducing the spread (i.e. increasing b) is shown in Figure 3.14. It is clearly evident that pore pressure redistribution is more prevalent in cases where there is a more concentrated region of initial excess pore water pressure.

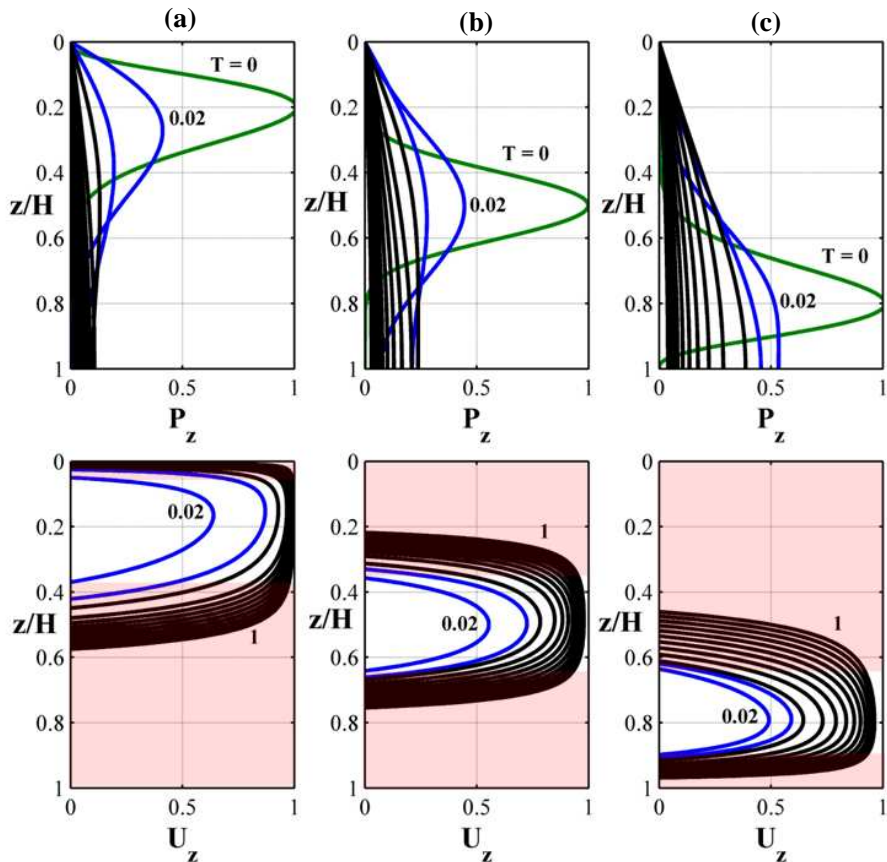


Figure 3.14 – Isochrones for skewed u_i -distributions with one-way drainage, where the maximum initial pressure occurs at (a) $Z = 0.2$, (b) $Z = 0.5$ and (c) $Z = 0.8$ for a spread of $b = 12$

3.3 Average degree of consolidation

The consolidation behaviour of a soil layer can also be analysed in terms of a global measurement of consolidation behaviour known as average degree of consolidation. The variation in average degree of consolidation with time is the focal point from which most consolidation properties are deduced.

3.3.1. Derivation

The average consolidation U represents the consolidation of the stratum as a whole and is given by the ratio between the consolidation settlement at time t and the value attained at the end of the consolidation process (s_c):

$$U = \frac{s(t)}{s_c} \quad (3.10)$$

Terzaghi's settlement expression is reliant upon the fundamental assumption that the average degree of consolidation, expressed in terms of settlements, is equal to the average degree of consolidation in terms of excess pore pressures. This assumption stems from the linear void ratio-vertical effective stress relationship outlined in Assumption 7. A minor elaboration of this assumption in terms of average degree of consolidation is provided in Terzaghi's *Theoretical Soil Mechanics* (1943), and the majority of geotechnical textbooks subsequently published simply accept that the average degree of excess pore pressure dissipation is equal to the degree of settlement (Taylor 1962, Lambe and Whitman 1969, Holtz and Kovacs 1981, Whitlow 1983, Powrie 1997, Lancellotta 2009, Sivakugan and Das 2009).

Therefore, it appears prudent to re-evaluate Terzaghi's original assumption that the average degree of pore pressure dissipation is equivalent to the percentage consolidation settlement for all distributions of initial excess pore water pressure. This can be done by calculating the consolidation settlement based on the volume of water exiting the drainage boundaries of the clay layer and comparing this with the expression proposed by Terzaghi:

$$U = \frac{s(t)}{s_c} = \frac{\int_0^H (u_i - u(t)) dz}{\int_0^H u_i dz} \quad (3.11)$$

Traditional method

According to traditional consolidation theory, the final or ultimate settlement (s_c) due to a change in effective stress ($\Delta\sigma'_v$) is given by:

$$s_c = m_v H_0 \Delta\sigma'_v \quad (3.12)$$

where H_0 = initial thickness of the clay stratum, and m_v = coefficient of volume compressibility, which describes the volumetric strain per unit stress increase. Consider a doubly drained layer as shown in Figure 3.15(a). Assuming that the u_i -distribution is shown by the continuous line in Figure 3.15(b), the settlement due to the dissipation of the entire excess pore pressure over an infinitesimal thickness (dz) is given by:

$$ds_c = m_v [u_i(z)] dz \quad (3.13)$$

Therefore, the final consolidation settlement due to the dissipation of the excess pore pressure within the entire layer of thickness H is;

$$s_c = m_v \int_{z=0}^H u_i(z) dz \quad (3.14)$$

where the integral component is the area bounded by the initial excess pore pressure distribution in Figure 3.15(b). After some time t has occurred, the initial excess pore pressure will have partially dissipated, and the resulting distribution can be described by $u(z,t)$.

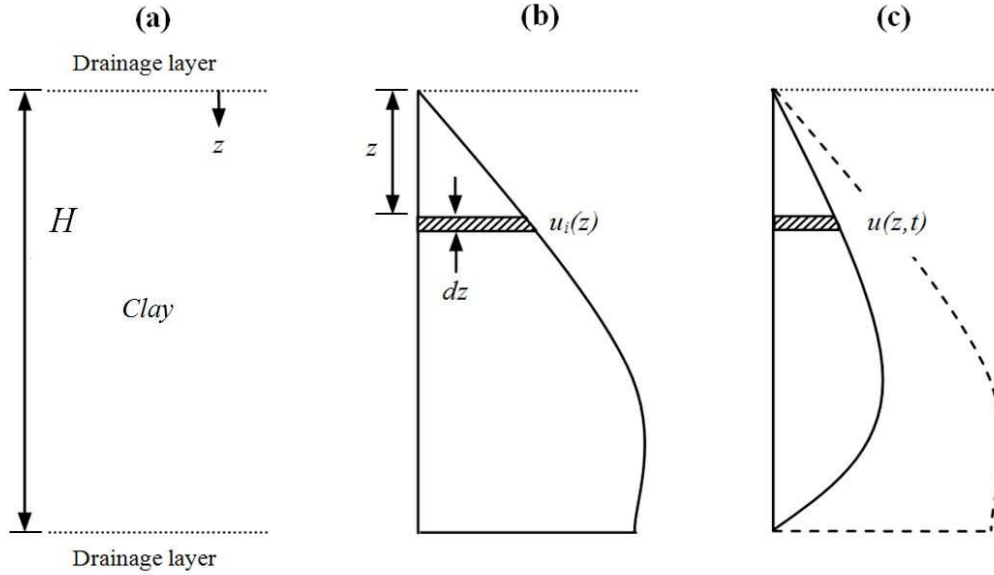


Figure 3.15 – Traditional settlement method: (a) doubly drained layer, (b) u_i -distribution, and (c) pore pressure dissipation

Therefore, the settlement that has taken place is simply the total settlement calculated using Eq. (3.14) minus the consolidation settlement that would occur due to the excess pore pressure distribution $u(z,t)$. Thus, the expression for settlement at some time t during consolidation can be written as follows (see Figure 3.15(c)):

$$s(t) = m_v \left[\int_{z=0}^H u_i(z) dz - \int_{z=0}^H u(z,t) dz \right] \quad (3.15)$$

For a given initial excess pore pressure distribution due to an applied load, Terzaghi's expression for the average degree of consolidation (U) in terms of consolidation settlement is subsequently represented by:

$$U = \frac{s(t)}{s_c} = \frac{m_v \left[\int_{z=0}^H u_i(z) dz - \int_{z=0}^H u(z,t) dz \right]}{m_v \int_{z=0}^H u_i(z) dz} = 1 - \frac{\int_{z=0}^H u(z,t) dz}{\int_{z=0}^H u_i(z) dz} \quad (3.16)$$

which is identical to Eq. (3.11). This is the expression traditionally used in geotechnical textbooks for deriving the equation for average degree of consolidation. The above derivation is valid for any initial excess pore water pressure distribution.

Discharge method

As defined in Chapter 2, the differential equation governing one-dimensional consolidation and the dissipation of excess pore water pressures is:

$$c_v \frac{\partial^2 u}{\partial z^2} = \frac{\partial u}{\partial t} \quad (3.17)$$

where c_v = coefficient of consolidation, u = excess pore water pressure, z = distance measured downward from the surface of the consolidating clay layer and t = time.

The cumulative discharge of water squeezed out of the doubly drained soil profile at any time during consolidation is the sum of the mass flux per unit area (q) at the top drainage boundary ($z = 0$), and the mass flux per unit area at the bottom drainage boundary ($z = H$) at some time t . Since Terzaghi's theory is one-dimensional, the discharge velocity can be represented as:

$$\mathbf{v} = -k_v \frac{\partial u}{\partial z} \hat{\mathbf{k}} \quad (3.18)$$

where $\hat{\mathbf{k}}$ is a unit vector pointing vertically downwards, k_v = permeability of the clay stratum and $\partial u / \partial z$ is simply the hydraulic gradient.

Thus, the mass flux per unit area at any point z at time t is given by:

$$q(z, t) = \mathbf{v} \cdot \hat{\mathbf{m}} \quad (3.19)$$

where $\hat{\mathbf{m}}$ is the unit normal in the direction of flow.

Hence, the cumulative discharge Q_t out of the soil profile at any time t is obtained by adding the two components at the top and bottom drainage boundaries as:

$$Q_t(t) = \int_{t=0}^t q(0, t) dt + \int_{t=0}^t q(H, t) dt \quad (3.20)$$

Since the normal vectors at $z = 0$ and $z = H$ are $-\hat{\mathbf{k}}$ and $\hat{\mathbf{k}}$ respectively, this becomes:

$$Q_t(t) = k_v \left[\int_{t=0}^t \left. \frac{\partial u}{\partial z} \right|_{z=0} dt - \int_{t=0}^t \left. \frac{\partial u}{\partial z} \right|_{z=H} dt \right] \quad (3.21)$$

To determine the total discharge out of the soil, the mass flux per unit area in Eq. (3.21) is simply evaluated at $t = \infty$ for the top and bottom boundaries.

$$Q_\infty = k_v \left[\int_{t=0}^{\infty} \frac{\partial u}{\partial z} \Big|_{z=0} dt - \int_{t=0}^{\infty} \frac{\partial u}{\partial z} \Big|_{z=H} dt \right] \quad (3.22)$$

Therefore, the normalised cumulative discharge U_Q through the soil at any time t , expressed as the fraction of the cumulative discharge at $t = \infty$ is a form of degree of consolidation that is given by:

$$U_Q = \frac{\int_{t=0}^t \frac{\partial u}{\partial z} \Big|_{z=0} dt - \int_{t=0}^t \frac{\partial u}{\partial z} \Big|_{z=H} dt}{\int_{t=0}^{\infty} \frac{\partial u}{\partial z} \Big|_{z=0} dt - \int_{t=0}^{\infty} \frac{\partial u}{\partial z} \Big|_{z=H} dt} \quad (3.23)$$

Upon re-examination of the original governing one-dimensional consolidation equation in Eq. (3.17), it is possible to definitively prove that the traditional and exact consolidation expressions are identical.

Eq. (3.23) can be rewritten as:

$$U_Q = \frac{- \int_{t=0}^t \frac{\partial u}{\partial z} \Big|_{z=0}^{z=H} dt}{- \int_{t=0}^{\infty} \frac{\partial u}{\partial z} \Big|_{z=0}^{z=H} dt} \quad (3.24)$$

After cancelling the negative signs and noting that

$$\frac{\partial u}{\partial z} \Big|_{z=0}^{z=H} = \int_{z=0}^H \frac{\partial^2 u}{\partial z^2} dz \quad (3.25)$$

Eq. (3.24) becomes

$$U_Q = \frac{\int_{z=0}^H \int_{t=0}^t \frac{\partial^2 u}{\partial z^2} dt dz}{\int_{z=0}^H \int_{t=0}^{\infty} \frac{\partial^2 u}{\partial z^2} dt dz} \quad (3.26)$$

where the order of integration in the numerator and the denominator were changed so that the integral with respect to depth is on the outside.

Upon consideration of the governing partial differential equation in Eq. (3.17), the time derivative can be substituted for the spatial derivative in Eq. (3.26) to give:

$$U_Q = \frac{\int_{z=0}^H \int_{t=0}^t \frac{\partial u}{\partial t} dt dz}{\int_{z=0}^H \int_{t=0}^{\infty} \frac{\partial u}{\partial t} dt dz} = \frac{\int_{z=0}^H u(z, t) \Big|_{t=0}^t dz}{\int_{z=0}^H u(z, t) \Big|_{t=0}^{\infty} dz} = \frac{\int_{z=0}^H u(z, t) dz - \int_{z=0}^H u(z, 0) dz}{\int_{z=0}^H u(z, \infty) dz - \int_{z=0}^H u(z, 0) dz} \quad (3.27)$$

As $t = \infty$, the excess pore water pressure approaches 0 (i.e. $u(z, \infty) = 0$). Also, the excess pore water pressure evaluated at time $t = 0$ is simply the initial excess pore water pressure u_i (i.e. $u(z, 0) = u_i$). Thus, Eq. (3.27) can be reduced to:

$$U_Q = 1 - \frac{\int_{z=0}^H u(z, t) dz}{\int_{z=0}^H u_i(z) dz} \quad (3.28)$$

This is identical to Terzaghi's expression for average degree of consolidation in Eq. (3.16).

3.3.2. Time factor review

For a case of uniform initial excess pore water pressure, the excess pore water pressure isochrones depicting the progression of consolidation during time for $T = 0.1, 0.2, \dots, 1.0$ are shown in Figure 3.16, where the soil layer is either doubly or singly drained.

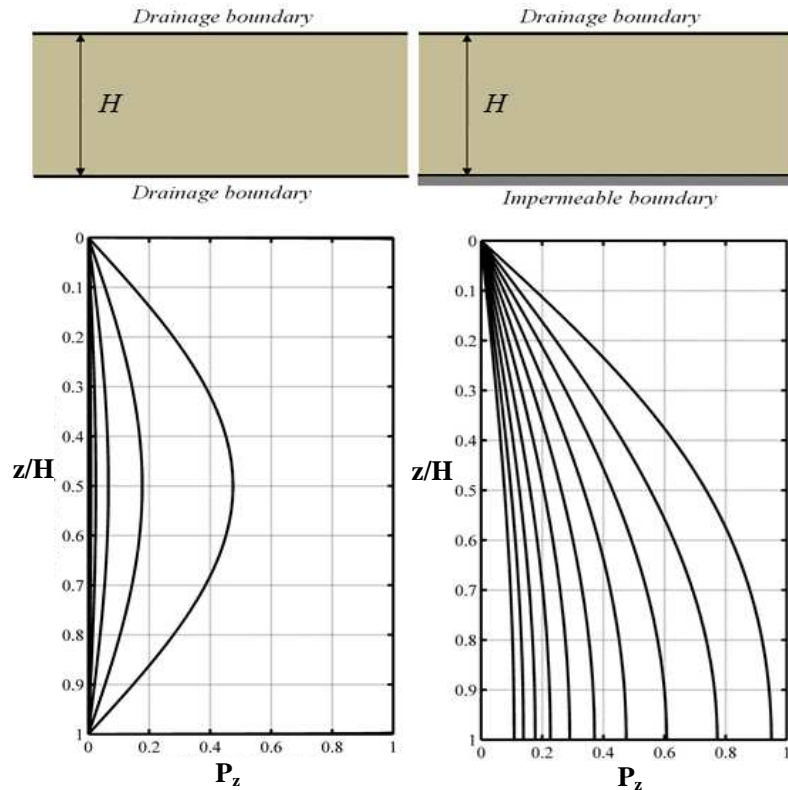


Figure 3.16 - Excess pore water pressure isochrones for a uniform u_i -distribution

As anticipated, the excess pore water pressure decays much more rapidly when the pore water is allowed to exit through two drainage boundaries. This decay can be viewed in terms of the overall settlement using the expression for average degree of consolidation as shown in Figure 3.17, where there is a separate curve for each drainage case.

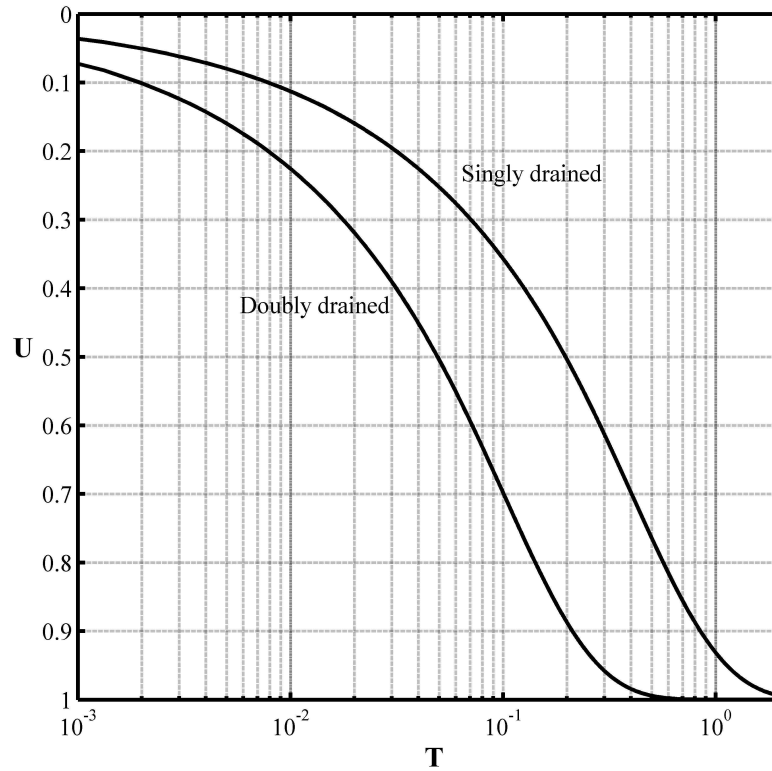


Figure 3.17 – Average degree of consolidation curves for singly and doubly drained layers

The beauty of the series solution which describes the decay of excess pore water within a layer subjected to a uniform distribution is that the percentage consolidation behaviour for each drainage case is identical when adjusted by a constant factor of time – the singly drained case merely achieves the same settlement four times slower than its doubly drained counterpart. Since the development of Terzaghi's consolidation equation, many geotechnical researchers have taken advantage of this relationship by introducing a variable referred to as maximum drainage path length (H_{dr}) so that the solution for both singly and doubly drained layers can be represented by a single average degree of consolidation curve which is based on the following series solution:

$$u = \sum_{n=1}^{\infty} \left[\frac{4\Delta\sigma_v}{(2n-1)\pi} \sin\left(\frac{(2n-1)n\pi z}{2H}\right) \right] \exp\left(-\frac{(2n-1)^2 \pi^2 T_c}{4}\right) \quad (3.29)$$

The series solution in Eq. (3.29) is the solution derived for the singly drained case in Chapter 2, where the conventional time factor is calculated using the drainage path length, rather than layer thickness:

$$T_c = \frac{c_v t}{H_{dr}^2} \quad (3.30)$$

Then, a thickness of $2H$ is considered for a doubly drained layer, and H is considered for a singly drained layer so that $H_{dr} = H$ for both drainage cases, since the maximum distance a water molecule must travel in the doubly drained case is half the total thickness.

When considering the $U_z - Z - T$ plot (degree of consolidation isochrones), the entire thickness from $z = 0$ to $2H$ is displayed – for a doubly drained case, the isochrones from 0 to $2H$ are applicable, but for a singly drained layer, the isochrones are only relevant from 0 to H , as shown in Figure 3.18.

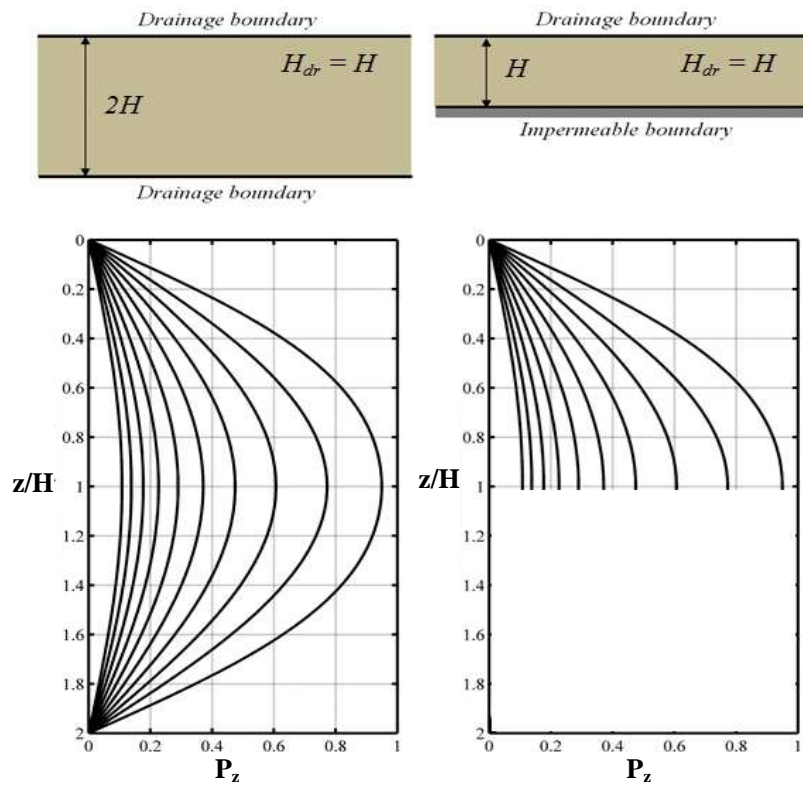


Figure 3.18 – Excess pore water pressure isochrones for a uniform u_i -distribution using the traditional expression for time factor (in terms of drainage path length)

The expression for the average degree of consolidation shown in Eq. (3.11) is evaluated the same way using the series solution in Eq. (3.29) – the limits are restricted to the domains that correspond to single or double drainage conditions. This results in the following standard average degree of consolidation plot (Figure 3.19), which is available in many geotechnical

textbooks. Since the drainage conditions are addressed within the time factor, only one curve exists for both drainage cases.

However, there is an inherent disadvantage associated with this scaling method – the variation in rates of consolidation for singly or doubly drained clay strata cannot be truly compared using Figure 3.19. This is because the traditional expression for time factor is technically in terms of two variables; time and number of drainage boundaries. As a result, all analyses within this thesis were conducted using a time factor that is in terms of layer thickness, and not drainage path length. This would slightly change the method in which the percentage consolidation of a layer is calculated, which can be illustrated using the following simple example.

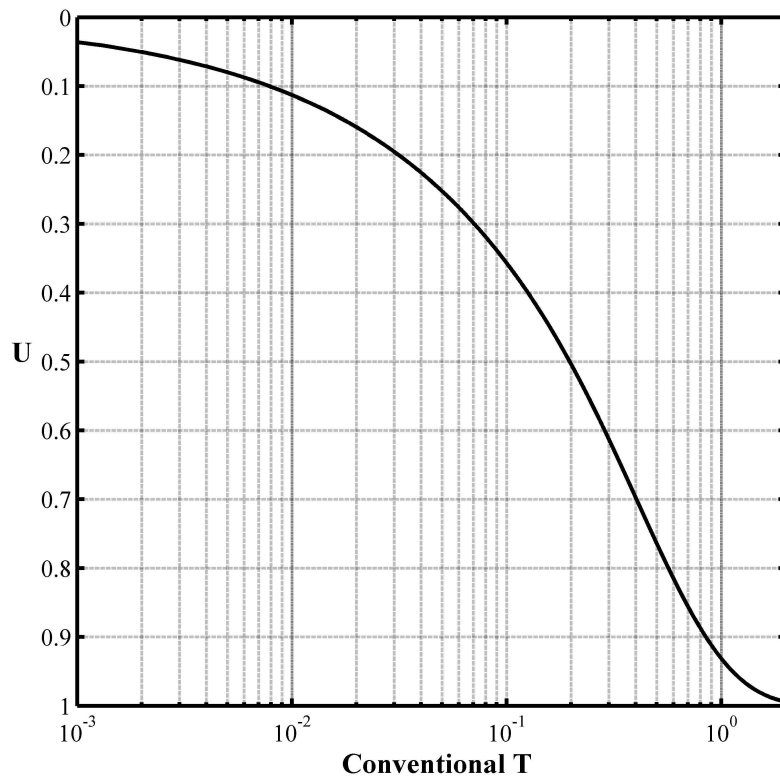


Figure 3.19 – Average degree of consolidation curves for singly and doubly drained layers in terms of the traditional time factor

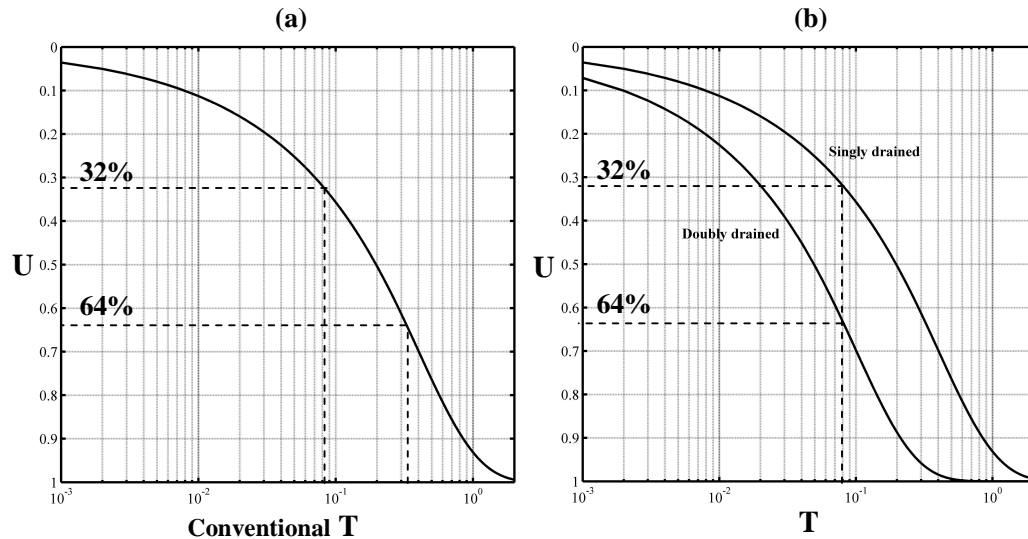
Consider the following problem:

A 15 m-thick deposit of Holocene clay exists underneath dredged clay at the Port of Brisbane. In some areas, this deposit is underlain by a layer of sand, whilst in other areas it is underlain by stiff, relatively impermeable clay. Assuming a coefficient of consolidation of 0.3 m²/year throughout, the Port wishes to know how the differences in drainage conditions will affect the percentage consolidation settlement that will occur after 10 years.

Table 3.1 - Example of traditional consolidation analysis

Drainage Configuration	Traditional method	Proposed method
Doubly drained	$H_{dr} = L/2 = 3 \text{ m}$ $T_c = \frac{c_v t}{H_{dr}^2} = \frac{(0.3)(10)}{3^2} = 0.333$	$H = 6 \text{ m}$ $T = \frac{c_v t}{H^2} = \frac{(0.3)(10)}{6^2} = 0.083$
Singly drained	$H_{dr} = L = 6 \text{ m}$ $T_c = \frac{c_v t}{H_{dr}^2} = \frac{(0.3)(10)}{6^2} = 0.083$	

Then, using the time factors calculated in Table 3.1, the percentage consolidation for each drainage case can be calculated as follows.

**Figure 3.20** – Comparing settlements for different drainage configurations using (a) traditional method, and (b) proposed method

As shown in Figure 3.20(a), it is difficult to compare the average degree of consolidation using traditional scaling methods. Furthermore, this scaling method is only applicable in cases where the initial distribution is symmetric about the middle of the clay layer (i.e. symmetric about $z = H$ if the layer is of thickness $2H$). That is, Eq. (3.29) can only be used to assess the consolidation behaviour of a singly drained layer of thickness H , if the mirror image of the u_i -distribution is reflected about the horizontal line at $z = H$ and isochrones are observed from 0 to H only. Here, every second series coefficient becomes 0 due to the initial symmetry of the excess pore pressure distribution. When considering a singly drained soil layer, users are simply advised to look only at the region 0 to H . It is

important to recognise that this technique is only applicable in situations where the u_i -distribution is symmetrically reflected about $z = H$.

For instance, if the consolidation behaviour of a singly drained layer subjected to a sinusoidal u_i -distribution using this reflection method was required, the sinusoidal function would need to be reflected about the midline ($z = H$), as shown in Figure 3.21(b) which provides U_z -isochrones and P_z -isochrones using this reflection technique, in comparison with those determined using the singly drained solution outlined previously. The isochrones in Figure 3.21(a) are identical to those in Figure 3.21(b) within the region 0 to H .

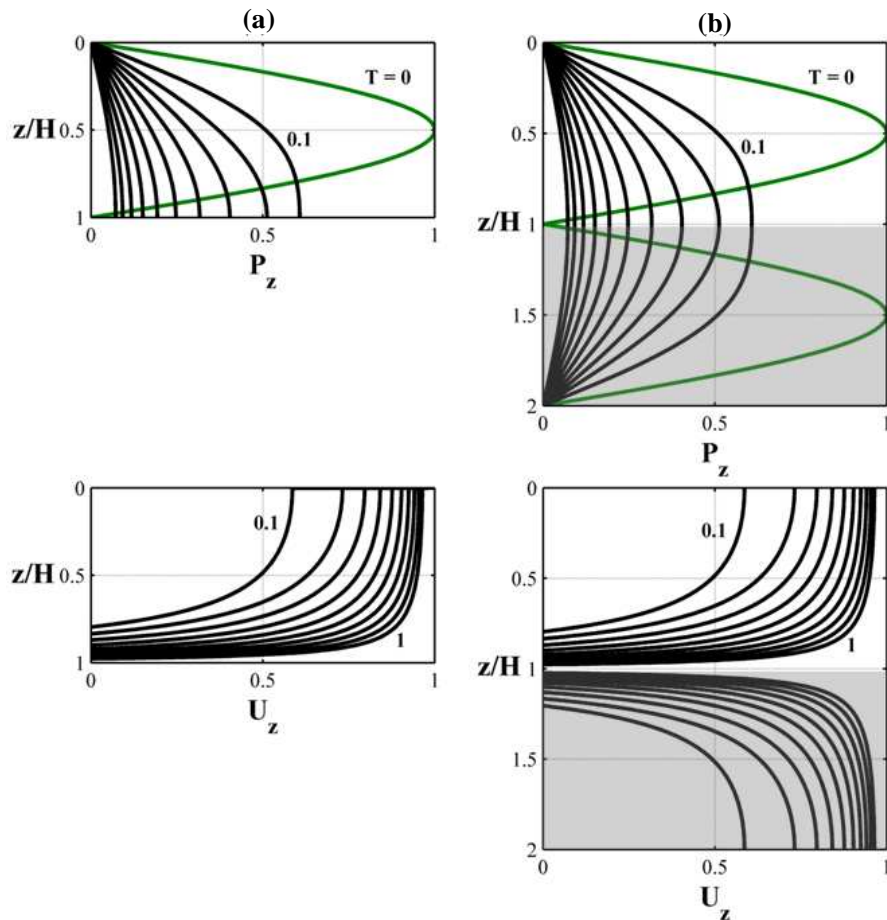


Figure 3.21 – U_z and P_z isochrones for a singly drained layer subjected to a sinusoidal u_i -distribution determined using (a) singly drained solution, and (b) reflection method

3.3.3. Percentage consolidation of non-uniform u_i -distributions

New $U - T$ curves can now be generated to compare singly and doubly drained settlements of a layer of thickness H subjected to various uniform and non-uniform u_i -distributions, where the effect of drainage conditions can be observed over a continuous period of

consolidation, as shown in Figures 3.22 to 3.24. If a user were to assess the effects of one- or two-way drainage for a designated stratum thickness using a time factor in terms of layer thickness, T is the same for both drainage configurations, and the overall differences in trends can be directly compared. That is, the differences in average degree of consolidation as a result of doubly or singly drained conditions can be visually observed over the entire period of consolidation since two $U - T$ curves are now available.

Using the conventional solitary $U - T$ curve, no *graphical* comparison can be made and the effect of one or two drainage boundaries on the consolidation settlement can only be determined for individual values of t . In this case, two different time factors would be required for each drainage case – these values would then be applied to the single $U - T$ curve to identify the corresponding U values for comparison. If the differences in settlement were required for the entire period of consolidation, this procedure would become quite time-consuming as two different time factor values would be required for each different value of t to determine the corresponding average degree of consolidation for an overall comparison.

The merits of axis scaling in $U - T$ curves are dependent upon the region of time over which the user wishes to analyse the average degree of consolidation. For example, if the consolidation settlement during the initial stages of construction is required, a $\log U - \log T$ or $U - \log T$ curve is often useful to amplify the early stages of consolidation. Many geotechnical textbooks have presented $U - T$ curves (using Terzaghi's time factor) with either no scaling (Taylor 1948, Scott 1963, Sowers 1979, Das 2009, Sivakugan and Das 2010, Coduto et al. 2011), a logarithmic scaling of only the T axis (Jumikis 1962, Leonards 1962, Berry and Reid 1987, Lancellotta 2009), or have presented $U - T$ curves in both forms (Terzaghi 1943, Terzaghi et al. 1996). $U - T$ curves for both singly and doubly drained strata subjected to key non-uniform u_i -distributions are shown in Figures 3.22 to 3.24.

Although the consolidation process theoretically ends when $t \rightarrow \infty$, in practice the process is often considered finished when $T \geq 2$ (Lancellotta 2009), which corresponds to 99.42% of the final consolidation settlement. This applies to both singly and doubly drained systems since T is dependent upon the maximum length of drainage path, and identical values of T would correspond to different original stratum thicknesses. However, by observing the average consolidation in terms of T , it is possible to specify this end-point for a clay stratum of constant thickness with either drainage configuration. As shown in Figs 3.22 to 3.24, the

process of consolidation can be considered finished when $T \geq 0.5$ for two-way drainage, in comparison with $T = 2$ for one-way drainage.

During the early stages of consolidation, when $T < 0.1$, having one or both of the axes in logarithmic scale enables a more precise definition of the values of T and U . For example, in Figure 3.22, all six cases appear to fall into two closely spaced single curves when the clay is doubly drained. These trends can be viewed more precisely using Figures 3.23 and 3.24. Similarly, for singly drained situations also, u_i -distributions (d) and (f) appear to be the same in Figure 3.22; the differences become more clear in Figs 3.23 and 3.24. During the later stages, when $T > 0.1$, having both T and U in arithmetic scale (see Figure 3.22) enables a more precise evaluation of the U and T values.

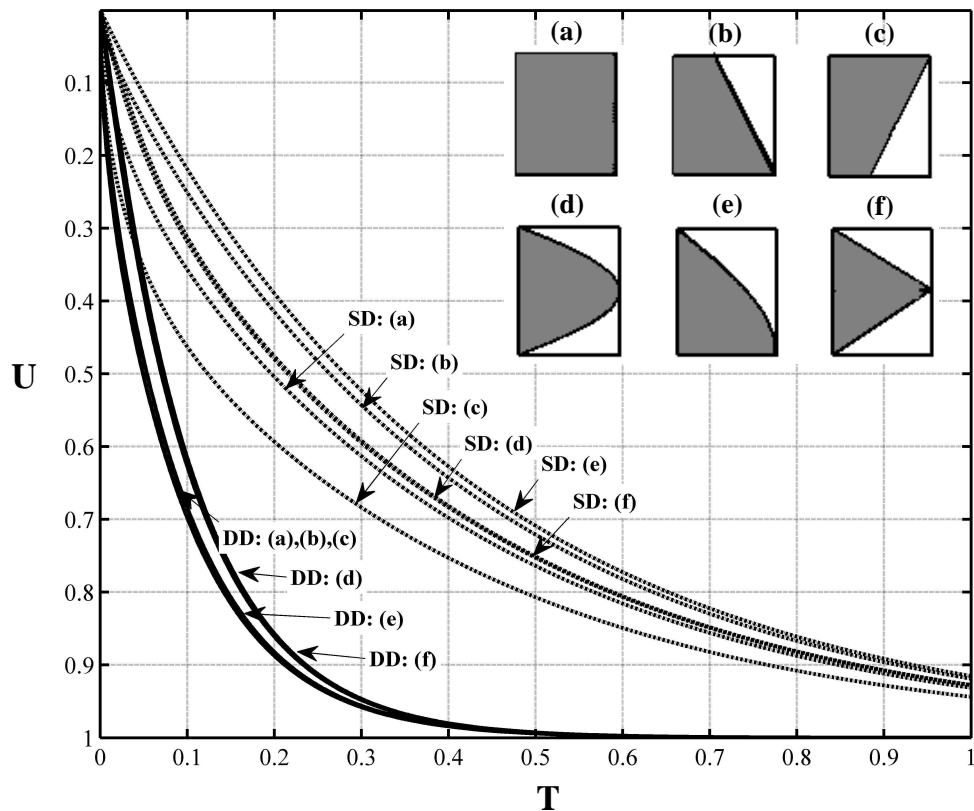


Figure 3.22 – U - T curves for a singly or doubly drained soil layer subjected to different u_i -distributions

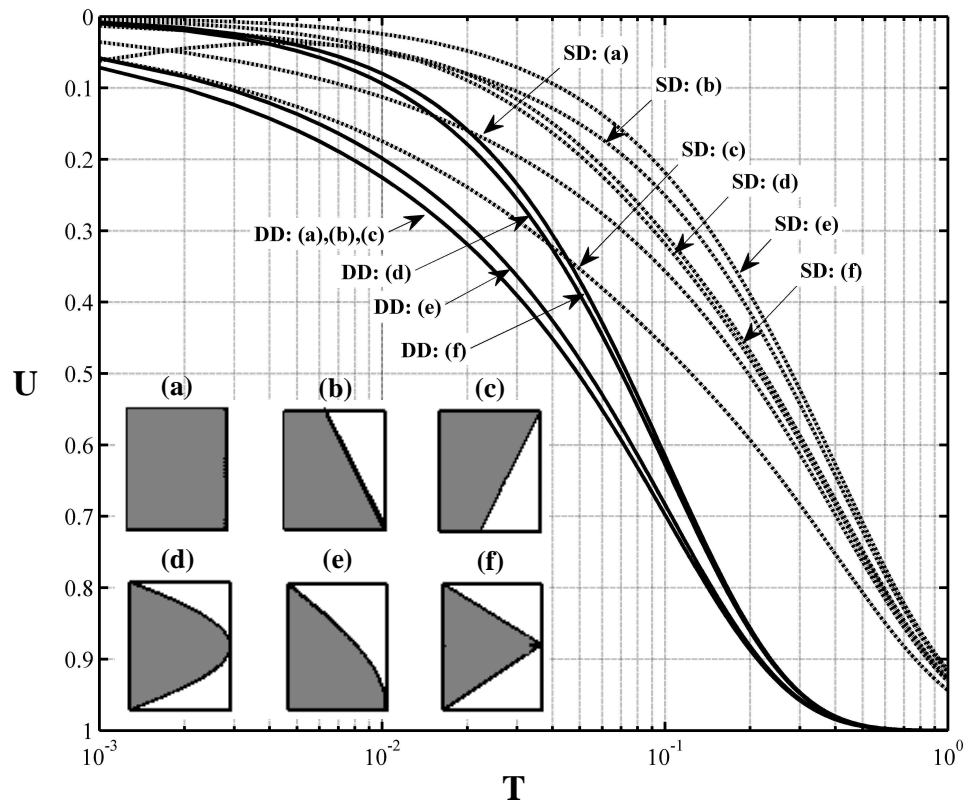


Figure 3.23 – U -log T curves for a singly or doubly drained soil layer subjected to different u_i -distributions

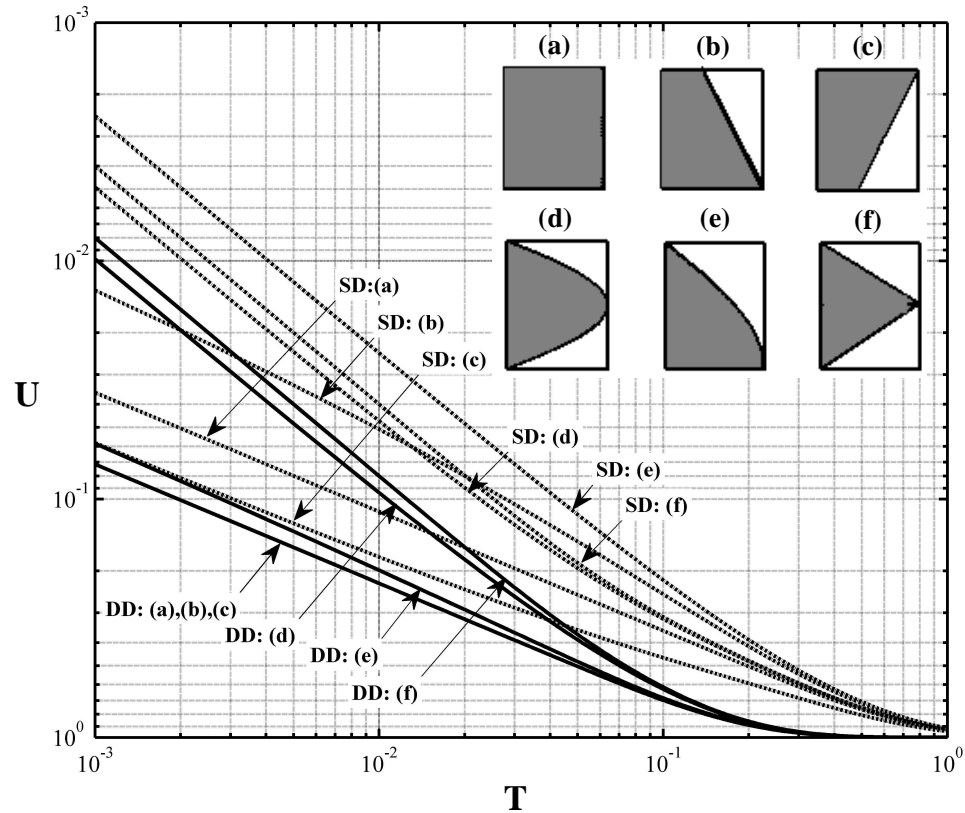


Figure 3.24 – $\log U$ -log T curves for a singly or doubly drained soil layer subjected to different u_i -distributions

Comparison with reported values

The significance of the average consolidation curve is well recognized when considering consolidation behaviour. Terzaghi and Frohlich (1936) have tabulated the $U - T$ values for a singly drained soil layer subjected to three basic cases of initial excess pore pressure; uniform, linearly increasing and linearly decreasing u_i -distributions. These values have been reproduced in tabular or graphical form in various geotechnical textbooks (Jumikis 1962, Craig 1974), without any apparent attempt to check these values. Singh (2005) compared these values with those obtained using the analytical solution for a linearly decreasing u_i -distribution, and observed that the previously reported values of U are inexact for low values of T . The average degree of consolidation curves calculated using the series solutions outlined previously are provided in conjunction with Terzaghi and Frohlich values for comparison in Figure 3.25, represented by the black and red dashed lines, respectively.

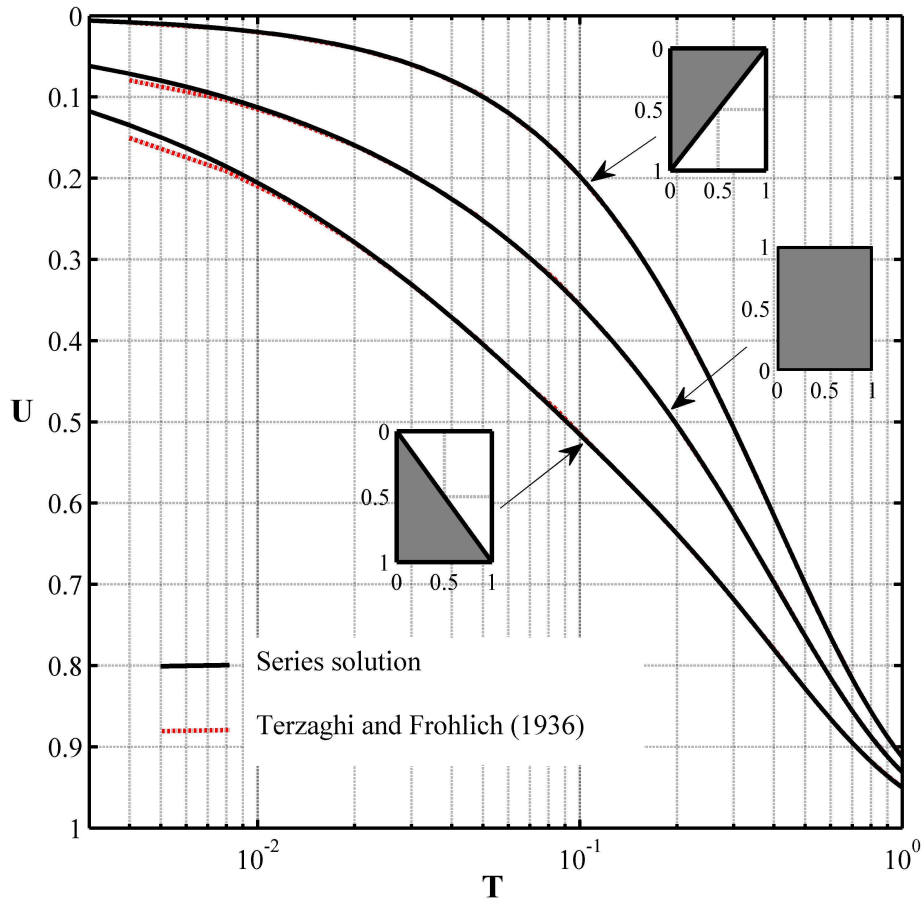


Figure 3.25 – $U-T$ curves for series solution results compared with Terzaghi and Frohlich (1936) tabulated values

The average consolidation curves generated for uniform and linearly decreasing cases of initial excess pore pressure show a deviation from the original values provided by Terzaghi

and Frohlich, further confirming results reported by Singh. However, it appears that the Terzaghi and Frohlich values corresponding to a linearly increasing u_i -distribution are comparatively accurate.

3.3.4. The relevance of drainage path length

By examining the relevance of drainage path length (H_{dr}), it is also possible to demonstrate the benefits of expressing the average degree of consolidation in terms of a time factor that is independent of drainage conditions (i.e. is in terms of layer thickness only).

History of H_{dr}

When Terzaghi first developed his one-dimensional consolidation theory, he referred to doubly drained clay layers as ‘open’ layers and singly drained layers as ‘half-closed’ layers irrespective of the u_i -distribution (Terzaghi 1943). He then directed the user to compute the time factor using half the layer thickness if doubly drained, and the total thickness if singly drained. From this, the term ‘maximum length of drainage path’ evolved and has been widely adopted by the geotechnical community as a physical explanation for Terzaghi’s drainage guidelines (Jumikis 1962, Scott 1963, Harr 1966, Winterkorn and Fang 1990, Powrie 1997, Das 2009, Holtz et al. 2010, Sivakugan and Das 2010 etc.). Some geotechnical textbooks further explain the term ‘maximum drainage path length’ as the maximum distance a water molecule must travel to exit the consolidating layer (Kaniraj 1988, Smith 2006, Helwany 2007, McCarthy 2007). As a result, the definition for H_{dr} can be interpreted one of two ways; as the relationship between equivalent thicknesses for singly and doubly drained layers, or as the maximum distance a water molecule must travel to leave the layer. Depending on the u_i -distribution, these two definitions are not always equal.

H_{dr} Definition A

It is widely accepted that for singly drained clay layers, the maximum drainage path length is the total thickness of the layer (H), whereas for doubly drained clay layers the drainage path length is half the thickness ($H/2$). Whilst it may be intuitively concluded that the drainage path length is therefore the thickness of the clay layer divided by the number of drainage boundaries, again this relationship only exists for uniform u_i -distributions. To determine H_{dr} for layers subjected to non-uniform u_i distributions, the correct definition of H_{dr} must first be understood. The expression for H_{dr} as it directly stems from Terzaghi’s work is actually a relationship between the effective thicknesses of singly and doubly

drained layers. That is, how much thicker must a doubly drained layer be to consolidate at the same rate as if it were singly drained? For example, for a case of uniform u_i , a singly drained layer of thickness H would consolidate at the same rate as a doubly drained layer that is twice as thick ($2H$). By determining this relationship between thicknesses, a single $U-T$ curve can be used for both drainage situations - the type of drainage situation is taken into account in the expression for time factor. From this, Terzaghi's definition for H_{dr} (Definition A) can be redefined as:

$$H_{dr} = f_H H \quad (3.31)$$

where H_{dr} is the doubly drained thickness used in the time factor expression (or H_{DD}) as a fraction of H which is the equivalent thickness of the singly drained layer (or H_{SD}), with f_H being the effective drainage path length factor. For a case of uniform u_i , it can be easily shown that $f_H = 0.5$:

If two separate series solutions are developed for each drainage situation using a constant layer thickness of H , it can be seen that a doubly drained layer will consolidate four times faster than its singly drained counterpart when the layer is subjected to a uniform u_i -distribution. That is, it will take four times as long for a singly drained layer to reach a particular consolidation settlement than if it were doubly drained. Thus, for a particular value of U :

$$T_{SD} = 4T_{DD} \quad (3.32)$$

where T_{SD} and T_{DD} are the time factors at a certain value of U for single and double drainage, respectively. Thus, in order to adopt only one solution and therefore require only one $U-T$ curve to describe both drainage cases, the decay of doubly drained pore pressure must be 'slowed down' by a factor of 4 as shown in Eq. (3.33). For a particular value of t :

$$T_{SD} = \frac{T_{DD}}{4} \quad (3.33)$$

$$\frac{c_v t}{H_{SD}^2} = \frac{c_v t}{4H_{DD}^2} \quad (3.34)$$

where H_{SD} is a nominal reference thickness of the clay layer (H), and H_{DD} is the thickness required to produce the same settlement values as the singly drained case. Since the properties of the soil (c_v) remain constant and the same point in time (t) is being considered, the expression in Eq. (3.34) can be reduced to:

$$H_{SD} = 2H_{DD} \quad (3.35)$$

$$\text{or } H_{dr} = 0.5H \quad (3.36)$$

Thus, a doubly drained layer must be twice as thick as a singly drained layer to produce the same variation in consolidation settlement with time (i.e. $f_H = 0.5$).

In computing the time factor for a singly drained clay layer, the layer thickness H can be used for any initial pore pressure distribution, whether symmetrical or otherwise. When it comes to doubly drained layers, it has been shown that H_{dr} can be taken as $H/2$ (or $f_H = 0.5$) only when the u_i -distribution is uniform. In order to deal with other situations where a doubly drained layer is subjected to non-uniform u_i -distributions, the values for f_H must be identified for each different distribution. The relationship between f_H and the average degree of consolidation (U) for key non-uniform distributions is shown in Figure 3.26.

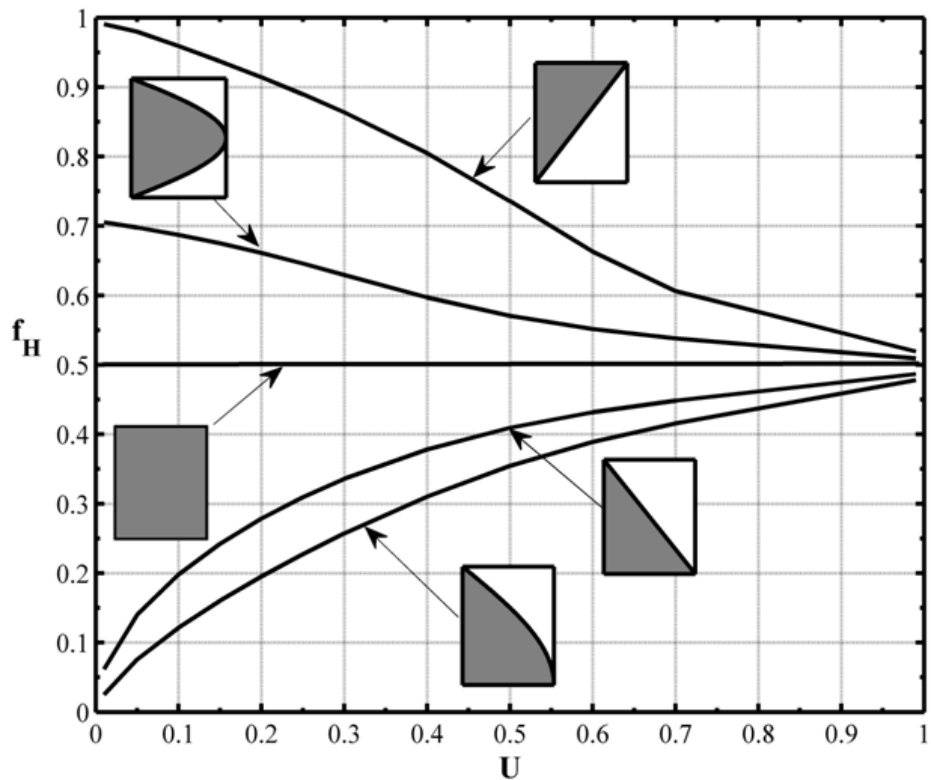


Figure 3.26 – Effective drainage path factor as a function of U for key u_i -distributions

It can be seen that f_H does not maintain a constant value, unlike the uniform u_i distribution where $f_H = 0.5$ at all times (or for all U). Given the $U - T$ curves for a singly drained

clay layer subjected to a particular non-uniform u_i -distribution, one could feasibly use Figure 3.26 to modify the time factor to also account for a doubly drained situation: H is simply multiplied by f_H in the expression for T . For example, for a uniform u_i distribution, $f_H = 0.5$ for all values of U and the effective drainage path length becomes $H/2$ which is the conventionally understood expression for H_{dr} . However, it is evident that for all non-uniform u_i -distributions, f_H varies with time, which indicates that any advantage associated with using H_{dr} in consolidation analyses is not present when considering non-uniform u_i -distributions. Instead, it is more convenient to eliminate H_{dr} as a variable and use two separate $U-T$ curves for each drainage situation (where T is in terms of H only and does not need to be adjusted).

The $U-T$ values provided by Terzaghi and Frohlich (1936) for a doubly drained layer subjected to non-uniform u_i -distributions such as; linearly increasing/decreasing, sinusoidal and half-sinusoidal were determined using the same procedure as with the uniform u_i -distribution. That is, the doubly drained layer thickness was initially designated as $2H$ to determine the corresponding $U-T$ values. In other words, the average consolidation behaviour represented by these $U-T$ values is actually four times ‘slower’ than it should be. The only way to rectify this is to adjust the time factor using $H_{dr} = H/2$ (i.e. $f_H = 0.5$) when determining the average degree of consolidation. However, as shown in Figure 3.26, f_H does not equal 0.5 for any of these non-uniform distributions. As a result, $H/2$ does not have any *physical* relevance in these cases in terms of drainage path length, and should be treated as a procedural adjustment only. This brings into question the benefit of designating the layer thickness as $2H$ in the initial development of the solution, which further supports the recommendation that separate $U-T$ curves be used, with no subsequent adjustments to the time factor.

H_{dr} Definition B

When the literal definition for H_{dr} as the ‘maximum distance a water molecule must travel to exit the consolidating layer’ is instead used (Definition B), quite different results to those established using Definition A are obtained. To determine the maximum distance a water molecule must travel, the changeover point between upward and downward flow (if both types are applicable) must be determined. This was done by observing the decay of excess pore pressure isochrones and noting the changes in hydraulic gradient with depth.

For one-dimensional consolidation, the discharge velocity at any point within a clay layer can be defined as:

$$v = k_v \left(\frac{1}{\gamma_w} \frac{\partial u}{\partial z} \right) \quad (3.37)$$

where k_v = vertical permeability of the clay stratum and $\frac{1}{\gamma_w} \frac{\partial u}{\partial z}$ is simply the hydraulic gradient, with γ_w being the unit weight of water.

Depending on whether $\frac{\partial u}{\partial z}$ is positive or negative, the flow can be upward or downward, respectively. The point at $\frac{\partial u}{\partial z} = 0$ indicates a point of no flow, and is the boundary condition that must be satisfied when dealing with an impervious layer. When this occurs at some point *within* the clay layer, it represents the cut-off point between upward and downward flow. Thus, the maximum drainage path length as defined by Definition B can be determined by observing the point at which $\frac{\partial u}{\partial z} = 0$ for each normalised excess pore pressure isochrone. An example of this is shown in Figure 3.27 for a linearly decreasing u_i distribution.

In the case of a doubly drained layer, two ‘maximum’ drainage path length values are obtained; one for upward flow where pore water exits the top boundary, and one for downward flow where pore water exits the bottom boundary. As shown in Figure 3.27(a), the maximum drainage path length (H_{dr}) at a particular time during consolidation (T) is obtained by selecting the larger of these two values. For the singly drained case, as in Figure 3.27(b), it can be seen that downward flow towards the impermeable boundary occurs during the early stages of consolidation. As a result, a drainage path length greater than the total thickness of the clay layer could exist in these situations, where a molecule of pore water travels downward initially, before moving upward towards the drainage boundary. However, for the purposes of this analysis, the maximum drainage path length (H_{dr}) has been selected as the *direct* distance a water molecule must travel to exit the layer (i.e. only upward flow is considered).

It can be seen from Figure 3.27(a) that during the early stages of doubly drained consolidation, the depth at which $\frac{\partial u}{\partial z} = 0$ is closer to the upper drainage boundary, and hence H_{dr} is significantly larger than $H/2$. As consolidation progresses, the isochrones tend to become symmetrical and H_{dr} tends toward $H/2$. From Figure 3.27(b), it is evident that the maximum drainage path length of upward flow is considerably shorter than H during the early stages of consolidation. However, as consolidation progresses H_{dr} tends toward H until upward flow dominates, at which point $H_{dr} = H$.

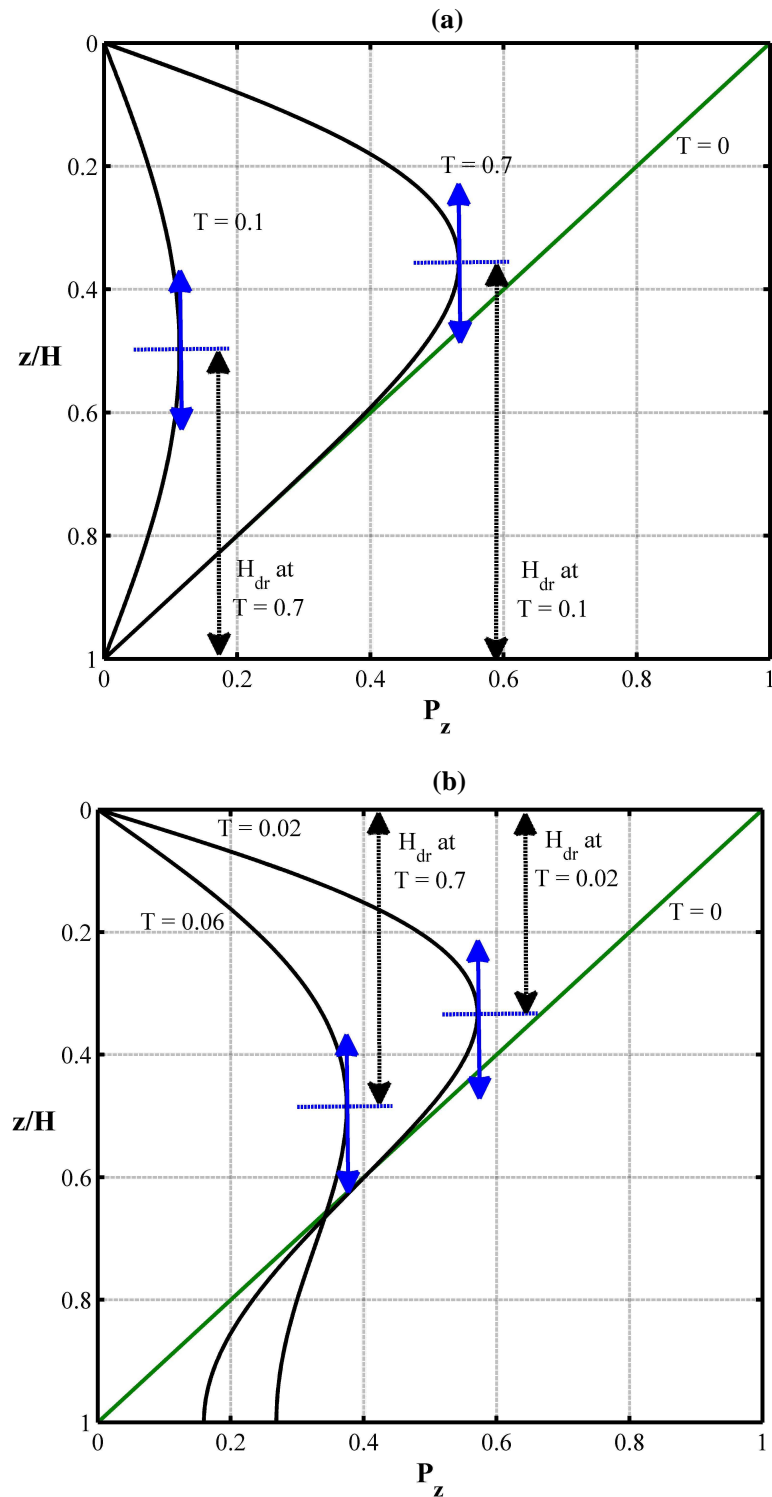


Figure 3.27 – Determination of maximum drainage path length for select isochrones for (a) doubly drained; or (b) singly drained consolidating layer

The variation of H_{dr} with time for a doubly drained layer subjected to key u_i -distributions is shown in Figure 3.28.

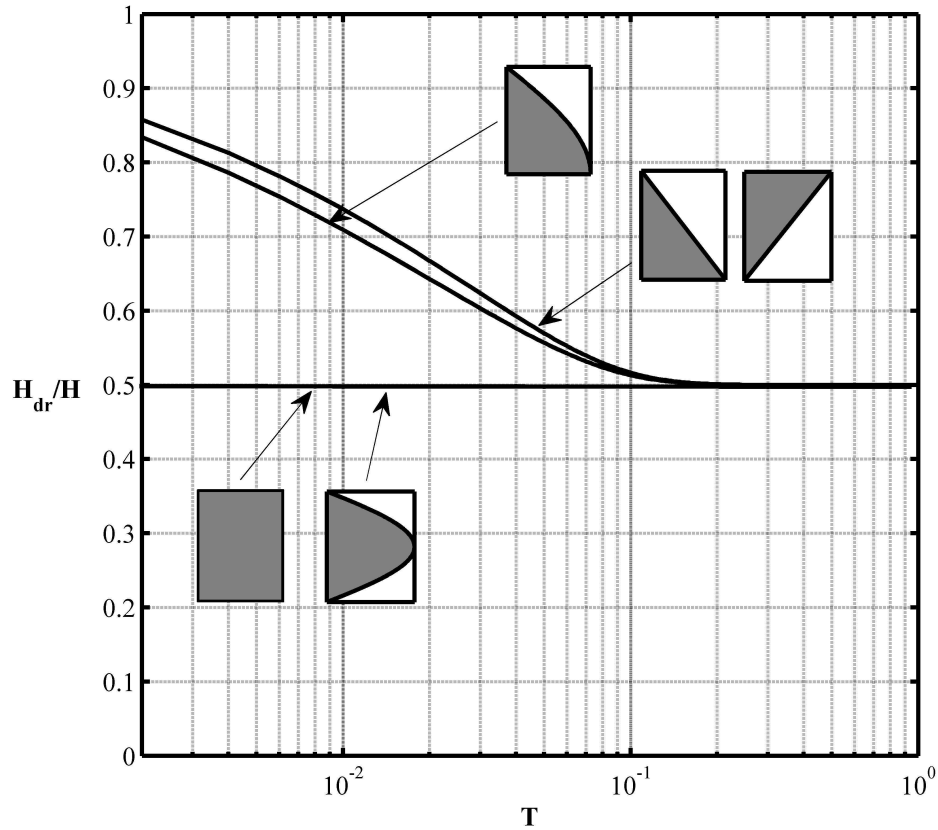


Figure 3.28 – Variation of maximum drainage path length with time for a doubly drained clay layer subjected to key u_i -distributions

It can be seen that when the u_i -distribution is symmetrical, the resulting decay of excess pore pressure isochrones also remains symmetrical about the horizontal line at $H/2$ and hence the maximum drainage path length remains constant throughout consolidation as $H/2$. As a result, the conventional expression for doubly drained maximum drainage path length ($H_{dr} = H/2$) is valid at all times during consolidation when considering symmetrical u_i -distributions such as uniform and sinusoidal shapes. For asymmetrical u_i -distributions such as linearly increasing/decreasing and half-sinusoidal distributions, H_{dr} varies with time, only returning to $H_{dr} = H/2$ at approximately $T = 0.2$.

For a singly drained consolidating layer (where the impermeable boundary is located at the base of the clay layer), H_{dr} varies with time in cases where pore pressure redistribution occurs during consolidation. The variation of H_{dr} with the time factor (T) is shown in Figure 3.29 for five different u_i -distributions.

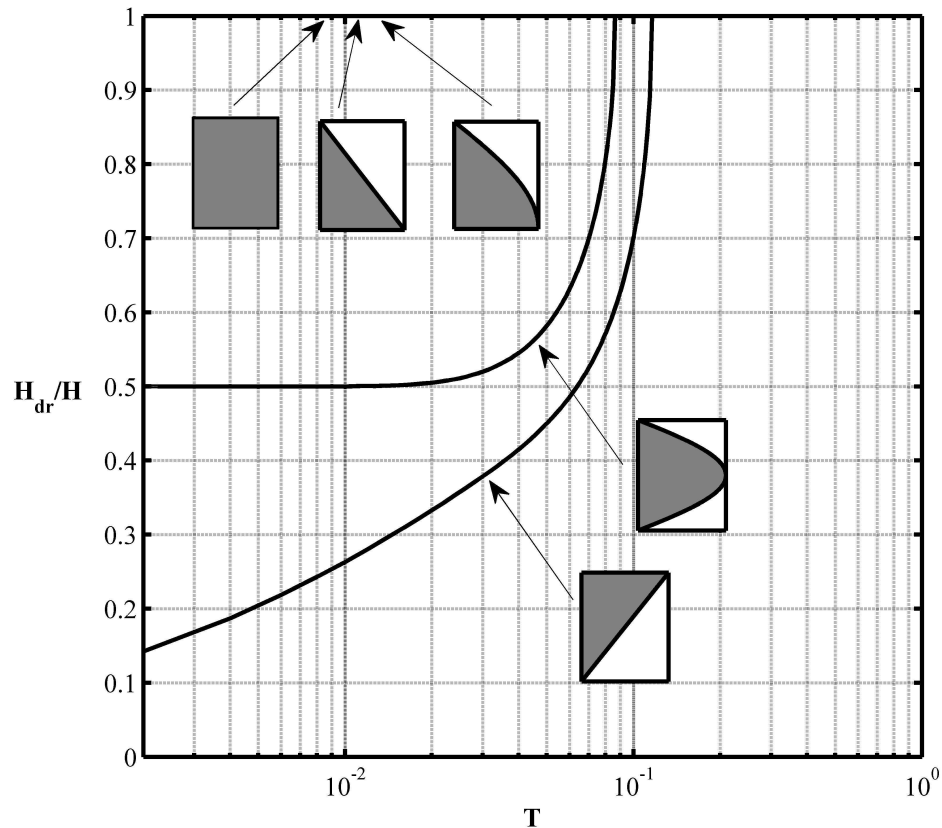


Figure 3.29 – Variation of maximum drainage path length with time for a singly drained clay layer subjected to key u_i -distributions

For uniform, half-sinusoidal and linearly increasing u_i -distributions, the maximum pore pressures occur at the bottom impervious boundary at all times, where $\partial u / \partial z$ is zero. Therefore, the maximum length of drainage path adheres to the conventional understanding of $H_{dr} = H$ for single drainage, but only for these distributions. For linearly decreasing and sinusoidal u_i -distributions, it takes quite a while for H_{dr} to reach the value of H .

Comparison of drainage conditions

Based on the example shown in Section 3.3.2, one might conclude that the settlement of a singly drained layer is always half of the settlement that would have occurred at the same time if the layer were instead doubly drained. However, in order to directly compare the effect of one or two drainage boundaries on the average degree of consolidation behaviour of a clay layer, the ratio between consolidation settlements during all stages of consolidation must be obtained, the results of which are shown in Figure 3.30, where the time factor is defined as $c_v t / H^2$.

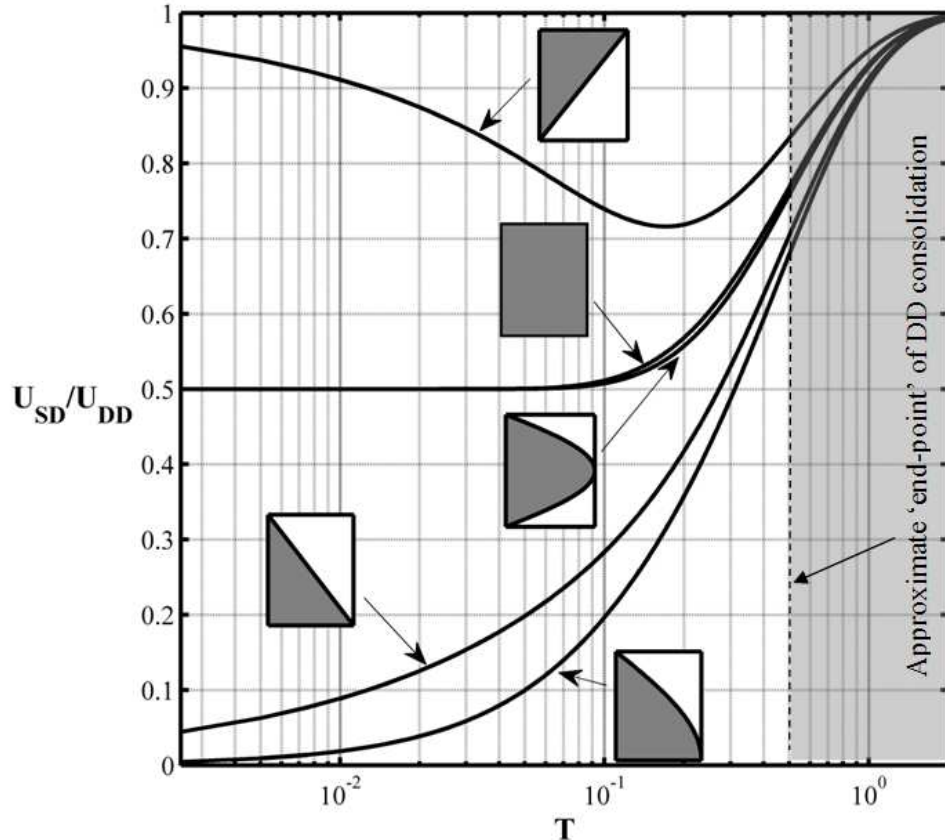


Figure 3.30 – A comparison between singly and doubly drained clay layers subjected to key u_i -distributions

For uniform and sinusoidal u_i -distributions, it can be seen that the settlement of a singly drained layer remains exactly half of the doubly drained settlement, but only until a time factor of approximately 0.07, which is well before the ‘end-point’ of doubly drained consolidation where $T = 0.5$ (or $T = 2$ for a singly drained layer) and $U = 99.42\%$.

The ratio between doubly and singly drained consolidation settlements for a linearly decreasing u_i -distribution show that at any time during consolidation, the settlement of a singly drained layer is never less than approximately 70% of the settlement that would occur if the layer were doubly drained. Alternatively, if a clay layer is subjected to half-sinusoidal or linearly increasing u_i -distributions, the effect of having an impermeable bottom layer dramatically reduces the rate of consolidation in comparison with the presence of a freely draining bottom layer.

3.3.5. Adjusting uniform results to account for non-uniform u_i -distributions

The variation in percentage consolidation (U) with time (T) that occurs within a clay layer initially subjected to a non-uniform variation in excess pore pressure can be quite difficult to evaluate, depending on the complexity of the non-uniform u_i -distribution. As a result, the $U - T$ values resulting from a uniform u_i -distribution are often adopted in consolidation analyses, as they are readily available in geotechnical literature and can be quite easily calculated. In this section, a simple method for adjusting uniform $U - T$ values to account for non-uniform initial excess pore pressure distributions has been proposed. This method takes advantage of the fact that at some key point during consolidation, the undissipated excess pore water pressure due to a non-uniform u_i -distribution becomes a fraction of the undissipated excess pore water pressure due to a uniform u_i -distribution, and this fraction remains constant for the remaining duration of the consolidation process.

Justification

The possibility of non-uniform u_i -distributions occurring in reality is already acknowledged in notable geotechnical textbooks (Terzaghi and Frohlich 1936, Taylor 1948), and is further supported by field evidence (e.g. Chu and Wan 2005). However, many consolidation analyses still adopt a uniform u_i -distribution and subsequently use the uniform $U - T$ curve only.

The rationale behind using the uniform $U - T$ curve to adequately represent consolidation can be attributed to; the similarity of $U - T$ curves resulting from different u_i -distributions, coupled with one-dimensional drainage simplifications, and the assumption of an idealized pressure-versus-void-ratio relationship (Taylor 1948). However, if the u_i -distribution is known (either through direct measurement or indirectly, through knowledge of the loading scenario), and one-dimensional consolidation can be reasonably assumed (or be adopted to estimate a conservative limit), why not strive for a more realistic estimate of the consolidation settlement by using the appropriate $U - T$ curve?

To justify the need for more careful consideration when selecting an appropriate initial excess pore pressure distribution and assess the validity of the rationale that all $U - T$ curves are ‘similar’, a graphical comparison between the average degree of consolidation of a layer subjected to non-uniform u_i -distributions (U) and the average degree of

consolidation of the same layer consolidating under a uniform u_i -distribution (U_{uni}) is shown in Figures 3.31 and 3.32 for one- and two-way drainage, respectively.

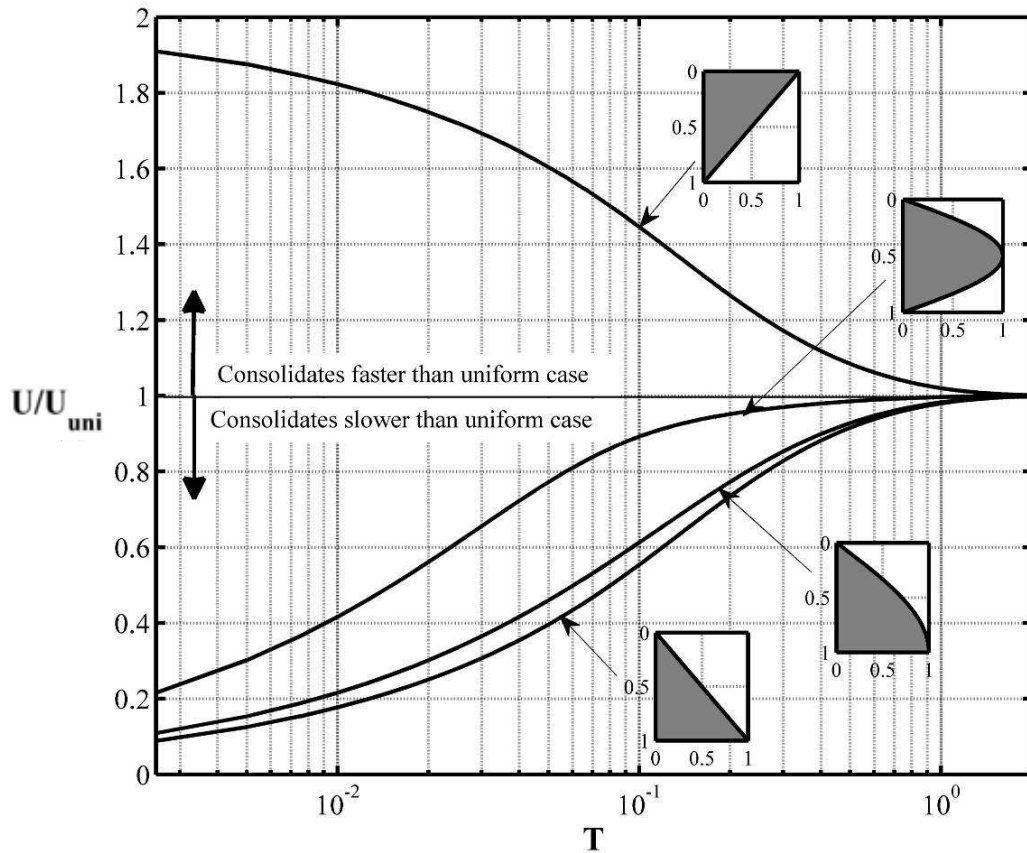


Figure 3.31 – Comparison between U values for non-uniform and uniform u_i -distributions with one-way drainage

If one-way drainage is present, choosing to adopt a uniform u_i -distribution instead of a sinusoidal, half-sinusoidal or linearly increasing u_i -distribution can result in gross over-estimations of consolidation settlement for a significant period of consolidation, especially during the early stages of consolidation, as shown in Figure 3.31.

A similar over-estimation of consolidation settlement would also occur when considering two-way drainage if a sinusoidal or half-sinusoidal u_i -distribution exists and the user selects a uniform u_i -distribution instead, as evidenced by Figure 3.32. This is practically relevant in cases where consolidation has already begun, but has occurred over an unknown period of time. When assuming the current pore pressure distribution as the u_i -distribution for the subsequent settlement analysis, a sinusoidal or half-sinusoidal pattern is appropriate.

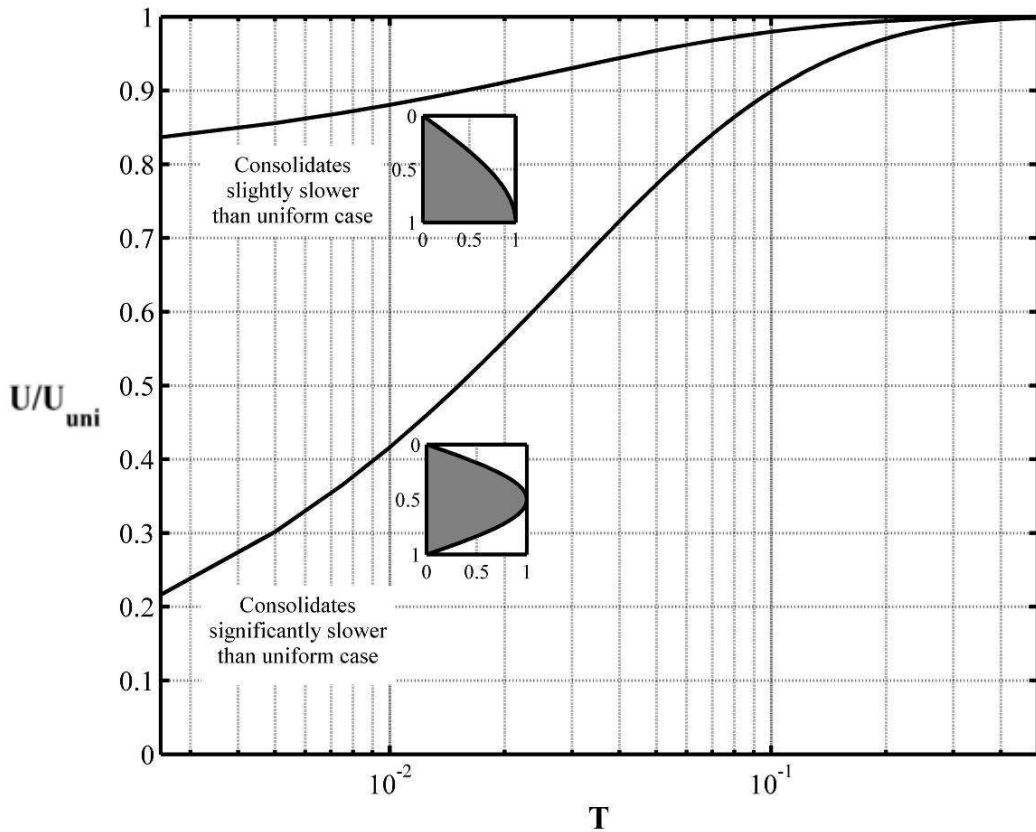


Figure 3.32 – Comparison between U values for non-uniform and uniform u_i -distributions with two-way drainage

Proposed method for determining $U-T$ curves

Perhaps the tedious nature involved with obtaining a set of $U - T$ values that correspond to non-uniform u_i -distributions may be a significant reason for past assumptions of a uniform u_i -distribution, the $U - T$ values of which are readily available in geotechnical literature. It would therefore be ideal to develop correction factors that can be directly applied to the widely available uniform $U - T$ values to adjust for different non-uniform u_i -distributions.

The excess pore water pressure isochrones for both uniform and linearly increasing u_i -distributions with two-way drainage at time factors of 0.02 and 0.1 are shown in Figure 3.33. It is evident that in the early stages (i.e. $T = 0.02$), the isochrone corresponding to the linearly increasing u_i -distribution is slightly skewed, but is forced towards a sinusoidal shape shortly thereafter by the boundary conditions (at approximately $T = 0.1$). In fact, the pore pressure isochrones in the early stages of consolidation for a *uniform* case of initial pore pressure are actually parabolic and do not become perfectly sinusoidal (or half-sinusoidal in

the case of one-way drainage) until $T = 0.1$ for two-way drainage or $T = 0.4$ for one-way drainage. However, at $T = 0.05$ for two-way drainage or $T = 0.2$ for one-way drainage the isochrone shapes deviate by less than 2.5% of their sinusoidal/half-sinusoidal counterparts, and can thus be considered sinusoidal/half-sinusoidal at and beyond these time factors.

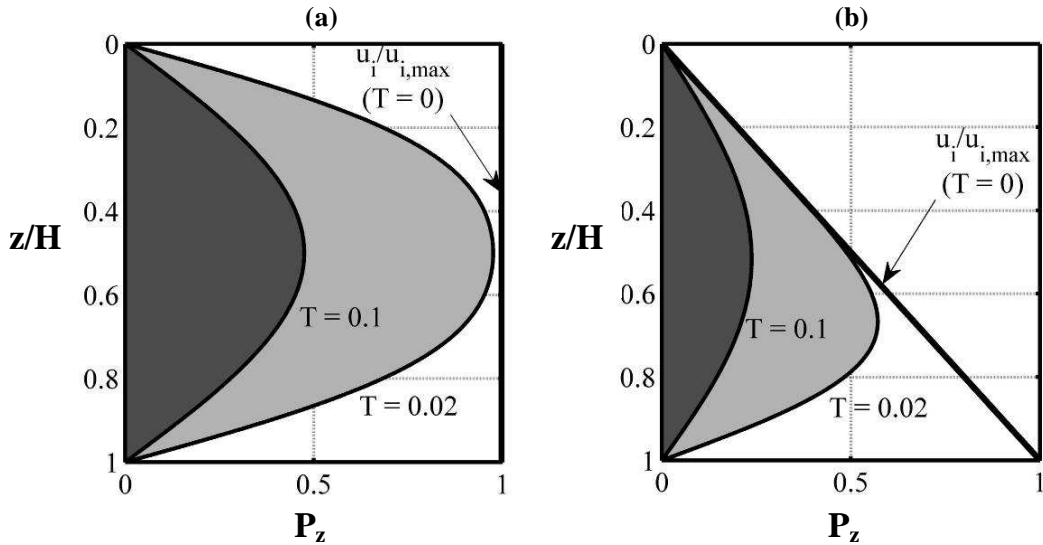


Figure 3.33 – Excess pore water pressure to decay for (a) uniform and (b) linearly increasing u_i -distributions with two-way drainage

The method used herein to develop adjustment factors is based on the principle that the decay of excess pore water pressure that occurs due to a non-uniform u_i -distribution will be slightly skewed in the early stages of consolidation, but will ultimately revert to a sinusoidal or half-sinusoidal shape, for two- and one-way drainage cases, respectively. Since the $U - T$ values resulting from a uniform u_i -distribution are readily available in literature, the decay of pore water pressure resulting from a uniform case is used as a base-line for comparison. By comparing the total excess pore pressure (i.e. area bounded by an isochrone) due a non-uniform u_i -distribution with the corresponding excess pore pressure resulting from a uniform u_i -distribution at a particular value of T , it is possible to determine when the decay of any non-uniform u_i -distribution becomes a (factor of) the ‘conventional’ uniform case. From this, a relationship between the ‘uniform’ $U - T$ values and the ‘non-uniform’ $U - T$ values can be established.

The development of this method can be illustrated using the simple example shown in Figure 3.33. The average degree of consolidation at $T = 0.1$ can be graphically characterized for each of the two u_i -distributions, as shown in Table 3.2, where the integrals are indicated by the shaded areas.

Table 3.2 – Graphical example illustrating Terzaghi's average degree of consolidation at $T = 0.1$

	Uniform	Linear
$\int_0^H u_i(z,0) dz$		
$\int_0^H u(z,T) dz$		
$U = \frac{\int_0^H u_i(z,0) dz - \int_0^H u(z,T) dz}{\int_0^H u_i(z,0) dz}$		

By examining the excess pore pressure left to decay for a uniform case at a specific time during consolidation, and comparing this with the remaining excess pore pressure for a non-uniform u_i -distribution corresponding to the same time factor, it is possible to determine a relationship between the U values of the two u_i -distributions. In essence, Terzaghi's expression for the average degree of consolidation is completed in two steps; first, the decay of excess pore pressure is observed relative to that generated by a uniform u_i -distribution, and then the original non-uniform u_i -distribution is taken into account. In order to do this, new notations are required, which are shown in Eqs. (3.38) and (3.39).

$$R_a = \frac{\left[\int_0^H u(z,T) dz \right]_{\text{non-uniform}}}{\left[\int_0^H u(z,T) dz \right]_{\text{uniform}}} \quad \text{e.g. } \begin{array}{c} \text{triangle} \\ \hline \text{square} \\ \text{circle} \end{array} \quad (3.38)$$

$$R_i = \frac{\left[\int_0^H u_i(z,0) dz \right]_{\text{non-uniform}}}{\left[\int_0^H u_i(z,0) dz \right]_{\text{uniform}}} = \left[\int_0^H u_i(z,0) dz \right]_{\text{non-uniform}} \quad \text{e.g. } \begin{array}{c} \text{triangle} \\ \hline \text{square} \\ \text{circle} \end{array} \quad (3.39)$$

where R_i is the ratio of the shaded areas in Eq. (3.39) that represent the initial excess pore pressures, and is constant for each unique u_i -distribution.

R_a is the ratio of 'non-uniform' to 'uniform' undissipated excess pore water pressure assessed at various values of T and can thus be expected to vary with time as consolidation

progresses. As shown in Figures 3.34 and 3.35, R_a reaches a constant value at a time factor of approximately 0.2 for one-way drainage, and 0.05 for two-way drainage.

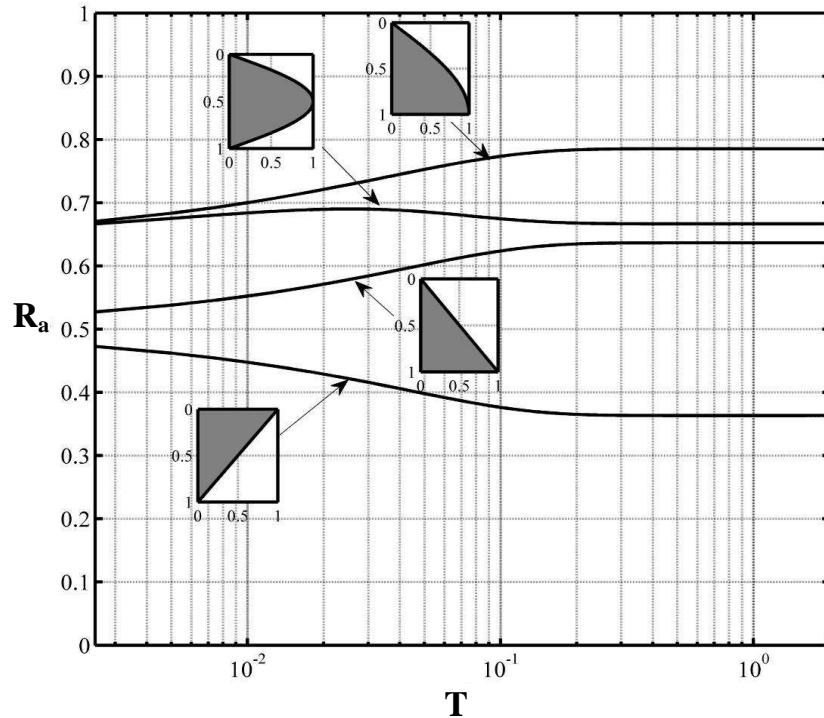


Figure 3.34 – Excess pore water pressure to decay for non-uniform u_i -distributions normalised by corresponding decay for a uniform u_i -distribution (one-way drainage)

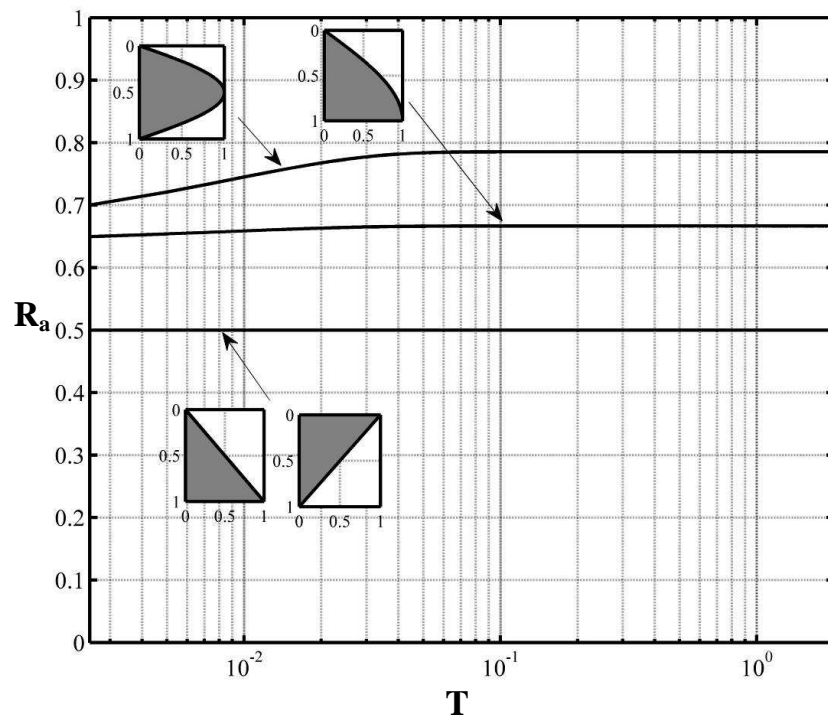
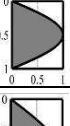
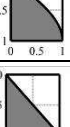
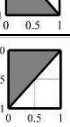
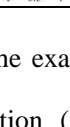


Figure 3.35 – Excess pore water pressure to decay for non-uniform u_i -distributions normalised by corresponding decay for a uniform u_i -distribution (two-way drainage)

This suggests that at these key points in time, herein referred to as T_a , the undissipated excess pore water pressure due to a non-uniform u_i -distribution will become some constant fraction of the corresponding undissipated pore pressure due to a uniform u_i -distribution. This fraction is the asymptotic or ultimate value of R_a (or $R_{a,ult}$) shown for each distribution in Figures 3.34 and 3.35, and conveniently summarized in Table 3.3.

Table 3.3 – Adjustment factors for key non-uniform u_i -distributions

u_i	R_i	Two-way drainage	One-way drainage
		$(T_a = 0.05)$	$(T_a = 0.2)$
	0.6366	0.7854	0.6667
	0.6366	0.6667	0.7854
	0.5	0.5	0.6366
	0.5	0.5	0.3634

Thus, for $T > T_a$, the exact average degree of consolidation values resulting from a non-uniform u_i -distribution (U_{non-u}) can easily and accurately be determined using the commonly available uniform U values (U_u) and adjusting them by the factors in Table 3.3 according to the relationship in Eq. (3.40).

$$U_{non-u} = 1 - \frac{R_a}{R_i} (1 - U_u) \quad (3.40)$$

For $T < T_a$, where R_a varies with T , the U_{non-u} values should be determined using the R_a values in Figures 3.34 and 3.35. Using Eq. (3.40) and the asymptotic values of R_a along with the corresponding values of R_i , a general expression for U_{non-u} in terms of U_u was developed for each non-uniform distribution. Values for U_{non-u} were then calculated for the *entire* period of consolidation using these expressions (and designated U_{eqn}) and compared with exact values of U_{non-u} (U_{exact}) as shown in Figures 3.36 and 3.37. As expected, for smaller values of U_{non-u} (which correspond to earlier values of T), the approximation becomes inaccurate, but to a relatively small degree.

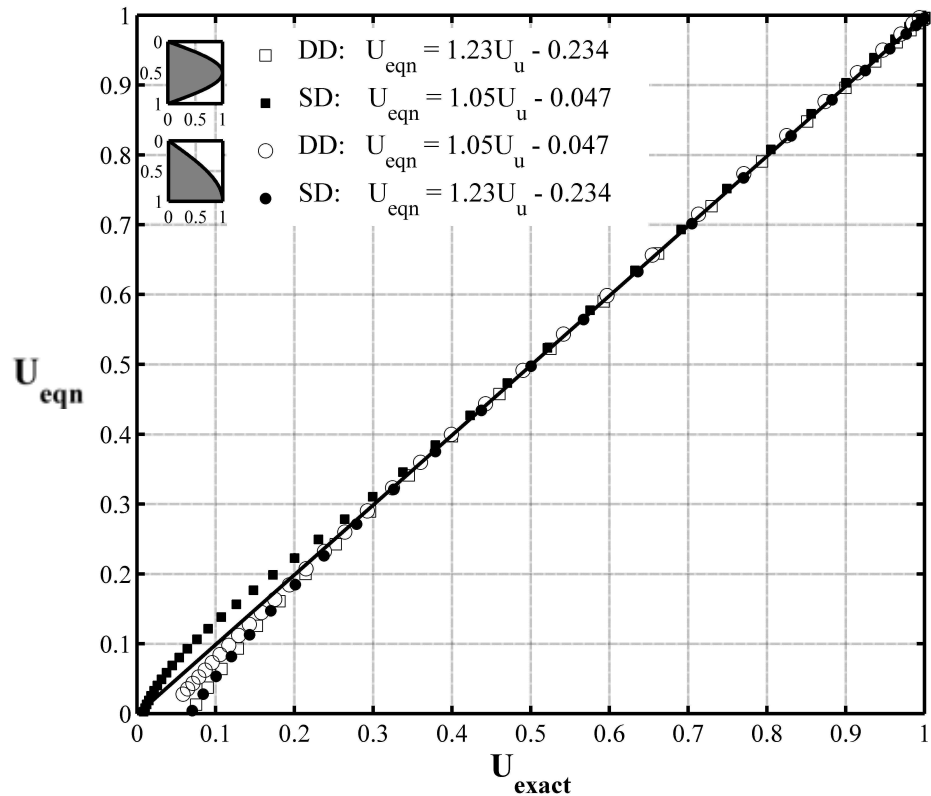


Figure 3.36 – Values of U calculated using the asymptotic values of R_a in Eq. (3.40) compared with exact values of U for sinusoidal and half-sinusoidal u_i -distributions

It should be noted that the equations developed using Eq. (3.40) are *exact* for the later stages of consolidation, when the initially non-uniform u_i -distribution has become perfectly sinusoidal (or half-sinusoidal in the case of one-way drainage). Obviously, when applied to the entire range of T , this expression will be inaccurate for the earlier stages of consolidation when the distribution of excess pore pressure is still skewed. However, a user can still feasibly determine the exact U_{non-u} value for a particular value of $T < T_a$ by selecting the appropriate value for R_a that corresponds to this T value from Figures 3.34 and 3.35 and using Eq. (3.40) along with the relevant U_u and R_i values. As shown in Figure 3.34, when considering one-way drainage, R_a does not significantly vary with time for the sinusoidal u_i -distribution. In fact, Eq. (3.40) can be applied to the entire period of consolidation (i.e. $T_a = 0$) in this case, whilst still yielding an acceptable RMS error of the order 10^{-3} . When considering two-way drainage (Figure 3.35) a satisfactory RMS error of the order 10^{-3} can be achieved if T_a is extended to include values of T greater than 0.03 for the sinusoidal case. For a half-sinusoidal u_i -distribution, T_a can be extended to incorporate

virtually the entire consolidation period ($T > 0.001$) whilst still maintaining an acceptable RMS error in the order of 10^{-3} .

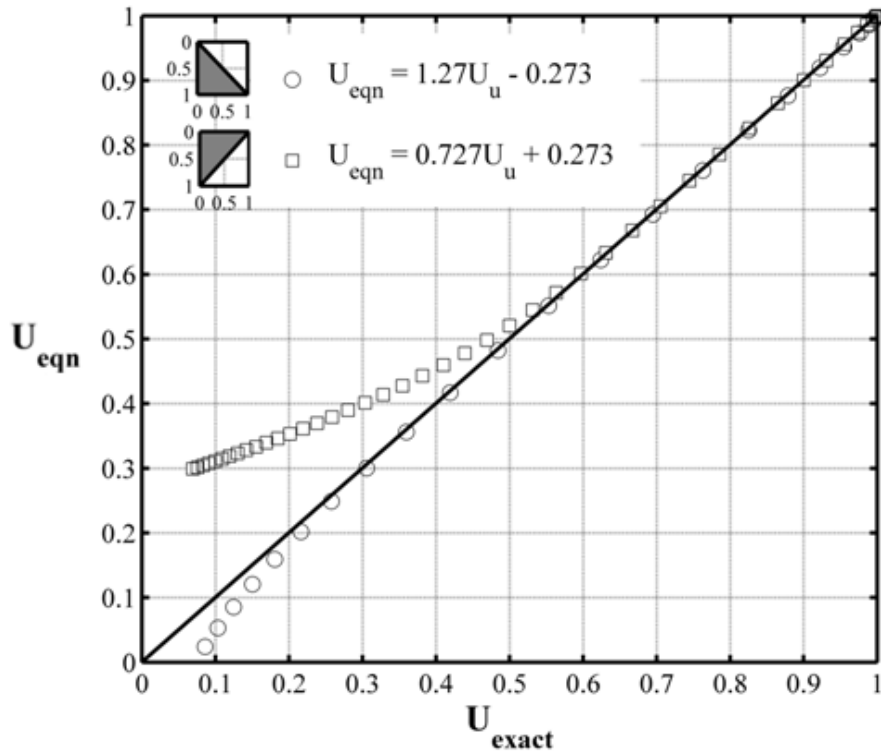


Figure 3.37 – Values of U calculated using the asymptotic values of R_a in Eq. (3.40) compared with exact values of U for linearly increasing and decreasing u_i -distributions with one-way drainage

It is obvious upon examination of Eq. (3.40) why the $U - T$ values for linear u_i -distributions are identical to those generated by a uniform u_i -distribution when considering two-way drainage; the decay of excess pore pressure is always exactly half that of the uniform case (i.e. $R_a = 0.5$), so that, when normalised by the initial excess pore pressure area ($R_i = 0.5$), the R_a / R_i component of Eq. (3.40) equals 1 and $U_{\text{non-u}} = U_u$.

For cases of one-way drainage, where the average degree of consolidation resulting from linear u_i -distributions is not identical to that resulting from a uniform u_i -distribution, the ultimate R_a ($R_{a,ult}$) value for various trapezoidal distributions (which mathematically exist between the triangular bounding cases) can be determined using the graph shown in Figure 3.38, where example cases have been shown for $R_i = 0.5, 0.7$ and 0.9 .

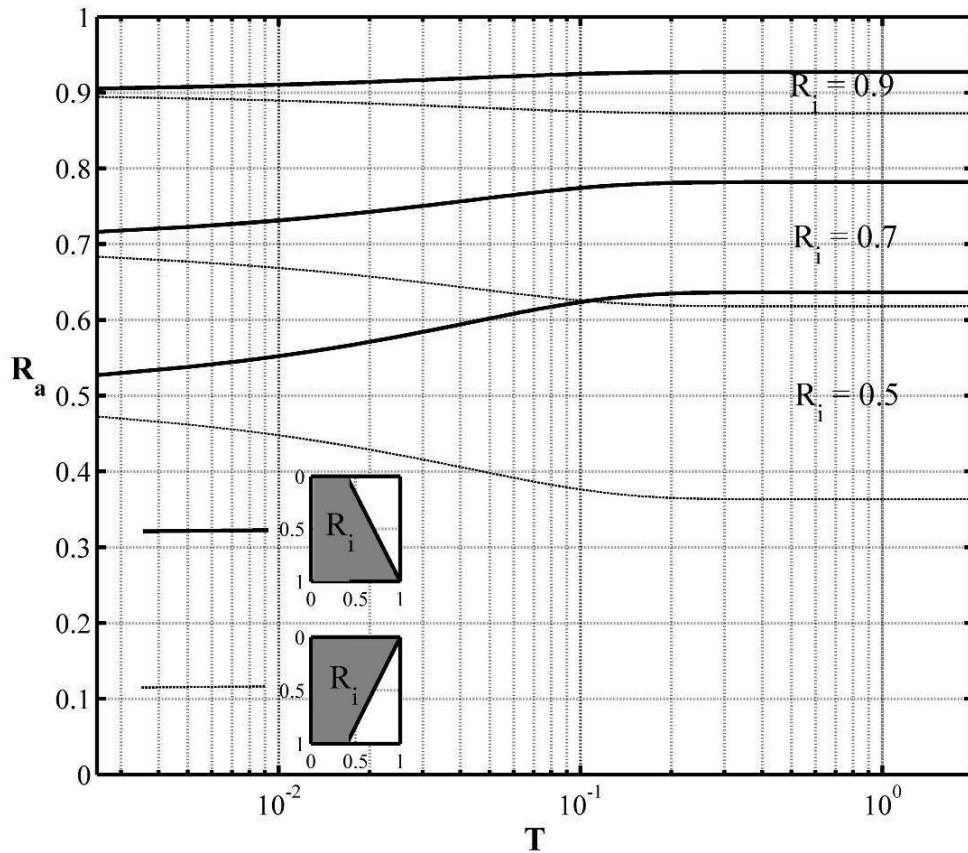


Figure 3.38 – Excess pore pressure to decay for linear u_i -distributions normalised by corresponding decay for a uniform u_i -distribution (one-way drainage)

Interestingly, but perhaps not surprisingly, the values of $R_{a,ult}$ vary linearly with R_i , as shown in Figure 3.39, which can feasibly be used to obtain the $U - T$ values for a layer with one-way drainage subjected to any variation of linear initial excess pore pressure. These factors were used in conjunction with Eq. (3.40) to determine the minimum value of T_a that would still yield an acceptable RMS error in the order of 10^{-4} . The T_a cutoff value required to maintain an RMS error of approximately 10^{-4} was found to linearly decrease as R_i increased, which is evident in Figure 3.38. That is, the region of consolidation that can be accurately described using Eq. (3.40) increases as the degree of linearity in the u_i -distribution decreases (i.e. as the u_i -distribution approaches a uniform shape).

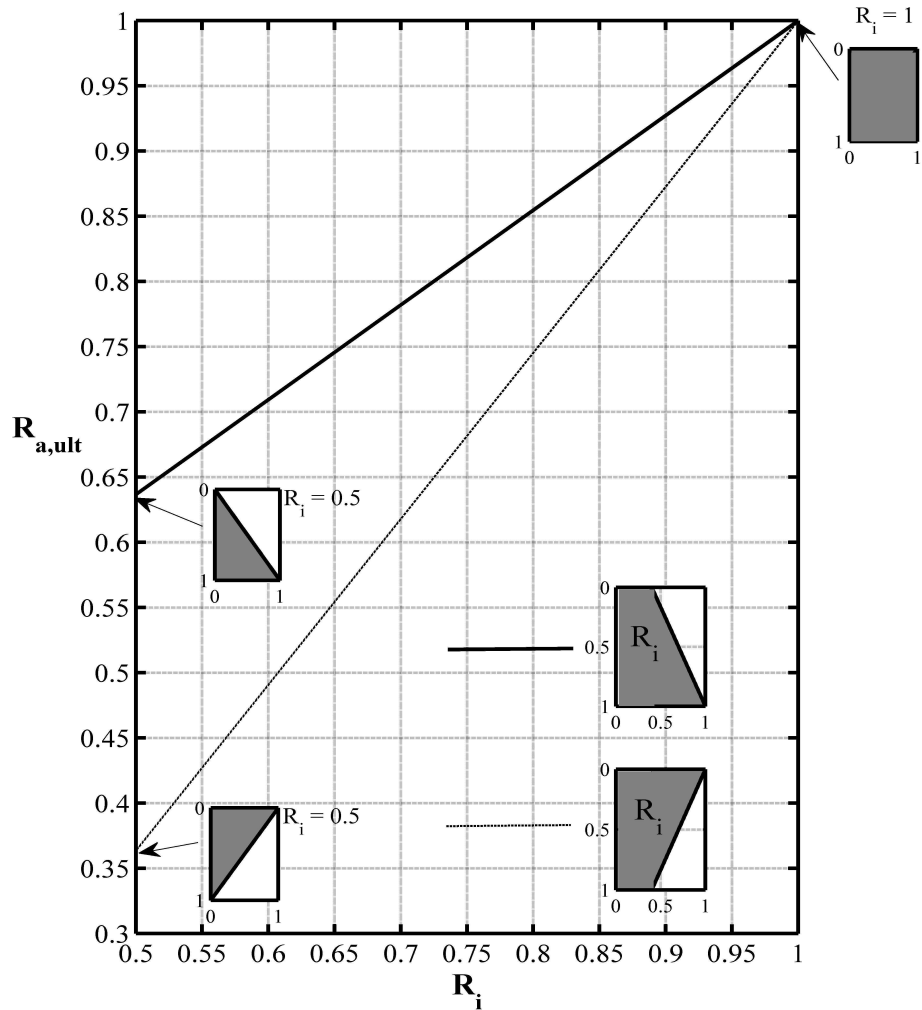


Figure 3.39 – Adjustment factors for using linear u_i -distributions

Thus, a unique and simplistic method for determining the average degree of consolidation of a layer (with one- or two-way drainage) subjected to a non-uniform initial excess pore water pressure distributions has been developed. All that is required to determine the non-uniform average degree of consolidation behaviour is some basic knowledge of the shape of the u_i -distribution and access to the widely available $U - T$ values associated with a uniform distribution of initial excess pore pressure. Using this method, a user can quickly obtain the non-uniform U values resulting from any number of key non-uniform u_i -distributions by adjusting the uniform $U - T$ values by some known factor. These factors have been provided in graphical and tabular form, and can be used to evaluate the average degree of consolidation of a layer subjected to sinusoidal, half-sinusoidal, and any variety of linear u_i -distributions.

3.4 Summary

The consolidation behaviour of a soil layer subjected to a variety of non-uniform u_i -distributions has been investigated in terms of both degree of consolidation isochrones and average degree of consolidation curves. In select cases (for both singly and doubly drained layers) the phenomenon of excess pore water pressure redistribution during consolidation was encountered. Here, the excess pore water pressures within some regions of the soil layer increased beyond their initial values during consolidation. When this occurs, it is difficult to infer any practical relevance from the degree of consolidation isochrones, as negative values are not feasible. As a result, in cases where pore pressure redistribution can be expected to occur, it is recommended that the dissipation of excess pore water pressure be viewed *directly* rather than scaling by the initial distribution to determine degree of consolidation.

The average degree of consolidation behaviour of a soil layer was also found to significantly depend upon the initial excess pore water pressure distribution. Using knowledge of the excess pore water pressure dissipation during consolidation, a simple method was developed which adjusts widely available percentage consolidation values for a uniform u_i -distribution to account for other possible non-uniform u_i -distributions.

Chapter 4: Coefficient of consolidation

4.1 General

When subjected to changes in applied stress, all soils undergo changes in volume. When considering one-dimensional strains, which are facilitated in an oedometer where loads are applied incrementally, these volume changes occur due to; initial or immediate compression, primary consolidation, and secondary compression or creep. Immediate settlement (also known as undrained, elastic or distortion settlement) occurs due to lateral movement of the soil in response to a change in vertical effective stress. This type of settlement is more prevalent in small loaded areas and occurs almost instantaneously with the application of load, before the onset of drainage. Although immediate settlement is technically not elastic, it is often calculated using elastic theory, particularly when considering cohesive soils (Fang 1991). Primary consolidation is the time-dependent settlement that occurs as the excess pore water pressure generated by the applied load increment dissipates via water being squeezed out of the soil. The consolidation settlement at which the excess pore water pressures have decayed to (approximately) zero is known as the ‘end of primary settlement’ or EOP settlement, designated by d_{100} . Secondary compression is the time-dependent compression that occurs at a virtually constant effective stress (Al-Zoubi 2010).

4.2 Current methods for determining c_v

Consolidation is due to a combination of soil properties, namely; permeability (k), which dictates the rate of pore fluid flow, and volume compressibility (m_v), which controls the development of excess pore water pressures within the soil, and therefore the duration of consolidation. Terzaghi’s theory quantifies the rate of consolidation using a parameter known as the coefficient of consolidation (c_v), which encapsulates both the permeability and compressibility of the consolidating soil. In the designs of foundations and embankments on clay subgrades, accurate predictions of settlement and pore water pressures are required to ensure these values are within acceptable limits. The accuracy of design predictions is reliant upon adequate input values of c_v . By ‘fitting’ the measured consolidation settlement ($d - t$ curve) to the theoretical percentage consolidation ($U - T$ curve) generated using Terzaghi’s theory for a uniform u_i -distribution, it is possible to determine a practical value of c_v for any type of soil. The settlement-time data obtained from laboratory oedometer tests can be analysed using a number of different curve-fitting procedures (Casagrande and Fadum 1940, Taylor 1948, Scott 1961, Cour 1971, Sivaram and Swamee 1977, Parkin 1978, Sridharan and Rao 1981, Robinson 1999, Mesri et al. 1999a, Feng and Lee 2001, Singh 2007). Since

Terzaghi's consolidation theory does not account for immediate or secondary settlement, these portions of the measured settlement-time curve must be removed before curve-fitting can take place.

The primary consolidation region of the settlement-time curve can be isolated by identifying and excluding the initial and secondary compression regions of the overall settlement curve. The immediate settlement, or settlement at the onset of primary consolidation (d_0), is often back-calculated by reverse extrapolating the early stage consolidation data. Two popular curve-fitting methods, Casagrande's log-time method (Casagrande and Fadum 1940) and Taylor's root-time method (Taylor 1948) both utilise the knowledge that the initial portion of the theoretical consolidation curve is parabolic (i.e. $U = 1.128\sqrt{T}$ for $U < 52.1\%$) in order to back-calculate d_0 . However, these curve-fitting procedures differ in their identification of d_{100} . Values of c_v generated using Taylor and Casagrande's curve-fitting procedures have been directly compared in previous studies (e.g. Sridharan et al. 1987, Duncan 1995, Cortellazzo 2002, Al-Zoubi 2010), and it is now widely accepted that values calculated using the root-time method are consistently larger than those calculated using the log-time method. This is due to discrepancies in identifying d_{100} – Casagrande's method generally predicts that the end-point of primary consolidation occurs much later during consolidation.

4.2.1. Validation of c_v values

Many of the existing curve-fitting procedures calculate c_v by fitting a single experimental point (e.g. d_{50}, t_{50} or d_{90}, t_{90}) to the corresponding percentage consolidation settlement-time factor values (e.g. 50%,0.049 or 90%,0.212) as shown:

$$c_{v,Taylor} = \frac{0.212 H_{90}^2}{t_{90}} \quad (4.1)$$

$$c_{v,Casagrande} = \frac{0.049 H_{50}^2}{t_{50}} \quad (4.2)$$

where t_{50} and t_{90} are the times at which primary consolidation is 50% and 90% completed, and H_{50} and H_{90} are the thicknesses of the clay layer at these times. Over the last five decades, attempts have been made to assess the accuracy of c_v values calculated from laboratory test data. In these investigations, researchers have usually adopted one of the following two approaches as a means of comparison;

- 1) The value of c_v calculated using a proposed or existing curve-fitting procedure is directly compared with that computed using the measured value of the permeability. In these instances, the permeability of the clay ($k_{v,measured}$) is usually measured during falling head permeability tests which are conducted at each loading increment. The value of c_v thus determined using the following expression:

$$c_{v,perm} = \frac{k_{v,measured}}{\gamma_w m_v} \quad (4.3)$$

can be seen as more realistic than the one interpreted from the curve-fitting procedures, where γ_w = unit weight of water and m_v = coefficient of volume compressibility. Results from oedometer tests with permeability measurements conducted on two types of normally consolidated Chicago clays (Al-Zoubi 2010) suggest that the Casagrande method yields c_v values that are 0.5 to 1.0 times those computed using $k_{v,measured}$ which is consistent with results reported by Mesri et al. (1994). In comparison, Taylor's method results in c_v values that are 1.0 to 2.0 times those computed using $k_{v,measured}$. These results allow no definitive conclusion to be drawn regarding the efficacy of one curve-fitting method over another.

- 2) The primary consolidation is compared with pore water pressure measurements to determine which curve-fitting procedure more appropriately predicts the end of primary settlement (d_{100}). Since Taylor and Casagrande's methods both employ similar techniques to calculate d_0 and therefore usually result in the same values (Sridharan et al. 1987), it follows that whichever method more accurately predicts d_{100} can be assumed to produce a more realistic c_v . To establish the end point of primary consolidation, a singly drained oedometer test is conducted and pore water pressure measurements are recorded at the impermeable base. Robinson (1999) conducted oedometer tests with permeability measurements on four types of soil (kaolinite, red earth, illite and bentonite) and found that the end of primary consolidation evaluated using Casagrande's method ($d_{100,C}$) more closely aligned with pore pressure measurements ($d_{100,pp}$) than the end of consolidation determined using Taylor's method ($d_{100,T}$) where $d_{100,T} \approx 0.85d_{100,pp}$. These results are supported by those found in similar studies (Mesri et al. 1999b, Al-Zoubi 2010), which suggest Casagrande's method may yield a better value of c_v than Taylor.

4.2.2. Limitations of current methods

Perhaps the biggest shortcoming of most curve-fitting methods lies within their calculation of c_v – the correlation between experimental and numerical settlement-time curves is used to calculate c_v , but for only *one* point (e.g. at 50% or 90% consolidation for Casagrande and Taylor methods, respectively). As a result, the user has no indication as to whether this predicted value of c_v is valid for the entire consolidation period as a whole. That is, if the user were to plot the experimental percentage of consolidation settlement versus time factor calculated using the predicted value of c_v , would the results align with Terzaghi's average degree of consolidation ($U - T$) curve at all times? To illustrate the importance of assessing the validity of predicted c_v values in this manner, two oedometer tests were conducted on a rapidly consolidating material comprising of 50% sand and 50% kaolinite (designated as K_{50}). The applied pressure was increased from 28 kPa to 444 kPa with LIR of unity. The properties of the clay are shown in Table 4.1 (column one). Values of c_v were calculated using the conventional Casagrande and Taylor curve-fitting procedures and fell within a realistic range of 2-3 m²/yr and 8-12 m²/yr, respectively. The experimental data, for all increments, were then converted into average degree of consolidation (U) and time factor (T) format using the following expressions:

$$U = \frac{d(t) - d_0}{d_{100} - d_0} \quad (4.4)$$

$$T = \frac{c_v t}{H(t)^2} \quad (4.5)$$

where $d(t)$ = dial gauge reading or settlement observed at time t , and $H(t)$ = thickness of the tested specimen at t (i.e. $H(t) = H_0 - d(t)$ where H_0 = sample thickness immediately prior to load application).

When Casagrande's c_v values were used to plot the experimental results against the theoretical percentage settlement curve as shown in Figure 4.1(a), a very poor fit was observed, although as expected, all the experimental points nicely aligned with theory at exactly 50% consolidation. The same exercise was repeated using Taylor's predicted c_v values and a significantly better fit was achieved, as shown in Figure 4.1(b). However, it is important to take note of the portion of the overall settlement-time data that Taylor's method actually attributes to primary consolidation. As shown in Figure 4.2(a), the values of d_0 predicted by each method agree quite well.

Taylor's method consistently results in a significantly smaller value of d_{100} – that is, the end of primary settlement is assumed to occur much earlier during consolidation. By predicting a significantly lower d_{100} , Taylor's method incorporates a significantly reduced portion of the settlement-time curve, thereby increasing the probability of a better correlation between experimental and theoretical results, as less data points are used overall.

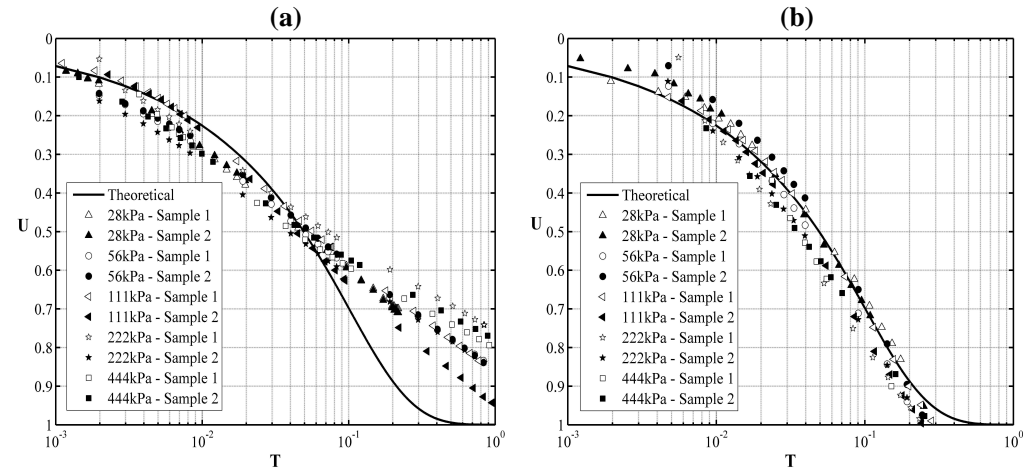


Figure 4.1 – Comparison between experimental and theoretical results using values of c_v calculated from (a) Casagrande and (b) Taylor curve-fitting methods

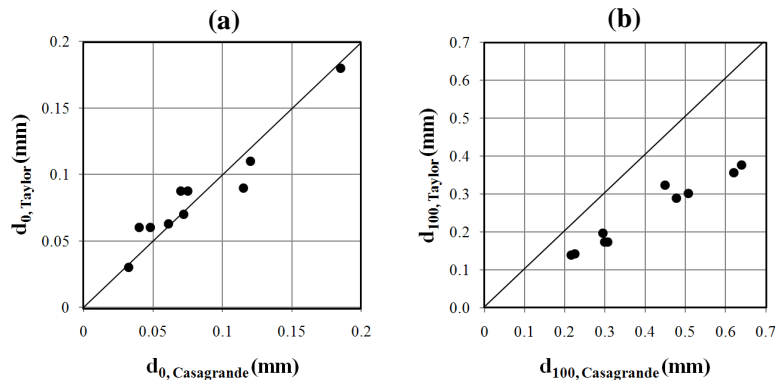


Figure 4.2 – Comparison between key curve-fitting values derived using Taylor and Casagrande's curve-fitting methods; (a) d_0 and (b) d_{100}

The proportion of laboratory test data that is actually attributed to primary consolidation by each method is graphically shown in Figure 4.3, where the total settlements (which include immediate consolidation and creep components) were measured over a period of 24 hrs. The applied pressures are also shown in the figure.

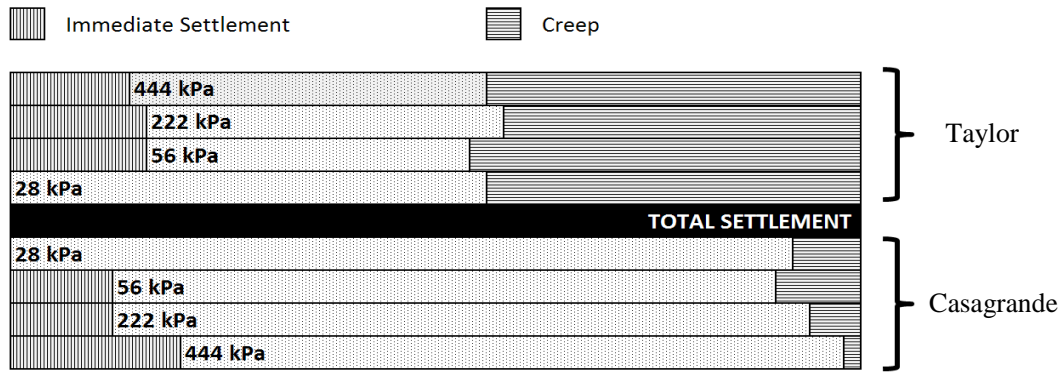


Figure 4.3 – Proportion of total settlement over a 24 hr period attributed to primary consolidation by each curve-fitting method

Once immediate and primary consolidation settlements have been isolated, logically the remaining settlement must be due to creep. Thus, for the case in question, Taylor's method predicts that a much larger portion of the 24 hr settlement is due to creep, in comparison with Casagrande's method, as shown in Figure 4.3.

Without resorting to more cumbersome methods of validation such as pore pressure or permeability measurements during consolidation, it is possible to assess the reliability of predicted c_v values by simply plotting the resulting percentage settlement curve against Terzaghi's $U - T$ curve and observing the correlation, as in Figure 4.1. This exercise was repeated for three different types of reconstituted, normally consolidated fine soil; a mixture of 50% Kaolinite and 50% very fine sand (K_{50}), a mixture of 60% Kaolinite and 40% coarse sand (K_{60}), and dredged mud obtained from the Townsville Port (DM). The properties of each soil are shown in Table 4.1. For each test, the applied pressure was increased from 7 kPa to 888 kPa with LIR of unity, with the exception of the K_{50} soil, which was only loaded from 28 kPa to 444 kPa.

Table 4.1 – Soil properties

Property	K_{50}	K_{60}	DM
Specific gravity	2.36	2.51	2.62
Liquid limit (%)	53	35	83
Plastic limit (%)	37	23	36
Plasticity index (%)	16	12	47
Sand (%)	49	39	9
Silt (%)	11	20	41
Clay (%)	40	41	50
Linear shrinkage (%)	5	6	18
USCS Symbol	MH	CL	CH

By converting each set of experimental data to $U - T$ form using the calculated c_v , d_0 and d_{100} values, it is possible to quantify the ‘fit’ between experimental and theoretical data through calculation of the root mean square (RMS) error. The RMS error can be determined using the following equation:

$$\varepsilon^2 = \frac{\sum_{n=1}^N (U_{Theor,n}(T) - U_{Exp,n}(T))^2}{N} \quad (4.6)$$

where $U_{Exp,n}$ = percentage settlement from experimental results (evaluated using d_0 and d_{100}) at time t during consolidation, $U_{Theor,n}$ = theoretical percentage settlement at that same time during consolidation (using the calculated c_v to convert t to time factor T) and N = total number of data points collected during testing. Since primary consolidation is the only type of settlement being considered, the RMS error is calculated for the settlement-time data points that fall within the limits of d_0 and d_{100} only.

4.2.3. Evaluation of c_v reliability

The values of c_v and key points during consolidation (namely d_0 and d_{100}) were evaluated using four different techniques; Taylor’s root-time method, Casagrande’s log-time method, Cour’s inflection point method (Cour 1971, Mesri et al. 1999a), and a new method developed during this investigation which utilises computational iterations to determine c_v , rather than the subjective manual curve-fitting or observation. For each of the load increments and all three soils shown in Table 4.1, the experimental $U - T$ data was plotted against the theoretical curve from which the RMS error was calculated. Values of RMS error ranged from 0.007 (indicating a very good fit) to 0.2 (indicating a very poor fit). Three example sets of $U - T$ curves are shown in Figure 4.4 to demonstrate the quality of fit associated with RMS errors of 0.166, 0.04 and 0.016.

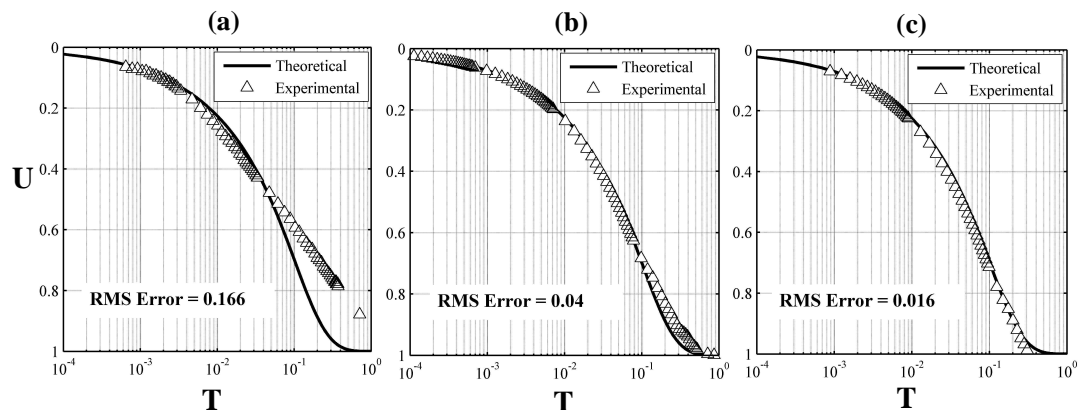


Figure 4.4 – Type of fit associated with RMS errors of (a) 0.166, (b) 0.04, and (c) 0.016

Although comparisons between experimental data and theoretical predictions in the form of average degree of consolidation and time factor exist in literature (e.g. Prasad and Rao 1995), they are few and far between, and to the authors' knowledge, have never been assessed in terms of root mean square error.

4.2.4. Automation of curve-fitting methods

To limit the degree of subjectivity introduced by manual curve-fitting (i.e. identifying creep, drawing tangents etc.), the following curve-fitting methods were automated by implementing their key components within the program MATLAB, which subsequently completed the curve-fitting process; Taylor's square-root of time method, Casagrande's log-time method, Cour's inflection point method, and a new method developed during this investigation. To do this, the following portions of the settlement-time curve needed to be defined;

- The early stage 'parabolic' region of the settlement-time curve;
- The inflection point or maximum gradient; and
- The 'straight-line' creep portion (when viewing the plot in logarithmic scale).

Calculate mode

The program that was developed using MATLAB, Cv_Calculate[®], was designed with two modes; a 'Calculate' mode, and an 'Analyse' mode, shown in Figure 4.5. When in Calculate mode, time-settlement data was analysed (using a variety of different curve-fitting methods) to give the following key output parameters;

- d_0 – dial gauge reading at 0% consolidation (mm)
- d_{100} – dial gauge reading at 100% consolidation (mm)
- c_v – coefficient of consolidation (m^2/yr)
- s_{total} – total settlement that occurred within the loading increment (mm)

In order to conduct this analysis, the following input parameters were required;

- Method – This drop-down box gives the user the option of analyzing the settlement-time data using a number of methods, namely; Casagrande, Taylor, Cour, Asaoka, Lovisa.
- Auto/manual – This set of radio buttons presents the user with an option of manual analysis. If this radio button is selected, the program will deliver a graph of time-settlement (in logarithmic or square-root time scale) that the user can analyse manually (i.e. draw the relevant tangents etc.). When viewing data for the first time, it is recommended that the 'manual' option be selected for a brief preliminary view

of data. This will provide information regarding immediate settlement, and whether this needs to be accounted for in the analysis.

- Initial thickness – This parameter is the thickness of the consolidating sample (mm) at the beginning of the load increment in question.
- Dial gauge number – The MATLAB program was coded to ensure minimal data manipulation was required. The James Cook University geotechnical laboratory in which these experiments were conducted contained four oedometers that all exported data simultaneously. As a result, an excel datasheet containing one column for time and four columns for relevant settlements of each oedometer was generated for each applied pressure increment. Instead of extracting the relevant data, this excel spreadsheet could be directly loaded into the program, and the appropriate dial gauge/oedometer number selected so that the correct set of settlement data was analysed.
- Excel file name – The name of the excel spreadsheet containing raw data automatically logged during testing is inputted in this dialogue box.
- Was there significant immediate settlement? – When identifying the initial parabolic region of the time-settlement curve, significant settlement needed to be excluded from the data. If a large portion of settlement occurred instantaneously during testing, the user has the option to ‘check’ the significant settlement box. In doing so, a default number of data points (5) are removed from the settlement-time data, thereby excluding the immediate settlement. When the box is checked, another input box also appears which gives the user the option of increasing the number of data points to exclude.

Cv_Calculate[®] was used to analyse data obtained from a number of different soil types. Whilst some of these soil types generated data that resembled the ideal ‘s-shaped’ curve (when in logarithmic scale) characteristic of primary consolidation, others exhibited curves that bore little resemblance to the ideal. In fact, when analyzing these datasets manually, it was often difficult to isolate the correct regions in which to draw the appropriate tangents. By using *Cv_Calculate*[®] to analyse the data instead, this element of user subjectivity was eliminated. Furthermore, the program was more than capable of analyzing these difficult cases, and had an overall success rate of 94% (when using the Taylor and Casagrande methods). In many cases, the Cour inflection point method failed to generate a value of c_v . However, this was no fault of the program, but was rather due to the absence of a clear inflection point within the experimental data.

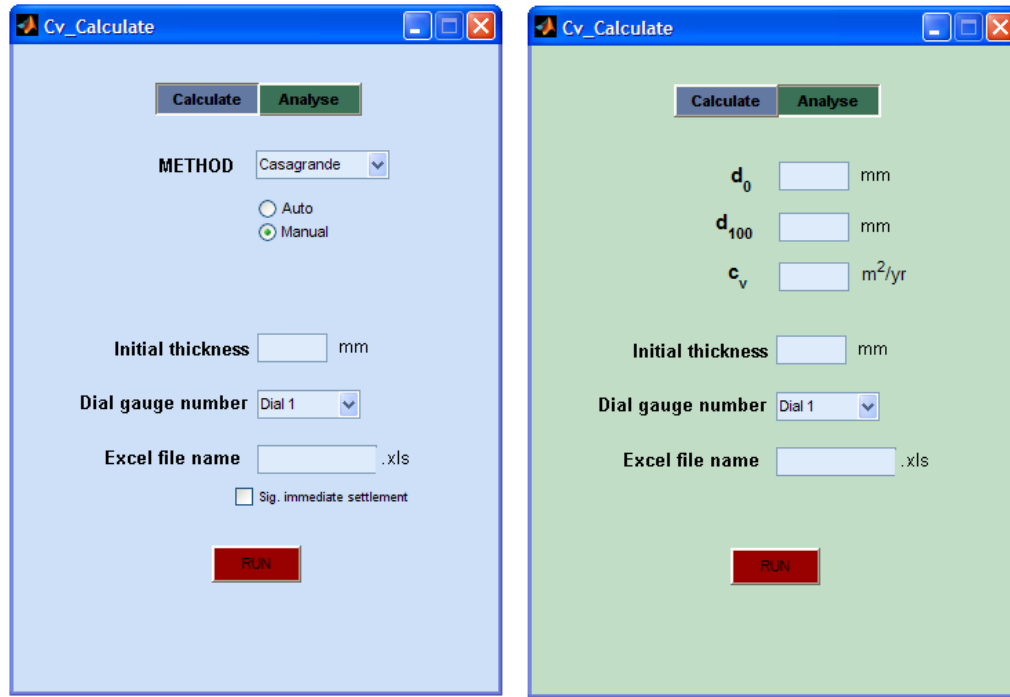


Figure 4.5 – Program used to analyse consolidation data

Taylor and Casagrande methods

The Taylor square root of time method generally yields larger values of c_v when compared with those determined using Casagrande's log-time method (Olson 1986, Sridharan et al. 1987, Pandian et al 1994).

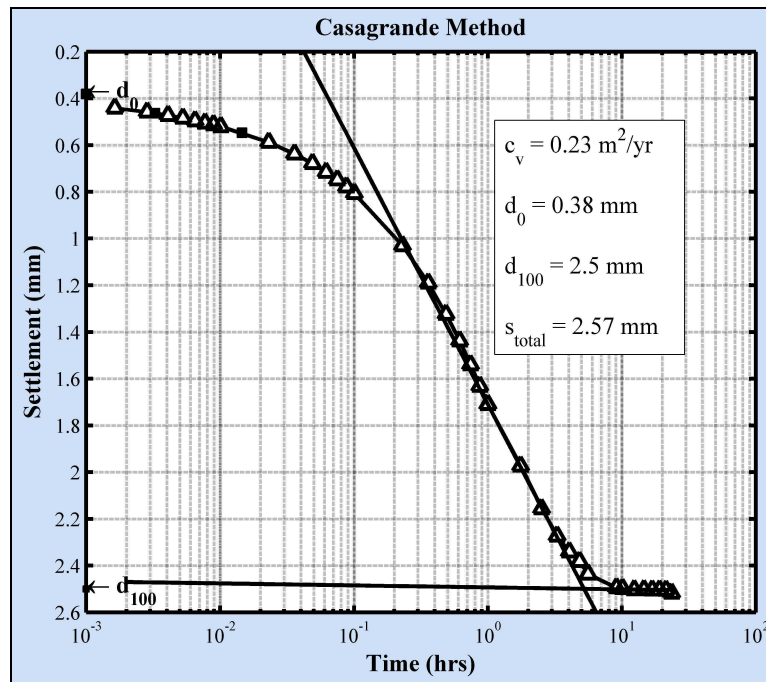


Figure 4.6 – Example analysis using Casagrande's log-time method

These methods are widely used, and will be elaborated upon in further detail later in this thesis. An example graphical output produced after selecting the Casagrande method is shown in Figure 4.6, which was obtained by analyzing the settlement-time data that resulted from applying 222 kPa to the *DM* soil. For the same set of data, the graph produced after selecting the Taylor method is shown in Figure 4.7.

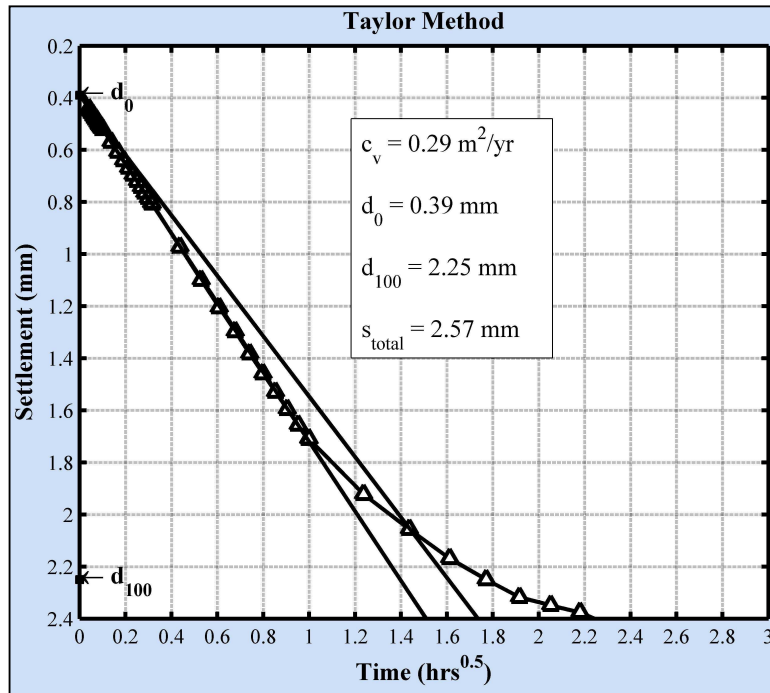


Figure 4.7 – Example analysis using Taylor's root-time method

Asaoka method

In 1978, Asaoka developed an approach to estimate the final consolidation settlement and coefficient of consolidation from settlement-time data obtained during a certain time period. The procedure for determining c_v using this method is summarised as follows;

- 1) Choose a time increment Δt to define the settlements d_t at times $t_0 + i\Delta t$ ($i = 0, 1, 2, \dots$).
- 2) Plot d_t versus d_{t-1} .
- 3) Draw a line through the points (d_t, d_{t-1}) and observe the settlement value corresponding to the point of intersection of the drawn line with a 45° line, indicating $d_t = d_{t-1}$. This will give the theoretical final settlement d_{100} .
- 4) Measure the slope of the line, β .
- 5) Calculate c_v using the following equation:

$$c_v = -C \frac{H^2}{\Delta t} \ln \beta \quad (4.7)$$

where C is a constant which is $5/12$ if singly drained, and $5/48$ if doubly drained, and H is the layer thickness.

For the same set of settlement data used previously, the graph shown in Figure 4.8 was obtained after selecting the Asaoka method in Cv_Calculate[®].

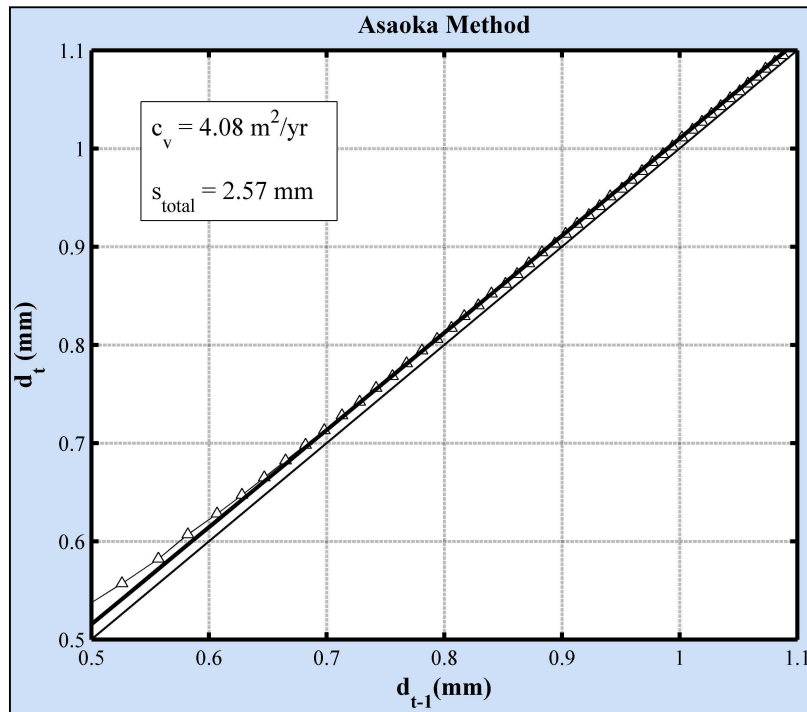


Figure 4.8 – Example analysis using the Asaoka method

As expected, the value of c_v generated using the Asaoka method was significantly greater than the values generated using the Taylor and Casagrande methods. This trend was consistent for all analyses, regardless of soil type.

Cour method

The inflection point method proposed by Cour (1971) involves the identification of an inflection or maximum gradient on the log-time plot of settlement data, which is known to correspond to 70% consolidation, according to Terzaghi's consolidation theory. It is suggested that the inflection point be determined one of two ways; by visual observation, or using the tangent method where the inflection point is selected as the point at which the absolute value of the slope of the tangent to the settlement-time curve is the maximum. Again, Cv_Calculate[®] was useful here as the degree of subjectivity associated with selecting the inflection point was removed. An output similar to that shown in Figure 4.9 was

generated for each settlement-time curve to evaluate c_v . Here, two graphs are provided; a graph of settlement versus time with the inflection point highlighted, and a graph of gradient versus time to illustrate how appropriate this inflection point is. In select cases, where the inflection point was absent, it was difficult to evaluate c_v using the Cour method. This phenomenon was also observed by Mesri and Godlewski (1977) who concluded that the Cour method is inapplicable for certain types of settlement-time curves.

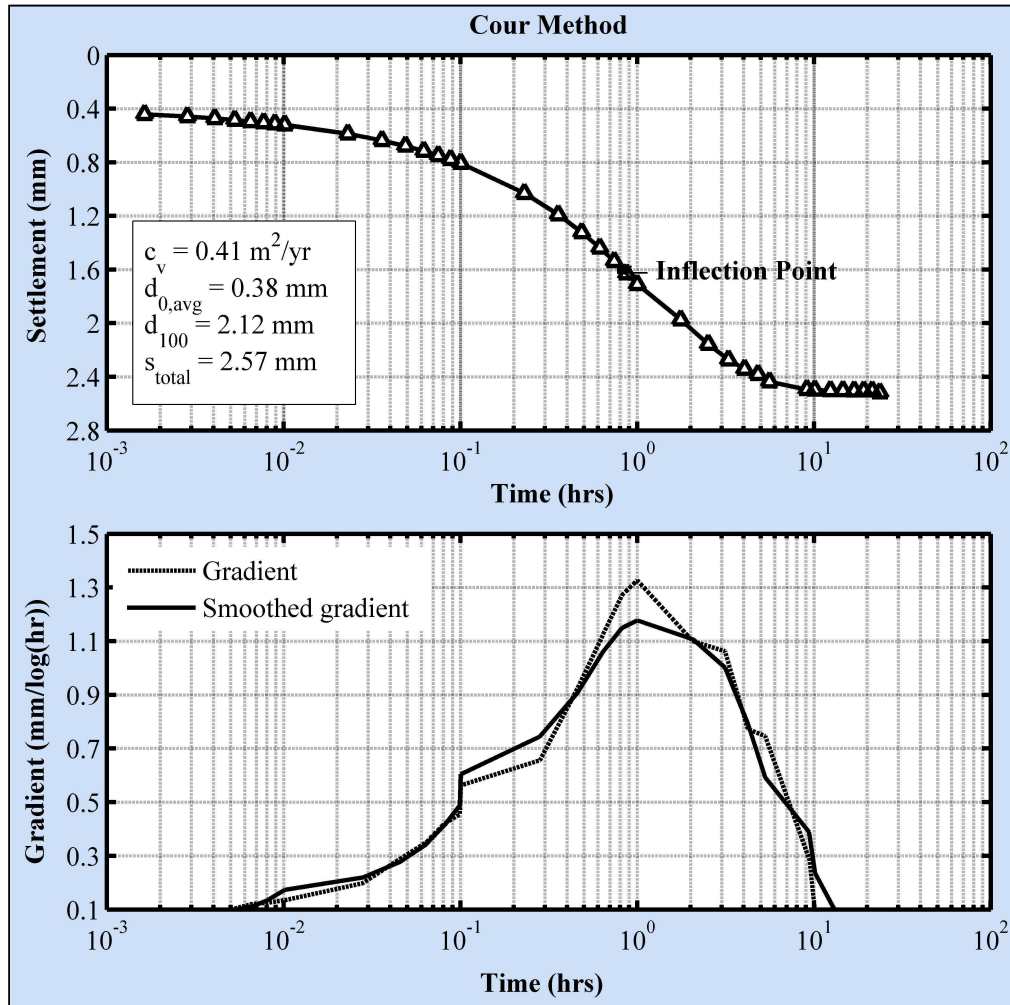


Figure 4.9 – Example analysis using Cour’s inflection point method

It is important to also address how the parameters d_0 and d_{100} shown in Figure 4.9 were obtained using the Cour method. As outlined previously, the Cour method culminates in a settlement value that corresponds to 70% primary consolidation. No further information regarding initial or end of primary settlement is actually required to calculate c_v – the only parameter resulting from the Cour method is d_{70} . Without another known reference point of

consolidation (i.e. d_0 or d_{100}), it is impossible to calculate the percentage consolidation (U) for the remaining settlement-time data and conduct a subsequent comparison between experimental and theoretical results. However, given the history of consistency between d_0 values calculated using the Taylor and Casagrande methods, it was considered appropriate to adopt an average of these two d_0 values ($d_{0,avg}$) and use this value to assess the c_v obtained using the Cour method. Using this value of d_0 and the corresponding value of d_{70} obtained during the analysis, it is easy to calculate a subsequent d_{100} value.

Proposed method for comparison – The variance method

A new approach was also developed during this investigation and implemented in Cv_Calculate[®], which draws upon some elements of previous curve-fitting methods whilst relying upon a ‘trial-and-error’ type procedure which was quantified using internal RMS error calculations. Since both Taylor and Casagrande’s methods utilise the initial parabolic nature of the settlement-time curve, it is not surprising they often produce similar (if not identical) values of d_0 . Consequently, the value used for the onset of primary consolidation (d_0) was the same as that adopted to analyse the c_v determined using the Cour method. This value is simply the average of the two d_0 values evaluated using the Taylor and Casagrande methods, denoted by $d_{0,avg}$.

When evaluating the end of primary settlement (d_{100}) a very different approach was used. The inconsistencies between values of d_{100} determined using various curve-fitting procedures suggest the traditional method of identifying graphical characteristics of the settlement-time curve to calculate this key parameter are at times inadequate. The proposed method for calculating d_{100} involved the following steps;

- 1) A wide and conservative range of possible values for d_{100} was selected. This range was arbitrarily divided into N evenly spaced points within the limits of $d_{100,min}$ and $d_{100,max}$:

$$d_{100,min} = d_{0,avg} + \frac{(d_f - d_{0,avg})}{2} \quad (4.8)$$

$$d_{100,max} = d_f \quad (4.9)$$

where d_f = dial gauge reading or settlement at the conclusion of the oedometer test.

This gives $1 \times N$ possible values for d_{100} . It was found that $N = 20$ was sufficient for most cases.

- 2) For each value of d_{100} within the N-point array (denoted by $d_{100,n}$), the settlement data was converted to percentage consolidation using the conventional expression for U :

$$U_{Exp} = \frac{d - d_{0,avg}}{d_{100,n} - d_{0,avg}} \quad (4.10)$$

In the oedometer tests reported herein, for every load increment where the settlement was recorded every second for 24 hours, up to 86,400 data points could be expected. If D represents the total number of data points, this step will produce a matrix of $D \times N$ values for U_{Exp} as shown in Figure 4.10.

	$d_{100,1}$	$d_{100,2}$	$d_{100,3}$	\dots	$d_{100,N}$
1	$U_{1,1}$	$U_{1,2}$	$U_{1,3}$	→	$U_{1,N}$
2	$U_{2,1}$	$U_{2,2}$	$U_{2,3}$	→	$U_{2,N}$
	↓	↓	↓		↓
D	$U_{D,1}$	$U_{D,2}$	$U_{D,3}$	→	$U_{D,N}$

Figure 4.10 – Schematic representation of Step 2; Calculating U_{Exp} using values of $d_{100,n}$

Here, $U_{20,8}$ means the degree of consolidation computed at the 20th data point using the 8th value of d_{100} . The value of T from Terzaghi's $U-T$ curve that corresponded to each value of U_{exp} was then explicitly determined. This was done by calculating a 'master' array of $U-T$ values using the solution to Terzaghi's consolidation equation in MATLAB. Here, a very large number of T values (upwards of 20,000) was used to evaluate U_{Terz} . Then, the value of T for which U_{Theor} most closely matched a particular value of U_{Exp} from this array was selected as the value of T that corresponded to U_{Exp} . As a result, this step results in a matrix of $D \times N$ values of T .

- 3) An individual value of c_v was then calculated for each data point using each of the T values determined in Step 2. Essentially, the experimental points were all forced to fit

the theoretical curve, and the c_v values that allowed this fit to be achieved were evaluated. Theoretically, if the ‘true’ value of d_{100} is used, these values of c_v should all be equal. However, as is often the case when applying theory to reality, experimental data are rarely ideal and a number of deviations from theory can be expected. As a result, the value of $d_{100,n}$ that produced the least *variance* in c_v values was reasonably assumed to be the ‘true’ end of primary settlement value. This ‘true’ value of d_{100} was established by calculating the variance in c_v values for each $D \times 1$ vector and adopting the value of d_{100} that produced the least variance, as demonstrated in Figure 4.11.

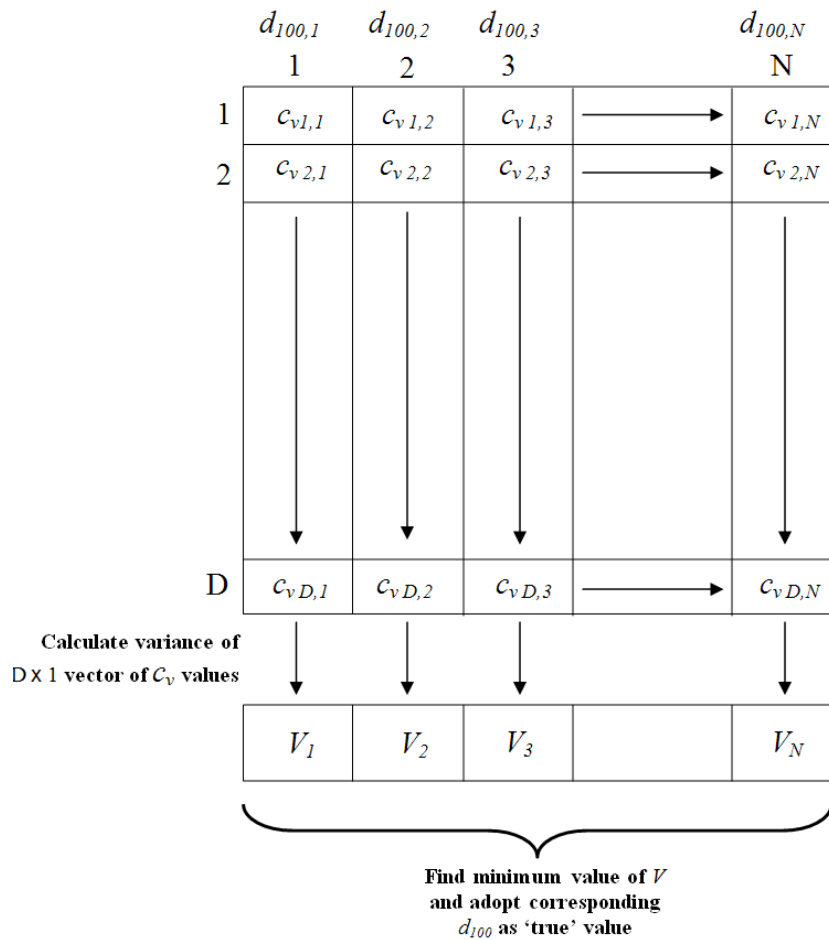


Figure 4.11 – Schematic representation of Step 3; Calculating d_{100} using the variance method

- 4) Once the ‘true’ value of d_{100} was established, the mean value of c_v was taken by averaging the entire array of c_v values that corresponded to that particular value of d_{100} . Finally, a more realistic value of c_v was determined by adjusting the mean value of c_v

by some factor (usually $\pm 10\%$ of the mean c_v value). This adjustment factor was selected based on a trial-and-error process similar to that used in Step 2, where a range of c_v values within the immediate vicinity of the mean c_v were selected, and the RMS error was calculated for each value of c_v (using the ‘true’ value of d_{100}). The value of c_v that produced the smallest RMS error was assumed to be the most realistic value of c_v .

An example output generated during the implementation of this method is shown in Figure 4.12.

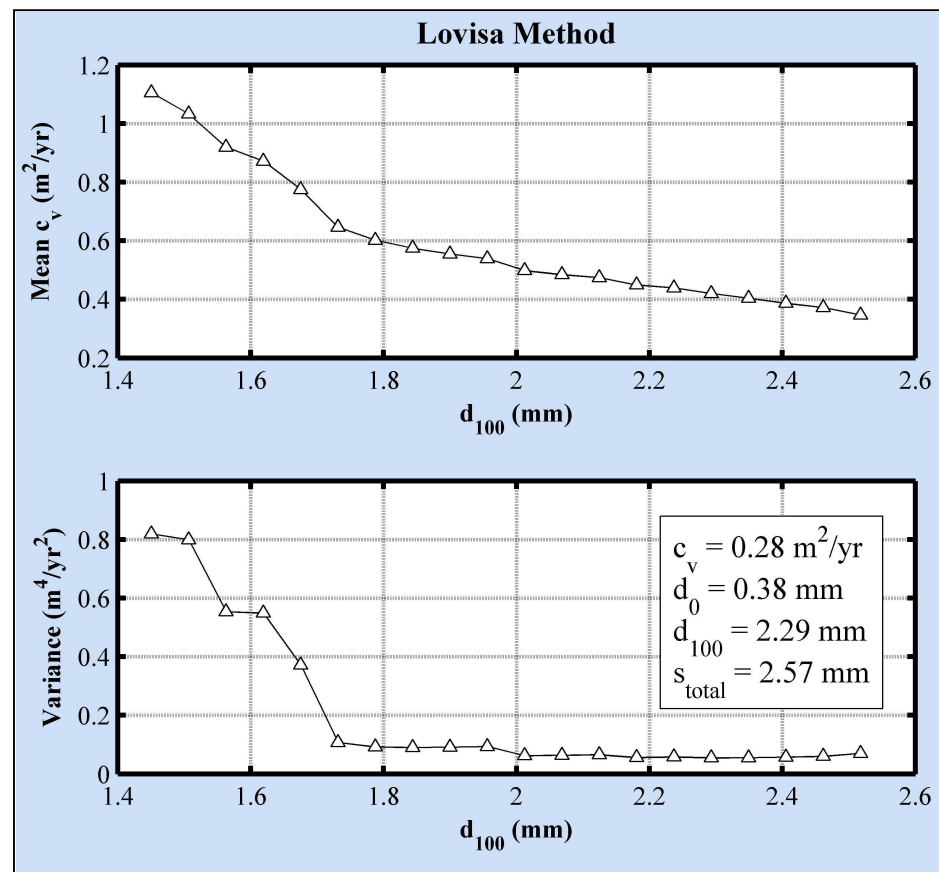


Figure 4.12 – Example analysis using the variance (or Lovisa) method

Analyse mode

Once a dataset has been analysed using the ‘Calculate’ mode, the user has a choice to assess the output parameters (namely d_0 , d_{100} and c_v) in order to determine how valid the generated value of c_v is when compared with the data as a whole.

For further clarification, the RMS error which quantifies the fit between experimental and theoretical data is also provided. For example, using the values obtained via the Taylor method, the graphical output shown in Figure 4.13 was generated when in ‘Analyse’ mode.

All simulations conducted using Cv_Calculate[®] were completed within 4 seconds. When using the Taylor, Casagrande, Cour and Asaoka methods, the run-time was approximately 1.8 seconds. However, the Lovisa method took slightly longer due to the trial-and-error approach. When in ‘Analyse’ mode, the run-time was never more than 3 seconds.

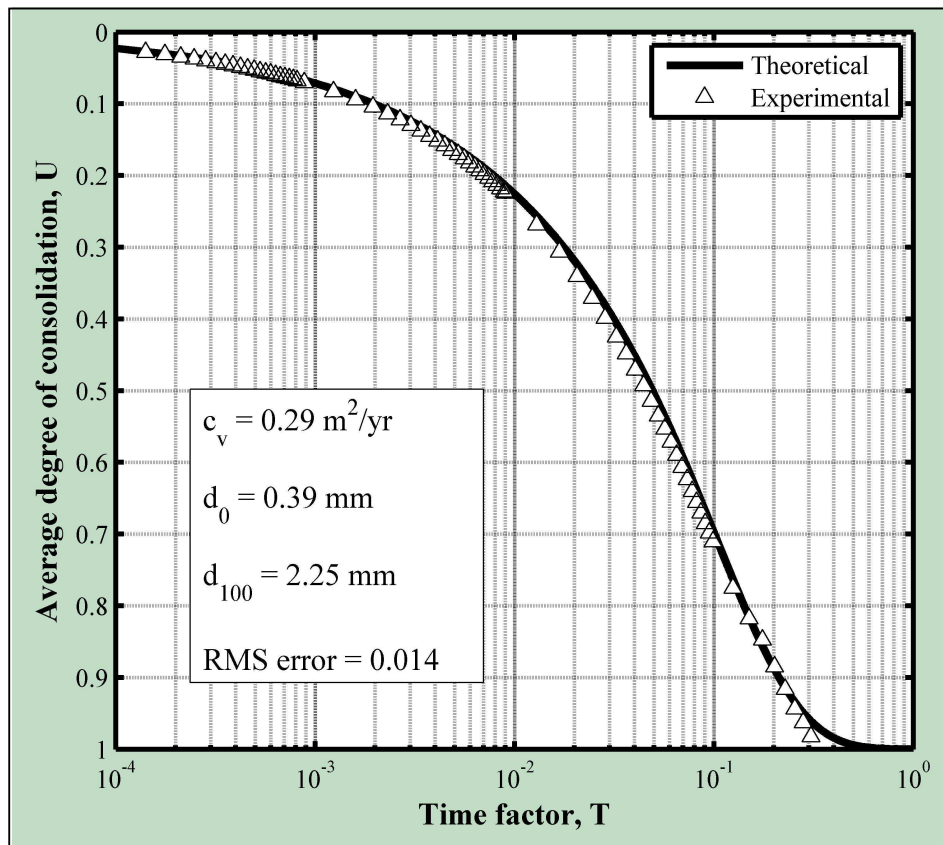


Figure 4.13 – Example fit between theoretical and experimental results

4.2.5. Comparison between experimental and theoretical results

Using Cv_Calculate[®], the values of c_v obtained by the three methods outlined previously (namely, Casagrande, Taylor and Cour) were then compared with the value of c_v obtained using the Lovisa method for each of the soils described in Table 4.1. The validity of each of the c_v values was also assessed using the ‘Analyse’ mode of Cv_Calculate[®]. In order to conduct this assessment, however, three parameters were required; d_0 , d_{100} and c_v . For this reason, the Asaoka method was excluded from the comparison.

The shape of settlement-time curves that occurred upon consolidation varied depending on the type of soil tested. This has been observed by previous researchers (e.g. Sridharan et al. 1987, Mesri and Godlewski 1977, Robinson 1999) and can be broadly attributed to the properties of the soil. An example of the shape of settlement-time curve resulting from an oedometer test where each of the three soils was subjected to an applied pressure of 28 kPa is shown in Figure 4.14. Settlement readings were taken every second over a 24 hr period which resulted in a very large data set (upwards of 84,600 points). For clarity, only a few experimental points from each set of data have been plotted in Figure 4.14.

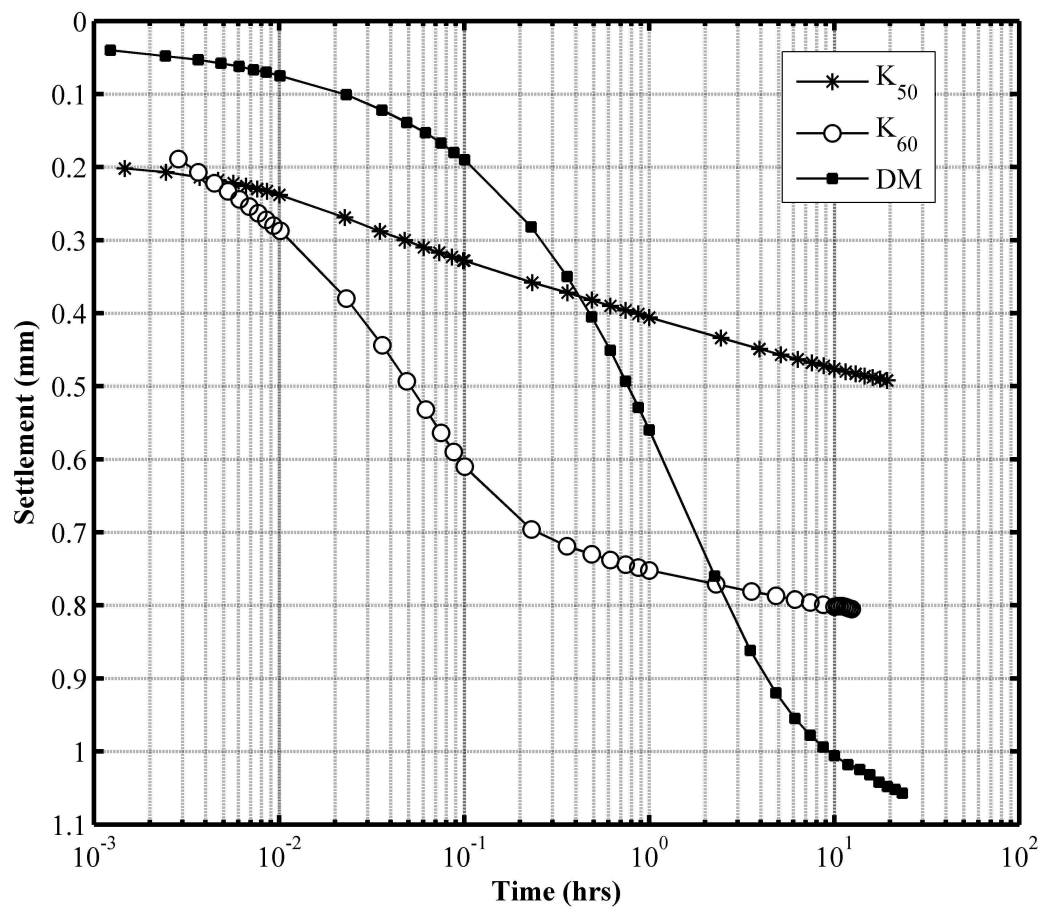


Figure 4.14 – Settlement-time curves for different soil types when consolidated under an applied stress of 28 kPa

As demonstrated in Figure 4.14, the K_{50} mix often produced a settlement-time curve that exhibited no distinguishable inflection point. This trend was observed for the entire range of applied stresses. The MATLAB program based on the Cour inflection point method subsequently failed in many cases. As a result, approximately 65% of the K_{50} data were unable to be examined using this method. Furthermore, the characteristic change in gradient at the onset of creep is also difficult to identify which makes the analysis of this data using

the other methods more difficult, with the exception of the Taylor method which does not require any information regarding secondary consolidation.

The d_0 values identified using the Taylor and Casagrande methods were consistently similar, for the three soils tested, as shown in Figure 4.15. This supports the adoption of an average value of d_0 when calculating c_v using the variance method (or Lovisa method) described herein.

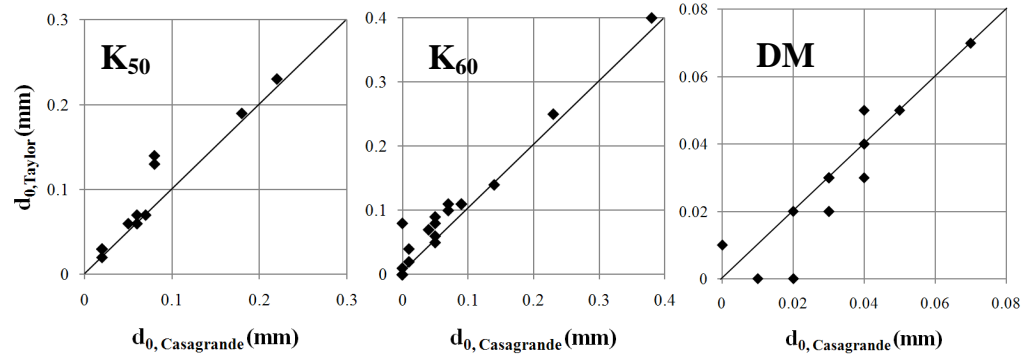


Figure 4.15 – Comparison between Taylor and Casagrande d_0 values for the three soils

The methods used by Taylor and Cour to pinpoint the end of primary settlement generally resulted in smaller values of d_{100} when compared with the values produced by the Casagrande method, which is evident in Figure 4.16. This trend is most pronounced for the K_{50} and DM soil types. For the K_{60} soil, values of d_{100} predicted by the Taylor, Cour and Lovisa methods are all generally in good agreement with the Casagrande d_{100} values. It can also be seen that the Lovisa method gives d_{100} values that are in closest agreement with Casagrande's d_{100} values, when considering all three soils.

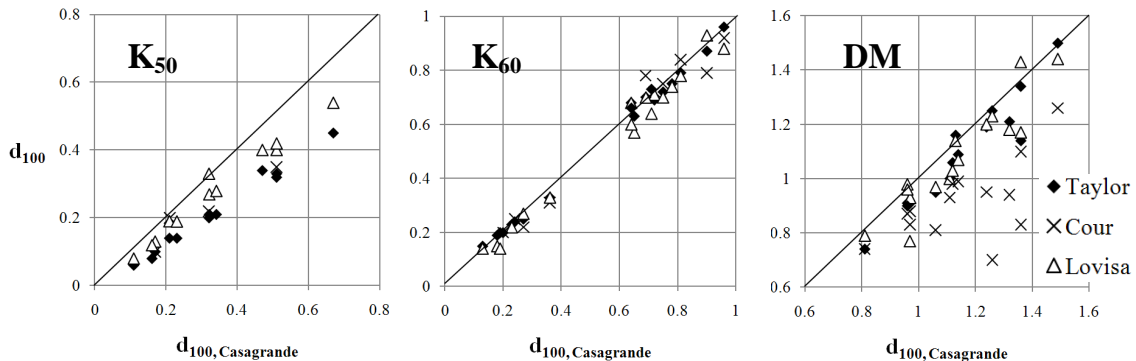


Figure 4.16 – Comparison between Taylor/Cour/Lovisa and Casagrande d_{100} values for the three soils tested (for stress range of 7 kPa to 888 kPa)

The effect of the conflicting values of d_{100} can be seen in the determination of c_v , the values of which are presented in Figure 4.17. For the K_{50} mix, Taylor's method often predicted a c_v value 3-6 times the magnitude of the value predicted by the Casagrande method. This was also observed for the DM soil, although to a lesser degree – values predicted by Taylor's method were only 1.2 times larger than their Casagrande counterparts. Taylor's method sometimes predicted a value of c_v that was *less* than that predicted by the Casagrande method (by a factor of 0.7 to 0.8) for the K_{60} mix.

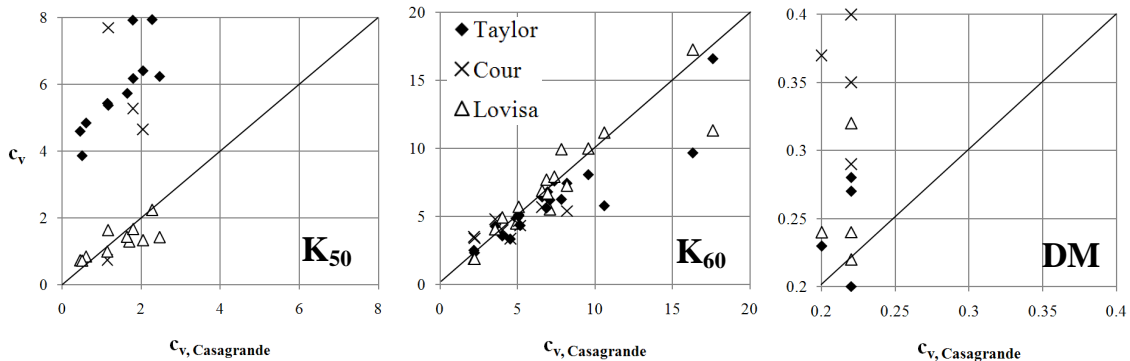


Figure 4.17 – Comparison between Taylor/Cour/Lovisa and Casagrande c_v values for the three soils tested (for stress range of 7 kPa to 888 kPa)

The predicted values of c_v and their corresponding RMS errors in relation to applied stress for the K_{50} soil are provided in Figure 4.18. The trend of increasing c_v with applied stress is evident regardless of the method used. Values of c_v calculated using the Lovisa method are generally in good agreement with those calculated using the Casagrande method. However, the corresponding RMS error associated with these values is significantly less for the Lovisa method when compared with the Casagrande method. This can be attributed to final step of the variance method which adjusts the mean c_v value by a certain factor, thereby resulting in a value of c_v that is more realistic.

Overall, the Taylor c_v values had the lowest RMS error and resulted in an experimental percentage settlement curve that most closely resembled the theoretical curve. However, the earlier statement regarding the portion of settlement that the Taylor method actually attributes to primary consolidation should be reiterated. By selecting a smaller segment of the overall settlement-time curve as primary consolidation, the probability of achieving a better fit is increased since less data points are used. In general, the lower RMS errors

associated with the Lovisa method, coupled with d_{100} values that are in close agreement with the Casagrande values, suggest that this method produces the most realistic value of c_v .

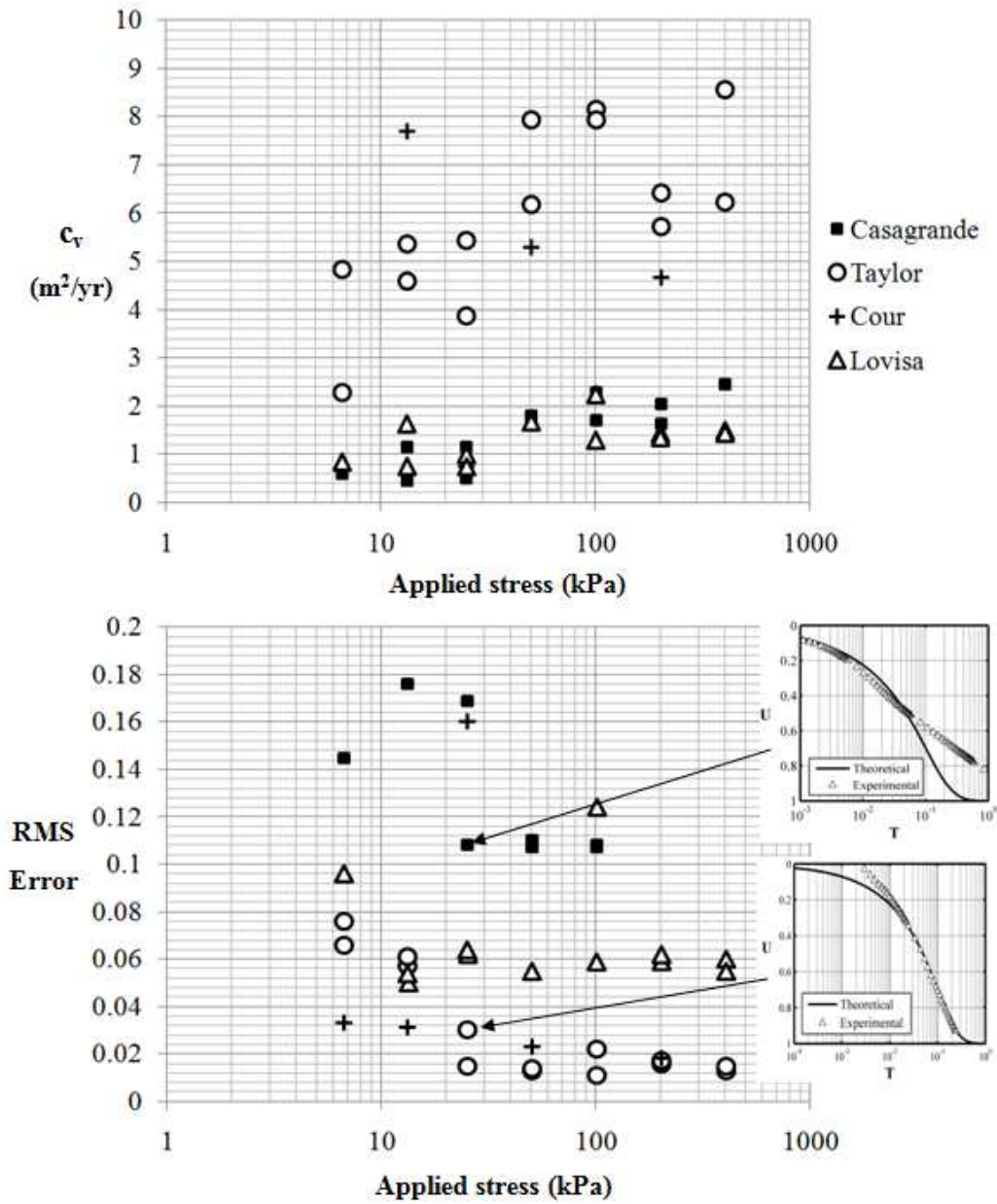


Figure 4.18 – Variation in predicted c_v values with applied stress and corresponding RMS error for K_{50} soil

A similar comparison between c_v values and applied stress along with the corresponding RMS error was also conducted for remaining two soils, K_{60} and DM , the results of which are shown in Figures 4.19 and 4.20, respectively. The increase in c_v with applied stress is

more pronounced for the K_{60} soil, which may be attributed to the significant percentage of coarse sand within the sample, in comparison with the much finer sand in the K_{50} sample.

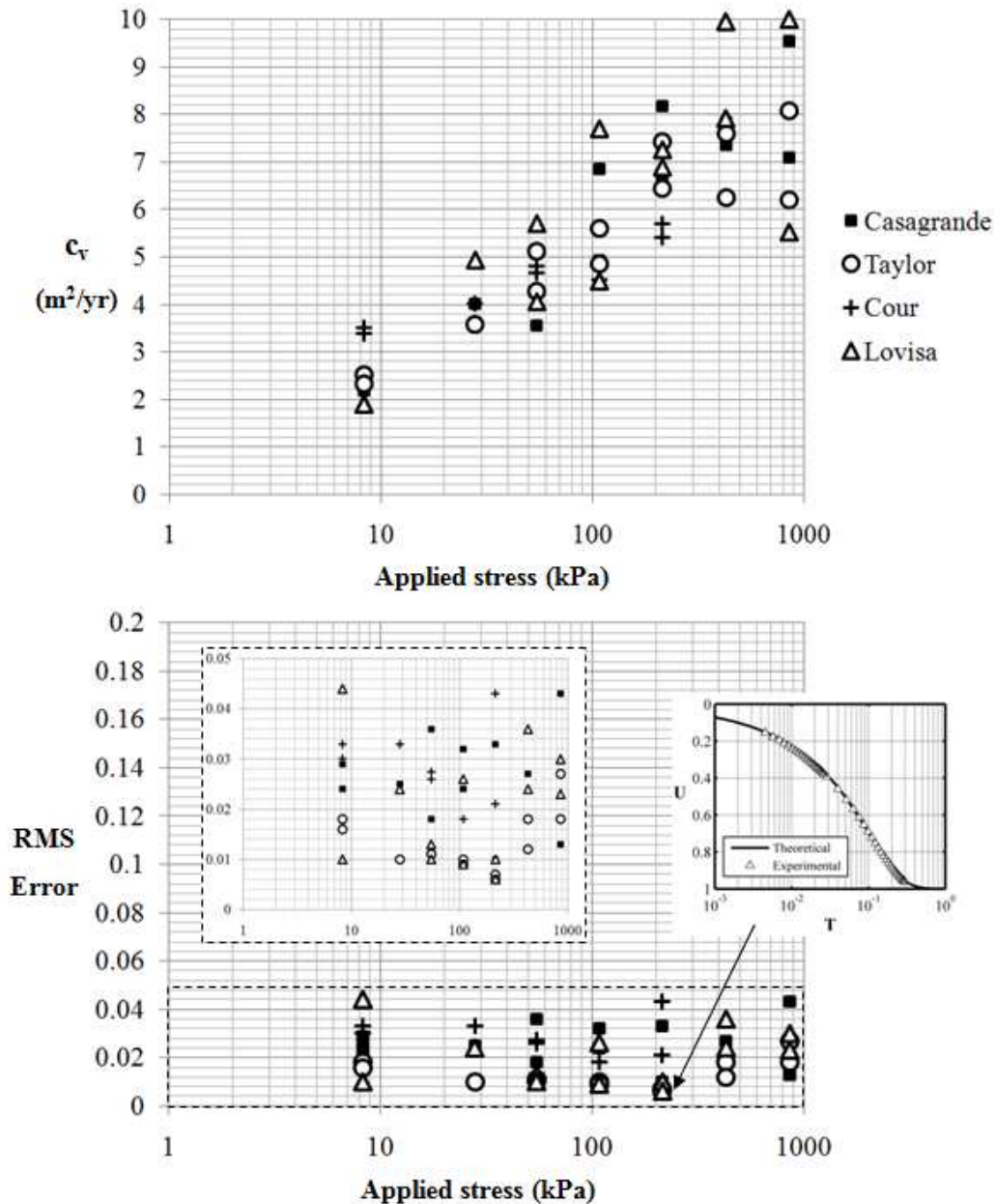


Figure 4.19 – Variation in predicted c_v values with applied stress and corresponding RMS error for K_{60} soil

The values of c_v determined using each method are all quite consistent within each stress increment, with the deviation between values becoming marginally greater as the applied stress increases. The RMS error for K_{60} is significantly less than that associated with K_{50} , implying that a better fit was achieved with the theoretical $U - T$ plots. Figure 4.19 also

shows the fit achieved between experimental and theoretical consolidation settlement using values calculated via the Lovisa method for one specific pressure increment where the RMS error was 0.006. It can thus be concluded that this soil type (60% Kaolinite, 40% coarse sand) more closely models the ideal consolidation behaviour predicted by Terzaghi's consolidation theory, in comparison with the K_{50} soil. The c_v and RMS error values for the DM soil are provided in Figure 4.20.

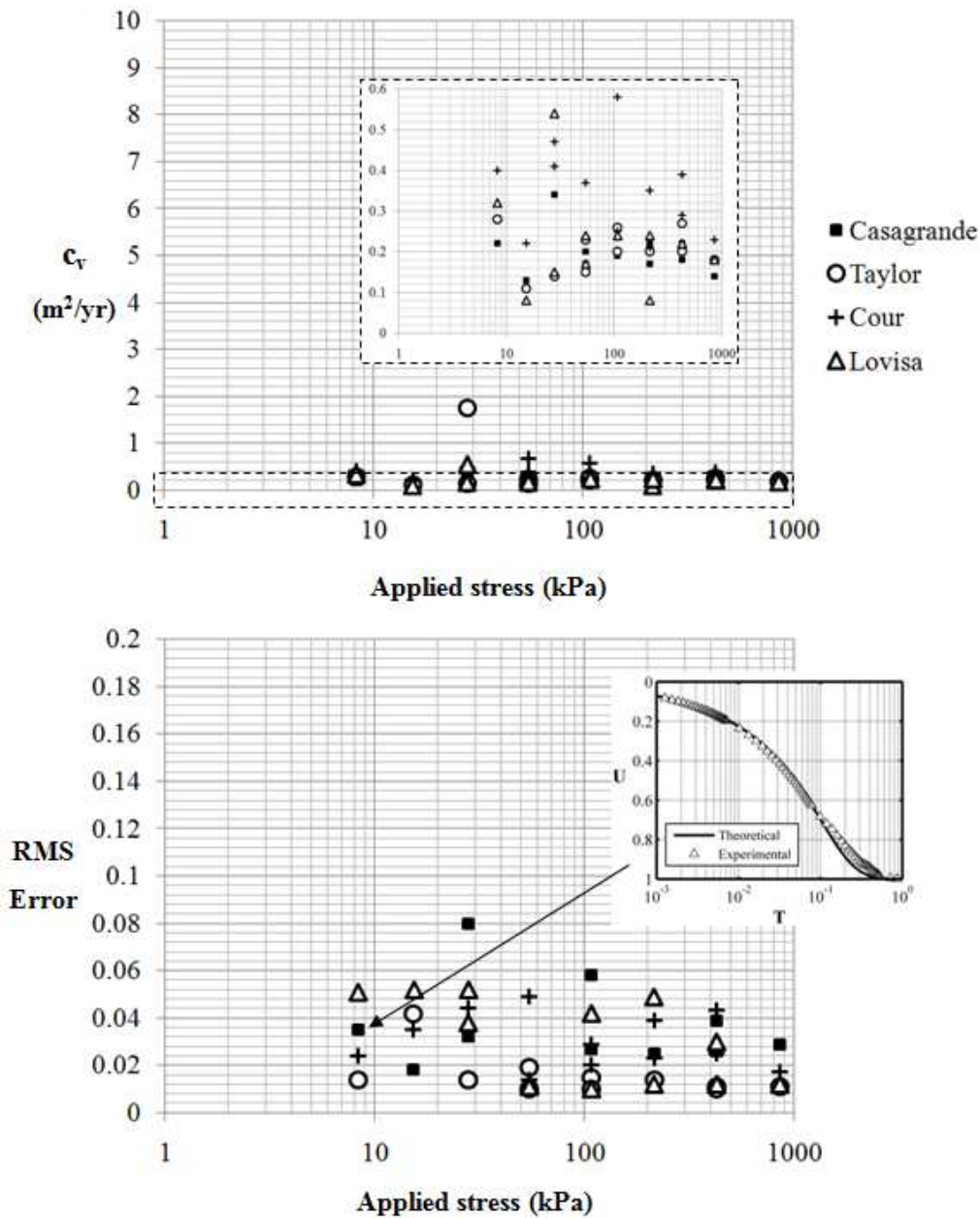


Figure 4.20 – Variation in predicted c_v values with applied stress and corresponding RMS error for DM soil

The coefficient of consolidation associated with the dredged mud was significantly less than the values of c_v associated with the K_{50} and K_{60} samples, often by an order of magnitude (discounting the c_v values predicted using the Cour method). With the exception of the Cour method, the Taylor, Casagrande and Lovisa methods all produced similar values of c_v . Since the rate of consolidation occurred much slower in comparison with the K_{50} and K_{60} samples, a larger portion of the primary consolidation settlement was able to be captured during testing. As a result, more weight should be given to the RMS errors associated with the DM c_v values, as these were determined using more available data points.

Although the Taylor method resulted in smaller RMS errors, the zone identified as primary consolidation is only a fraction of the actual primary consolidation. The actual region of primary consolidation appears to be more appropriately identified using the Casagrande method, which is supported by results gathered using the Lovisa method, where a similar region of primary consolidation was usually isolated. However, the lower RMS errors associated with the Lovisa method suggest that the corresponding values of c_v may be more realistic. This can be attributed to the type of approach used to determine c_v ; the Casagrande method ultimately fits only one point of experimental data to theory, whereas the Lovisa method utilises *all* data points to determine an appropriate value of c_v .

Thus, it can be concluded that the efficacy of the designated curve-fitting method is very much dependent upon the shape of the settlement-time curve generated during testing, and is thus dependent upon the type of soil tested (Crawford 1964). For soils that do not exhibit ‘ideal’ settlement-time curves, it is unreasonable to assume that the c_v calculated by fitting a single experimental point to theory is entirely accurate. When the values of c_v calculated using these single-point methods were used to convert experimental data into average degree of consolidation, a poor fit between Terzaghi’s average degree of consolidation curve and that generated from the experimental data was often observed.

It is also important to consider the effect of secondary compression (or creep) and how this may distort interpretation of laboratory test data when determining c_v . The curve-fitting methods along with the proposed computational method both rely on Terzaghi’s consolidation theory which applies to primary consolidation only. Such a situation is never realized in practice, and at best, the soil may abide by Terzaghi’s consolidation theory over certain specific stages of the consolidation process, and not throughout (Sridharan and Prakash 1995). This deviation between experimental results and theory may explain why

some curve-fitting methods fail to adequately evaluate a reasonable c_v , such as when the Casagrande method was used to analyse laboratory data obtained during tests on the K_{50} mix. Studies conducted by Sridharan et al (1995) showed that if creep is a dominant factor in consolidation, the resulting value of c_v predicted using this data will be less than the actual value.

4.3 Tall oedometer

Oedometers used for one-dimensional consolidation tests are proportioned such that their height/diameter ratio lies in the range of 0.17 to 0.40. Sometimes, it is desirable to test a soil specimen that has a significantly larger height to diameter ratio, where the wall friction has to be considered in the analysis. Such tall oedometers can become useful tools in consolidation tests, if the wall friction can be accounted for rationally.

4.3.1. Background

The standard oedometer test, also referred to as consolidation test or one-dimensional compression test, is a classical laboratory test used to determine consolidation and swelling parameters of a saturated soil specimen. The standard oedometer test is usually carried out on a cylindrical sample of saturated soil with dimensions of 75 mm diameter and 14-25 mm thickness. As specified in ASTM standards (ASTM D2435), the ratio of height to diameter of an oedometer sample should be greater than 0.17 (to avoid disturbance during trimming), but less than 0.4 to reduce the influence of friction along the lateral surface. By ensuring the sample dimensions remain within these limits, any effect of wall friction can be ignored and a uniform initial excess pore pressure distribution can be reasonably assumed. If the height of the sample is much greater than its diameter, stress transfer occurs between the soil mass and the adjacent rigid wall. As a result, a stress-redistribution process occurs where differential straining mobilizes shear stresses and transfers part of the applied pressure from the yielding soil mass to relatively stable neighboring non-yielding walls (Ting et al. 2010). This phenomenon is referred to as arching when dealing with mine stopes, where large underground voids in the form of rectangular prisms are backfilled with mine tailings. In cases where the height of the oedometer is much greater than its diameter, a uniform initial excess pore water pressure distribution can no longer be reasonably assumed. In order to identify the actual initial excess pore water pressure variation with depth and account for this in the analysis, the effects of wall friction must be considered.

Randolph et al. (1991) conducted a one-dimensional analysis of soil plugs in pipe piles. It was shown that, under drained loading conditions, arching within the pipe pile leads to

significant frictional capacity of the plug, thus causing the pile to fail in ‘plugged mode.’ However, when faster rates of loading are considered (i.e. undrained loading), the pile can fail in ‘unplugged mode,’ with shear failure occurring between the soil plug and the pile shaft. Ladd et al. (1994) investigated the effect of arching in relation to consolidation analysis of Boston Blue clay upon which an embankment was constructed. In this study, a decrease in total vertical stress at the centerline below the embankment occurred during consolidation, whilst the vertical stress increased beyond the toe of the embankment. Nguyen (2002) also noted that this decrease in total vertical stress under an embankment is contrary to the common assumption that the total vertical stress remains constant during consolidation. Consideration was given to arching effects in an analysis conducted by Helinski et al. (2010), who developed a coupled two-dimensional finite element model of mine backfilling with cemented tailings. An investigation on the effects of consolidation on arching in storage bins for cohesive materials was conducted by Guan (2007). The height to equivalent diameter for the model bin was 0.92, and results indicated that the location of arching was highly dependent upon the moisture content of the material, which in this case, was wheat flour.

4.3.2. Development of analytical solution

By using classical arching theory (Marston 1930, Terzaghi 1943), an analytical expression for the vertical stress distribution within an oedometer was developed, taking into account the effects of wall friction. Through this derivation, the height to diameter ratio of 0.4 proposed by ASTM standards can be verified. Furthermore, this analysis will provide information regarding the initial excess pore water pressure distributions accounting for wall friction, so that realistically, a soil can be consolidated in an oedometer of any given dimensions. Rather than increasing the diameter by impractical proportions just to test a sample of larger thickness, a tall apparatus with a more realistic diameter can now be used with due consideration to the friction. This has many practical applications, particularly when determining the consolidation properties of a fast-consolidating soil such as mine tailings. Furthermore, this analysis may prove useful in situations where slurry consolidation is carried out using tall consolidometers.

The proposed derivation is dependent upon the assumption that the vertical normal stresses are uniformly distributed at any depth, and that the adhesion between the oedometer walls and the soil is equal to the cohesion of the soil. Figure 4.21 shows a schematic diagram of a tall oedometer with height H and diameter D , which contains a dry soil of unit weight γ .

In order to determine the variation in effective stress with depth, the following forces acting on the horizontal element of thickness dz at a depth z from the top of the oedometer must be determined:

- The self-weight dW of the element

$$dW = \gamma \left(\frac{\pi D^2}{4} \right) dz \quad (4.11)$$

where γ = dry unit weight of the soil.

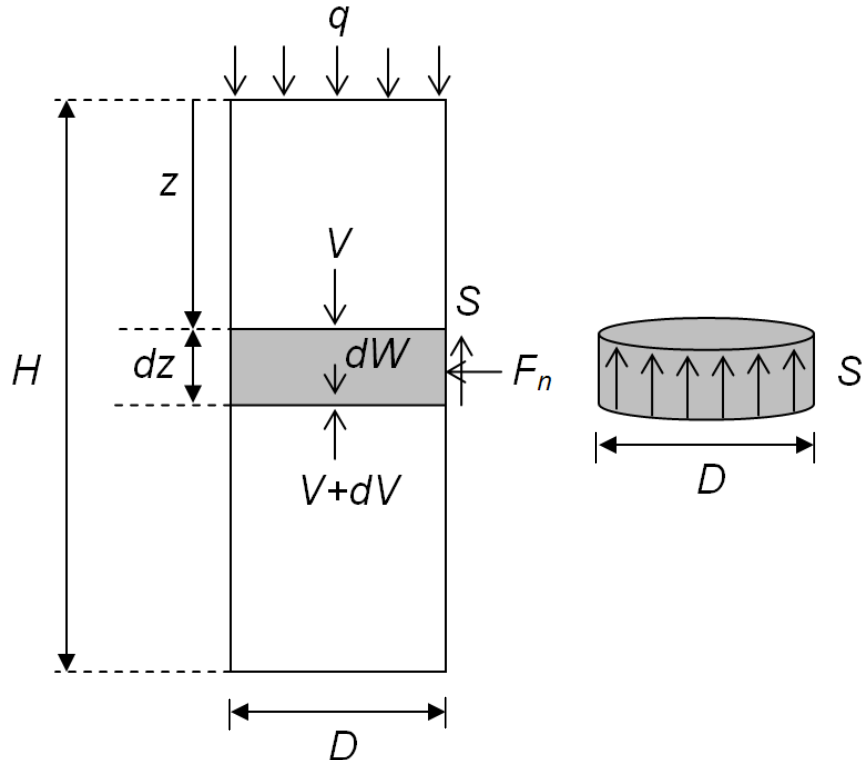


Figure 4.21 – Schematic diagram of tall oedometer

- The vertical force V acting on the layer at depth z :

$$V = \sigma_z \left(\frac{\pi D^2}{4} \right) \quad (4.12)$$

where σ_z = effective vertical stress at depth z . It also follows that the vertical force acting upward at the bottom of the element at position $z + dz$ must be

$$V + dV = (\sigma_z + d\sigma_z) \left(\frac{\pi D^2}{4} \right) \quad (4.13)$$

- The shear force S acting over the oedometer wall-soil interface at depth z :

$$S = \tau(\pi D)dz \quad (4.14)$$

where τ = shear stress along the wall at depth z . The maximum shear stress mobilized at the oedometer wall-soil interface can be determined using the Mohr-Coulomb strength criterion as

$$\tau = c + \sigma_x \tan \delta \quad (4.15)$$

where c = cohesion of the soil; σ_x = normal stress acting on the plane, and δ = interface friction angle. The relationship between the vertical and the horizontal stresses can be expressed as

$$\sigma_x = K\sigma_z \quad (4.16)$$

where K = lateral pressure coefficient or the ratio of horizontal stress to vertical stress. Substituting Eqs. (4.15) and (4.16) into Eq. (4.14) gives:

$$S = (c + K\sigma_z \tan \delta)(\pi D)dz \quad (4.17)$$

The equilibrium of vertical forces acting on the element leads to

$$0 = V + dV - V - dW + S \quad (4.18)$$

or

$$0 = dV - dW + S \quad (4.19)$$

Substituting Eqs. (4.11), (4.13) and (4.17) into (4.19) gives:

$$d\sigma_z = \left[\gamma - \frac{4c}{D} - \frac{4K\sigma_z \tan \delta}{D} \right] dz \quad (4.20)$$

or

$$d\sigma_z = (P - Q\sigma_z)dz \quad (4.21)$$

where

$$P = \gamma - \frac{4c}{D} \quad (4.22)$$

and

$$Q = \frac{4K \tan \delta}{D} \quad (4.23)$$

At $z = 0$, $\sigma_z = q$. Therefore, Eq. (4.21) can be solved as:

$$\int_q^z \frac{1}{P - Q\sigma_z} d\sigma_z = \int_0^z dz \quad (4.24)$$

or

$$\sigma_z = \frac{P}{Q} \left(1 - e^{-Qz} \right) + q e^{-Qz} \quad (4.25)$$

which on substitution from Eqs. (4.22) and (4.23) becomes

$$\sigma_z = \frac{\gamma D - 4c}{4K \tan \delta} \left(1 - e^{-4K \tan \delta \left(\frac{z}{D} \right)} \right) + qe^{-4K \tan \delta \left(\frac{z}{D} \right)} \quad (4.26)$$

which can be rewritten to incorporate the height-to-diameter (H / D) ratio of an oedometer:

$$\sigma_z = \frac{\gamma D - 4c}{4K \tan \delta} \left(1 - e^{-4K \tan \delta \left(\frac{H}{D} \right) \left(\frac{z}{H} \right)} \right) + qe^{-4K \tan \delta \left(\frac{H}{D} \right) \left(\frac{z}{H} \right)} \quad (4.27)$$

As shown in Eq. (4.26), the vertical effective stress within the soil at a depth z is the combination of two components; the soil self-weight, and the external applied pressure. The self-weight component increases with depth, whilst the effect of the applied pressure decreases with depth. Depending upon factors such as the oedometer height and diameter, either the soil component or applied pressure component will dominate. To illustrate this, some nominal yet realistic soil parameters were selected, and the vertical effective stress due to each component was evaluated using the following expressions:

$$\text{Self - weight : } \sigma_{S-W} = \frac{\gamma D - 4c}{4K \tan \delta} \left(1 - e^{-4K \tan \delta \left(\frac{z}{D} \right)} \right) \quad (4.28)$$

$$\text{Applied pressure : } \sigma_p = qe^{-4K \tan \delta \left(\frac{z}{D} \right)} \quad (4.29)$$

Eq. (4.26) is simply the addition of Eqs. (4.28) and (4.29). For clays, realistic ranges of values for dry unit weight, effective friction angle, and effective cohesion are 14-21 kN/m³, 15-30°, and 0-15 kPa, respectively. As evident in Eq. (4.28), a large effective cohesion will only reduce the impact of the self-weight component that contributes to the vertical effective stress. Thus, in order to analyse the significance of the self-weight component in Eq. (4.26), a small value of effective cohesion (2 kPa) was selected conservatively. The dry unit weight and effective friction angle were chosen to be 17 kN/m³ and 25°, respectively.

Because the oedometer walls are assumed to be rigid, lateral strain can be neglected and K can be assumed as $K_0 = 1 - \sin \phi'$. Furthermore, it was assumed that $\delta = 0.5\phi'$ at the soil-wall interface since oedometer walls are commonly made of stainless steel. The range of applied pressures investigated was selected based on pressures commonly encountered in standard oedometer tests (i.e. 5, 10, 20, 40, 80, 160, 320 kPa). By conducting a simple analysis using Eqs. (4.28) and (4.29) and varying the diameter (from 0.5-4 m) for each trial

of applied pressure, an upper limit was arbitrarily identified, below which the self-weight of the soil can be considered negligible and applied pressure dominates.

This is illustrated for an example applied pressure of 80 kPa shown in Figure 4.22 which shows the variation in effective stress with depth as the diameter increases, whilst maintaining a height/diameter ratio of 1. It should be noted that the horizontal distance between the applied pressure component (solid line) and the effective stress incorporating self-weight (dotted line) is the self-weight contribution. It is thus apparent that for smaller diameters, the vertical effective stress is governed predominantly by the applied pressure. By conducting this comparison for each pressure, it was concluded that if $q/\gamma D$ remains approximately greater than 10, the component of effective stress due to self-weight (Eq. 4.28) can be considered negligible.

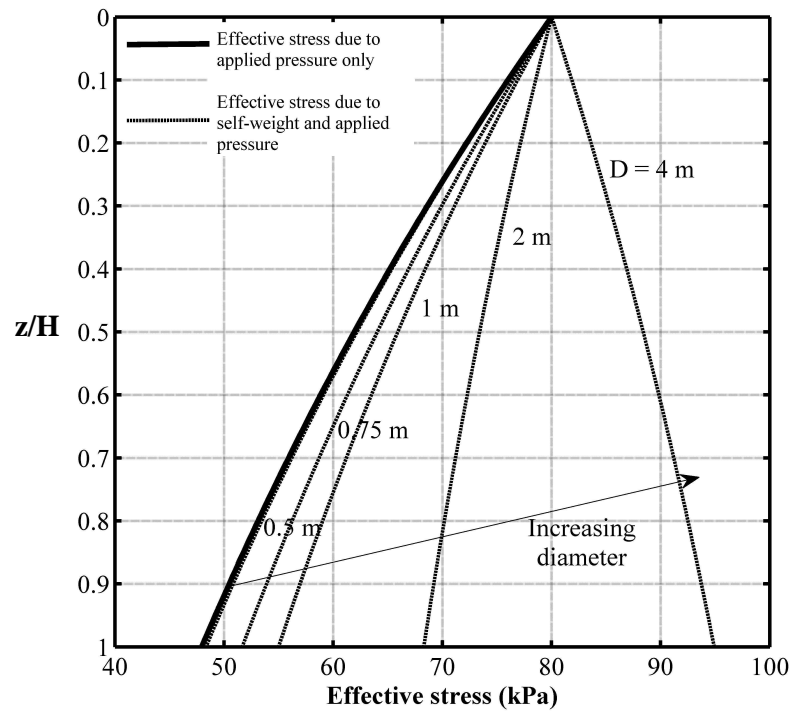


Figure 4.22 – Variation in effective stress with depth and increasing diameter for an applied pressure of 80 kPa

As a result, for $q/\gamma D > 10$ the variation of effective stress with depth in Eq. (4.26) can be reduced to:

$$\sigma_z = q e^{-4K \tan \delta \left(\frac{z}{D} \right)} \quad (4.30)$$

The applied vertical stress distribution (Eq. 4.30) is instantaneously translated into the initial pore water pressure distribution that drives the consolidation process. Therefore, Eq. (4.30) can also be written as

$$u_i = q e^{-4K \tan \delta \left(\frac{z}{D} \right)} \quad (4.31)$$

where u_i is the initial excess pore water pressure, since the load is initially taken entirely by the pore water within the saturated soil. Eq. (4.31) can again be rearranged in terms of the height-to-diameter ratio of the oedometer apparatus, and normalised with respect to the applied pressure (so that the maximum value encountered will be 1).

$$\frac{u_i}{q} = e^{-4K \tan \delta \left(\frac{H}{D} \right) \left(\frac{z}{H} \right)} \quad (4.32)$$

The simplification of Eq. (4.27) to Eq. (4.32) can be further justified by observing the effect of varying the H / D ratio with applied pressure. For this analysis, a nominal diameter of 0.5 m was selected. The results are shown in Figure 4.23, where the dotted line indicates the effective stress including both components of self-weight and applied pressure, whereas the solid line indicates the applied pressure only.

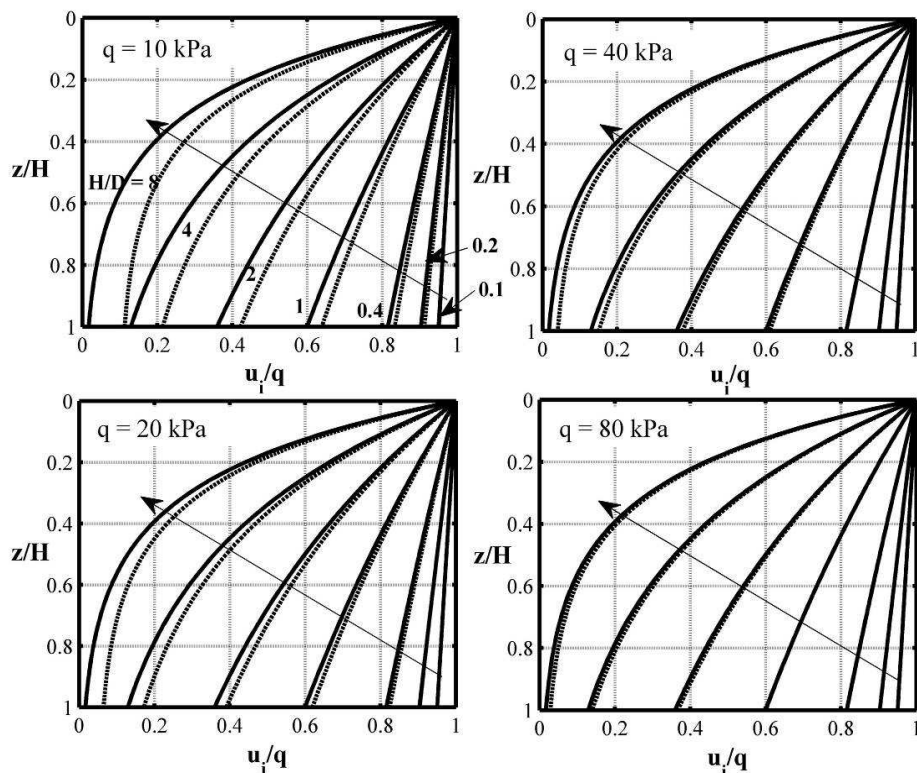


Figure 4.23 – Variation in u_i with z/H and increasing H/D for a diameter of 0.5 m (Legend – see Figure 4.22)

The arrows show the trend in results as the height of the oedometer (in comparison with the diameter) is increased. It can be seen from Figure 4.23 that the self-weight component increases with depth in all cases. The relative magnitude of this component decays with increasing applied pressure (q) and decreasing H/D .

In general, once the applied pressure is greater than approximately 20 kPa, the effective stress is governed primarily by the applied pressure. For example, at 80 kPa, the effective stress is approximately equal to the applied pressure component only, which still decreases with depth due to the wall friction. This corresponds to a $q/\gamma D$ ratio of 9.5 which aligns with earlier observations. For applied pressures greater than 80 kPa, there is insignificant change in the $u_i/q - z/H$ plot as deduced from Figure 4.23.

Effect of varying height to diameter ratio

Using the expression for the normalised initial excess pore water pressure distribution in Eq. (4.32), the effect of varying the height-to-diameter ratio of the oedometer was investigated in situations where $q/\gamma D > 10$. Here, the effective friction angle was maintained at 25° . The initial distribution that can be expected when adhering to the standard recommendation that H/D be less than 0.4 is also shown in Figure 4.24.

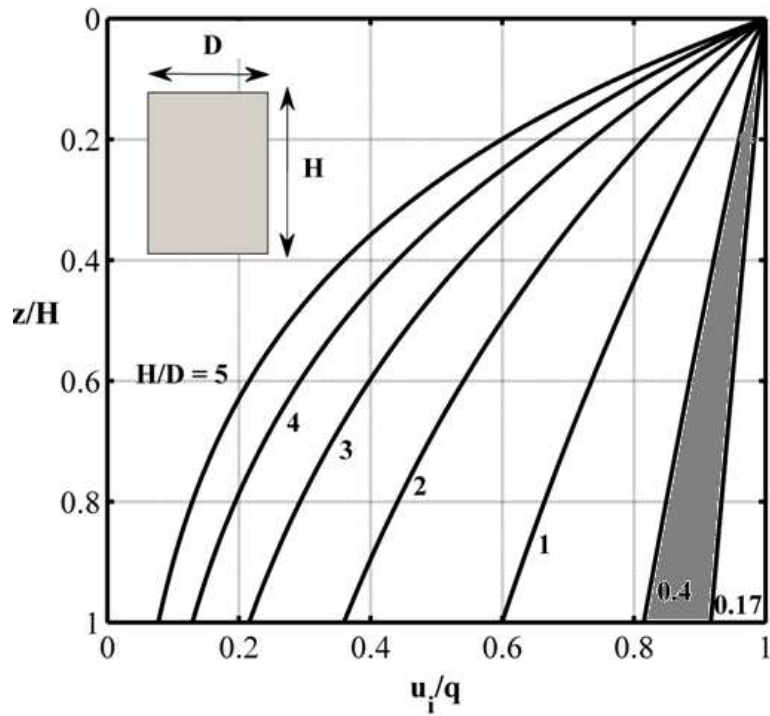


Figure 4.24 – Variation in u_i with z/H , assuming $q/\gamma D > 10$ (i.e. neglecting the self-weight component)

ASTM standards also recommend H / D be greater than 0.17 to avoid disturbance during trimming. Within this narrow band ($0.17 < H / D < 0.4$) which is also shown in Figure 4.24, data analyses of settlement-time results can be conducted using Terzaghi's traditional average degree of consolidation curve, which is based upon a *uniform* initial excess pore water pressure distribution. Although the initial pore pressure distribution resulting from $H / D = 0.4$ is not technically uniform, it is still considered reasonable to use consolidation theory based on a uniform initial distribution in this case. However, for values of H / D greater than 0.4, this may no longer be a realistic assumption. In order to determine whether an analysis in terms of uniform initial excess pore water pressure is applicable, the average degree of consolidation versus time factor plots (Figure 4.25) were developed for the initial pore water pressure distributions shown in Figure 4.24. For the singly drained case, drainage was allowed through the surface only.

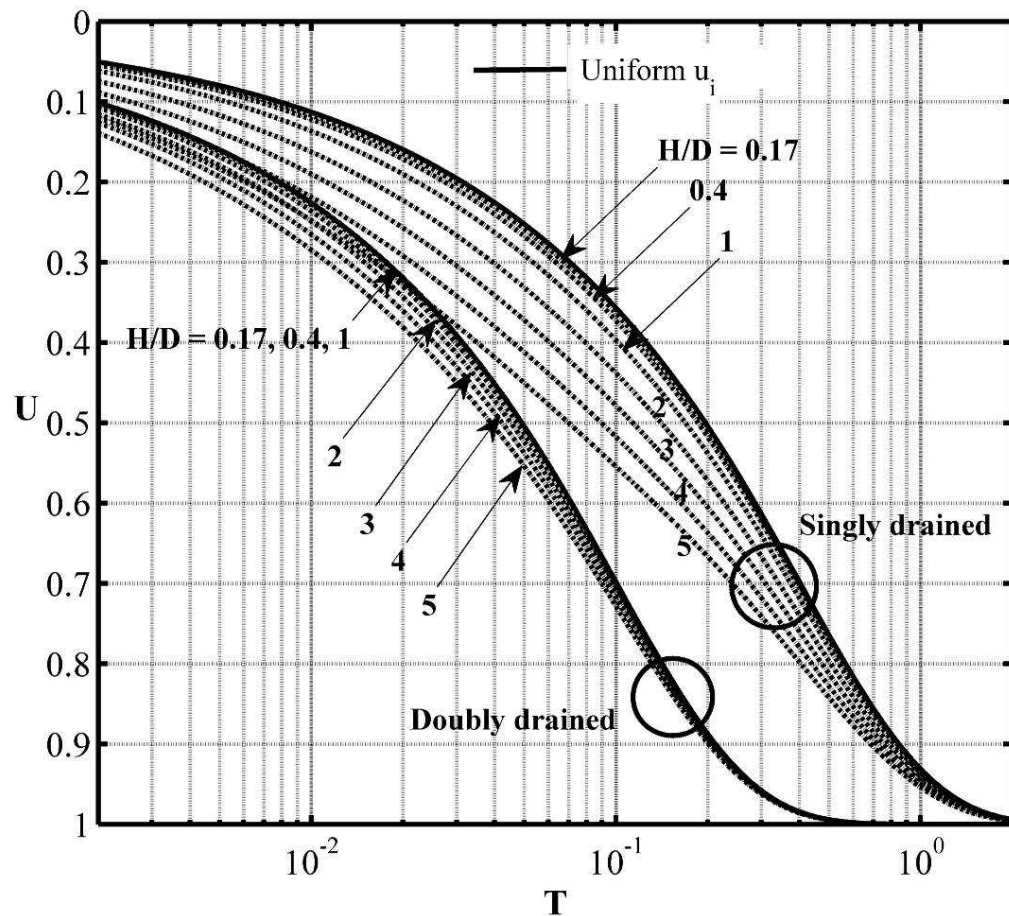


Figure 4.25 – Average degree of consolidation behaviour due to initial excess pore pressure distributions resulting from H/D ratios of 0.17, 0.4, 1, 2, 3, 4, 5 for both singly and doubly drained cases

As demonstrated in Figure 4.25, increases in sample height (with respect to diameter) have less of an effect when doubly drained conditions are maintained, in comparison with cases

where the soil is singly drained. In fact, the average degree of consolidation behaviour due to initial excess pore water pressure distributions resulting from H/D ratios less than 2 is very similar to that resulting from a case of uniform initial excess pore water pressure, when dealing with a doubly draining sample. However, when drainage is prevented through the base of the soil layer, the average degree of consolidation only resembles the uniform case for H/D values less than 0.4. This corresponds with the value specified by ASTM standards and means conventional restrictions regarding analysis using uniform $U-T$ values apply to cases where the sample is singly drained.

Applied pressure vs. self-weight

It has been shown that as long as $q/\gamma D > 10$, the self-weight component of the soil can be neglected and Eq. (4.26) can be reduced to Eq. (4.30). However, if the self-weight component of the soil is included, any number of initial excess pore water pressure (u_i) distributions can be produced, where u_i can increase, decrease or remain approximately constant with depth, depending on the applied pressure (q) and oedometer diameter (D). This is illustrated in Figure 4.26, where the u_i -distribution for H/D ratios of 3 and 5 is provided for three different $q/\gamma D$ values less than 10 (1, 2 and 5), where self-weight cannot be ignored.

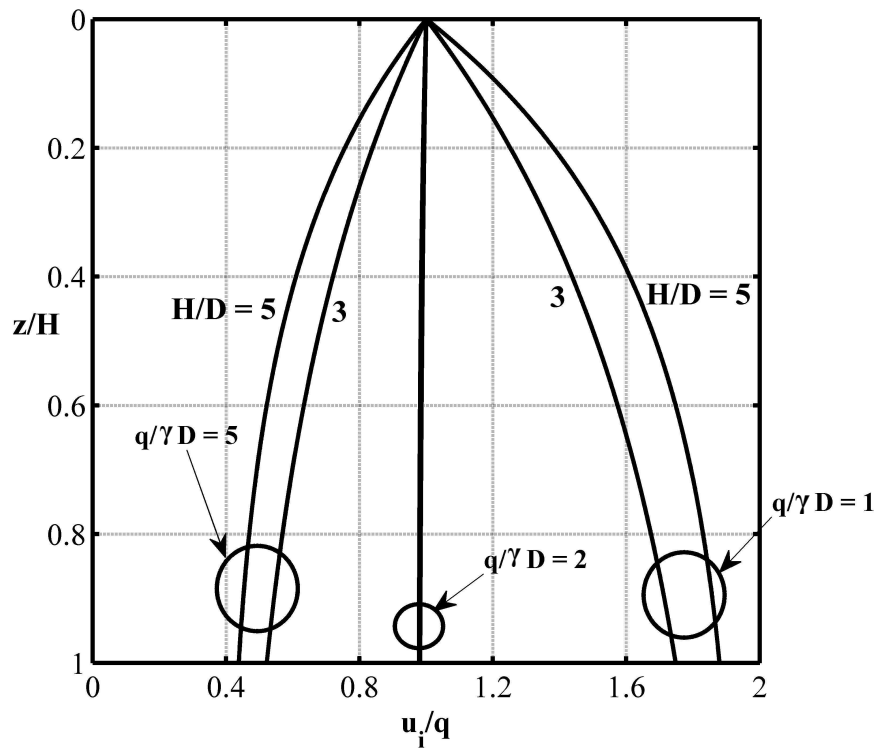


Figure 4.26 – Variation in u_i with z/H and $H/D = 3$ and 5 for $q/\gamma D = 1, 2$ and 5

It can be seen that when $q/\gamma D = 2$, the u_i -distribution is approximately uniform and equal to the applied surcharge. When $q/\gamma D > 2$, the applied pressure begins to dictate the shape of the u_i -distribution, and stress transfer to the oedometer walls causes the pore pressure to decrease with depth.

As shown previously, when $q/\gamma D$ reaches 10, the self-weight of the soil becomes negligible and only applied stress needs to be considered. However, when $q/\gamma D < 2$, the self-weight of the soil becomes the dominating factor, and the initial excess pore water pressure correspondingly increases with depth.

In general, as the H/D ratio increases, the u_i -distribution becomes more skewed and further removed from a linear nature. This becomes important when considering the percentage consolidation of a doubly drained layer, where it is widely known that the $U-T$ variation due to linear and uniform u_i -distributions is identical. Thus, when the u_i -distribution generated by Eq. (4.26) resembles an approximately linear profile, the resulting $U-T$ curve can be expected to follow the uniform case, as shown in Figure 4.27.

When there is limited skewness (i.e. $H/D \leq 3$), the u_i -distribution is approximately linear, and doubly drained consolidation follows the uniform case. When $q/\gamma D < 2$, the average degree of consolidation proceeds slower than the uniform case, regardless of whether the layer is singly or doubly drained. Conversely, when $q/\gamma D > 2$, consolidation proceeds comparatively faster than the uniform case. These results can be summarised (see Table 4.2) to illustrate which combinations of H/D and $q/\gamma D$ generate a solution that conforms to the uniform percentage consolidation curve when the self-weight of the soil is either considered or ignored.

Table 4.2 – Limiting values of H/D for $q/\gamma D$ values where the average degree of consolidation resembles the uniform u_i case

	Singly drained	Doubly drained
Self-weight and applied pressure considered	$q/\gamma D < 2$	$H/D \leq 0.5$
	$q/\gamma D = 2$	All H/D
	$q/\gamma D > 2$	$H/D \leq 0.5$
Self-weight ignored	$q/\gamma D > 10$	$H/D < 0.4$
		$H/D < 2$

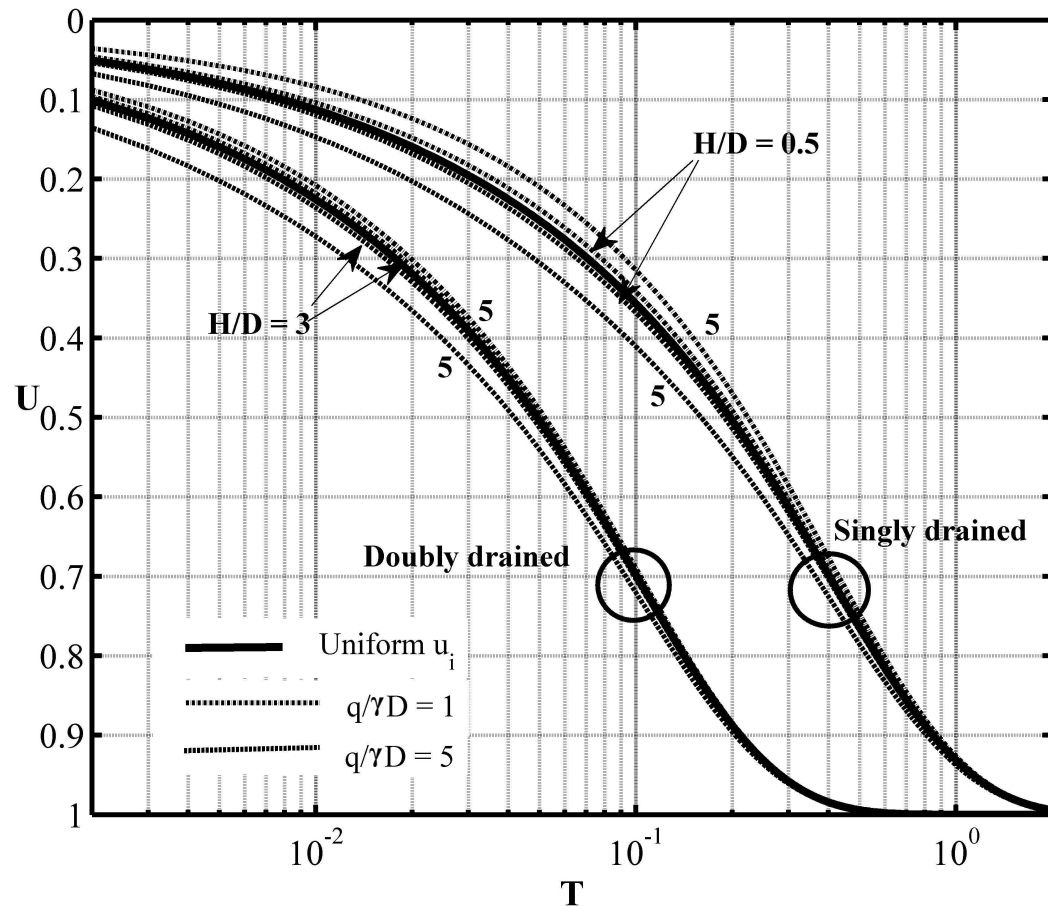


Figure 4.27 – Average degree of consolidation behaviour due to initial excess pore pressure distributions resulting from u_i distributions where $q/\gamma D = 1$ and 5 and $H/D = 3$ and 5, and 0.5 and 5 for both doubly and singly drained cases, respectively.

4.3.3. Experimental Investigation

The coefficient of consolidation (c_v) of a soft soil is traditionally determined using curve-fitting procedures such as Taylor's root-time method (Taylor 1948) and Casagrande's log-time method (Casagrande and Fadum 1940). Here, the measured consolidation settlement is 'fitted' to the theoretical percentage consolidation curve generated using Terzaghi's theory, which is based on a uniform distribution of initial excess pore water pressure. As a result, the popular curve-fitting methods developed by Taylor and Casagrande are only applicable for cases where a uniform initial pore water pressure distribution can be reasonably assumed, or where the average degree of consolidation behaviour closely resembles the uniform $U - T$ curve. Based on the results shown in Figures 4.25 and 4.27, the Taylor and Casagrande curve-fitting methods *can* apply to tall samples in select cases.

When dealing with small diameters (which will usually ensure that $q/\gamma D > 10$), the self-weight component of Eq. (4.26) can be ignored, and the u_i distribution can be expected to follow Eq. (4.30). Thus, the Taylor and Casagrande methods can apply when H/D is greater than the recommended 0.4, as long as the sample remains doubly drained and H/D does not exceed 2. However, for singly drained cases (e.g. when pore water pressure measurements are required), the sample must adhere to the recommended dimensions ($0.17 < H/D < 0.4$) in order to realistically use the Taylor and Casagrande curve-fitting methods. Thus, for cases where $q/\gamma D > 10$, the recommended sample dimensions can therefore be amended to;

Table 4.3 – Modified sample dimensions

	Singly drained	Doubly drained
ASTM D2435		$0.17 < H/D < 0.4$
Proposed modification	$0.17 < H/D < 0.4$	$0.17 < H/D < 2$

In order to verify the arbitrarily defined cut-off values of H/D for the doubly drained case in Table 4.3, consolidation tests were carried out in a tall oedometer. The settlement-time results from these tests were then analysed using Taylor and Casagrande's curve-fitting procedures to determine the coefficient of consolidation of the soil. These values were then compared with values of c_v determined using standard oedometer tests. If the amended proportions for H/D in Table 4.3 are correct, the values of c_v obtained from tall oedometer test data should align with values of c_v obtained from standard oedometer test data.

Apparatus and testing procedure

The tall oedometer shown in Figure 4.28 was used to conduct consolidation tests on the K_{60} soil outlined in Chapter 4 (see Table 4.1 for properties). Incremental loading was carried out via hydraulic pressure application with a load increment ratio (LIR) of unity. The sample deformation with time was measured under applied pressures of 10, 20, 40, 80, 160, 300 and 600 kPa until creep was reached so that the Casagrande method could be used to complement values obtained using the Taylor method. These applied pressures correspond to $q/\gamma D$ values of 7.4 (10 kPa) to 445 (600 kPa). Thus, with the exception of the 10 kPa applied pressure, the aforementioned limit, $q/\gamma D > 10$, was maintained, thereby ensuring the self-weight of the soil could be ignored. It should be noted that the conditions for uniform u_i specified in Table 4.2 were still met when $q = 10$ kPa (or $q/\gamma D = 7.6$), which meant that data obtained during this loading increment could still be conducted using the

uniform $U - T$ curve (i.e. traditional Taylor and Casagrande curve-fitting techniques apply).

In order to accommodate the diaphragm shown in Figure 4.28, h was required to be a minimum of 30 mm. For this study, the initial dimensions of the sample were 77 mm diameter and 165 mm thickness. Over the duration of testing, the tall sample experienced a total 65 mm of settlement. As a result, the settlement-time curves generated during each load increment covered a range of H / D values from 2.1 (at 10 kPa) to 1.3 (at 600 kPa).

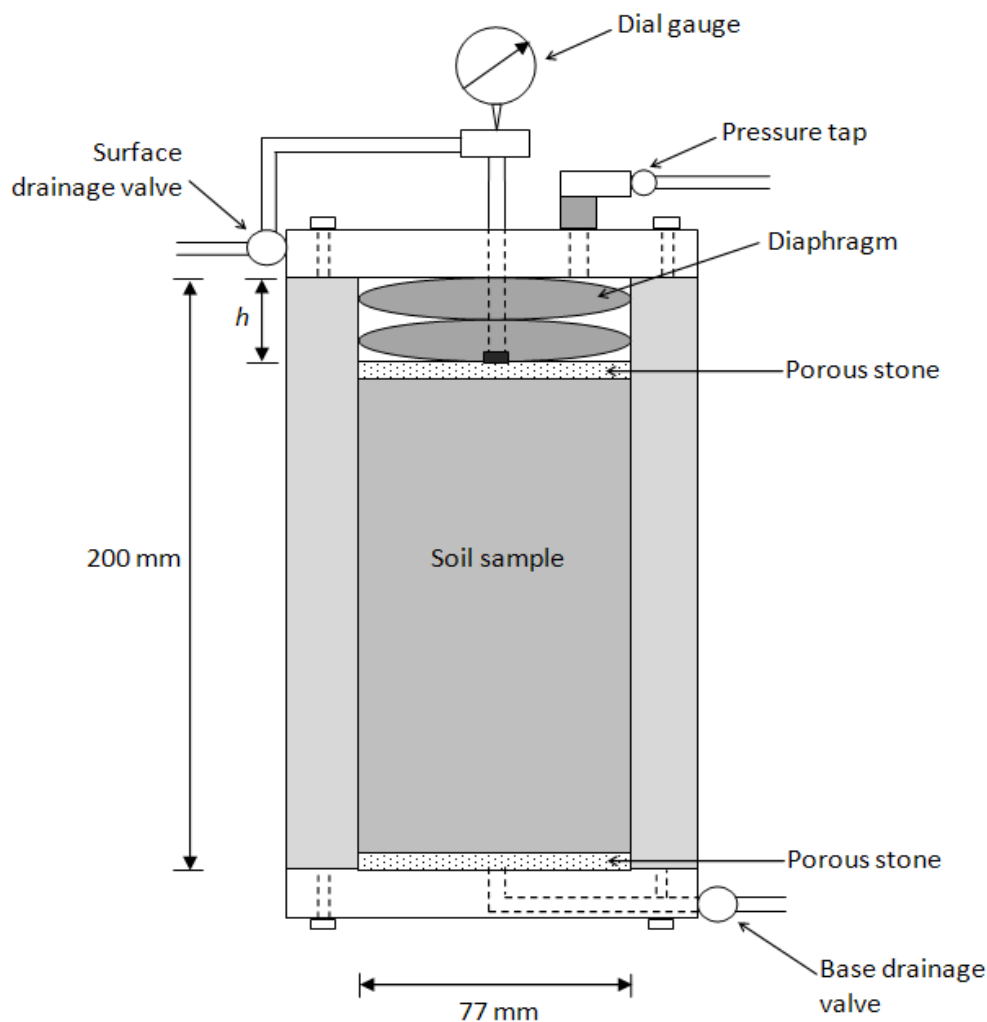


Figure 4.28 – Schematic of tall oedometer apparatus

A series of oedometer tests were also carried out according to ASTM standards (ASTM D2435) for applied pressures of 8, 15, 30, 55, 108, 215, 429 and 856 kPa. The standard oedometer apparatus ensured that the sample had initial dimensions of 63 mm diameter and 20 mm thickness, which corresponds to a H / D ratio of 0.3.

Sensitivity analysis with regards to effective friction angle

The effect of friction angle (ϕ') on the initial excess pore water pressure distribution of the sample was assessed using $H/D = 2.1$, as this was the largest value encountered during testing. Eq. (4.32) can therefore be rearranged to incorporate the effective friction angle as follows:

$$\frac{u_i}{q} = e^{-8.4 \tan(0.5\phi')(1-\sin\phi')\left(\frac{z}{H}\right)} \quad (4.33)$$

Jaky's equation (1948) for the lateral earth pressure coefficient was again applied ($K_0 = 1 - \sin\phi'$) and the interface friction angle was calculated as $\delta = 0.5\phi'$.

The effect of the self-weight component on u_i was neglected. Values of ϕ' were varied from 15° to 35° and, as shown in Figure 4.29, the difference between initial excess pore water pressure distributions for each case was relatively minor.

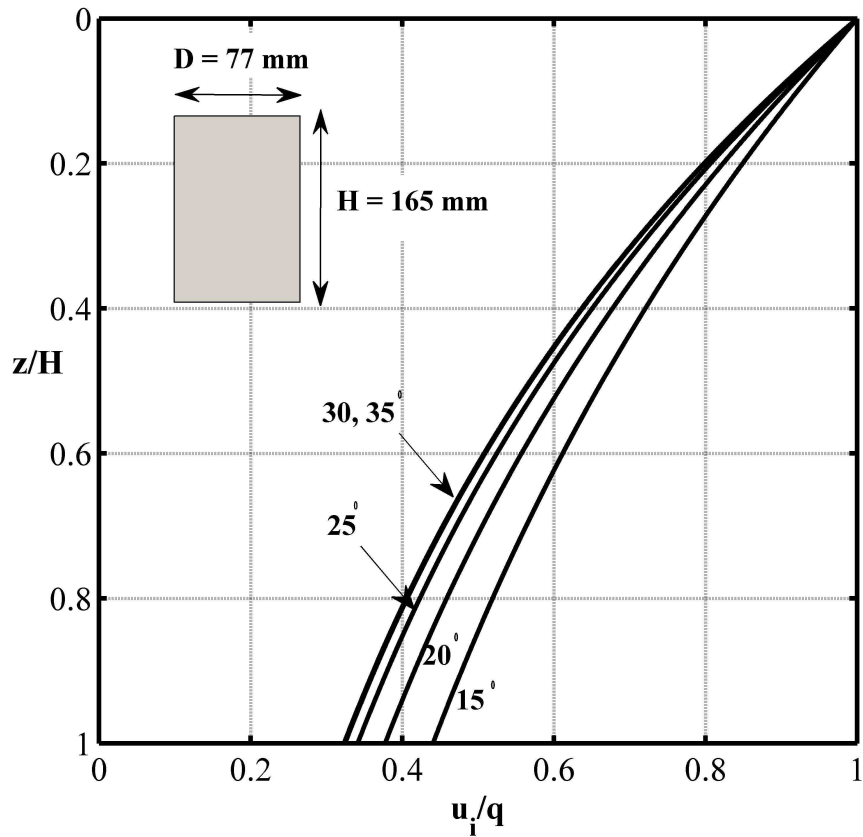


Figure 4.29 – Effect of friction angle on u_i -distribution where $H/D = 2.1$

Furthermore, when each of these five distributions was used to determine the change in average degree of consolidation (U) with time (T), there was no visible difference between the generated $U - T$ curves, for both singly and doubly drained situations. That is, despite

the difference in u_i -distributions as a result of variations in ϕ' , essentially only one $U - T$ curve is generated, which suggests that the initial excess pore water pressure distribution is relatively insensitive to changes in effective friction angle. This is illustrated in Figure 4.30 which shows the $U - T$ curves for each distribution shown in Figure 4.29 for both singly and doubly drained cases. For the doubly drained case (which are the conditions that are maintained in this investigation), the $U - T$ curves are practically identical to that obtained using a uniform initial excess pore water pressure distribution.

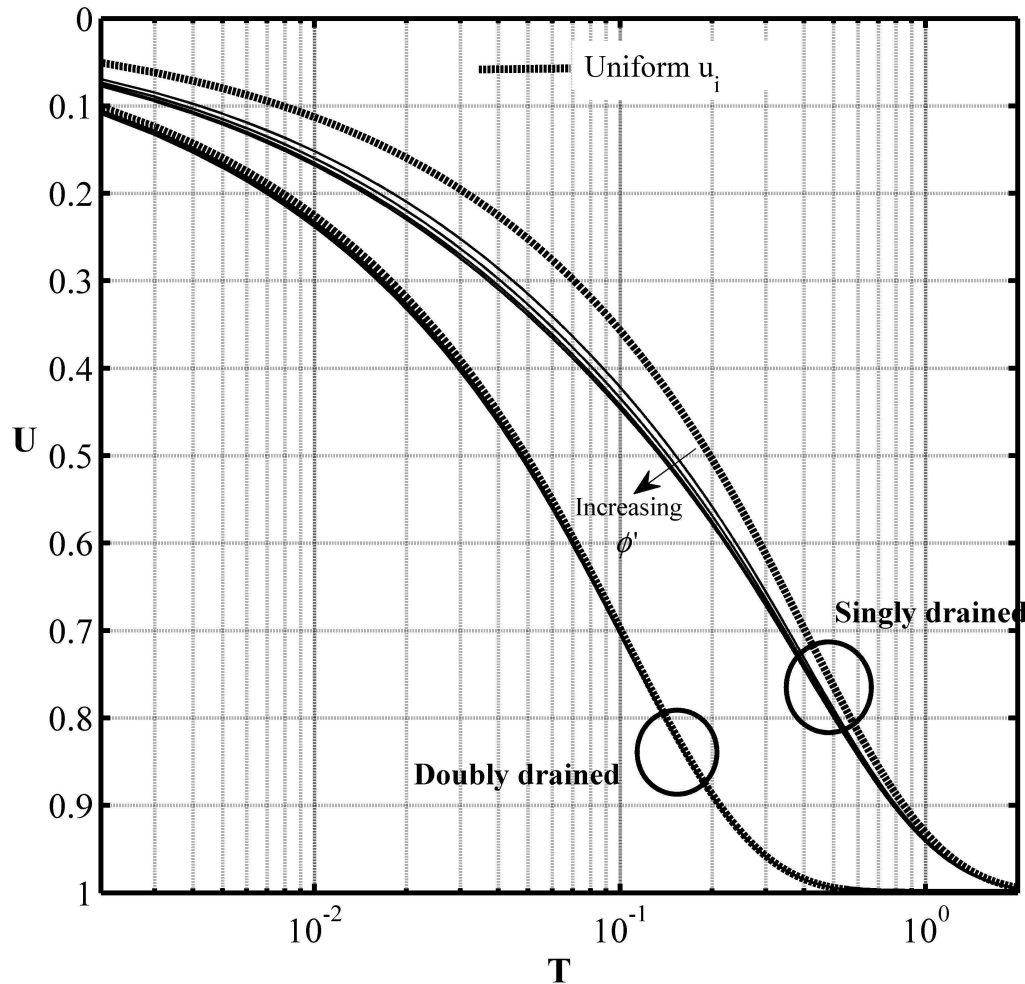


Figure 4.30 – Average degree of consolidation behaviour due to u_i -distributions resulting from ϕ' values of 15° , 20° , 25° , 30° and 35° for both singly and doubly drained cases, where $H/D = 2.1$

Sensitivity analysis with regards to interface friction angle

The effect of the interface friction angle (δ) on the initial excess pore water pressure distribution of the sample was also assessed using $H/D = 2.1$ and $\phi' = 25^\circ$. By varying

δ/ϕ' from 0 to 1, the effect of wall roughness on the initial excess pore water pressure distribution was analysed using the following equation:

$$\frac{u_i}{q} = e^{-4.85\left(\frac{z}{H}\right)\tan \delta} \quad (4.34)$$

The resulting initial excess pore water pressure distributions are shown in Figure 4.31, and the corresponding $U-T$ curves are provided in Figure 4.32.

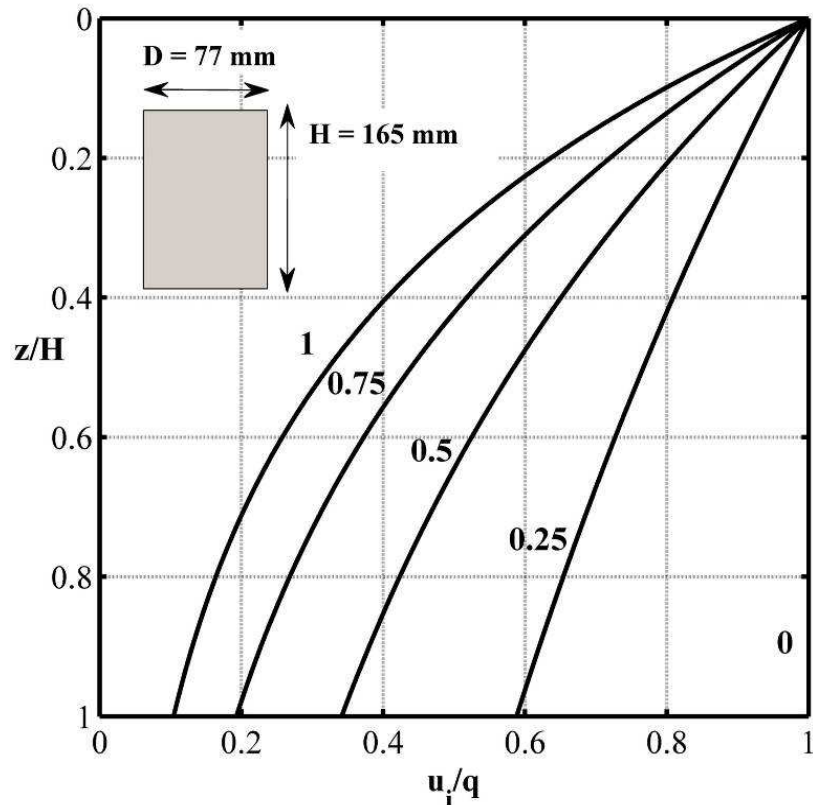


Figure 4.31 – Initial excess pore water pressure distributions resulting from δ/ϕ' values of 0 to 1

It is evident that the initial excess pore water pressure distribution is highly sensitive to wall roughness. For $\delta/\phi'=0$ (i.e. smooth wall), the initial pore pressure distribution is uniform. For $\delta/\phi'=1$ (i.e. very rough wall), only 11% of the applied pressure is transferred to the bottom of the oedometer. This sensitivity translates to the average degree of consolidation behaviour, although to a lesser extent when considering a doubly drained layer. For a doubly drained layer with low to moderate wall friction, with $\delta/\phi' \leq 0.5$, the $U-T$ variation is approximately identical to that for a uniform initial excess pore water distribution.

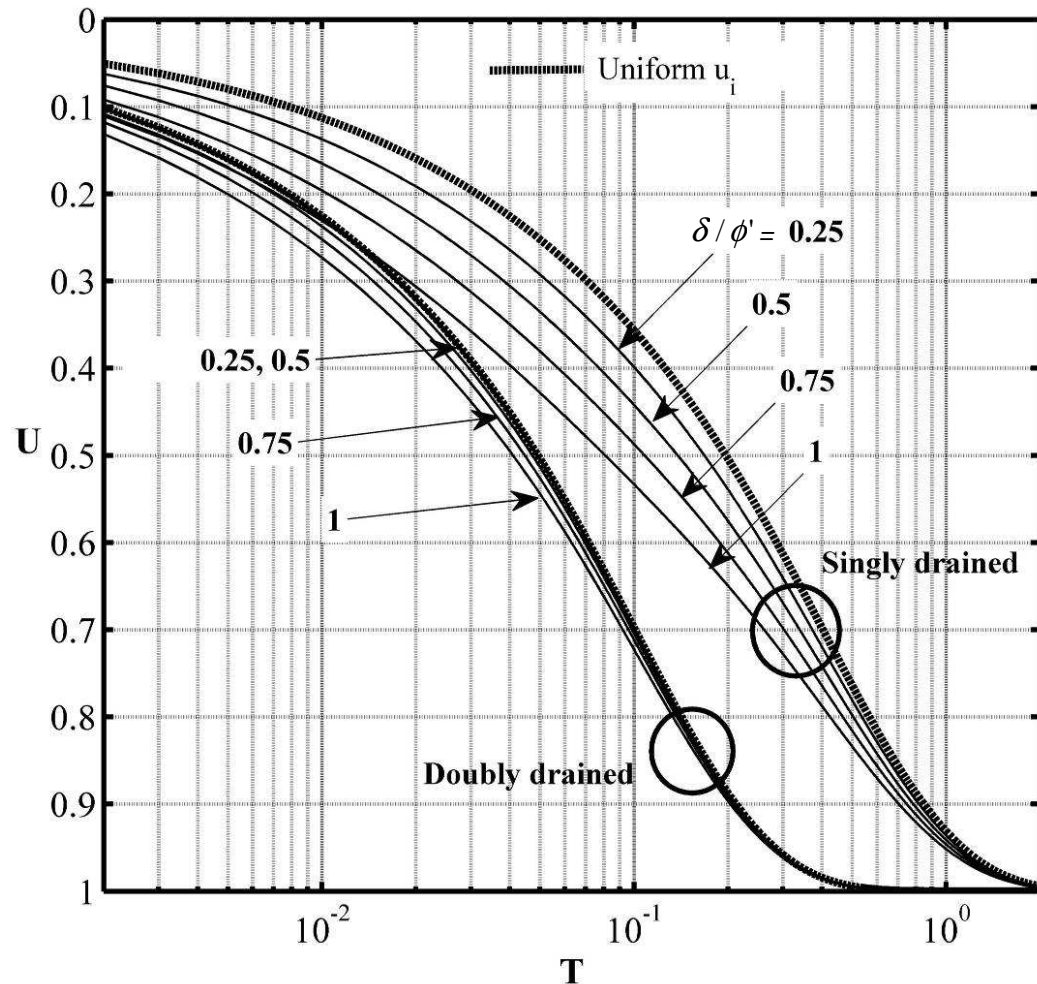


Figure 4.32 – Average degree of consolidation behaviour due to u_i -distributions resulting from δ/ϕ' values of 0, 0.25, 0.5, 0.75 and 1 for both singly and doubly drained cases, where $H/D = 2.1$ and $\phi' = 25^\circ$

Results

The settlement-time data gathered from each load increment was analysed using both Taylor and Casagrande curve-fitting methods to determine whether the values of c_v obtained from tall oedometer test data aligned with values obtained using standard testing methods. Although it is widely accepted that the Taylor method will yield larger values of c_v than the Casagrande method, the sandy clay used in this study resulted in similar values of c_v regardless of the method used to analyse data. In general, values of c_v calculated using the Taylor method were within 4% of values calculated using the Casagrande method. As a result, it was considered reasonable to obtain an average of these values. The variation in c_v with applied stress for both the tall and standard oedometer data sets is shown in Figure 4.33.

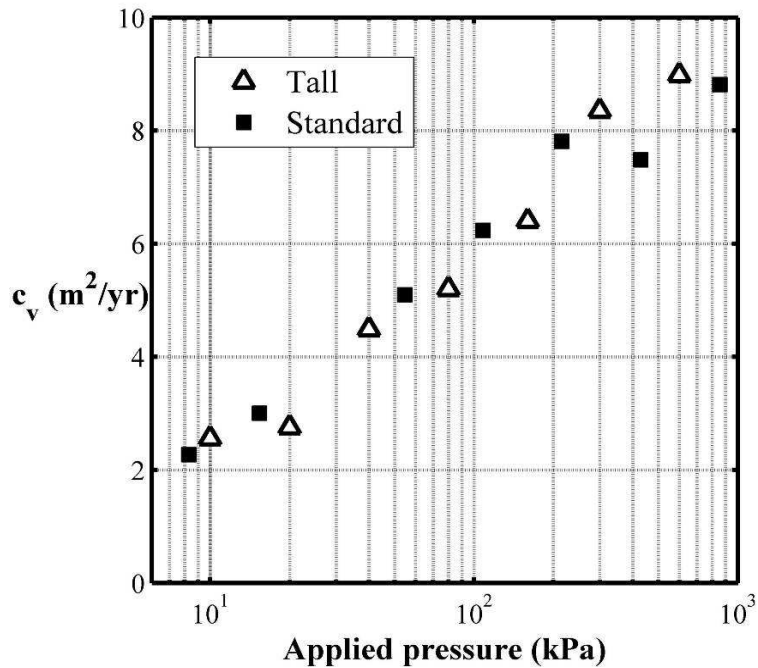


Figure 4.33 – Variation in c_v values determined using data obtained from tall and standard oedometer tests

As anticipated, the c_v values closely align with each other and display nearly identical trends of increasing c_v with increasing applied pressure. This supports the modified $H/D \approx 2$ cut-off point proposed in Table 4.3, for a doubly drained system.

The average degree of consolidation curves generated by the proposed analytical solution suggest that despite wall friction, traditional consolidation analyses using the popular Taylor and Casagrande curve-fitting methods can be used to analyse data obtained from a tall, doubly draining sample for select combinations of applied pressure, height and diameter. Experimental results also support this conclusion, as the value of c_v obtained from data gathered during tall oedometer testing (where $H/D = 2.1$) was approximately equal to the values obtained from standard oedometer tests.

4.4 Calculating c_v from data due to non-uniform u_i -distributions

The coefficient of consolidation (c_v) is often determined by comparing the characteristics of the experimental and theoretical consolidation using empirical curve-fitting procedures which are based on the theoretical $U-T$ curve generated by a layer subjected to a uniform initial excess pore water pressure (u_i) distribution. Two notable examples include

Casagrande's log-time method, and Taylor's square-root of time method. The results obtained using these curve-fitting methods are also applicable to cases where consolidation is driven by a linear distribution of u_i , but only if the layer is doubly drained. Although it is widely accepted that singly drained consolidating layers subjected to linear u_i -distributions produce quite different $U - T$ curves, no effort has yet been made to adjust Taylor's and Casagrande's techniques to account for these differences.

Since the development of the Casagrande and Taylor curve-fitting methods, a number of alternative procedures for the determination of c_v have been proposed (Cour 1971, Sivaram and Swamee 1977, Sridharan and Rao 1981, Mikasa and Takada 1986, Raju et al. 1995, Singh 2005), many of which have been critically reviewed by Shukla et al. (2009). However, due to the inherent simplicity and relative accuracy of the methods developed by Casagrande and Taylor, their curve-fitting procedures are still foremost in evaluating the coefficient of consolidation, and can produce reliable values of c_v in many instances, as demonstrated in Section 4.2.

Although Terzaghi's theory is based upon a number of assumptions (e.g. saturated soil, homogeneous properties etc.), most curve-fitting procedures currently used to calculate c_v rely on a further assumption of uniform initial excess pore pressure (u_i). In this section, Taylor and Casagrande's curve-fitting methods are modified to account for a variety of non-uniform initial excess pore pressure distributions. In order to generalise these curve-fitting procedures, it is first necessary to develop approximations to describe different regions of the $U - T$ curves, from which adjustment factors can be inferred.

4.4.1. Development of approximate solutions

The $U - T$ curve generated by the Fourier solution to Terzaghi's one-dimensional consolidation equation for a uniform u_i -distribution with one-way drainage can be approximated using two empirical expressions that apply to separate regions of the $U - T$ curve. The following expressions were developed by Taylor (1948) and apply to the relevant regions of the $U - T$ curve:

$$U = \sqrt{\frac{4}{\pi}T} \quad U < 0.6 \quad (4.35)$$

$$U = 1 - 10^{-1.0716T - 0.09119} \quad U > 0.6 \quad (4.36)$$

In the same year, Fox also provided similar approximations (Eqs. 4.37 and 4.38), although the region of U over which these equations apply varies slightly from the cut-off point ($U = 0.6$) suggested by Taylor.

$$U = \sqrt{\frac{4}{\pi} T} \quad U < 0.503 \quad (4.37)$$

$$U = 1 - \frac{8}{\pi^2} \exp\left(\frac{-\pi^2}{4} T\right) \quad U > 0.503 \quad (4.38)$$

The root mean square (RMS) error for the Taylor and Fox equations and their corresponding domains was evaluated, to compare the accuracy of their $U - T$ approximations, given by Eqs. (4.35) to (4.38). Taylor and Fox's expressions to approximate the first part of the $U - T$ curve are identical – it is only the domains that vary. The domain suggested by Fox resulted in a slightly smaller RMS error of 1.3×10^{-4} in comparison with Taylor's RMS error of 1.1×10^{-3} , when compared with Terzaghi's exact solution. These values are similar to those provided by Chan (2003), where the largest relative difference between the approximate solution proposed by Fox and the exact solution was shown to be 1.5×10^{-3} . The RMS errors generated by the approximations for the second part of the $U - T$ curve (Eqs. 4.36 and 4.38) were 3.7×10^{-5} and 3.7×10^{-4} for the Taylor and Fox expressions, respectively.

Since the $U - T$ curves generated by various other non-uniform u_i -distributions are often quite similar in shape to the uniform u_i $U - T$ curve, it follows that expressions of the form used by Taylor and Fox can also be used as approximations for these non-uniform u_i $U - T$ curves. However, it should be noted that the domains over which these approximations apply will vary depending upon the u_i -distribution, as each resulting $U - T$ curve is unique. Eqs. (4.35) and (4.36) can be generalised as follows, where the domains indicate the region over which the approximation is valid;

$$\text{Approximation 1} \quad U = AT^B \quad 0 \leq U \leq U_{\text{limit}} \quad (4.39)$$

$$\text{Approximation 2} \quad U = 1 - 10^{CT+D} \quad U_{\text{limit}} \leq U \leq 1 \quad (4.40)$$

where A , B , C and D = constants unique to each u_i -distribution.

Non-linear least squares method

Using the program MATLAB, the method of non-linear least squares was used to determine the constants in Eqs. (4.39) and (4.40) for key u_i -distributions. For each expression within a

particular u_i -distribution, the RMS error was evaluated for a variety of domains until an acceptable level of accuracy was reached. For the purposes of this analysis, an RMS error less than 1.0×10^{-4} was selected as an appropriate limit.

To determine the value of U_{limit} for each expression, and thus evaluate the domains over which the approximations are valid, the RMS error was plotted against a range of values of U_{limit} , as shown in Figure 4.34(a) which is for the simple case of uniform u_i .

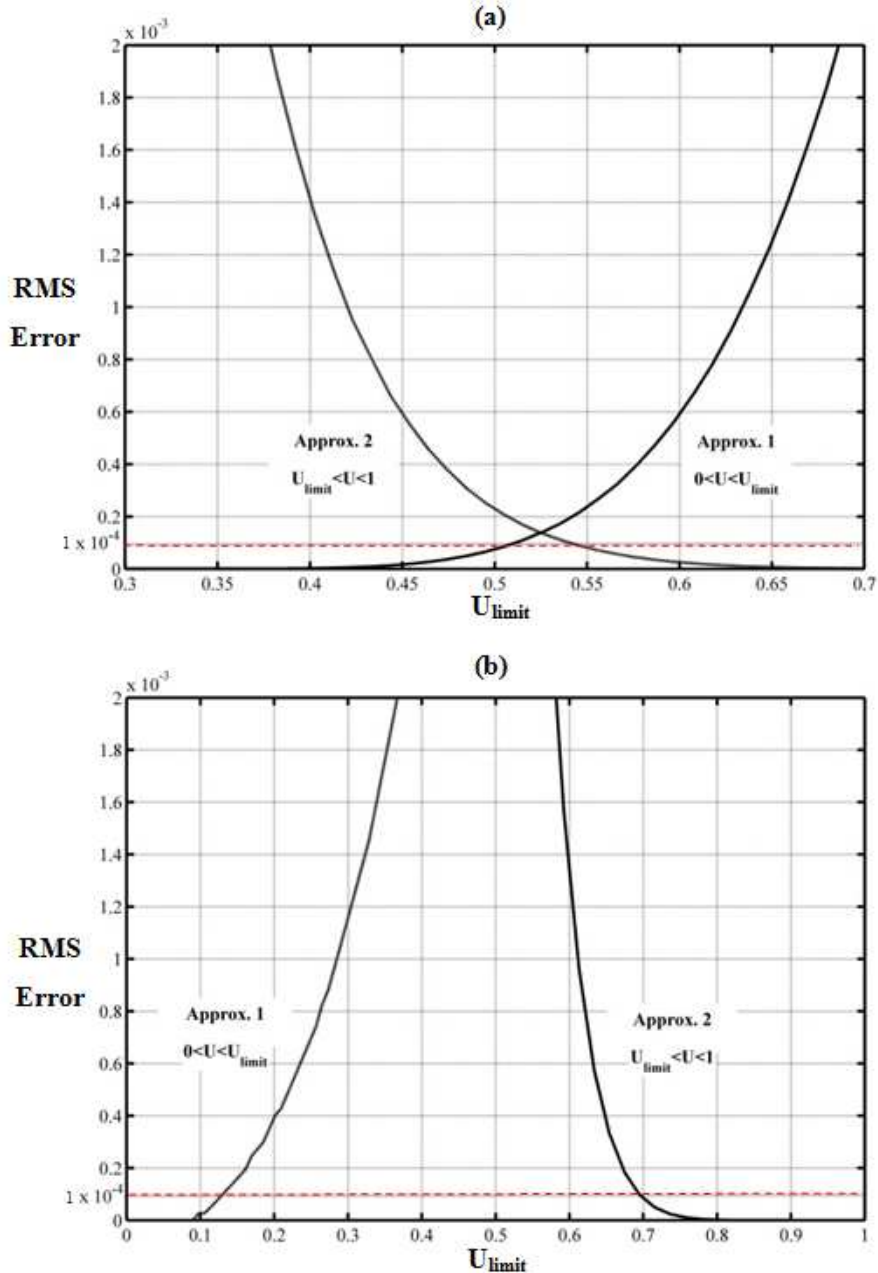


Figure 4.34 – RMS error for (a) uniform u_i -distribution, and (b) a linearly decreasing u_i -distribution (singly drained).

The value of U_{limit} that corresponded to an RMS error of 1.0×10^{-4} was selected for each approximation to evaluate the appropriate domains. For example, for a uniform u_i -distribution, Figure 4.34(a) was used to determine the upper limit of U for the first approximation as 52%, which is consistent with the value of 52.1% specified by Chan (2003). From Figure 4.34(a), the lower limit of U for the second approximation was also determined (54%).

It should be noted that the value of U_{limit} is not always the same for each of the expressions in Eqs. (4.39) and (4.40). In fact, for some non-uniform u_i cases, a large portion of the $U - T$ curve cannot be described by these expressions. This is evident in Figure 4.34(b), where there is a large difference between the upper and lower limits of Approximations 1 and 2 (15% and 69%, respectively).

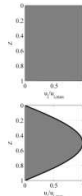
U-T approximations for non-uniform u_i -distributions

Using the procedure outlined above, approximations were developed for some key initial excess pore pressure distributions, namely: linearly increasing u_i , linearly decreasing u_i and sinusoidal u_i , supplemented with the commonly used uniform u_i for validation purposes. When generating the solutions for a singly drained layer, the impermeable boundary was located at the bottom of the soil layer.

Separate functions are provided for each drainage configuration within a particular u_i -distribution since the c_v -calculation procedures outlined in this study do not use H_{dr} , but instead adopt two different values of T for singly and doubly drained situations. The approximation functions for a doubly drained layer are shown in Table 4.4.

Table 4.4 – $U-T$ approximations for two-way drainage

Approximation 1		Approximation 2	
Equation	Domain	Equation	Domain
$U = 2.25T^{0.5}$	$0 \leq U \leq 0.52$	$U = 1 - 10^{-4.29T - 0.091}$	$0.57 \leq U \leq 1$
$U = 8.23T^{0.97}$	$0 \leq U \leq 0.11$	$U = 1 - 10^{-4.29T}$	$0 \leq U \leq 1$



It is widely known that a doubly drained layer subjected to a uniform u_i -distribution produces the same $U - T$ curve as that subjected to a linearly increasing or decreasing u_i -distribution with two-way drainage. Thus, the equations for a uniform u_i -distribution shown in Table 4.4 also apply to linearly increasing and decreasing u_i -distributions, but only if two-way drainage is facilitated. For a singly drained soil layer, the approximation equations and their corresponding domains are shown in Table 4.5.

The approximations in Tables 4.4 and 4.5 have also been plotted against the theoretical $U - T$ curve for each u_i -distribution in Figures 4.35 to 4.38. The inset of each graph is simply the same plot with both axes transformed into logarithmic scale. The solid lines represent the approximate solution, and the lighter dashed lines indicate the exact solution.

Table 4.5 – $U-T$ approximations for one-way drainage

Approximation 1		Approximation 2	
Equation	Domain	Equation	Domain
$U = 1.13T^{0.5}$	$0 \leq U \leq 0.52$	$U = 1 - 10^{-1.07T-0.091}$	$0.54 \leq U \leq 1$
$U = 1.96T^{0.99}$	$0 \leq U \leq 0.18$	$U = 1 - 10^{-1.07T-0.23}$	$0.39 \leq U \leq 1$
$U = 1.91T^{0.48}$	$0 \leq U \leq 0.15$	$U = 1 - 10^{-1.07T+0.014}$	$0.69 \leq U \leq 1$
$U = 3.93T^{0.96}$	$0 \leq U \leq 0.04$	$U = 1 - 10^{-1.07-0.071}$	$0.57 \leq U \leq 1$

As highlighted previously, the approximations in Eqs. (4.39) and (4.40) are at times unable to capture the entire $U - T$ curve. This is more pronounced in the case of a sinusoidal u_i -distribution (Figure 4.38) with one-way drainage, where it is impossible to approximate almost half of the entire $U - T$ curve.

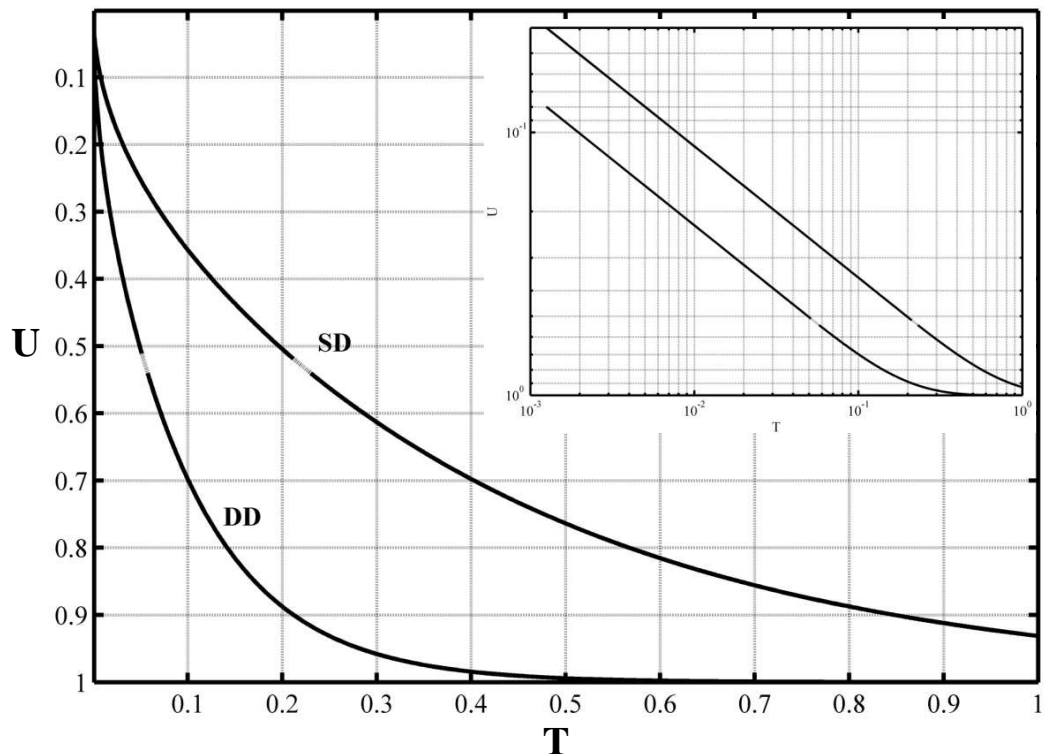


Figure 4.35 – U - T approximation curves for a uniform u_i -distribution with one- or two-way drainage

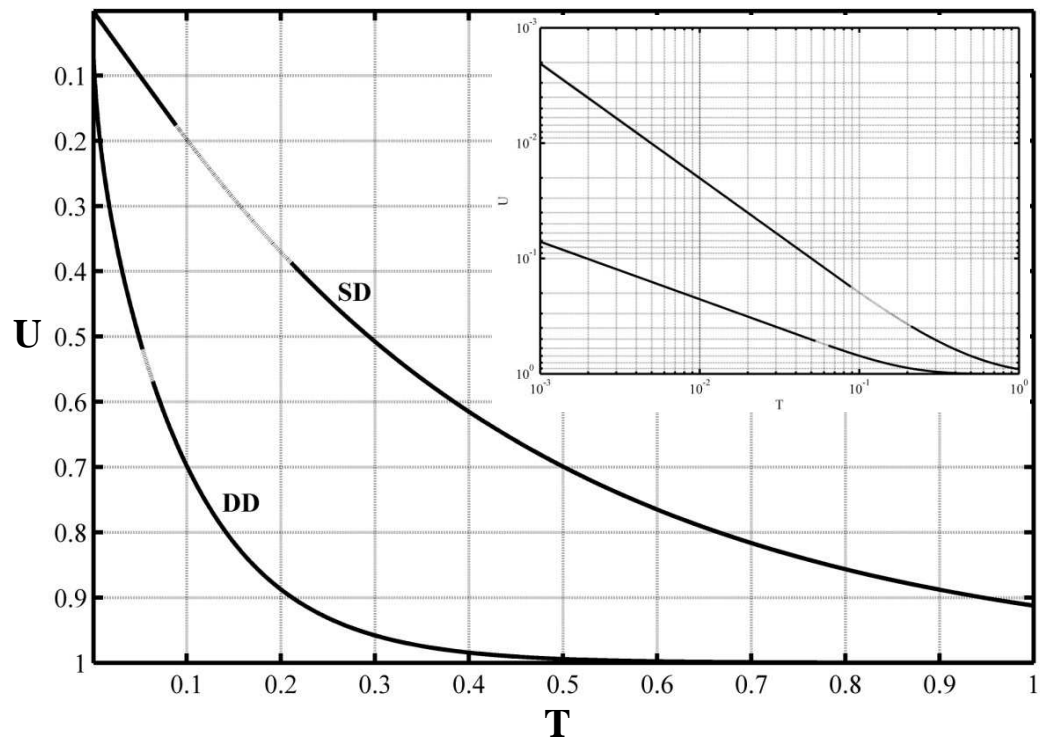


Figure 4.36 – U - T approximation curves for a linearly increasing u_i -distribution with one- or two-way drainage

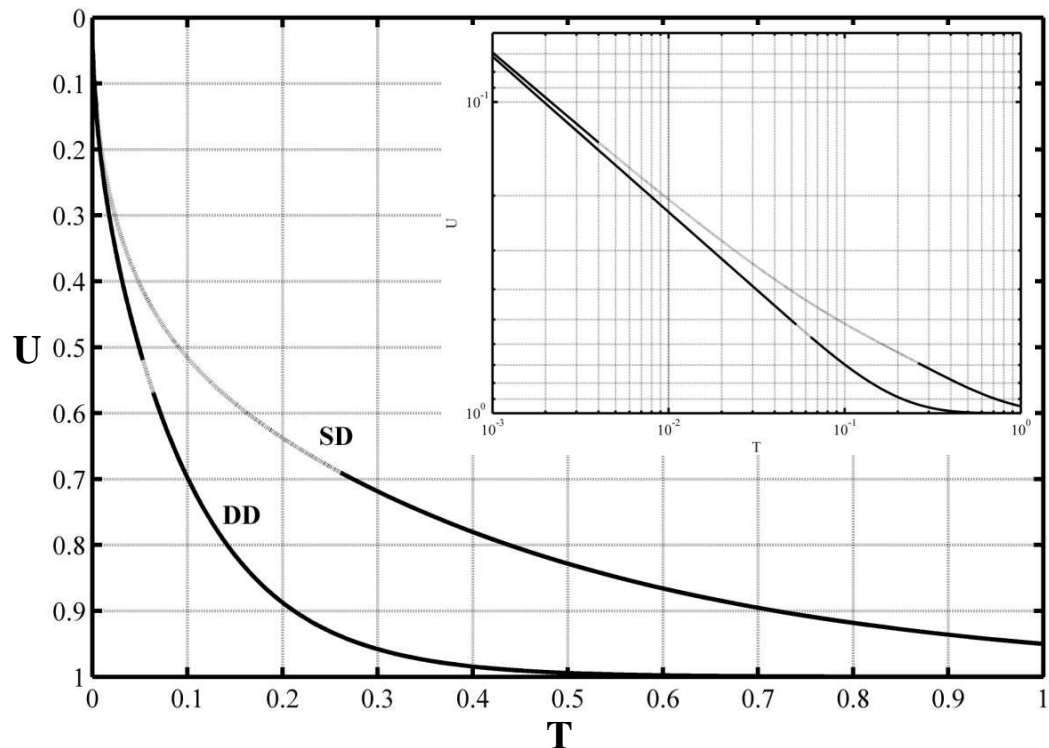


Figure 4.37 – U - T approximation curves for a linearly decreasing u_i -distribution with one- or two-way drainage

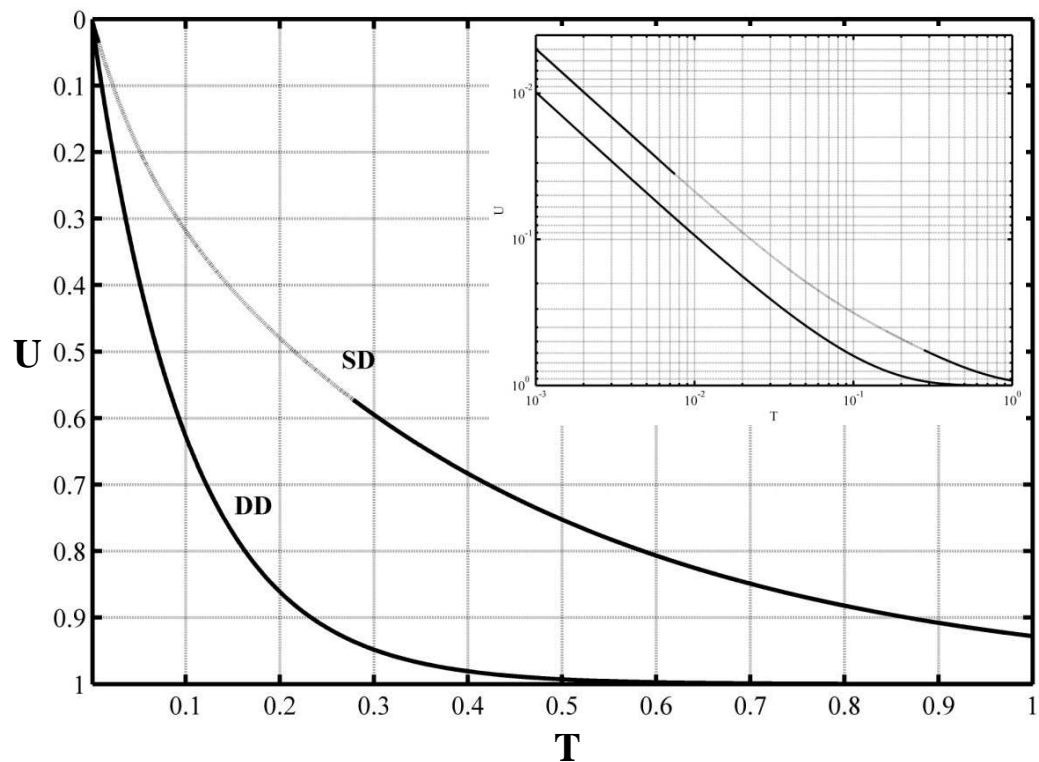


Figure 4.38 – U - T approximation curves for a sinusoidal u_i -distribution with one- or two-way drainage

4.4.2. Generalisation of curve-fitting procedures

The curves of settlement readings versus time (taken from field or laboratory tests) for a given load increment are often similar in shape to the theoretical average degree of consolidation (U) versus time factor (T) curves. Casagrande and Taylor took advantage of this similarity by developing empirical curve-fitting procedures that fit approximately the observed data to the Terzaghi (1925) theory of consolidation. These curve-fitting procedures rely on the following expression to calculate c_v :

$$c_v = \frac{TH_{dr}^2}{t} \quad (4.41)$$

where c_v = coefficient of consolidation, T = time factor that corresponds to a particular percentage consolidation settlement, t = actual time taken to reach that particular consolidation settlement and H_{dr} = maximum length of drainage path, which can vary depending on whether the soil layer is singly or doubly drained. As established previously, it is counterintuitive to work in terms of H_{dr} when dealing with non-uniform u_i -distributions, so the generalised procedures outlined herein will be in terms of H , as

$$c_v = \frac{TH^2}{t} \quad (4.42)$$

Log-time method

The proposed log-time method is a generalized form of Casagrande's log-time method that can account for any non-uniform u_i -distribution. Here, the plots of settlement readings versus time are used in conjunction with the theoretical consolidation curves to establish the point at which primary consolidation is 50% complete, and thereby determine the coefficient of consolidation. The procedure for the determination of c_v is as follows;

- 1) For a given applied load, plot the settlement readings (d) as a function of log-time ($\log t$) and connect with a smooth curve as shown in Figure 4.39.
- 2) Determine d_{100} . To estimate the point of 100% primary consolidation, extend the linear tail of the curve back toward the y-axis. Then draw a line tangent to the point of inflection in the central portion of the curve. The intersection point of these two lines is deemed the end-point of primary consolidation ($U = 1$). Determine d_{100} from the point where the lines intersect. Leonards and Girault (1961) have shown that using tangents to

determine the inflection point of the $d - \log t$ curve results in values of t_{100} that correlate closely to the time at which excess pore pressure approaches zero.

- 3) *Determine d_0 .* Select a time t_x in the initial part of the curve, and calculate t_y such that $t_y = f_C t_x$, where f_C is a factor that is dependent upon the initial excess pore-water pressure distribution and drainage configuration. (Note: For a uniform u_i -distribution, $f_C = 4$ for both one- and two-way drainage configurations). Observe the compression readings that correspond to t_x and t_y (d_x and d_y respectively). Determine the compression reading at the commencement of primary consolidation (d_0) as $d_0 = d_x - \Delta d$ where $\Delta d = d_y - d_x$.
- 4) *Determine t_{50} .* Calculate $d_{50} = (d_{100} + d_0)/2$ and observe the corresponding time (t_{50}).
- 5) *Determine c_v .* Using t_{50} , calculate c_v by substituting the known variables into Eq. (4.42), where T_{50} is obtained from the relevant $U - T$ curve or design tables (Tables 4.6 and 4.7), and H is used instead of H_{dr} . (Note: For a uniform u_i -distribution, $T_{50} = 0.197$ if singly drained, and $T_{50} = 0.049$ if doubly drained.)

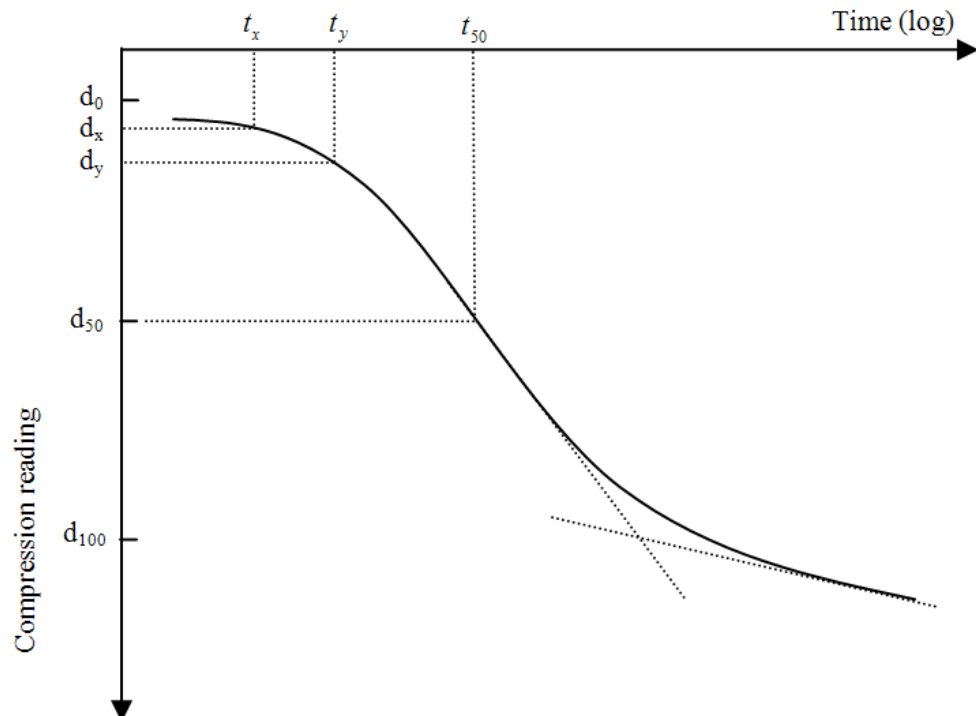


Figure 4.39 – Evaluation of c_v using log-time method

Time exponent method

The time-exponent method outlined in this investigation is a generalized form of Taylor's square root of time method that can accommodate any non-uniform u_i -distribution. As with the log-time method, a similar outcome is required so that Eq. (4.42) can be used to calculate c_v . Using the following time-exponent method, the point at which primary consolidation is 90% complete can be evaluated.

- 1) For a given applied load, plot the settlement readings (d) as a function of time to the power of the exponent B (t^B) as shown in Figure 4.40, where B is dependent upon the initial u_i -distribution. (Note: For a uniform u_i distribution, $B = 0.5$ and the user is directed to take the square root of time values, hence Taylor's 'square root of time' method.)
- 2) Determine d_0 . Ignoring the first few data points, which are usually attributed to immediate settlement and therefore outside the scope of primary consolidation, draw a line through the linear portion of the $d - t^B$ curve. The point where the line intersects the y-axis is the settlement reading at zero deformation (d_0), and signifies the beginning of primary consolidation ($U = 0$).
- 3) Determine t_{90} . When the consolidation plot deviates from linearity, the abscissa of the $d - t^B$ curve becomes greater than that of the straight line segment by a factor which is denoted by f_T at 90% consolidation. If the first straight line is of the form $d' = gt^B + d_0$ where g is the gradient obtained in Step 2, draw a second straight line of the form $d' = (g / f_T)t^B + d_0$ until it intersects the actual $d - t^B$ curve. Observe the corresponding time (t_{90}^B). (Note: For a uniform u_i -distribution, $f_T = 1.15$ for both one- and two-way drainage.)
- 4) Determine c_v . Using t_{90} , calculate c_v by substituting the known variables into Eq. (4.42), where T_{90} is obtained from the relevant $U - T$ curve or design tables (Tables 4.6 and 4.7), and H is the thickness of the soil layer. (Note: For a uniform u_i -distribution, $T_{90} = 0.848$ if singly drained, and $T_{90} = 0.212$ if doubly drained.)

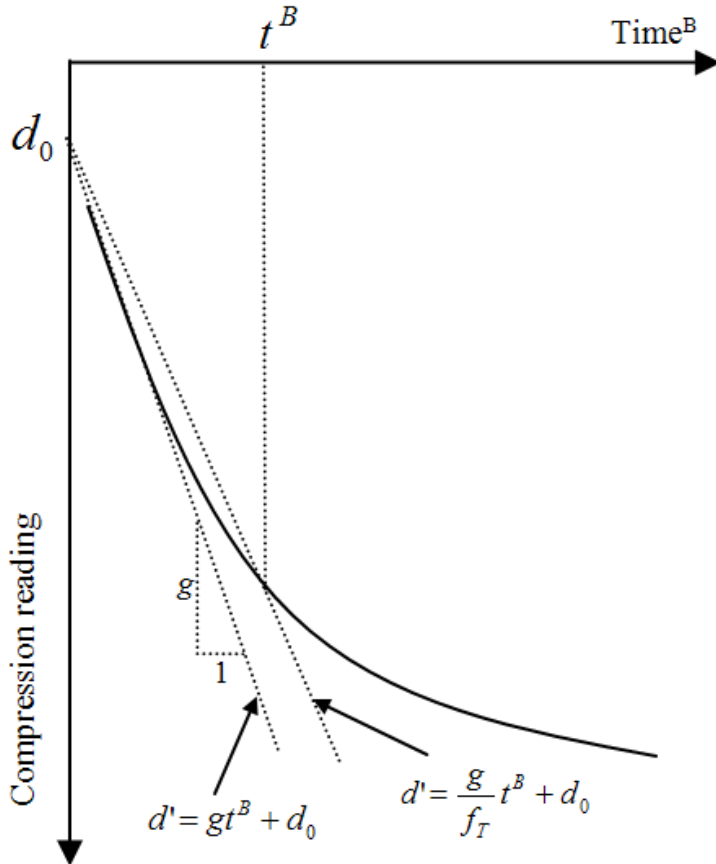


Figure 4.40 – Evaluation of c_v using time-exponent method

4.4.3. Evaluation of adjustment factors

The equation for approximating the first part of the $U - T$ curve (Approximation 1) can be used to derive the curve-fitting procedures proposed by Taylor and Casagrande. In this study, the following expressions were developed using the properties of Taylor and Casagrande's curve-fitting methods along with Eq. (4.39) in order to evaluate the curve-fitting factors f_c and f_T for the u_i -distributions outlined previously:

$$f_T = \left[0.848 \exp\left(\frac{0.1054 + \ln A}{B}\right) \right]^B \quad (4.43)$$

$$f_c = \exp\left(\frac{0.693}{B}\right) \quad (4.44)$$

where A and B = approximation function constants, which are unique to each u_i -distribution and can be found in Tables 4.4 and 4.5.

The curve-fitting constants for doubly and singly drained soil layers are shown in Tables 4.6 and 4.7, respectively. It can be seen that the ratio of singly to doubly drained T values is exactly 4 when considering a uniform u_i -distribution. This ratio is consistent for the entire range of U – that is, a doubly drained layer consistently consolidates four times faster than its singly drained counterpart. This is where the theory for the conventional expression for drainage path length (H_{dr}) originates. However, as soon as a non-uniform u_i -distribution is considered, the ratio between singly and doubly drained T values ceases to remain constant and in fact varies with time. Furthermore, the ratio between T values at key points during consolidation (i.e. 50% and 90% consolidation required for curve-fitting methods) no longer equals 4 for these non-uniform u_i -distributions. As a result, the advantage of working in terms of H_{dr} is no longer available, and any effort to include this variable can actually complicate consolidation calculations.

Table 4.6 – f_C and f_T curve-fitting factors for two-way drainage

Log-time method		Time-exponent method	
f_C	T_{50}	f_T	T_{90}
4.00	0.049	1.15	0.212
2.04	0.070	2.23	0.233

Table 4.7 – f_C and f_T curve-fitting factors for one-way drainage

Log-time method		Time-exponent method	
f_C	T_{50}	f_T	T_{90}
4.00	0.197	1.15	0.848
2.01	0.294	2.07	0.946
4.23	0.090	1.82	0.718
2.05	0.215	3.86	0.866

As demonstrated for a case of uniform u_i , Taylor and Casagrande's curve-fitting methods are only effective if there is a sufficient region over which the approximation for the first

part of the $U - T$ curve (Approximation 1) applies. When a non-uniform u_i -distribution is considered, the valid domain for Approximation 1 decreases from 52% (for the uniform case) to less than 18%. When using the log-time method, this reduced domain can make the evaluation of d_0 (Step 3) difficult since the region over which f_C applies is also reduced. The time-exponent method relies on the user being able to objectively identify the ‘straight-line’ portion of the transformed settlement-time curve. A reduced domain for Approximation 1 can thereby introduce a certain degree of subjectivity to the curve-fitting method, as the user has a smaller ‘straight-line’ region to work with.

4.5 Summary

Existing curve-fitting techniques for determining the coefficient of consolidation have been critically reviewed using oedometer data gathered from tests conducted on different soil types. Furthermore, a new method independent of curve-fitting has been proposed, which utilises the computational abilities of MATLAB to back-calculate a value for c_v . Results suggest that the efficacy of each method is dependent upon the soil properties, and whether secondary compression is prevalent. Furthermore, modifications have also been developed to adjust current curve-fitting techniques so that they can be applied to any set of settlement-time data, regardless of the initial excess pore water pressure distribution that generated this data.

The parameter, coefficient of consolidation, was also discussed in relation to average degree of consolidation. Popular curve-fitting techniques that fit experimental data to the theoretical average degree of consolidation curve in order to back-calculate consolidation parameters were critically reviewed using copious experimental data. A new oedometer apparatus was also discussed, where the effect of skin friction was incorporated into the initial excess pore water pressure distribution. Conclusions derived from this research were then experimentally verified using a tall oedometer. Finally, popular curve-fitting techniques (Taylor’s square-root of time method, and Casagrande’s logarithm-time method) were modified so that they can be applied to any set of settlement-time data, regardless of the initial excess pore water pressure distribution.

Chapter 5: Experimental validation of pore pressure redistribution and curve-fitting procedures

5.1 General

The phenomenon of pore pressure redistribution outlined in Chapter 3 can be experimentally verified by simulating a non-uniform u_i -distribution which is known to elicit this redistribution of excess pore water pressures. The simplest non-uniform initial excess pore water pressure distribution that can be recreated within a laboratory setting is a sinusoidal u_i -distribution. This can be achieved by conducting a standard doubly drained oedometer test and waiting a short period for the dissipation of excess pore water pressures to reach a sinusoidal shape. Pore pressure redistribution is known to occur when a *singly* drained layer is subjected to a sinusoidal u_i -distribution. Thus, by halting drainage from one of the two drainage boundaries in the doubly drained test once the pressures have reached their sinusoidal shape, a sinusoidal u_i -distribution with one-way drainage situation can be successfully replicated.

This principle can be further applied to assess the efficacy of two of the curve-fitting procedures outlined in Chapter 4; the sinusoidal u_i -distribution with one-way drainage, and the sinusoidal u_i -distribution with two-way drainage.

5.2 Pore pressure redistribution

As explained in Chapter 3, the phenomenon of pore pressure redistribution is likely to occur in cases where a significant portion of the u_i -distribution is located within a small region of the consolidating soil layer. The probability of this redistribution occurring is further compounded in singly drained soil layers, especially when this region is located close to the impervious boundary.

The existence of this pore pressure redistribution phenomenon can be verified either using field data collected from a region where a non-uniform u_i -distribution was known to exist and tracking the pore water pressure dissipation during consolidation, or by conducting a simple experiment in the laboratory where a non-uniform u_i -distribution is recreated. Here, the tall oedometer apparatus described in Chapter 4 becomes very useful.

5.2.1. ‘Arched’ u_i -distribution with one-way drainage

The distribution of excess pore water pressure within the tall oedometer is known to be non-uniform in shape, according to the derivation outlined previously. Since this non-uniform u_i -distribution was derived using classical arching theory, it will be referred to herein as an ‘arched’ u_i -distribution. If the layer is singly drained, the dissipation of excess pore water pressure can be expected to follow the pattern outlined by the pore pressure isochrones in Figure 5.1(a), which clearly exhibit pore pressure redistribution.

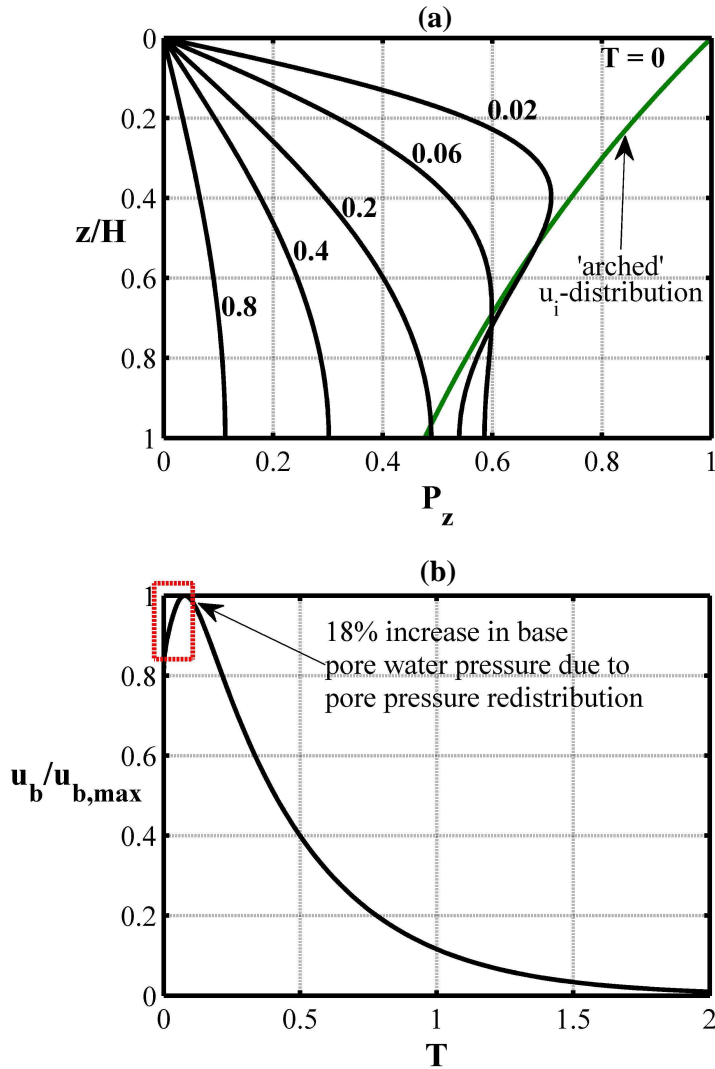


Figure 5.1 – Consolidation behaviour due to an arched u_i -distribution in terms of (a) pore pressure isochrones for $T = 0.02, 0.06, 0.1, 0.2\dots 1.0$, and (b) variation in pore pressure at $z = H$ with T

Theoretically, by conducting a singly drained test in the tall oedometer and measuring pore water pressures at the base of the apparatus, this pore pressure redistribution can be confirmed. The base pore water pressures (u_b) are expected to follow the trend shown in

5.1(b) which was theoretically obtained using the pressure values at $z = H$ from Figure 5.1(a). It should be noted that the base pore water pressures in Figure 5.1(b) have been normalised by the maximum base pressure value ($u_{b,\max}$), which is equal to the 62% of the pressure applied to the surface of the sample, assuming $c' = 25 \text{ kPa}$, $\phi' = 25^\circ$, $\delta = 0.5\phi'$, and $\gamma = 17 \text{ kN/m}^3$.

When this experiment was conducted in the laboratory, the initial increase in excess pore water pressure characteristic of pore pressure redistribution was difficult to capture. This was attributed in part to the sensitivity of the pressure transducer, and to the relatively small expected increase in pore water pressure as evident in Figure 5.1(b) (i.e. an increase of only 18% is expected). Thus, a non-uniform u_i -distribution that exhibits a more pronounced redistribution of excess pore water pressure during consolidation was needed.

5.2.2. Sinusoidal u_i -distribution with one-way drainage

An alternative u_i -distribution that is known to yield a greater degree of pore pressure redistribution was achieved by conducting an oedometer test that was initially doubly drained, but was switched to singly drained some short time later by closing the base drainage valve. At the instant base drainage was halted, designated by t_{block} , the distribution in excess pore water pressure can be considered non-uniform (and approximately sinusoidal) in shape. The process from t_{block} onwards can thus be treated as a singly drained layer subjected to a sinusoidal u_i -distribution, which is known to elicit severe pore pressure redistribution (see Figure 3.12).

This doubly-to-singly drained process was conducted within the tall oedometer apparatus described in Chapter 4, which is known to produce an arched u_i -distribution. It is important to halt base drainage at a point in time at which the excess pore pressure distribution is as close to sinusoidal as possible, whilst still allowing sufficient time to capture the subsequent progression of singly drained consolidation. Thus, the *exact* point at which the excess pore water pressure becomes sinusoidal must be determined.

According to Figure 5.2, which ‘fits’ sinusoidal distributions to the actual decay of excess pore water pressure due to an arched u_i -distribution, the isochrones do not become sinusoidal in appearance until approximately $T \approx 0.1$. This can be more precisely confirmed using a ratio of undissipated excess pore water pressure of an arched u_i -distribution in

comparison with the undissipated excess pore pressure of a purely sinusoidal u_i -distribution. This is similar to the procedure outlined in Chapter 3, where the variable R_a was introduced to compare non-uniform u_i -distributions with a uniform u_i -distribution, which can be adjusted to incorporate a sinusoidal u_i -distribution rather than a uniform u_i -distribution as follows:

$$R_a = \frac{\left[\int_0^H u(z, T) dz \right]_{\text{arched}}}{\left[\int_0^H u(z, T) dz \right]_{\text{sinusoidal}}} \quad (5.1)$$

In Eq. (5.1), the numerator represents the total undissipated excess pore water pressure due to an arched u_i -distribution at some point during consolidation (T) and the denominator denotes the total undissipated excess pore water pressure due to a sinusoidal u_i -distribution at that same point in time.

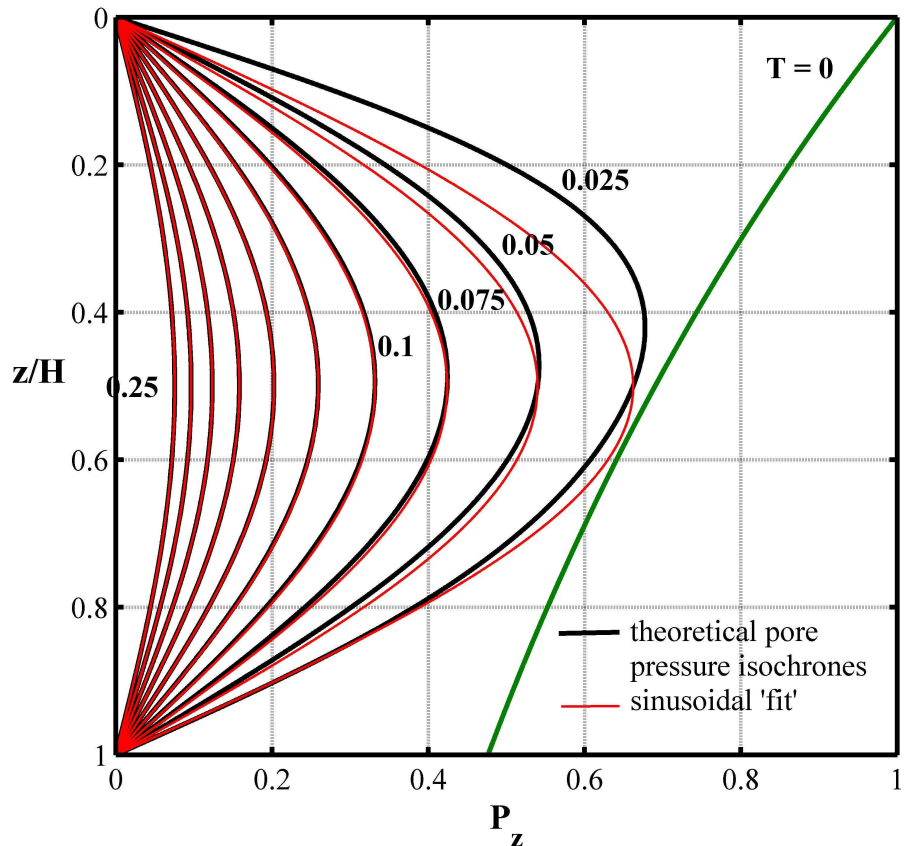


Figure 5.2 – Pore water pressure isochrones due to an arched u_i -distribution with accompanying sinusoidal approximations

The ratio of these values (R_a) varies with time and is highly dependent upon sample dimensions – smaller values of H / D see the excess pore water pressure tending towards a sinusoidal shape (i.e. $R_a = 1$) much earlier during consolidation. A plot of R_a from Eq. (5.1) with T in Figure 5.3 shows that the isochrones due to an arched u_i -distribution where the sample height to diameter (H / D) ratio is less than 2 become perfectly sinusoidal at $T = 0.07$. For larger H / D ratios, the isochrones do not become sinusoidal until $T = 0.09$.

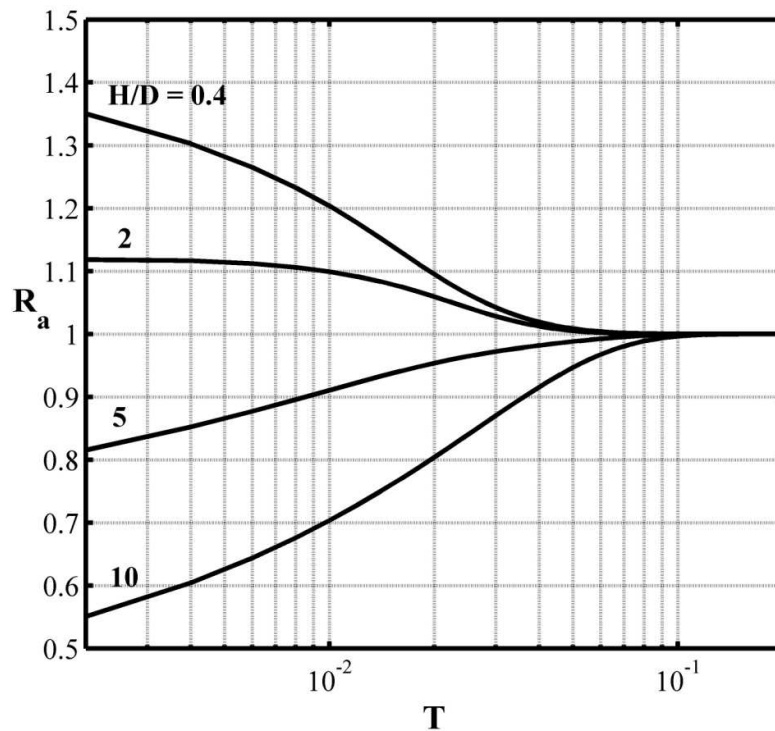


Figure 5.3 – Tendency of pore water pressure isochrones to become sinusoidal in shape for different H/D values, under doubly drained conditions

Assuming a sinusoidal u_i -distribution, a graph similar to that shown in Figure 5.1 can be developed, which is shown in Figure 5.4. In this case, the maximum base pore pressure was determined to be 61.1% of the applied pressure. In contrast with the arched u_i -distribution in Figure 5.1, the sinusoidal u_i -distribution results in a more pronounced peak in base pore water pressures shortly after the singly drained test has commenced, as shown in Figure 5.4(b). This peak in base pore water pressure is a clear indication of pore pressure redistribution. Thus, if the experimental measurement of base pore water pressures during testing exhibits this time lag before reaching the maximum pressure, pore pressure redistribution can be said to occur.

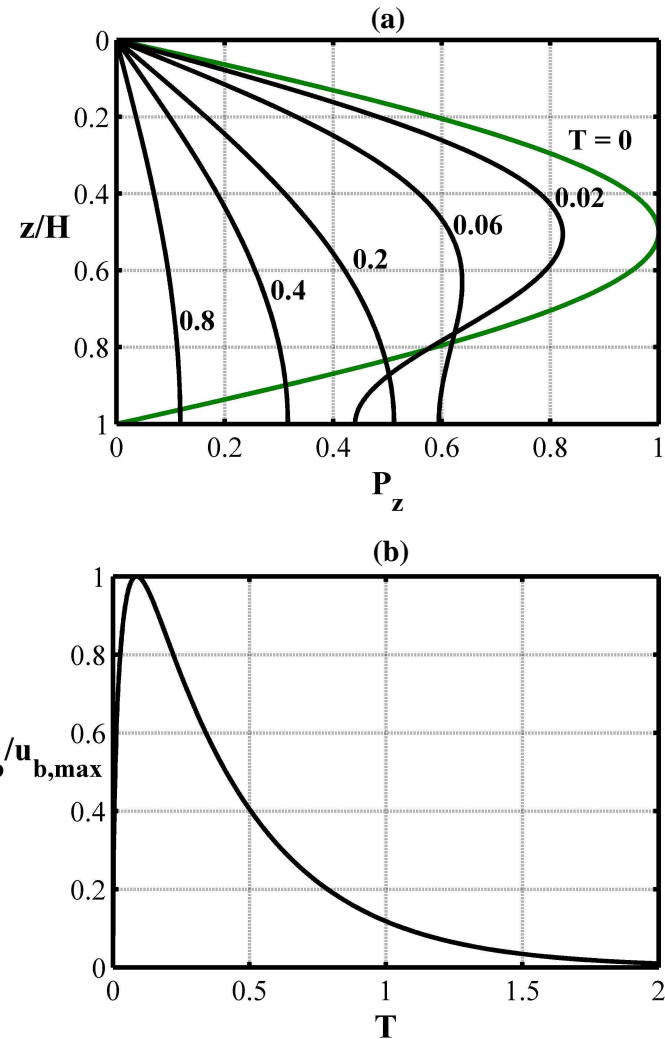


Figure 5.4 – Consolidation behaviour due to a sinusoidal u_i -distribution in terms of (a) pore pressure isochrones for $T = 0.02, 0.06, 0.1, 0.2 \dots 1.0$, and (b) variation in pore pressure at $z = H$ with T

Testing went ahead using a known soil with already determined consolidation properties. A number of tests were conducted, all of which yielded very similar results. An example of the analysis that took place is as follows. First, the soil was loaded into the tall oedometer in slurry form and allowed to settle overnight. Any excess water was siphoned off the surface the following morning, after which a small pressure of 20 kPa was applied. Loading was then increased according to LIR of unity until 160 kPa was reached, with doubly drained conditions maintained throughout. For the subsequent applied surcharge of 300 kPa, the doubly-to-singly drained test was conducted and base pore pressures recorded.

The K_{60} soil described in Table 4.1 (Chapter 4) was used for these tests. According to the research conducted in Chapter 4, the anticipated value of c_v for this soil and under the applied pressure range of 140-350 kPa is approximately $7.0\text{-}9.0 \text{ m}^2/\text{yr}$. The height of the sample at the start of testing was 129 mm. By combining these parameters, the earliest time

at which base drainage must be halted ($t_{block,sin}$) in order to achieve a sinusoidal distribution of excess pore water pressure can be calculated as follows:

$$t_{block,sin} = \frac{T_s H_0^2}{c_{v,min}} \quad (5.2)$$

where T_s is the time factor at which pore pressures are sinusoidal (0.07 from Figure 5.3), H_0 is the height of the sample upon application of 300 kPa applied pressure and $c_{v,min}$ is taken as the minimum possible value of c_v ($7.0 \text{ m}^2/\text{yr}$) for that pressure increment in order to determine a conservative value for $t_{block,sin}$. The test was subsequently conducted for $t_{block} = 2 \text{ hrs}$ (which is greater than the calculated value for $t_{block,sin} = 1.46 \text{ hrs}$), after which time pore water pressures at the bottom of the specimen were manually recorded until consolidation was complete. In order to verify the experimental data using theory, the raw data had to be adjusted – the base pore water pressures were normalised by the maximum value achieved during testing, and the times at which these pressures were recorded were then converted to time factor values. To do this, a value of c_v was required. After manually varying the input c_v value within MATLAB, the best fit between experimental and theoretical data was found to occur when $c_v = 8.5 \text{ m}^2/\text{yr}$, which lay within the anticipated region of c_v values ($7.0\text{-}9.0 \text{ m}^2/\text{yr}$). The results are displayed in Figure 5.5 which shows a good alignment between experimental results and the theoretical curve from Figure 5.4(b).

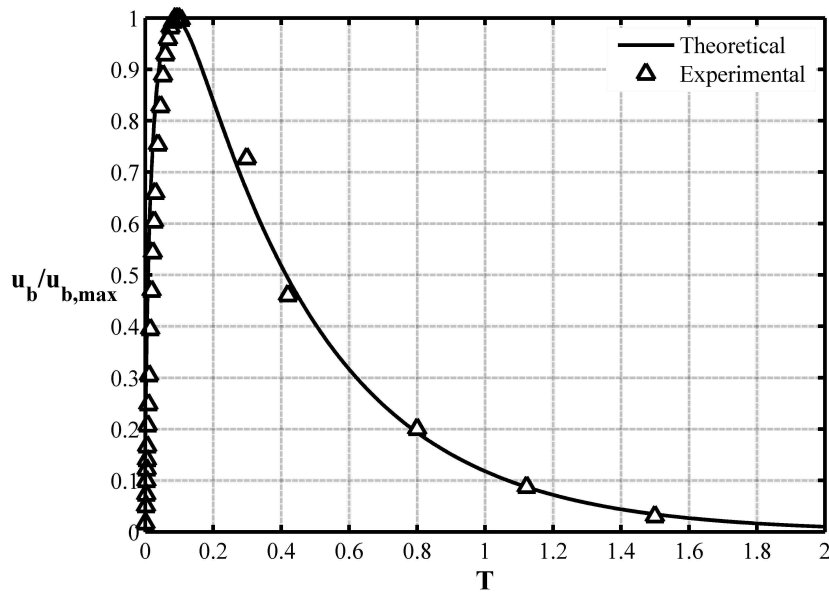


Figure 5.5 – Variation in experimental and theoretical base pore water pressure with time for a sinusoidal u_i -distribution with one-way drainage

Whilst the experimental *trend* closely models theory, there were some discrepancies between the maximum base pore water pressures achieved during testing and the theoretical maximum. For an applied surcharge of 300 kPa (increased by 140 kPa from 160 kPa), the theoretical maximum base pore water pressure that should occur during testing is $0.611 \times 140 = 85.5$ kPa. However, the maximum pressure that was achieved during testing was 40 kPa, which is only 47% of the theoretical maximum. This discrepancy was attributed to the stiffness of the pore water pressure measuring system which potentially allowed partial drainage of pore water from the base of the sample. Other past investigations involving recordings of base pore water pressure encountered similar partial drainage problems (Whitman et al. 1961, Perloff et al. 1965, Robinson 1999). Despite this minor discrepancy, the results support the theory and provide evidence of the pore pressure redistribution phenomenon.

5.3 Generalised curve-fitting procedures

Using the same principle of doubly-to-singly drained testing to create a non-uniform u_i -distribution that is sinusoidal in shape, some of the modified curve-fitting procedures developed in Chapter 4 (Section 4.4) can be easily verified.

5.3.1. Singly drained layer subjected to a sinusoidal u_i -distribution

Using the approach outlined in Section 5.2, it is also possible to verify the modified curve-fitting procedure proposed in Chapter 4 (Section 4.4) for a singly drained soil layer subjected to a sinusoidal u_i -distribution. These tests were conducted using the tall oedometer apparatus outlined in Chapter 4.

Experimental Strategy

Consider the average degree of consolidation curves shown in Figure 5.6. The $U - T$ curve 1-2-3 depicts the rate of consolidation of a doubly drained soil layer subjected to a uniform (or arched as long as $H / D < 2$) u_i -distribution. The consolidation process (shown in blue) 1-2-4 is part doubly drained, and part singly drained. From 1 to 2, the layer is doubly drained. At 2, the base drainage valve is closed and the system becomes singly drained which leads to a much slower rate of consolidation (as outlined by 2 to 4 in comparison with 2 to 3). Provided the distribution of excess pore water pressure with depth at the time drainage is halted (t_{block}) is sinusoidal, the section between points 2 and 4 can be treated as a new consolidation process which equates to a singly drained layer subjected to a sinusoidal u_i -distribution. Excluding any previous settlement, this process can also be represented by

the green $U - T$ curve (where the average degree of consolidation was calculated using a sinusoidal u_i -distribution). Thus, if this test were reproduced within a laboratory setting, the data obtained from points 2 to 4 could feasibly be analysed using the modified curve-fitting procedure for a singly drained layer subjected to a sinusoidal u_i -distribution to obtain the c_v value of the soil.

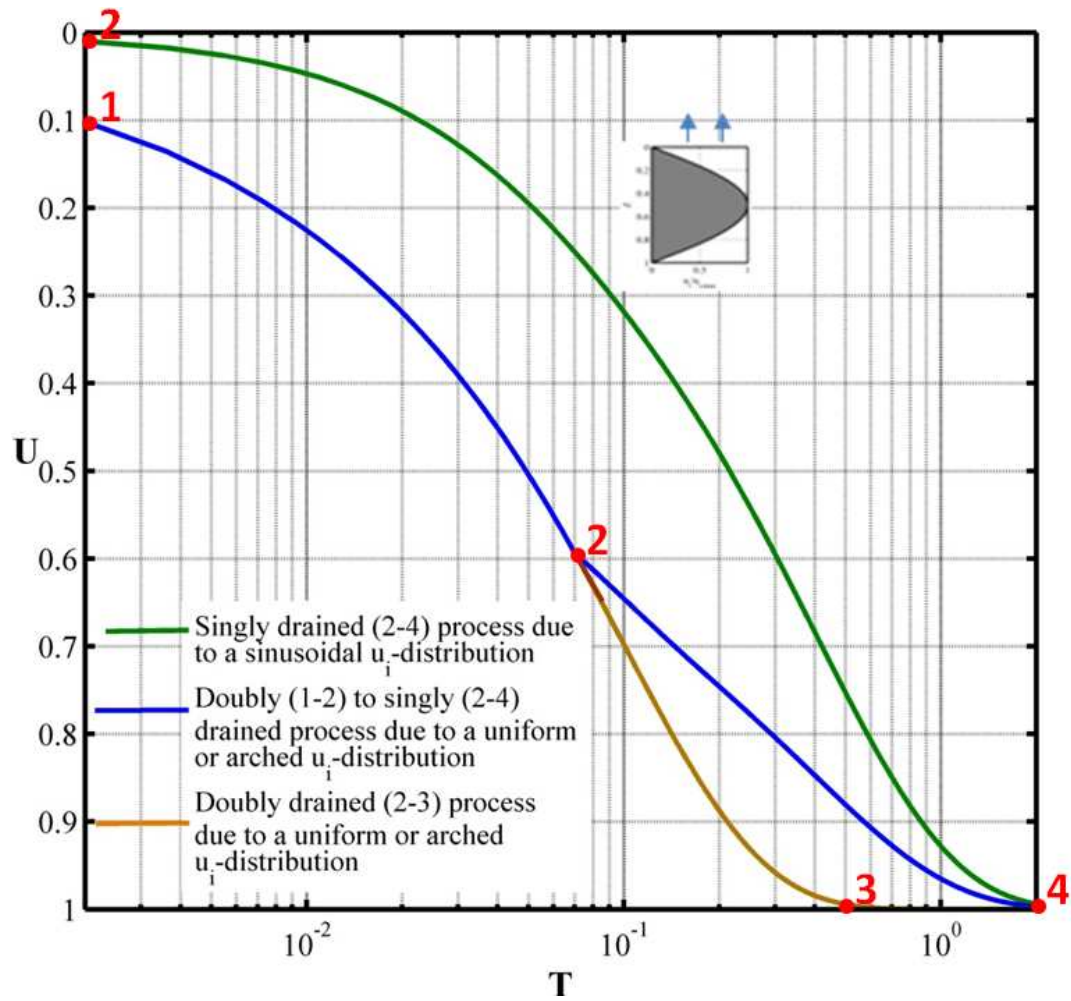


Figure 5.6 – Average degree of consolidation curves translating a doubly drained layer to a singly drained layer subjected to a sinusoidal u_i -distribution

This process was carried out using the K_{60} soil described in Chapter 4, where the initial height of the sample was varied to assess the effect of the H/D ratio. As outlined in Chapter 4, the expected value of c_v for this soil within the applied pressure range of 80-160 kPa is approximately $5.5\text{-}9.0 \text{ m}^2/\text{yr}$. A summary of the theoretical $t_{block,sin}$ values calculated using Eq. (5.2) from two tests conducted under 160 kPa applied pressure is shown in Table

5.1, along with the actual t_{block} values used during testing, their corresponding values of T_{block} , and the settlement measured at t_{block} (s_{block}).

Table 5.1 – Details of doubly drained to singly drained testing

		Test 1	Test 2
Experimental parameters	H_0 (mm)	141	100
	H / D	1.84	1.32
	s_{block} (mm)	3.22	3.57
	t_{block} (mins)	98	40
	T_{block}	0.05	0.04
Limiting factor	$t_{block,sin}$ (mins)	133	67

As shown in Table 5.1, the times at which base drainage was halted during Tests 1 and 2 were actually less than the conservative value of $t_{block,sin}$ calculated using Eq. (5.2). Thus, further examination is required to determine if, and how closely the percentage consolidation of a singly drained layer subjected to one of these not-yet-sinusoidal isochrones ($T < 0.07$) behaves in comparison to a singly drained layer subjected to a sinusoidal u_i -distribution.

As established previously, once the base drainage valve has been closed, any subsequent consolidation can be treated as an entirely new consolidation process where the pore water pressure distribution at T_{block} is treated as the new ‘initial’ distribution, where T_{block} is the time factor corresponding to t_{block} . By selecting particular isochrones and treating them as new ‘initial’ distributions, it is possible determine the value of T_{block} for which the problem behaves as if the u_i -distribution were perfectly sinusoidal. For instance, if the pore pressure isochrones due to an arched u_i -distribution in Test 1 (where $H / D = 1.84$, from Table 5.1) are revisited, it can be seen that the isochrones *appear* sinusoidal before they technically become sinusoidal. This is evident in Figure 5.7 where the blue isochrones are purely sinusoidal (according to the $T = 0.07$ cut-off established previously) and the red isochrones have yet to become sinusoidal.

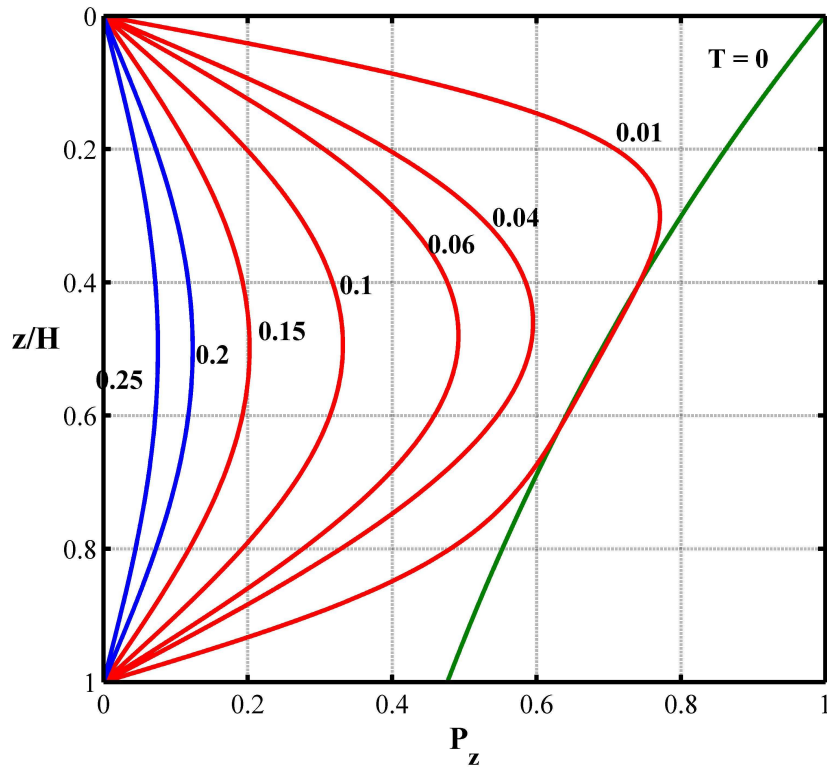


Figure 5.7 – Excess pore water pressure isochrones due to an arched u_i -distribution with two-way drainage

It was considered appropriate to conduct a comparison in terms of average degree of consolidation, since the modified curve-fitting procedures are reliant on this parameter. This exercise was completed for small values of T_{block} (0.01 and 0.04), where it is known that the distribution of excess pore water pressure is not yet completely sinusoidal. The results are shown in Figure 5.8, where the blue $U-T$ curve indicates the consolidation behaviour of a singly drained soil layer subjected to a true sinusoidal u_i -distribution. The isochrones corresponding to $T_{block} = 0.01$ and 0.04 (due to an arched u_i -distribution with two-way drainage) were used as ‘initial’ excess pore water pressure distributions with subsequent one-way drainage to generate $U-T$ curves for comparison with the $U-T$ curve resulting from a sinusoidal u_i -distribution with one-way drainage (shown in blue). It is evident that if bottom drainage is halted even in the very early stages of consolidation, the subsequent process still closely follows the sinusoidal $U-T$ curve.

Using Figure 5.8, it can be concluded that as long as $T_{block} > 0.04$, any consolidation settlement that occurs during the singly drained portion of the test can be independently analysed using the modified curve-fitting technique for a sinusoidal u_i -distribution (with

one-way drainage). Thus, even conservatively, the values of T_{block} in Table 5.1 still meet this requirement.

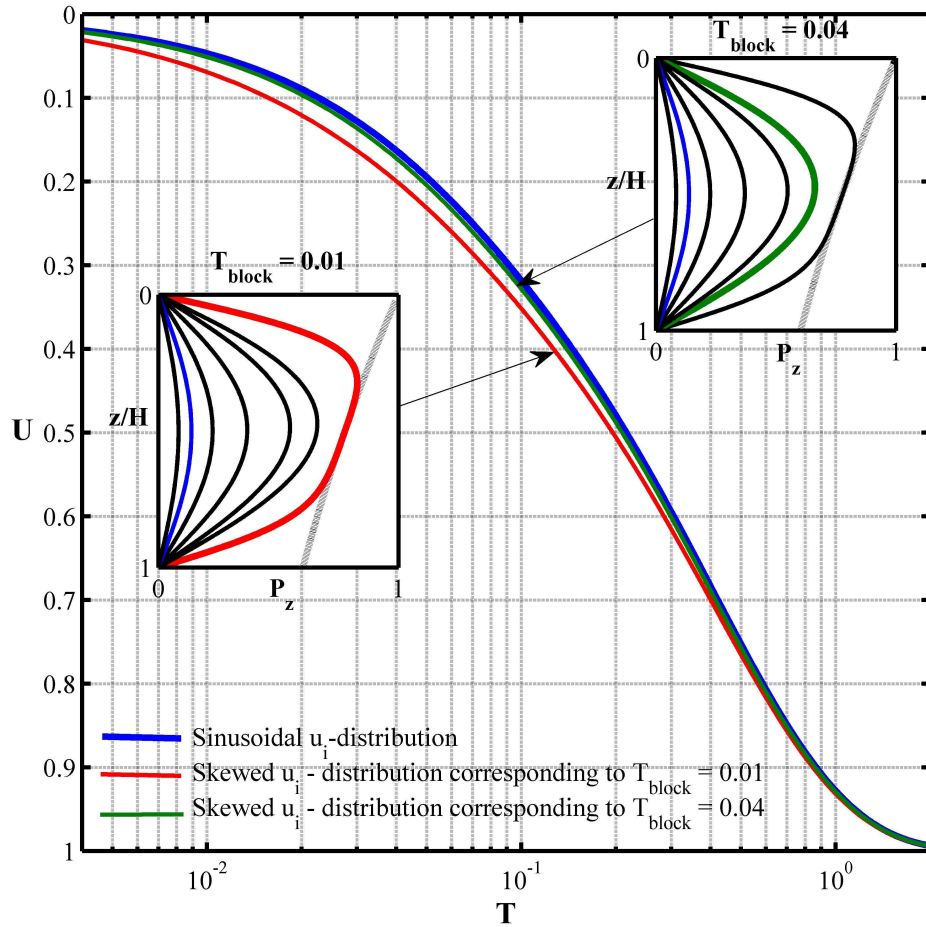


Figure 5.8 – Average degree of consolidation curves using $T_{block} = 0.01$ and 0.04 isochrones of an arched u_i -distribution as ‘initial’ u_i -distributions with subsequent one-way drainage

Results – Singly drained consolidation process (2 to 4)

Using the factors provided in Chapter 4 (Section 4.4), Figures 5.9 and 5.10 were developed, each of which depict the modified Casagrande and Taylor curve-fitting methods for a sinusoidal u_i -distribution with one-way drainage.

Based on the data obtained from the singly drained portion of the process only (from points 2 to 4 in Figure 5.6), subsequent values of c_v were predicted using the modified Casagrande and Taylor methods (denoted by $c_{v,Cas}$ and $c_{v,Tay}$ respectively). In Test 1 (i.e. the 141 mm thick sample), approximately 50% of the total settlement data occurred under singly drained conditions, whereas in Test 2, 70% of the data corresponded to singly drained conditions, each of which were used in the modified curve-fitting techniques.

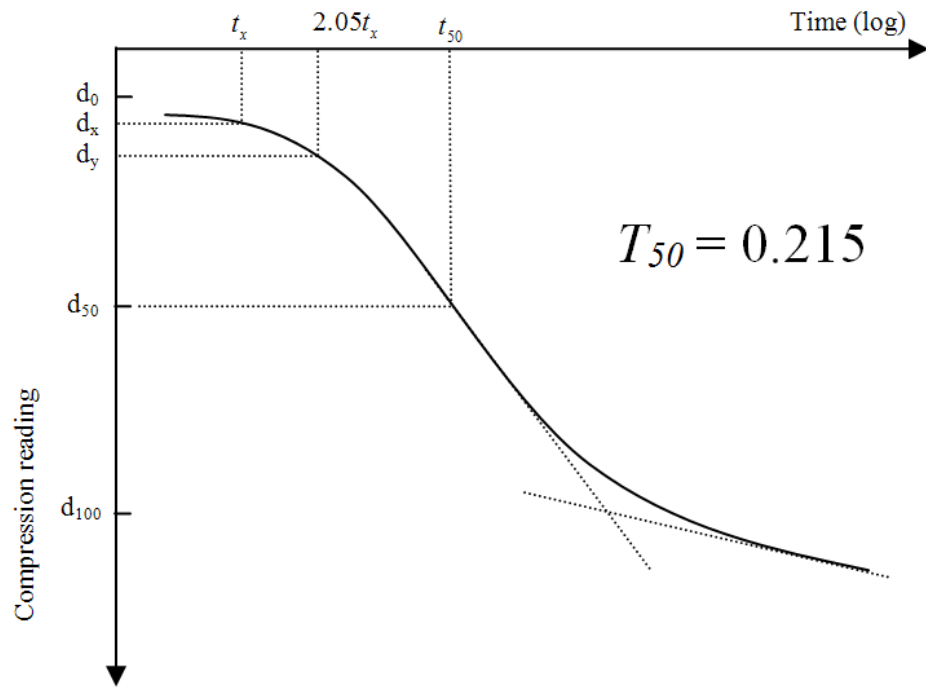


Figure 5.9 – Modified Casagrande curve-fitting procedure for a singly drained layer subjected to a sinusoidal u_i -distribution

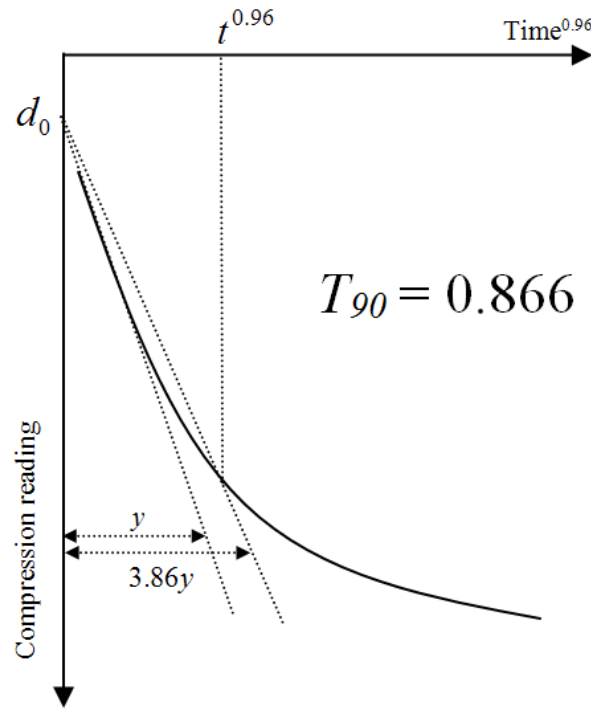


Figure 5.10 – Modified Taylor curve-fitting procedure for a singly drained layer subjected to a sinusoidal u_i -distribution

Using the settlement data corresponding to the singly drained portion of the test only, the *modified* Taylor and Casagrande curve-fitting methods were used to determine the value of c_v . To do this, it was first necessary to subtract t_{block} from all singly drained t values so that the x -axis of the sinusoidal singly drained plot spanned from $t = 0$ to $t_{100} - t_{block}$ rather than t_{block} to t_{100} . An example analysis is shown in Figure 5.11 for the Test 1 settlement data.

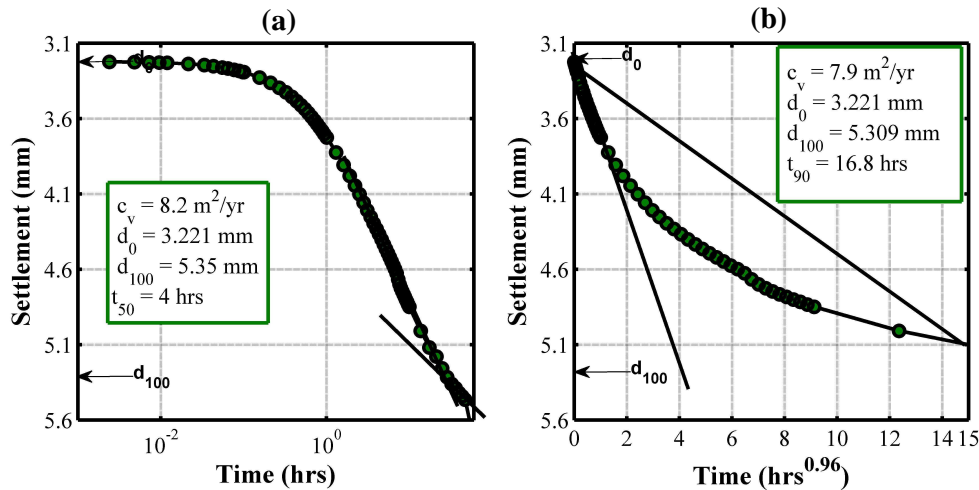


Figure 5.11 – Example analysis using (a) modified Casagrande curve-fitting technique, and (b) modified Taylor curve-fitting technique

It should be noted that the ‘initial’ thickness (H_0) used to conduct these analyses was calculated by subtracting the total settlement that occurred during the doubly drained process (s_{block}) from the actual initial thickness.

Results – Doubly-to-singly drained consolidation process (1 to 4)

Although the expected range of c_v values for the K_{60} mix operating under an applied pressure of 160 kPa is already known ($5.5\text{--}9.0 \text{ m}^2/\text{yr}$), the c_v value for each particular doubly-to-singly drained test was also determined using a trial-and-error type procedure implemented in the program MATLAB. Here, the *entire* set of data was fitted to the theoretical curve contained within points 1 and 4 in Figure 5.6. To do this, the settlement readings taken during testing had to be scaled to reflect percentage consolidation. Thus, the compression readings that corresponded to 0% and 100% primary consolidation were required. This was done using the same tangent principles behind determining d_0 and d_{100} in the traditional Casagrande method. Then, all compression readings were converted to percentage consolidation.

Using various values of c_v , the raw times corresponding to each compression reading were converted to time factor values which were then plotted against percentage consolidation. Based on results collected during Test 1, the value of c_v that gave the best fit (when viewing the process as a whole) was $7.0 \text{ m}^2/\text{yr}$, which lies within the expected region. This value was also independently achieved using the results collected during Test 2 which suggests confidence in the repeatability of the test. The resulting plots of experimental data versus the theoretical $U - T$ curve (from points 1 to 4 in Figure 5.6) are shown in blue in Figures 5.12 and 5.13 for Tests 1 and 2, respectively. The singly drained portion of the blue $U - T$ curve in Figures 5.12 and 5.13 was theoretically determined for $T_{block} = 0.06$ and 0.08 , and $T_{block} = 0.05$ and 0.06 for Test 1 and Test 2, respectively, to cover the expected range of c_v values (from $6.0\text{--}8.0 \text{ m}^2/\text{yr}$). This was deemed necessary due to the circular nature of the problem; to calculate the value of c_v , the experimental data must be fitted to the theoretical curve, which also requires the value of c_v .

The values of c_v obtained using the modified curve-fitting procedures applied to the singly drained data only resulted in the following values for $c_{v,Cas}$ and $c_{v,Tay}$: 7.9 and 8.2 , and 7.6 and $8.3 \text{ m}^2/\text{yr}$ for Tests 1 and 2, respectively. These values were used to non-dimensionalise the experimental data for comparison with the theoretical $U - T$ curve. The results shown in green in Figures 5.12 and 5.13 represent the non-dimensionalised experimental data obtained from the singly drained portion of the tests only, which are in close agreement with the theoretical curve for a sinusoidal u_i -distribution with one-way drainage.

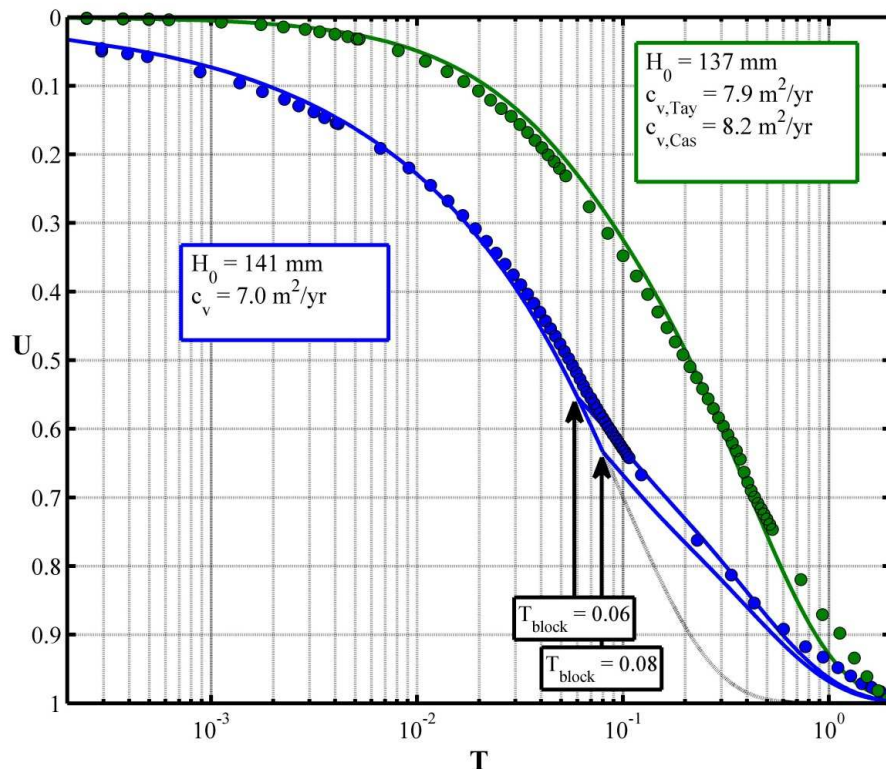


Figure 5.12 – Comparison between values of c_v obtained using trial and error versus modified curve-fitting technique (sample of 141 mm height subjected to an applied load of 160 kPa)

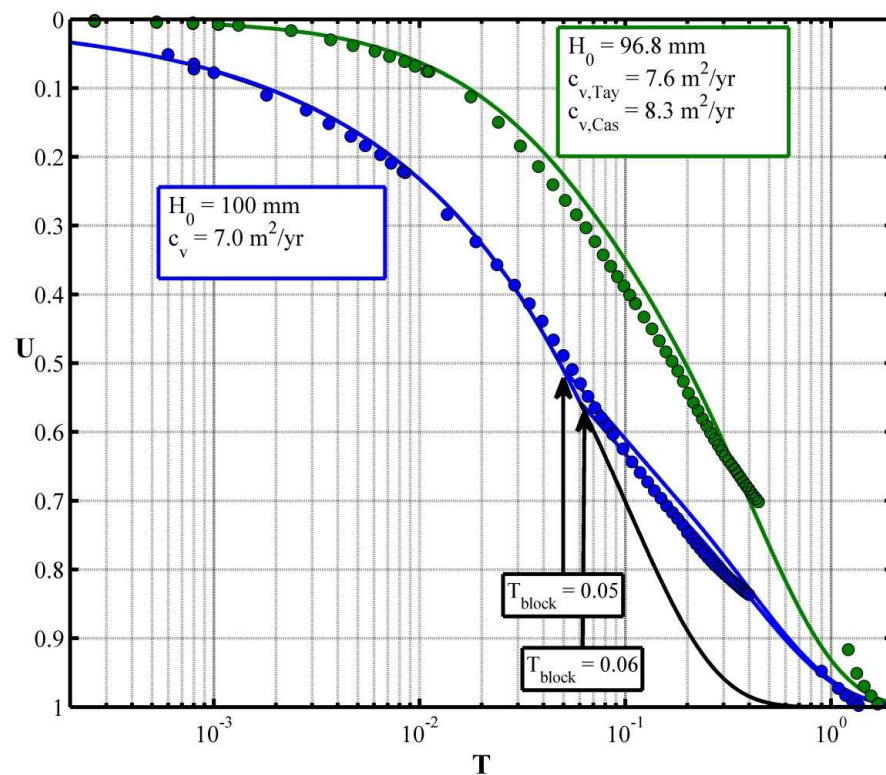


Figure 5.13 – Comparison between values of c_v obtained using trial and error versus modified curve-fitting technique (sample of 100 mm height subjected to an applied load of 160 kPa)

A summary of the consolidation parameters obtained using the modified curve-fitting methods in comparison with the ‘true’ values evaluated using the trial-and-error MATLAB process is provided in Table 5.2.

Table 5.2– Results from Tests 1 and 2 obtained using (a) MATLAB trial-and-error, and (b) modified curve-fitting techniques

(a)		(b)	
		Total (1 to 4)	Sine (2 to 4)
Test 1	d_0 (mm)	0.42	Percentage data used
	d_{100} (mm)	5.4	t_{block} (min)
	c_v (m^2/yr)	7.0	d_0 (mm)
Test 2	d_0 (mm)	1.7	Casagrande d_{100} (mm)
	d_{100} (mm)	5.9	c_v (m^2/yr)
	c_v (m^2/yr)	7.3	Taylor d_0 (mm)
Test 1			d_{100} (mm)
			c_v (m^2/yr)
			Percentage data used
Test 2			t_{block} (min)
			d_0 (mm)
			Casagrande d_{100} (mm)
Test 2			c_v (m^2/yr)
			Taylor d_0 (mm)
			d_{100} (mm)
Test 2			c_v (m^2/yr)

Overall, these results suggest the modified Casagrande and Taylor curve-fitting methods are effective in evaluating the coefficient of consolidation of a singly drained soil layer subjected to a sinusoidal u_i -distribution. Furthermore, this exercise could potentially be repeated to verify the efficacy of the modified curve-fitting method corresponding to a doubly drained layer subjected to an half-sinusoidal u_i -distribution. Here, the test would begin as a singly drained process and then revert to doubly drained conditions after an half-sinusoidal u_i -distribution was achieved.

5.3.2. Doubly drained layer subjected to a sinusoidal u_i -distribution

Using the same principles outlined in Section 5.3.1, it is possible to also verify the modified Taylor and Casagrande curve-fitting procedures for a doubly drained layer subjected to a sinusoidal u_i -distribution. In fact, it is much easier to do this since any portion of the data obtained during a conventional oedometer test can be used (after the pore pressure has become sinusoidal).

Experimental Strategy

As demonstrated in Figures 3.34 and 3.35, where the variation in R_a with T was observed for non-uniform u_i -distributions in comparison with a uniform u_i -distribution, the time factor at which the pore pressure decay of a uniform u_i -distribution becomes sinusoidal is approximately 0.03, provided the soil layer is doubly drained. Thus, any portion of settlement corresponding to $T > 0.03$ can be analysed using the modified curve-fitting procedures for a sinusoidal u_i -distribution with two-way drainage. This is illustrated by Figure 5.14, which provides the average degree of consolidation curves due to uniform and sinusoidal u_i -distributions for a doubly drained soil layer.

The $U - T$ curve 1-2-3 corresponds to the percentage settlement-time curve obtained during traditional oedometer testing.

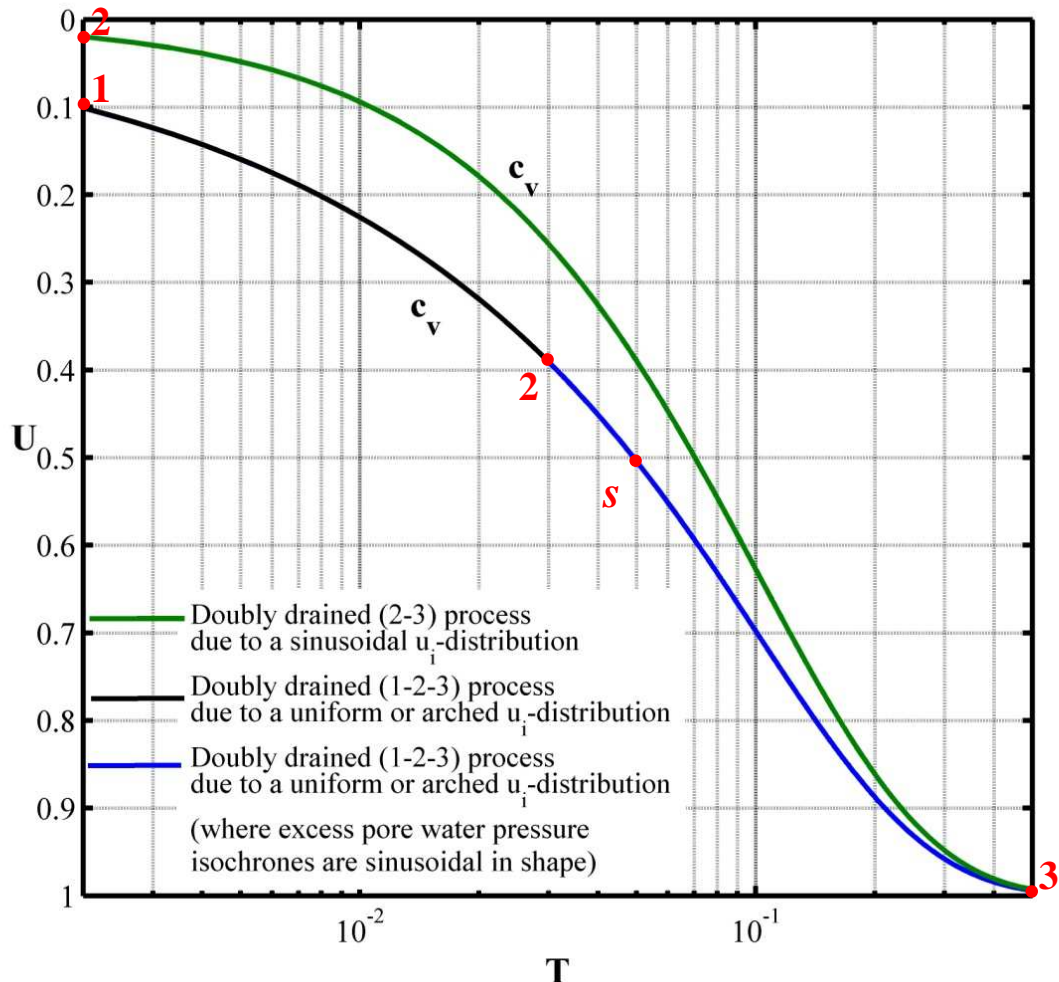


Figure 5.14 – Average degree of consolidation curves translating a doubly drained layer subjected to uniform or sinusoidal u_i -distributions

The blue portion of this curve (from 2 to 3) depicts the percentage consolidation that occurs when the excess pore water pressure isochrones are sinusoidal in shape. The data obtained between points 2 and 3 can thus be analysed using the modified curve-fitting procedure for a sinusoidal u_i -distribution with two-way drainage (denoted by the green curve in Figure 5.14). In fact, unlike the singly drained procedure outlined in Section 5.3.1, *any* set of data obtained between s and 3 (where s is an arbitrary point within the region 2 to 3) can be analysed using this method since the distribution in excess pore water pressures remains sinusoidal throughout. This means that, in essence, there are *multiple* values of c_v that can be obtained from just *one* oedometer test, which may be useful for validation purposes. Using settlement data corresponding to the sinusoidal portion of the test only, the modified Taylor and Casagrande curve-fitting methods were used to determine the value of c_v . The time chosen from which to analyse the sinusoidal data (t_s) was varied, so that different portions of the sinusoidal section were analysed.

For this doubly drained analysis, two different soil samples were used (K_{60} and DM) along with two different oedometer apparatus', the tall oedometer described previously and a standard oedometer. The earliest conservative time from which data could be extracted ($t_{s,\sin}$) was calculated using Eq. (5.2) and is shown in Table 5.3, along with actual testing parameters.

Table 5.3– Details of doubly drained testing

		Data set 1	Data set 2
Experimental parameters	Test type	Standard	Tall
	Soil type	DM	K_{60}
	Applied pressure (kPa)	8.29	160
	Expected c_v range (m ² /yr)	0.2-0.4	5.5-9.0
	H_0 (mm)	19.6	111
	H / D	0.3	1.6
	s_{s1} (mm)	1.8	2.8
	t_{s1} (min)	66	47
Limiting factors	T_{s1}	0.07	0.04
	$t_{s,\sin}$ (min)	30	47
	T_s	0.03	0.04

Although two sets of data were extracted from the settlement-time data obtained from one oedometer test, only the first settlement-time point (s_{s1}, t_{s1}) from which data was extracted is provided in Table 5.3 to ensure it meets the limiting criterion (i.e. $T_{s1} \geq T_s$).

Results

Using the factors provided in Chapter 4 (Section 4.4), Figures 5.15 and 5.16 were developed, each of which depict the modified Casagrande and Taylor curve-fitting methods for a sinusoidal u_i -distribution with two-way drainage. Using the data from two independent doubly drained oedometer tests, values of c_v were subsequently predicted using the modified Casagrande and Taylor methods ($c_{v,Cas}$ and $c_{v,Tay}$ respectively).

When conducting the modified curve-fitting analysis, it was necessary to shift each data set back to $t = 0$, as if each were its own new consolidation test. To do this, t_s was subtracted from all t values within the selected data segment so that the x -axis of the sinusoidal doubly drained plot spanned from $t = 0$ to $t_{100} - t_s$ rather than t_s to t_{100} (similar to the procedure outlined in Section 5.3.1).

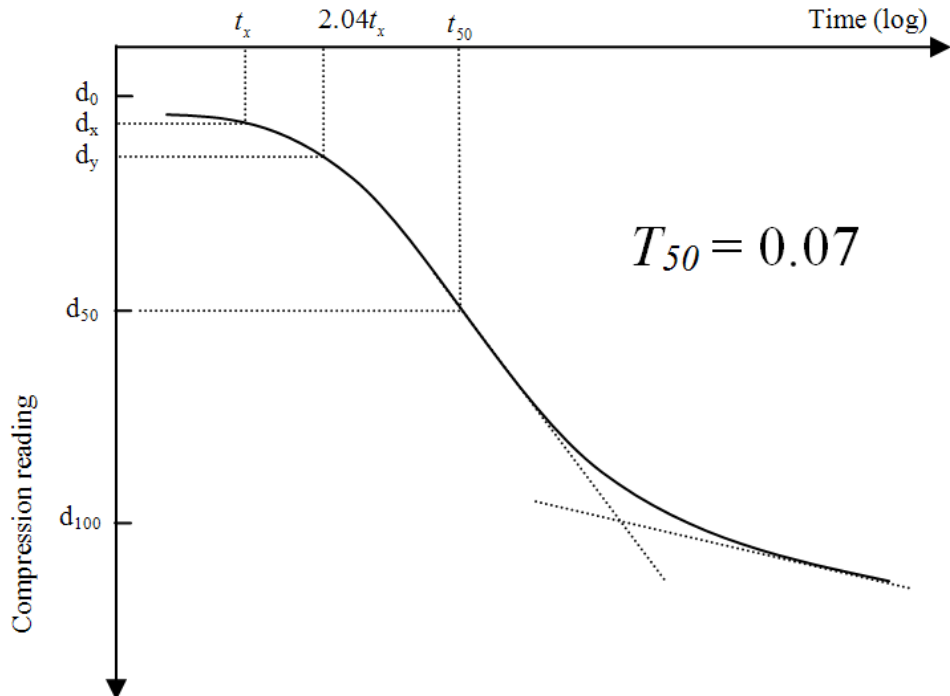


Figure 5.15 – Modified Casagrande curve-fitting procedure for a doubly drained layer subjected to a sinusoidal u_i -distribution

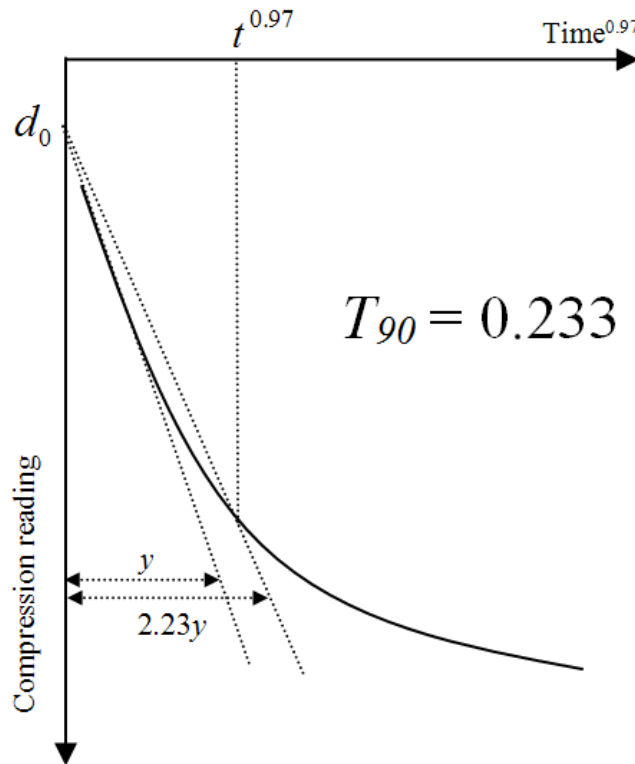


Figure 5.16 – Modified Taylor curve-fitting procedure for a doubly drained layer subjected to a sinusoidal u_i -distribution

For the Casagrande analysis, the experimental settlement (d) was plotted against logarithm of time (t), as shown in Figures 5.17 and 5.18 which correspond to data sets 1 and 2, respectively. The $d - \log t$ curves for both uniform and sinusoidal cases are shown on the one plot for clarification purposes. However, the analysis for each case was conducted using separate plots so that the y -axis could be adjusted accordingly for accuracy.

In Figures 5.17 and 5.18, points 1 to 3 indicate the set of data that was analysed using the traditional Casagrande curve-fitting method. The data between points 2a and 3 was extracted and shifted back so that the array of time values for this data began at $t \approx 0$ hrs. The subsequent $d - \log t$ plot was then analysed using the modified Casagrande method for a sinusoidal u_i -distribution with two-way drainage. This procedure was repeated for the smaller set of compression data contained with points 2b to 3. It is clearly evident that point 2a in Figures 5.17 and 5.18 (selected at $t = 66$ min and 47 min, respectively) adhere to the restrictions set by $t_{s,\sin}$ calculated using Eq. (5.2), provided in Table 5.3. It should be noted that any point between $t_{s,\sin}$ and 3 could have been selected to analyse the data – the points 2a and 2b were simply arbitrarily selected.

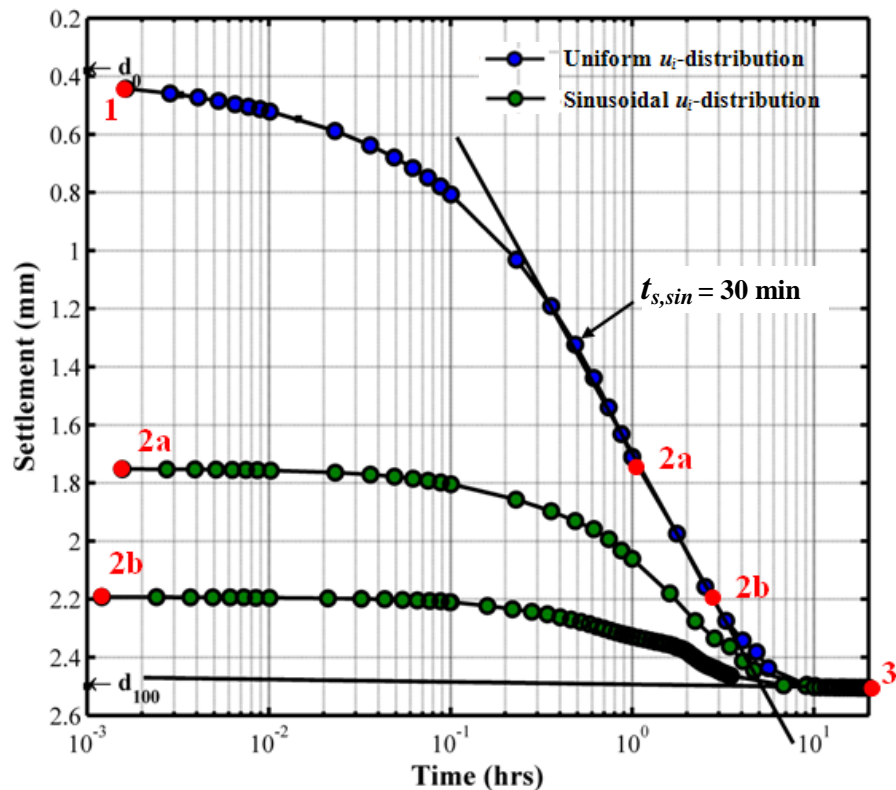


Figure 5.17 – Analysis of data set 1 using traditional and modified Casagrande curve-fitting techniques

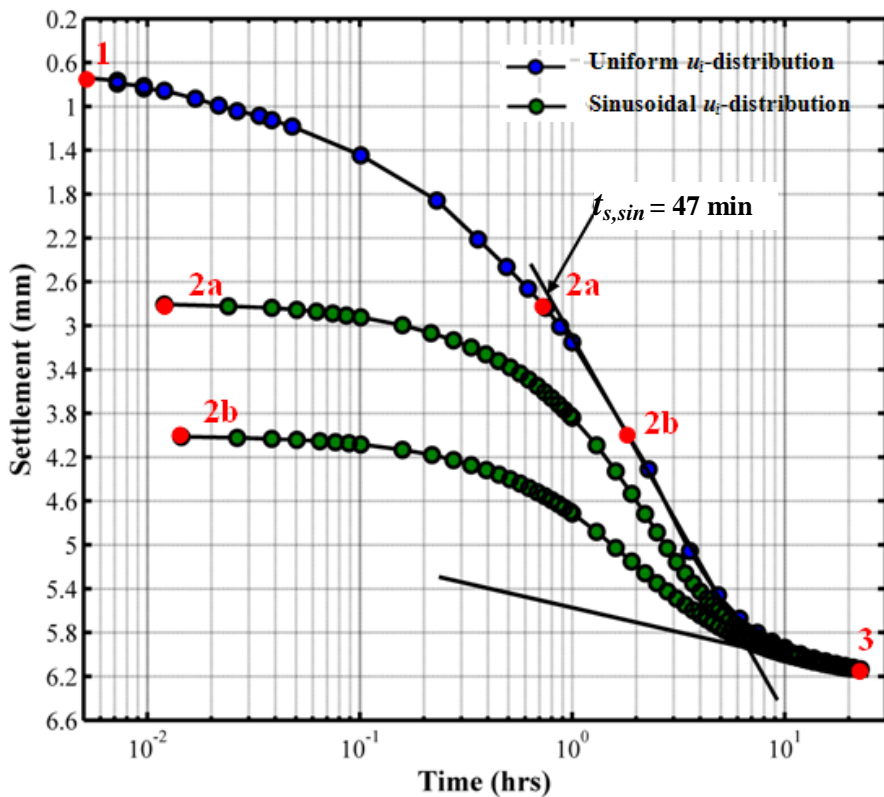


Figure 5.18 – Analysis of data set 2 using traditional and modified Casagrande curve-fitting techniques

When using the modified Casagrande method, d_0 was easily identified as the settlement corresponding to t_s . The settlement corresponding to 100% primary consolidation (d_{100}) was identical to the value determined using the traditional Casagrande method. Overall, the major contributor to the difference in methods is the value of T_{50} , which is 0.07 compared with the value corresponding to a uniform u_i -distribution which is 0.049.

For the Taylor analysis in traditional terms, the experimental settlement was plotted against $t^{0.5}$ as shown in Figures 5.19 and 5.20, which correspond to data sets 1 and 2, respectively. However, when using the modified Taylor method, the x -axis must be of the form $t^{0.97}$ (see Table 4.4) in order to adequately capture the initial ‘straight-line’ portion of the. As a result, the sinusoidal $d - t^{0.97}$ curves are shown as insets in Figures 5.19 and 5.20. The tangent lines characteristic of the Taylor method have been included in Figures 5.19 and 5.20 for the uniform case and the first sinusoidal set of data (from points 2a to 3) to illustrate the differences in methods.

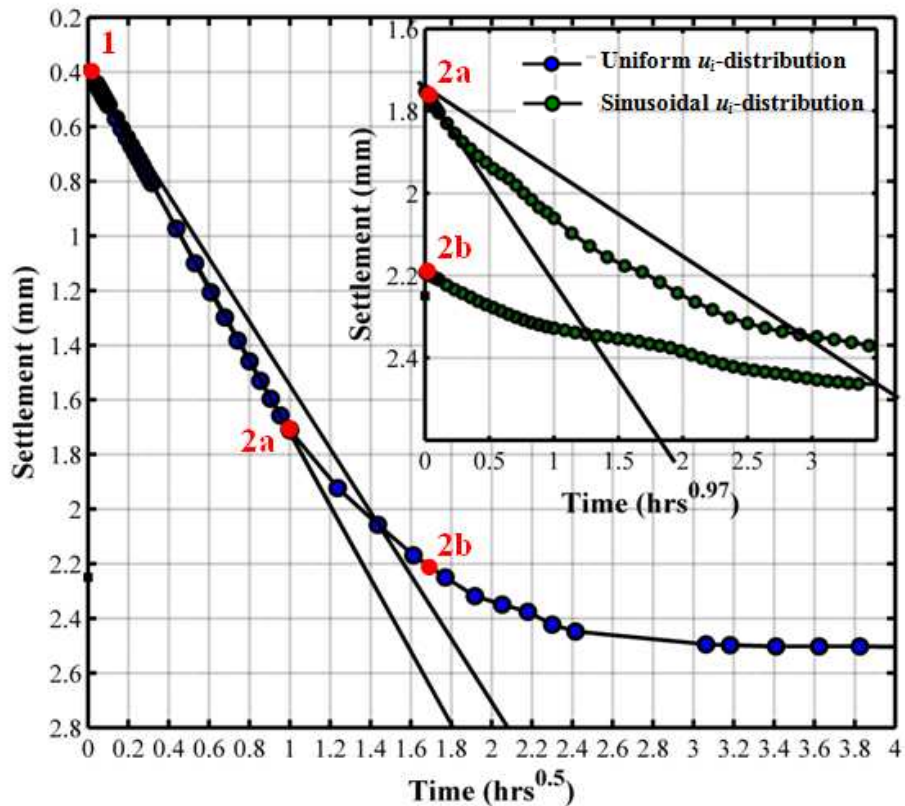


Figure 5.19 – Analysis of data set 1 using traditional and modified Taylor curve-fitting techniques

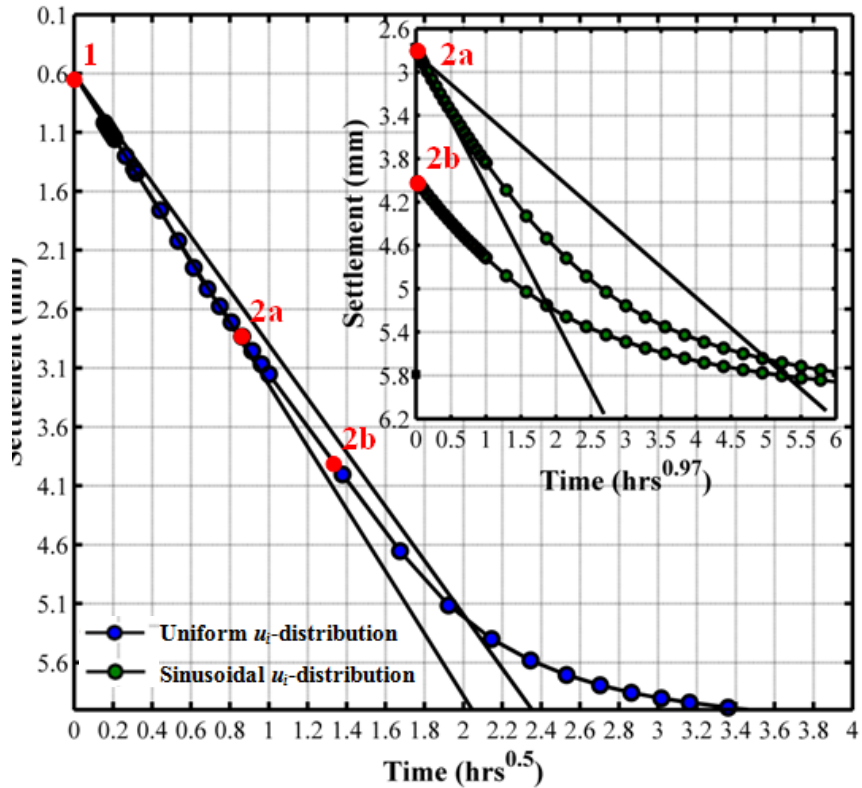


Figure 5.20 – Analysis of data set 2 using traditional and modified Taylor curve-fitting techniques

It is important to note that the straight-line portion of the sinusoidal $d - t^{0.97}$ curve is much smaller than that of the uniform $d - t^{0.5}$ curve. This can be explained by re-examining Table 4.4, which shows that the ‘straight-line’ approximation for the sinusoidal case only applies to 11% of the total settlement, whereas the ‘straight-line’ portion of the uniform case applies to 52% of the total settlement. Thus, when using the modified Taylor method, it is important not to try and force the line through more data points than necessary.

In order to verify the values of c_v calculated using the modified curve-fitting methods for a sinusoidal u_i -distribution with two-way drainage, the data as a whole (i.e. a doubly drained layer subjected to a uniform u_i -distribution) was also analyzed using traditional Casagrande and Taylor curve-fitting methods for comparison. A summary of the consolidation parameters obtained using the traditional and modified curve-fitting methods for data sets 1 and 2 is provided in Table 5.4. The values of c_v obtained by applying the modified Casagrande method to the sinusoidal data are consistently less than the values obtained using the traditional method, but only to a very small degree (approximately 15%). This is also evident upon examination of the c_v values obtained using the Taylor method. Overall, c_v

values obtained using modified curve-fitting methods aligned with those obtained traditionally, even when only 29% of the data was used in the analysis (as was the case for the Sine 2b-3 analysis in data set 1).

Table 5.4 – Results obtained using traditional and modified curve-fitting techniques to analyse data sets 1 and 2

		Uniform	Sine	
Data set 1	Percentage data used	100%	47%	29%
	t_s (hrs)	0	1.1	2.6
	d_0 (mm)	0.38	1.8	2.2
	Casagrande	d_{100} (mm)	2.5	2.5
		c_v (m^2/yr)	0.23	0.19
		d_0 (mm)	0.39	1.8
Data set 2	Taylor	d_{100} (mm)	2.3	2.4
		c_v (m^2/yr)	0.29	0.22
		Percentage data used	100%	61%
	t_s (min)	d_0 (mm)	0.40	2.8
		d_{100} (mm)	5.9	5.9
		c_v (m^2/yr)	6.9	5.9
	Casagrande	d_0 (mm)	0.61	2.8
		d_{100} (mm)	5.8	5.9
		c_v (m^2/yr)	5.9	5.7
	Taylor	d_0 (mm)	0.40	4.0
		d_{100} (mm)	5.9	5.9
		c_v (m^2/yr)	6.9	5.9

Although the differences between the traditional and modified curve-fitting methods appear minor, it is important to acknowledge the importance of these differences. For example, if the *traditional* Casagrande method was used to analyse the *sinusoidal* data, the predicted values of c_v would be approximately 50% less than the actual value. This variation would be further exacerbated if the traditional Taylor method was used instead of the modified method, where c_v values as much as 10 times the actual c_v of the soil can be expected. Clearly, the modifications to the traditional curve-fitting methods play a significant role in the determination of accurate values of c_v in these sinusoidal u_i -distribution cases.

In order to make a definitive conclusion regarding the efficacy of the modified curve-fitting methods, the experimental data was plotted against theoretical values using each set of parameters from Table 5.3 similar to the analysis conducted in Section 4.2. These results are shown in Figures 5.21 and 5.22, which correspond to data sets 1 and 2, respectively. In general there is a close agreement between theoretical and experimental results. However, it appears that the Taylor method consistently outperforms the Casagrande method in terms of the fit achieved between experimental data and theory.

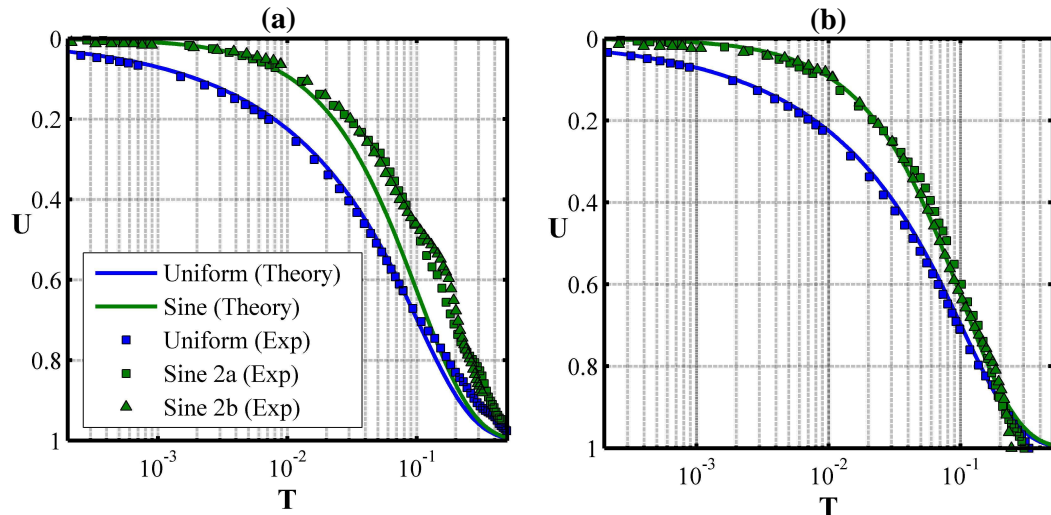


Figure 5.21 – Experimental vs theory using (a) $c_{v,Cas}$ and (b) $c_{v,Tay}$ for data set 1

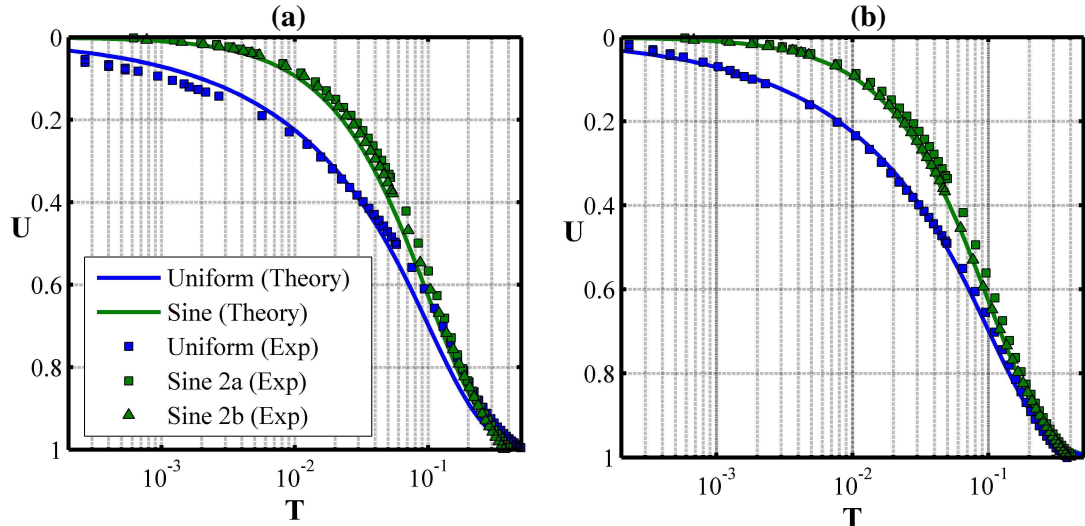


Figure 5.22 – Experimental vs theory using (a) $c_{v,Cas}$ and (b) $c_{v,Tay}$ for data set 2

The modified curve-fitting procedures were successfully used to analyse the data obtained during the doubly drained consolidation of a soil layer. It is possible to apply the same principle to a singly drained layer. Here, the modified curve-fitting method for a half-sinusoidal u_i -distribution with one-way drainage would be used to analyse the data instead.

5.3.3. Practical Implications

The proposed modified curve-fitting methods have many potential applications when it comes to back-calculation of the coefficient of consolidation, and in field predictions of settlement. In fact, by using these methods, some common difficulties regarding back-calculation of consolidation properties can be avoided. For instance, if an initial period of

settlement versus time is unknown, the remaining data that was collected need not be discarded. An analysis using sinusoidal or half-sinusoidal curve-fitting procedures (for doubly or singly drained layers, respectively) can still take place *at any time*, as long as consolidation is not yet complete.

Furthermore, if the soil layer being considered was initially subjected to an unknown non-uniform u_i -distribution, the majority of settlement behaviour can still be predicted using the sinusoidal or half-sinusoidal solutions since the decay of excess pore water pressure will inevitably return to one of these shapes. That is, some short time later (depending, of course, on the coefficient of consolidation and thickness of the soil being considered), the process will have returned to a familiar sinusoidal/half-sinusoidal process where the consolidation behaviour is known.

The prediction of c_v has long been a contentious issue among geotechnical engineers, as evidenced by the numerous evaluation techniques available in literature. Many of these methods require complicated analysis techniques, while others are as unreliable as they are simple. Many geotechnical engineers and laboratory technicians will invariably return to the widely used Taylor and Casagrande methods to analyse settlement-time data. The benefits of using one of the modified curve-fitting procedures proposed within this study to analyse data obtained from a laboratory oedometer test are threefold;

1. The user is sure to be already familiar with the basic steps involved in the popular Taylor and Casagrande curve-fitting methods. The advantage associated with the modified Taylor and Casagrande methods is that the overall procedure remains the same – it is only the curve-fitting *parameters* that are adjusted to account for the sinusoidal/half-sinusoidal u_i -distribution.
2. Depending on the type of soil being tested, immediate settlement can introduce complications regarding identification of the start of primary consolidation (d_0). Since the modified curve-fitting methods exclude the initial portion of the settlement-time data anyway, immediate settlement is no longer an issue and the evaluation of d_0 becomes considerably more straightforward.
3. Multiple values of c_v can be obtained from just one set of data, which can be extremely useful when there is some existing doubt as to the validity of the conventionally calculated c_v . For example, when the settlement-time curve does not

follow the ideal ‘s-shape’ (when in log-scale), the prediction of c_v can become more subjective. In these cases, it would be unwise to rely on a single value of c_v .

Although there are numerous advantages to the aforementioned techniques for calculating c_v , these methods are still reliant on Terzaghi’s one-dimensional consolidation theory which does not account for secondary compression (or creep). Rather, to use these methods, the assumption that creep begins at the end of primary consolidation must be valid. Depending on the type of soil, this assumption may have a significant impact on the determination of the coefficient of consolidation.

5.4 Summary

By recreating a non-uniform initial excess pore water pressure distribution within a laboratory setting, important theoretical results gathered in Chapters 3 and 4 were experimentally verified. The phenomenon of pore pressure redistribution during consolidation was successfully verified for a sinusoidal u_i -distribution with one-way drainage. Data gathered from these tests were also analysed using the modified curve-fitting procedure for a sinusoidal u_i -distribution with one-way drainage. The calculated c_v values align with those determined using standard oedometer testing and analysis. The modified curve-fitting technique for a sinusoidal u_i -distribution with two-way drainage was also experimentally validated, and potential applications of this technique were explored.

Chapter 6: Time-dependent loading

6.1 General

In certain geotechnical applications, it is necessary to estimate the consolidation settlement of a soil layer that is subjected to an increase in vertical total stress that occurs over a prolonged period of time. Structural loading on a foundation, or surcharge loading on a clay layer, are cases where time-dependent loading must be considered – the assumption of an instantaneously applied load no longer applies. Over the years, several methods for calculating primary consolidation settlements that occur under time-dependent loading have been developed (Gibson 1958, Olson 1977, Zhu and Yin 1998, Conte and Troncone 2006, Zhu and Yin 2005, Hsu and Lu 2006, Hanna et al. 2011). Olson (1977) derived a mathematical solution to one-dimensional consolidation for constant rate loading (or ramp loading) in which the vertical total stress is assumed to be uniform with depth. That is, a uniform initial excess pore pressure distribution was considered. Hsu and Lu (2006) extended Olson's work by allowing c_v to vary with applied pressure.

Studies conducted by Gibson (1958) account for the compression of the soil layer during deposition. Schiffman and Stein (1970) proposed a general solution for multi-layered clay undergoing one-dimensional consolidation that accounts for the loading history. Zhu and Yin (1998) extended the investigation into ramp loading by considering an excess pore water pressure distribution that varies linearly with depth and time. Conte and Troncone (2006) used Fourier analysis to study consolidation due to time-dependent loading including static and cyclic loads. Their theoretical results were verified using laboratory test data and case histories.

Hanna et al. (2011) recently proposed a simple and easily applicable method for calculating construction and post-construction settlements, which is further explored within this chapter. Here, the initial distribution of excess pore water pressure is assumed to remain constant over the depth of the soil layer.

6.2 Ramp loading

In field scenarios, a load is rarely applied instantaneously, but instead is applied in steps as construction or preloading takes place. This stepped construction can be approximated by a constant rate of loading, or ramp loading (RL) as shown in Figure 6.1.

By reducing the loading to a constant rate, and discretising the ramp loading into infinitesimal pressure increments (as in Figure 6.2) an expression for the percentage

consolidation at the end of constant rate loading can be developed (Hanna et al. 2011). This relationship is dependent upon the assumption that the infinitesimally applied loads all generate a uniform distribution of excess pore water pressure with depth.

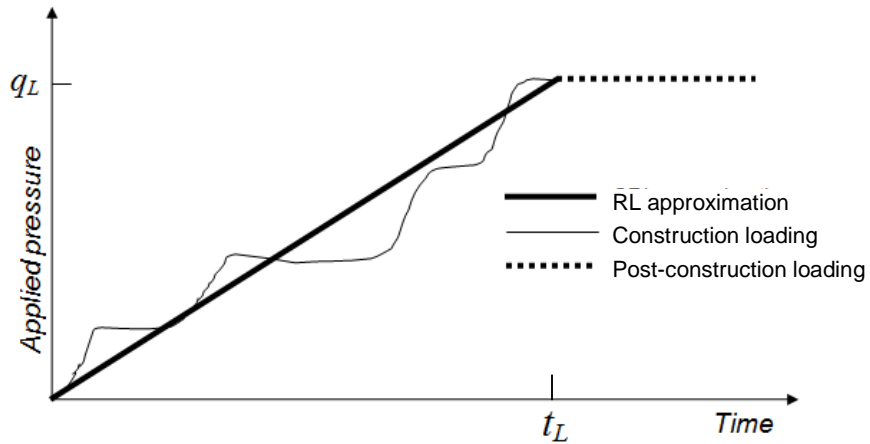


Figure 6.1 – Approximating actual loading rate with constant rate loading

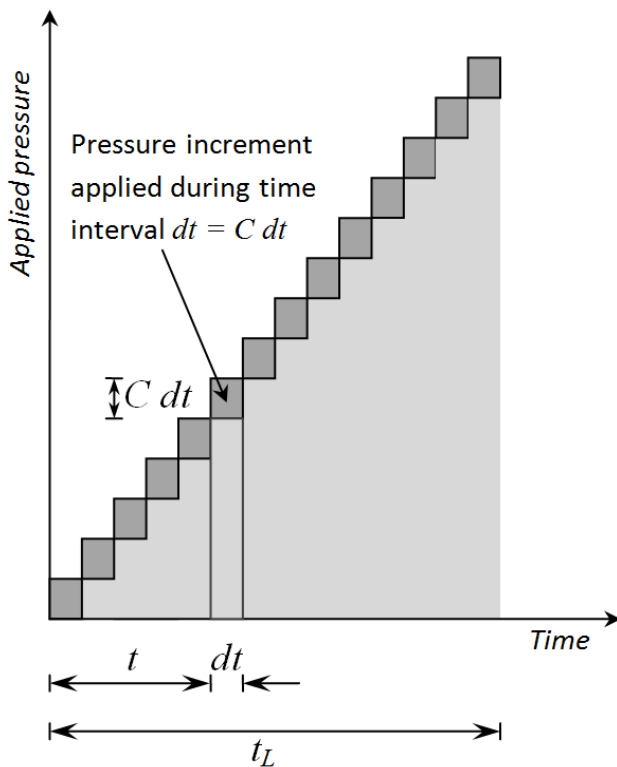


Figure 6.2 – Infinitesimal pressure increments applied during loading

It is assumed that the total applied pressure on the soil layer is applied at a rate, C . If the pressure is applied consistently over the time period t_L (i.e. construction time), the total

pressure (q_L) at the end of loading is Ct_L (see Figure 6.1). If the loading were instantaneous, this would equate to the initial excess pore water pressure, u_i . That is,

$$u_i = Ct_L \quad (6.1)$$

Similarly, the pressure applied on the soil layer during an infinitesimal time period (dt) is Cdt (as in Figure 6.2). This translates to an infinitesimal increase in excess pore water pressure (Δu_i) of Cdt , at time t , throughout the soil layer.

At the completion of loading (i.e. at t_L), some of this excess pore water pressure will have dissipated. The fraction of excess pore water pressure dissipated at t_L is U_{t_L-t} , where U_{t_L-t} is the average degree of consolidation during the time period t_L-t , developed using Terzaghi's consolidation theory. This can be written as:

$$\Delta u_i - \Delta u_{t_L} = U_{t_L-t} Cdt \quad (6.2)$$

where Δu_i = initial excess pore water pressure increase due to the infinitesimal pressure increment Cdt , and Δu_{t_L} = corresponding excess pore water pressure from this pressure increment that remains undissipated at t_L .

By adding all infinitesimal time intervals, the excess pore water pressure that has dissipated at t_L is given by:

$$u_i - u_{t_L} = \int_{t=0}^{t_L} U(t_L - t) Cdt \quad (6.3)$$

where u_{t_L} = excess pore water pressure at t_L , taking into account the entire loading over the duration t_L . This is a fraction of u_i (Eq. 6.1) after allowing for pore pressure dissipation during time t_L . Eq. (6.3) can also be written as:

$$u_i - u_{t_L} = \int_{t=0}^{t_L} U(t) Cdt \quad (6.4)$$

The expression for average degree of consolidation at t_L can thus be determined:

$$U_L = \frac{u_i - u_{t_L}}{u_i} = \frac{\int_0^{t_L} U(t) Cdt}{Ct_L} = \frac{\int_0^{t_L} U(t) dt}{t_L} \quad (6.5)$$

Eq. (6.5) can also be written as:

$$U_L = \frac{\int_0^{T_L} U(T) dT}{T_L} \quad (6.6)$$

where

$$T_L = \frac{c_v t_L}{H^2} \quad (6.7)$$

Using Eqs. (2.44) and (2.45) and applying them to Eq. (6.6), an expression for U_L can be derived for both singly and doubly drained soil layers:

$$U_{L,SD} = 1 - \frac{1}{T_L} \sum_{n=0}^{\infty} \frac{32}{[(2n-1)\pi]^4} \left[1 - \exp\left(-\frac{[(2n-1)\pi]^2 T_L}{4}\right) \right] \quad (6.8)$$

$$U_{L,DD} = 1 - \frac{1}{T_L} \sum_{n=0}^{\infty} \frac{2(1-(-1)^n)}{n^4 \pi^4} \left[1 - \exp(-n^2 \pi^2 T_L) \right] \quad (6.9)$$

The proposed expression for constant rate loading can be used as the baseline for determining the construction and post-construction consolidation settlements for any loading period (t_L). Here, the following adjustments are required;

During Construction ($t < t_L$) – The ‘final’ consolidation settlement at the end of loading (U_L) is proportionally reduced to reflect the fraction of load being applied at t . If the load accumulated at time t is represented by $q(t)$ and the total load at the end of loading is given by q_L , the consolidation settlement during construction can be calculated as follows:

$$U_{t < t_L} = U_L \left(\frac{q(t)}{q_L} \right) \quad (6.10)$$

Post-construction ($t > t_L$) – The problem can now be treated as an instantaneous case, where the ‘initial’ excess pore pressure distribution (at $t = t_L$) is assumed to be sinusoidal or half-sinusoidal for doubly and singly drained layers, respectively. This assumption is based on the knowledge that the excess pore pressure isochrones take a sinusoidal or half-sinusoidal shape during consolidation (when considering a uniform initial excess pore water pressure distribution). The post-construction consolidation settlements can thus be calculated using the following equation:

$$U_{t > t_L} = U_L + (1 - U_L) U_{t=t_L} \quad (6.11)$$

where U_L = average degree of consolidation at the end of constant rate loading (t_L). The U_{t-t_L} values are those generated by a sinusoidal/half-sinusoidal initial distribution (due to an instantaneously applied load), which are commonly available in literature. These values should be selected and used in Eq. (6.11) according to the following time factor:

$$T_{t-t_L} = \frac{c_v(t-t_L)}{H^2} \quad (6.12)$$

The complete post-construction settlement can be plotted in relation to construction settlement by then plotting all $U_{t>t_L}$ values at T values that have been shifted to account for the loading period (i.e. $T = T_{t-t_L} + T_L$).

Using this procedure and Eq. (6.8), the theoretical settlement-time curves (shown in blue) were developed for a singly drained case where the loading period varied according to $T_L = 0.05, 0.2, 0.4$ and 0.8 , and are shown in Figure 6.3. The ramp loading (RL) curve generated using Eq. (6.8) has also been provided for clarity. It can be seen that the $U - T$ curves intersect the base RL curve at their respective $T = T_L$ values.

Since these $U - T$ curves were required for a *singly* drained case, the distribution of excess pore water pressure at the end of loading was assumed to follow a half-sinusoidal shape. Consequently, the U_{t-t_L} values used in the post-construction adjustments are due to a half-sinusoidal distribution with one-way drainage. To illustrate the need for this modification, the settlement-time curves that would result from an assumption of uniform excess pore water pressure at the end of loading have also been provided in Figure 6.3 (denoted by the green lines). Clearly, the rate of settlement is considerably over-estimated if the assumption of uniform excess pore water pressure at T_L is adopted in place of a half-sinusoidal distribution. In fact, for a loading period of $T_L = 0.05$, the rate of settlement using this uniform assumption actually surpasses the rate of settlement of an instantaneously loaded, singly drained layer (denoted by the red line).

In order to verify the half-sinusoidal assumption when adjusting for post-construction settlement, the ‘true’ theoretical settlement-time curves have also been provided in Figure 6.3. These curves were developed using a discretised approach which is further elaborated upon in Section 6.3. It is clearly evident from Figure 6.3 that the assumption of a half-sinusoidal distribution of excess pore water pressure at T_L is valid for most loading periods. However, when the load is applied very quickly (i.e. for small values of T_L), the ramp

loading solution actually underestimates the rate of consolidation by a small degree. This is because the distribution of excess pore water pressure at these times is actually parabolic in nature, and has not yet become sinusoidal.

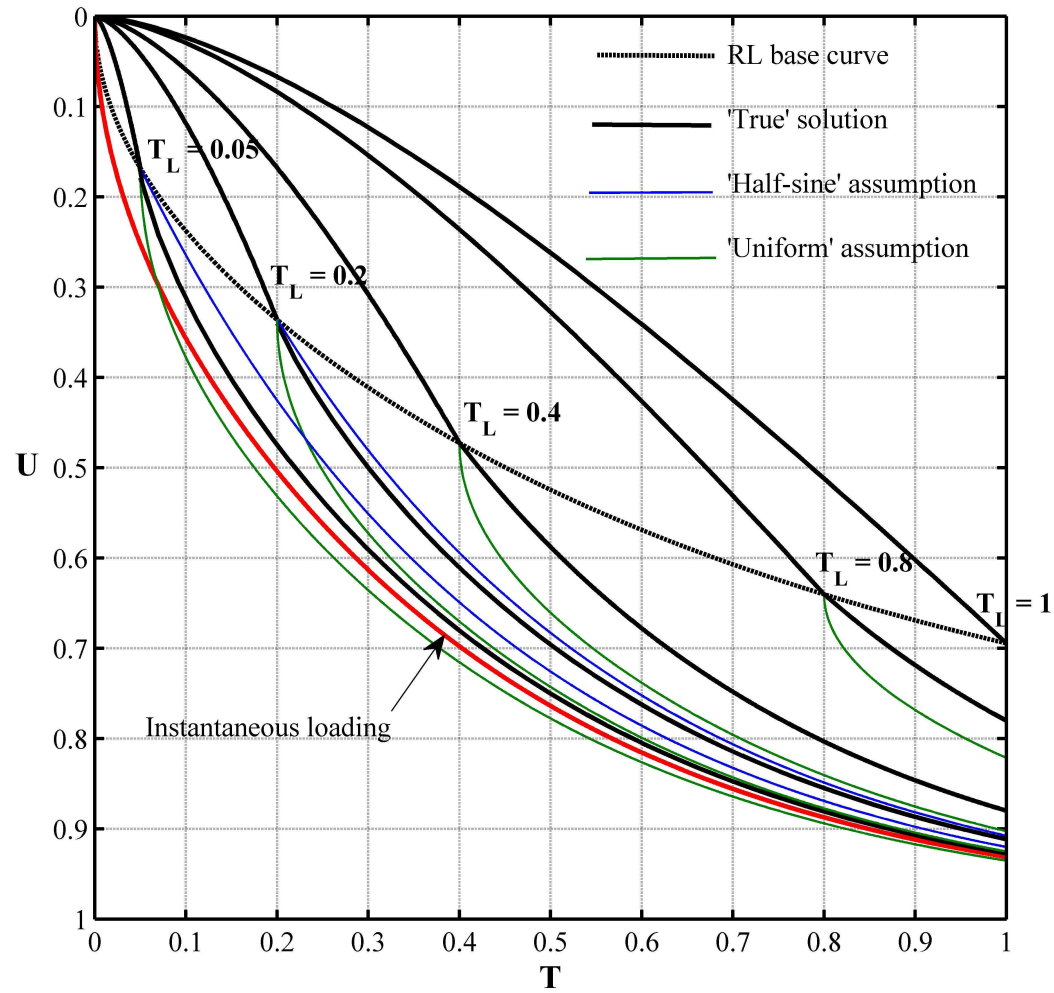


Figure 6.3 – During and post-construction consolidation settlement for various construction times (T_L) with one-way drainage permitted

Since the total applied load in Eq. (6.1) was assumed to adhere to a uniform u_i -distribution (which has a solution that is interchangeable between singly and doubly drained cases), the same settlement-time curves as those shown in Figure 6.3 can be expected for the doubly drained case, but using Eq. (6.9) along with T_L values that are 4 times less than the singly drained case (i.e. $T_L = 0.0125, 0.05, 0.1$ and 0.2). Furthermore, the post-construction settlement-time portion of the curves would require U_{t-t_L} values that correspond to a sinusoidal u_i -distribution with two-way drainage, rather than the half-sinusoidal u_i -distribution with one-way drainage used to develop Figure 6.3.

6.2.1. Approximations for ramp loading

It is widely known (Taylor 1948, Fox 1948) that the early stages of consolidation (for $U < 0.52$) can be mathematically approximated using an exponential function of the form, as outlined in Section 4.4.1:

$$U = AT^B \quad (6.13)$$

where $A = 1.128$ and $B = 0.5$ for a case of uniform initial excess pore pressure where the load is applied instantaneously.

Using the procedure outlined in Section 4.3.1, this exponential approximation (Eq. 6.13) was also found to apply to the entire region of construction settlement ($t < t_L$), regardless of T_L . However, the constants A and B are dependent upon T_L . Adjusting the constants A and B was sufficient to adequately capture the entire construction portion of the settlement-time curve. The variation in these approximation constants with time is shown in Figure 6.4.

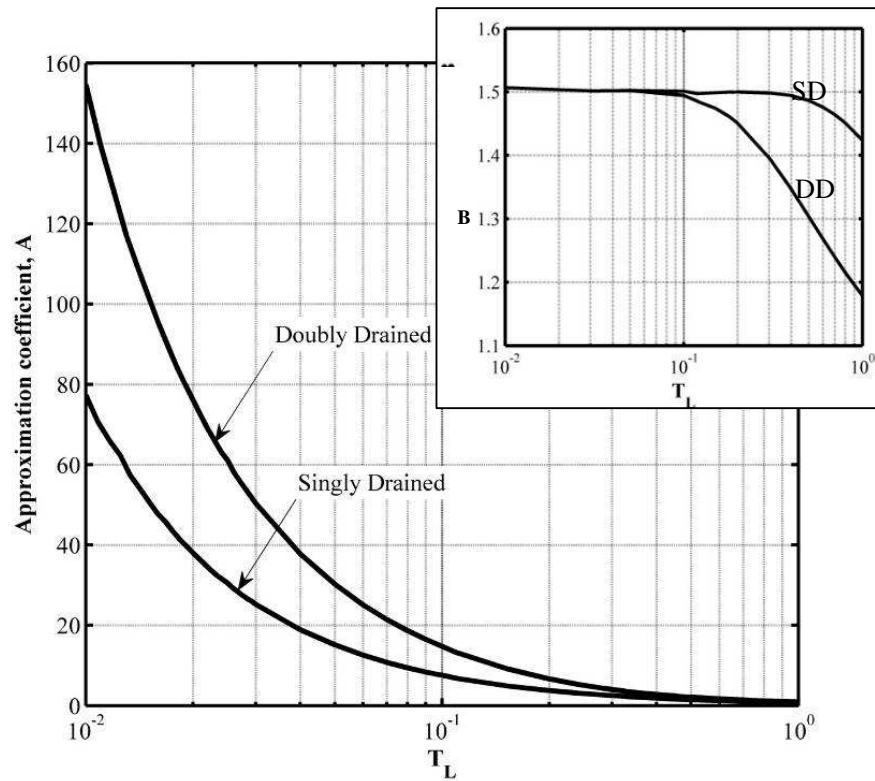


Figure 6.4 – Approximation constants

For cases where one-way drainage is permitted, assuming a constant value of $B = 1.5$ as the power constant and adjusting A accordingly will result in root mean square (RMS) errors less than 0.002.

6.3 Discretised loading

To assess the assumption of a sinusoidal/half-sinusoidal ‘initial’ excess pore pressure distribution at $t = t_L$, the consolidation settlement resulting from time-dependent loading was determined using an alternative approach. Here, the constant rate loading was actually simulated by applying finite but very small ‘instantaneous’ loads, where each increment had a uniform variation in pressure with depth. Thus, the process was still analytically examined, but using the solution to Terzaghi’s consolidation theory in Eq. (3.17) for an instantaneously applied load. Here, the total load q_L , was divided into a large number of increments (each with magnitude Δq) which were applied in a discrete fashion over the course of t_L .

In each case, the load increment was allowed to decay for some fraction of time (ΔT), upon which the next load increment would be added, and subsequent pore pressure decay allowed. By increasing the number of increments (i.e. reducing the magnitude of Δq and ΔT), it is possible to determine the point at which this discretised loading effectively becomes constant rate or ramp loading.

An example of this process is shown in Figure 6.5 for a loading period of $T_L = 0.3$ where two-way drainage was facilitated. Here, the number of loading increments was increased until the consolidation settlement approached the settlement generated using the ‘true’ ramp loading expression. This procedure was repeated for a number of other values of T_L to confirm the limiting value of ΔT . It was found that if the time factor between loading increments was less than 0.0143, the discretised loading could be considered constant rate loading.

Using this discretised approach, the validity of the sinusoidal/half-sinusoidal assumption used in Eq. (6.11) was examined. It was found that for values of $T > 0.2$ and $T > 0.05$ for one- and two-way drainage, respectively, this assumption is completely valid. However, for values of T less than 0.2 and 0.05 (for one- and two-way drainage), the post-construction settlements are underestimated, and consolidation actually proceeds slightly faster than anticipated as shown in Figure 6.3. This can be attributed to the shape of the excess pore pressure isochrones – in the early stages of consolidation, the shapes of pore pressure isochrones resulting from a uniform initial excess pore pressure distribution are actually parabolic rather than sinusoidal.

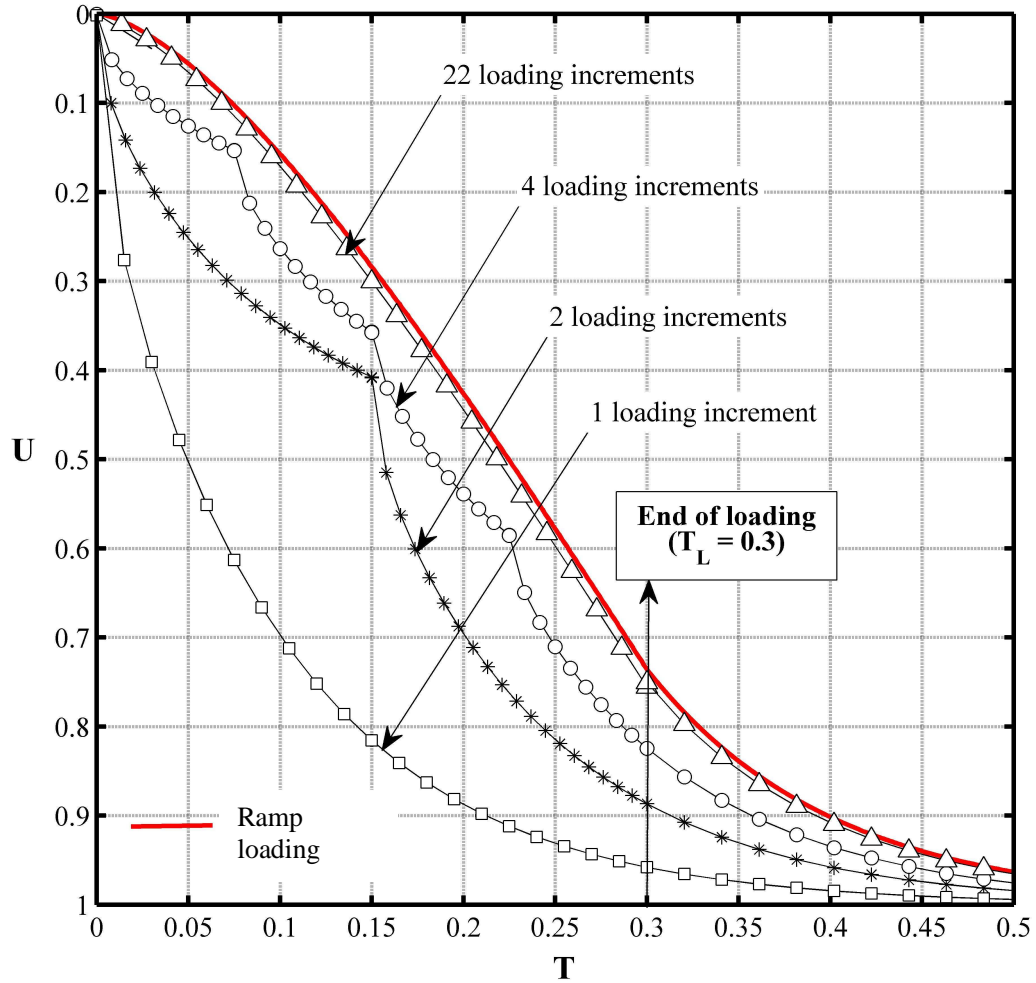


Figure 6.5 – Effect of varying number of loading steps within construction period of T_L for a doubly drained layer

This is further highlighted in Figure 6.6, where the actual pore pressure isochrones resulting from a uniform initial distribution operating under one-way drainage are shown along with half-sinusoidal approximations. As suggested by the constant rate loading comparison, the isochrones do not become sinusoidal in shape until $T = 0.2$ (or $T = 0.5$ in the case of two-way drainage).

This discretised approach has many applications beyond constant rate loading. For example, surcharge preloading usually takes place in large ‘steps’, where a quantity of fill is deposited and allowed to sit for weeks before another deposition occurs. As a result, even the assumption of ramp loading in these cases might be unreasonable. Instead, the discretised approach outlined in this study can be used to assess the percentage consolidation that will occur given any variety of fill history.

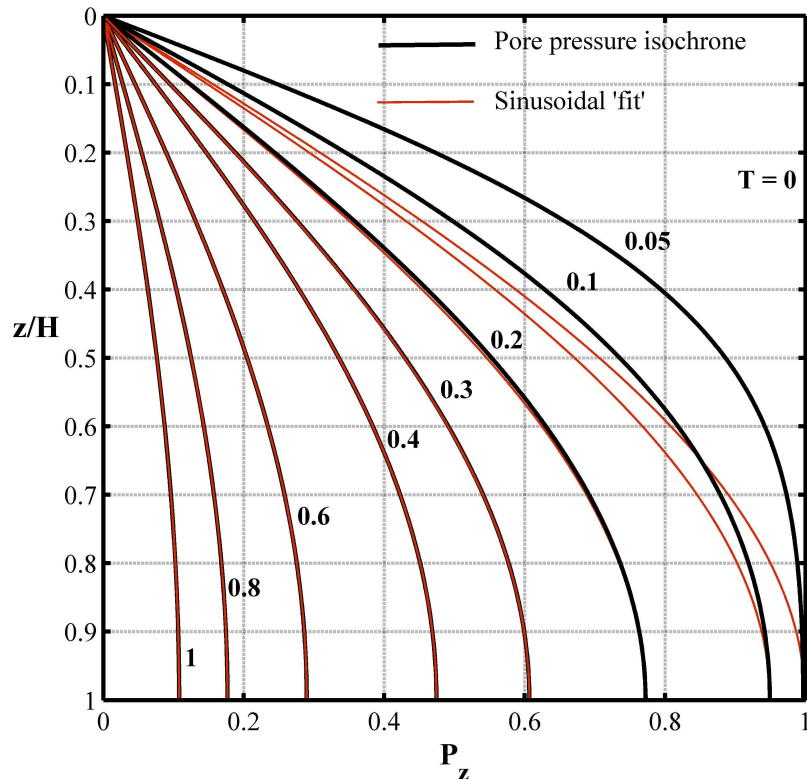


Figure 6.6 – Pore pressure isochrones as they become sinusoidal

6.4 Experimental investigation

Using the knowledge that applying load increments at time factor intervals of less than $T = 0.0143$ will result in a ramp loading-type problem, an experimental study was conducted to complement the analytical results. Time-dependent loading tests were carried out using the K_{50} soil mix described in Table 4.1.

6.4.1. Discretised approaching constant rate loading

Two independent oedometer tests were conducted simultaneously (labelled Specimen 1 and 2), under doubly drained conditions. The relevant consolidation parameters including applied stress, total primary consolidation settlement and initial thickness are provided in Table 6.1.

Table 6.1 – Consolidation parameters

Specimen	q (kPa)	ΔH (mm)	H_0 (mm)
1	108	0.206	18.576
	215	0.272	18.241
2	108	0.257	18.887
	215	0.38	18.429

The total pressure was applied over a period of two hours, which corresponds to a time factor of approximately 0.3, based on c_v values established previously using standard oedometer tests. The load was divided into 240 increments which ensured a small enough ΔT of 0.00125 (i.e. ramp loading could be reasonably assumed). Physically, this required spooning sand into a hanging bucket every 30 seconds. The results for each sample are shown in Figure 6.7, and demonstrate a close agreement between the theoretical constant rate loading curve and experimental discretised loading curve.

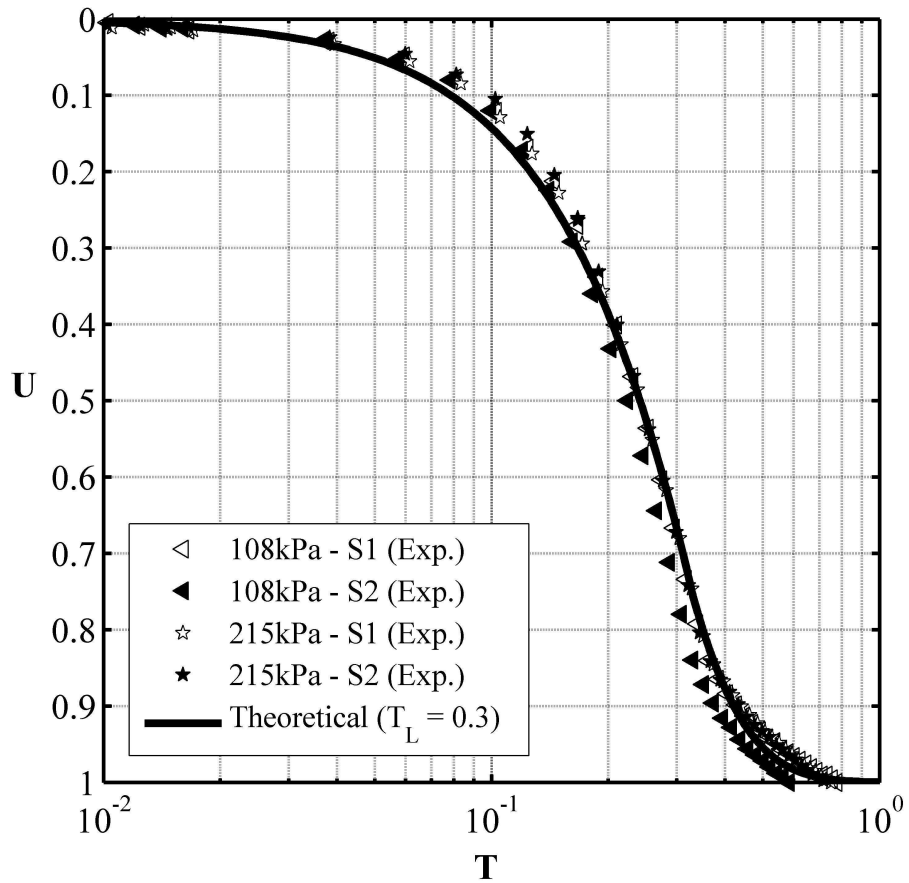


Figure 6.7 – Experimental vs. theoretical time-dependent loading

6.4.2. Construction settlements

When the construction settlement versus time is normalised with respect to the end of loading values, it can be seen that all construction settlements occur within a relatively narrow band, regardless of clay type and loading duration. At the end of loading, $t = t_L$ and $s = s_L$. Therefore, it follows that;

$$\frac{t}{t_L} = \frac{T}{T_L} \quad (6.14)$$

and

$$\frac{s}{s_L} = \frac{U}{U_L} \quad (6.15)$$

where $t < t_L$ (i.e. only considering settlement s that occurs during construction). Here, U and U_L are both based on the same final consolidation settlement that occurs due to the applied pressure q .

The resulting plot of settlement normalised with respect to the settlement at the end of loading (U / U_L) versus time normalised with respect to the loading duration (T / T_L) can be seen in Figure 6.8, which is supplemented with experimental data (see Table 6.2).

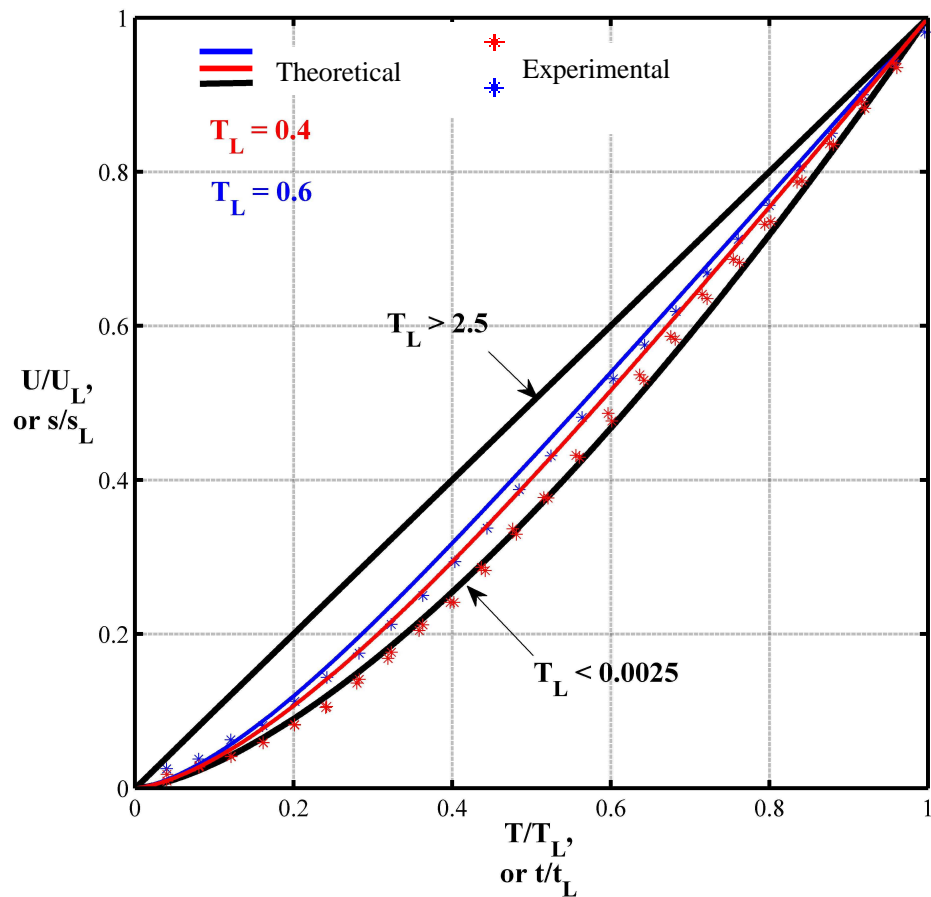


Figure 6.8 – Theoretical and experimental construction settlements normalised by constant rate loading parameters

When conducting the theoretical analysis, a wide range of T_L values was considered, ranging from 0.0025 to 2.5 which covers rapid (almost instantaneous) to very slow loading. It is evident from Figure 6.8 that, irrespective of the coefficient of consolidation or loading duration, the U/U_L versus T/T_L plot lies within a very narrow band. Essentially, this plot is insensitive to the type of clay (i.e. c_v) and duration of loading (t_L).

This was confirmed by conducting further laboratory oedometer tests on the K_{50} mix (Specimens 1 and 2 from Section 6.4.1), where the loading period (t_L) and total applied load (q) were varied. The normalised settlement-time plots for two load increments, corresponding to $T_L = 0.4$ and 0.6 are also shown in Figure 6.8. Key consolidation parameters (c_v, H_0 etc.) used to generate the normalised settlement-time plots are shown in Table 6.2. Values of c_v calculated using the constant rate loading data align quite well with values obtained during conventional oedometer tests where the load was applied instantaneously.

Table 6.2 – Consolidation parameters for comparison of pre-construction settlements within the oedometer specimen

Specimen	q (kPa)	ΔH (mm)	H_0 (mm)	t_0 (hrs)	s_0 (mm)	T_L	c_v (m^2/yr)
1	107.6	0.206	18.576	2	0.17	0.4	0.6
	215.1	0.272	18.241	2	0.22	0.4	0.6
	429.6	0.467	17.85	1	0.34	0.6	1.7
2	107.6	0.257	18.887	2	0.212	0.4	0.6
	215.1	0.38	18.429	2	0.3	0.4	0.6

These results suggest that it is possible to determine the coefficient of consolidation from a single field measurement of settlement that occurred during the loading period. From this, the entire settlement-time plot can subsequently be generated.

6.5 Summary

By extending Terzaghi's one-dimensional consolidation equation to constant rate or ramp loading, an expression for the degree of consolidation as a function of time factor was developed. Here, the distribution of excess pore water pressure at the end of the construction period was assumed to be sinusoidal or half-sinusoidal in shape, for doubly and singly drained cases, respectively. By simulating a discretised approach within the program MATLAB, this expression was verified for large construction periods. When loading took place relatively quickly (i.e. when the loading time factor was less than 0.2 and 0.05 for one-

and two-way drainage, respectively), the sinusoidal/half-sinusoidal assumption was found to be inaccurate. Furthermore, the discretised loading approach was found to approach a constant rate or ramp loading problem when the time factor increment between loading intervals was less than 0.0143.

Chapter 7: Summary, conclusions and recommendations

A summary of this dissertation, conclusions and recommendations for possible future work have been discussed in this chapter.

7.1 *Summary*

The solution to Terzaghi's famous one-dimensional consolidation equation can be freely found in literature, and is based on a number of assumptions, some of which are considered more reasonable than others. Most importantly, infinitesimal deformations are assumed to occur in the vertical direction only, and a linear relationship between void ratio and effective stress is also assumed. Although other more complex models do exist which address these assumptions in a better way, many geotechnical engineers revert back to using Terzaghi's one-dimensional theory as it is considerably more straightforward, and requires minimal effort to use. The purposes of this study have been to investigate aspects of Terzaghi's consolidation theory, in particular the assumption of uniform initial excess pore water pressure, to see if it is possible to extend the solution whilst maintaining the simplicity that makes Terzaghi's solution so attractive.

The results obtained during this study were developed by solving Terzaghi's consolidation equation within the program MATLAB, where a collocation approach was adopted to solve for series coefficients. The analytical option for solving Terzaghi's consolidation equation has often been avoided in the past due to problems associated with Gibbs phenomenon which can occur when discontinuities are present in the initial condition. However, using a novel method of truncation developed in this study, Gibbs phenomenon was easily avoided.

The common assumption of a uniform initial distribution of excess pore water pressure within a loaded soil layer has permeated all other aspects of consolidation analyses. For instance, common procedures currently used to analyse laboratory data in order to determine the consolidation properties of a soil, are based on this assumption. The term 'maximum drainage path length' has also become a standard consolidation term that is used in everyday analyses, despite the fact that it is only practically relevant for a case of uniform initial excess pore water pressure.

This investigation has served to bridge this gap in knowledge by developing a general solution to Terzaghi's consolidation equation that can cater for any initial distribution of excess pore water pressure. Theoretical results obtained during this analysis were also applied to practical situations in a laboratory setting. These results show that pore pressure

redistribution during consolidation is a genuine phenomenon and can be realistically expected to occur in singly drained layers where the majority of initial excess pore water pressure is located near the surface of the layer (when the impervious boundary is located at the base of the layer).

By modifying current curve-fitting procedures which are used to back-calculate consolidation parameters, there are now fewer restrictions on the scope of data that can be analysed. That is, settlement-time data is no longer confined to cases where a uniform distribution of initial excess pore water pressure is present.

Knowledge of the dissipation of excess pore water pressure throughout consolidation was also applied to time-dependent loading cases. Once construction is complete, the distribution in excess pore water pressure can be reasonably assumed to conform to a sinusoidal/half-sinusoidal shape in doubly/singly drained cases. This assumption proved useful when evaluating post-construction settlements. Thus, by conducting a thorough investigation into the inner workings of consolidation, it is possible to apply established consolidation principles to new and exciting geotechnical problems.

7.2 **Conclusions**

In this investigation, research has been carried out to determine the effect of various non-uniform initial excess pore water pressure distributions on the consolidation behaviour of soil. A summary of the pertinent findings can be found below.

7.2.1. **Excess pore water pressure dissipation**

The consolidation behaviour of a soil stratum subjected to various non-uniform initial excess pore water pressure distributions, most of which may occur under foundation and embankment loading, was analysed in terms of excess pore water pressure to create a general picture of the dissipation process duration consolidation. Depending on the drainage conditions (i.e. whether the layer is singly or doubly drained), a range of different consolidation responses were observed. As highlighted in many geotechnical textbooks, the percentage settlement with time of a doubly drained layer subjected to a uniform initial pore pressure distribution is identical to a case of linear initial excess pore water pressure. However, the *dissipation* of excess pore water pressure during consolidation is unique for each of these cases.

The phenomenon of pore pressure redistribution was observed in both singly and doubly drained layers, where the values of excess pore water pressure within some parts of the soil layer actually increased above their initial values during consolidation. In doubly drained

layers, pore pressure redistribution was considered most likely to occur when the non-uniform initial pore pressure distribution contained a concentrated region of excess pore water pressure and minimal pressures elsewhere in the layer. In singly drained layers, pore pressure redistribution was prevalent in cases where the initial excess pore water pressure distribution contained minimal values of pressure at the impermeable boundary. The existence of this phenomenon brings into question the value of the term ‘degree of consolidation’ which would actually be negative at depths where pore pressure redistribution occurred during consolidation. In these cases, it is best to view the consolidation process in terms of the unscaled pore pressure dissipation.

7.2.2. Average degree of consolidation

The magnitude of consolidation settlement is often calculated using Terzaghi’s expression for average degree of consolidation (U) with respect to time. Developed during a time of limited computing capabilities, Terzaghi’s series solution to the one-dimensional consolidation equation is traditionally generalized using a dimensionless time factor (T), where a single $U - T$ curve is used to describe the consolidation behaviour of both singly and doubly drained strata. As a result, any comparisons between one- and two-way drainage are indirect, and confined to discrete values of time. By introducing a modified time factor in terms of layer thickness (H) instead of the maximum drainage path length (H_{dr}), it is possible to observe the effect of drainage conditions over a continuous range of time, for a variety of asymmetric initial excess pore pressure distributions.

A simple method for adjusting uniform $U - T$ values to account for non-uniform initial excess pore pressure distributions was also developed, which makes use of the highly prevalent $U - T$ values corresponding to a uniform distribution of initial excess pore water pressure. This method takes advantage of the fact that at some key point during consolidation, the undissipated pressure associated with a non-uniform initial distribution will become a fraction of the undissipated pressure associated with a uniform initial distribution, and this fraction will remain constant for the remaining duration of consolidation.

7.2.3. Coefficient of consolidation – uniform initial excess pore water pressure distributions

The coefficient of consolidation (c_v) is traditionally determined by fitting observed settlement-time data to the theoretical average degree of consolidation versus time factor relationship developed by Terzaghi. Although it is widely accepted that different curve-

fitting methods can produce different values of c_v , very few comparisons have been conducted to assess the validity of these methods. In this study, the settlement-time data gathered from conventional oedometer tests conducted on three different clays were analysed using three common curve-fitting techniques; the Casagrande log-time method, Taylor's root-time method and the Cour inflection point method. A new method proposed by the authors for calculating c_v , which abandons the traditional curve-fitting approach in favor of a computational-based approach, was also used to compare these results. In order to assess the validity of each c_v value, the experimental results were compared with the theoretical average degree of consolidation curve and quantified using the root mean square (RMS) error. The efficacy of the designated curve-fitting method was found to significantly depend upon the 'shape' of the settlement-time curve generated during testing. In general, the Taylor method predicted larger values of c_v than the Casagrande method, and correspondingly smaller RMS errors. The variance method resulted in values of c_v that more closely matched those generated using the Casagrande method. However, smaller RMS errors were achieved using the variance method which suggests that this technique may produce a more realistic estimate of c_v than the Casagrande method.

7.2.4. Tall oedometer

Currently, standard practice requires the height to diameter ratio of a consolidating sample to remain less than 0.4 to avoid any effect of wall friction, where stress transfer occurs between the soil mass and rigid oedometer ring edge. As a result, in order to adhere to standard recommendations, the height of a consolidating sample is restricted to small thicknesses (such as the nominal 20-25 mm) to avoid requiring an overly large diameter and very heavy loads. To account for this, an analytical expression for the initial excess pore water pressure distribution which incorporates the effect of wall friction was developed in terms of the height (H) to diameter (D) ratio of the consolidating sample. It has been shown that when $H \leq 2D$ and the applied pressure increment is greater than 10 times the product of the unit weight and the specimen diameter, the self-weight component of the initial excess pore water pressure distribution can be ignored. For such cases, when the specimen is doubly drained, the variation in percentage consolidation with time factor is the same as that for a uniform initial pore pressure distribution, which is the condition assumed in traditional oedometer testing. When self-weight is considered, the percentage consolidation also follows the uniform $U-T$ curve as long as $H \leq 3D$ for doubly drained cases, and $H \leq 0.5D$ for singly drained cases.

The average degree of consolidation curves generated by the proposed analytical solution suggest that despite wall friction, traditional consolidation analyses using the popular Taylor and Casagrande curve-fitting methods can be used to analyse data obtained from a tall, doubly draining sample for select combinations of applied pressure, height and diameter. Experimental results also support this conclusion, as the values of c_v obtained from data gathered during tall oedometer testing (where $H / D = 2.1$) were approximately equal to the values obtained from standard oedometer tests.

7.2.5. Coefficient of consolidation – non-uniform initial excess pore water pressure distributions

The coefficient of consolidation (c_v) is often determined by comparing the characteristics of the experimental and theoretical consolidation using empirical curve-fitting procedures which are based on the theoretical $U - T$ curve generated by a layer subjected to a uniform initial excess pore water pressure distribution. However, in cases where settlement-time data is a result of a non-uniform initial pore pressure distribution, these curve-fitting procedures are no longer valid. In this part of the investigation, a generalised procedure for Taylor and Casagrande's popular curve-fitting procedures was proposed, where the user is directed to select appropriate adjustment factors, depending on the type of non-uniform initial excess pore pressure distribution encountered. These factors were determined by approximating separate regions of the $U - T$ curves using simple power and exponential functions. In non-uniform cases where the power approximation only captures a small portion of the $U - T$ curve it may be difficult to objectively use the corresponding modified curve-fitting procedure.

One-way drainage

A non-uniform initial excess pore water pressure distribution in the form of a sinusoidal shape was generated using traditional oedometer testing so that data obtained from a non-uniform initial excess pore water pressure distribution could be analysed. First, a doubly drained oedometer test was initiated. Then, some short time after consolidation had begun, the base drainage tap was closed so that the process reverted to one-way drainage. At the moment the base tap was closed, the distribution in excess pore water pressure can be said to be sinusoidal in shape (due to the nature of pore pressure dissipation in two-way drainage cases). Thus, any data obtained after this point can technically be analysed using a modified curve-fitting procedure that applies to a sinusoidal initial distribution with one-way drainage. This was completed using a soil of known consolidation properties. Values of c_v obtained

using the ‘singly drained’ data were in good agreement with values obtained via standard oedometer tests which suggest that the proposed modifications to Taylor and Casagrande’s curve-fitting methods are sound.

Two-way drainage

During any doubly (or singly) drained standard oedometer test, the excess pore water pressure distribution within the soil layer will revert to a sinusoidal (or half-sinusoidal) shape some short time after consolidation has commenced. Thus, after excluding any data before this point in time, the remaining settlement-time data can be analysed using one of the modified curve-fitting procedures for a sinusoidal (or half-sinusoidal) initial excess pore pressure distribution with two- (or one-) way drainage. In fact, since the distribution of excess pore water pressure after this point in time remains sinusoidal (or half-sinusoidal) for the rest of the consolidation process, this principle can be applied to any portion of data. As a result, numerous values of c_v can be calculated using just one set of settlement-time data.

This principle was applied to two different soil types of known consolidation properties. The modified curve-fitting technique that corresponds to a sinusoidal initial excess pore pressure distribution with two-way drainage was verified in both cases and produced values of c_v that were in close agreement with those obtained using traditional curve-fitting methods.

7.2.6. Time-dependent loading

Terzaghi’s one-dimensional consolidation equation can be extended to constant rate of loading, where an expression for the degree of consolidation as a function of time factor can be generated. Using this expression, no further approximations are required, other than the principle of superposition. However, this solution is dependent upon the assumption that, at the end of loading, the undissipated excess pore water pressure will be sinusoidal/half-sinusoidal in shape due to the pore pressure dissipation occurring at the drainage boundaries during loading. Thus, any subsequent consolidation will adhere to the solution corresponding to a sinusoidal/half-sinusoidal ‘initial’ excess pore water pressure distribution.

An alternative approach using a discretisation technique was also developed to complement the constant rate loading approach, where the total applied load was divided into a large number of increments, each of which was ‘instantaneously’ applied at select time intervals, where the applied pressure increment was uniform with depth. When these time factor intervals became less than 0.0143, this discretised approach effectively became a constant rate loading problem. Once this alternative method was validated, the construction settlements for small loading periods were evaluated and compared with those determined

using the true constant rate loading approach. It was found that the assumption of a sinusoidal/half-sinusoidal distribution of excess pore water pressure at the end-point of loading is unrealistic for small loading periods, since the distribution in excess pore water pressure at the end of these shorter loading periods is still parabolic in shape. However, the sinusoidal/half-sinusoidal assumption still produces results that are far more accurate than if an assumption of uniform excess pore water pressure was used.

7.3 Recommendations for future research

Some light has been focused on the untapped potential of Terzaghi's one-dimensional consolidation theory. Without requiring any new knowledge of data analysis techniques, a procedure through which *multiple* values of c_v can be evaluated using *one* set of data has been established. This technique draws upon the principles of consolidation in relation to non-uniform initial excess pore water pressure distributions which have been thoroughly explored throughout this investigation. In doing so, a number of other potential research avenues have emerged which can be used to conduct further research in this area. Some recommendations for future research are;

7.3.1. Partial drainage boundaries

This research was based on a 'black-and-white' approach to drainage conditions, where a boundary is considered either drained or undrained. In reality, drainage conditions fall somewhere between these absolutes. The presence of a partially draining boundary has been incorporated into Terzaghi's consolidation theory in the past, but only when considering a uniform initial excess pore water pressure distribution. Thus, it may be useful to investigate the effects of non-uniform initial distributions on the consolidation behaviour of a partially draining soil layer.

This solution could also be extended to investigate the consolidation behaviour of a multi-layer system where the settlement of contiguous consolidating layers needs to be assessed.

7.3.2. Soil properties that vary with depth

The solution to Terzaghi's consolidation theory developed during this research is reliant upon the assumption that soil properties remain constant with depth. In some cases, key consolidation parameters such as permeability and volume compressibility actually vary with depth within a consolidating layer. By incorporating this variation into the solution and assessing the effects of non-uniform initial excess pore water pressure distributions on the subsequent progression of consolidation, it may be possible to develop an analytical solution that more closely resembles a practical situation.

7.3.3. 2D and 3D effects

The results reported in this investigation are all for a case of one-dimensional consolidation. By extending this theory to incorporate a two- or three-dimensional system, it may be possible to more accurately model the effects of non-uniform initial excess pore water pressure distributions on the consolidation behaviour of a soil layer.

7.4 *Final comments*

Through-out this investigation, one cannot help but admire the reoccurring theme of how Terzaghi's solution time and again returned respectable results, richly deserving of its broad use and appeal amongst practicing engineers and researchers. An important contribution to Terzaghi's success would have to be the solution's simplicity in application. Modern solutions that return more reliable results encompassing a broader range of applications may naturally see adoption, however a solution only becomes great if that power is coupled with a simplicity in application. It is my hope that the work presented within this study has not broken that vital property while contributing some measure of improvement that will continue to propagate Terzaghi's success.

References

- ASTM D2435-04. Standard methods for one-dimensional consolidation properties of soils using incremental loading.
- Al-Zoubi, M. S. (2010). "Consolidation analysis using the settlement rate-settlement (SRS) method." *Applied Clay Science*, 50(1), 34-40.
- Arfken, G. (1970). *Mathematical Methods for Physicists*, : Academic Press, New York.
- Asaoka, A. (1978). "Observational procedure of settlement prediction." *Soils and Foundations*, 18(4), 87-101.
- Berry, P. L., and Reid, D. (1988). *An Introduction to Soil Mechanics*, McGraw-Hill, London.
- Carslaw, H. S. (1930). *Introduction to the theory of Fourier series and integrals*, Dover Publications Inc., New York, 3rd edn.
- Casagrande, A., and Fadum, R. E. (1940). Notes on soil testing for engineering purposes. *Publication 268*, Harvard University, Cambridge.
- Chan, A. H. C. (2003). "Determination of the coefficient of consolidation using a least squares method." *Geotechnique*, 53(7), 673-678.
- Chan, A. H. C. (2006). "Discussion: Determination of the coefficient of consolidation using a least squares method." *Geotechnique*, 56(1), 73-76.
- Chu, J., and Wan, S.W. (2005). "Estimation of degree of consolidation for vacuum preloading projects." *International Journal of Geomechanics ASCE*, 5(2), 158-165.
- Coduto, D. P., Yeung, M-C. R., and Kitch, W. A. (2011). *Geotechnical Engineering: Principles and Practices*, Pearson Higher Education, Upper Saddle River, 2nd edn.
- Conte, E. And Troncone, A. (2006). "One-Dimensional Consolidation under General Time-Dependent Loading," *Canadian Journal of Geotechnical Engineering*, 43(11), 1107-1116.

Cortellazzo, G. (2002). "Comparison between laboratory and in situ values of the coefficient of primary consolidation c_v ." *Canadian Geotechnical Journal*, 39(1), 103-110.

Cour, F. R. (1971). "Inflection point method for computing C_v ." *Journal of Soil Mechanics and Foundations Division ASCE*, 97(SM5), 827-831.

Craig, R. F. (1974). *Soil Mechanics*, Van Nostrand-Reinhold, New York, 186-187.

Crawford, C. B. (1964). "Interpretation of the consolidation test." *Journal of Soil Mechanics and Foundation Engineering Division ASCE*, 90(SM5), 87-102.

Das BM. (2009). *Principles of Geotechnical Engineering*, 7th edn. Cengage Learning, Stamford.

Duncan, M. J. (1995). "Discussion of 'Limitations of conventional analysis of consolidation settlement.'" *Journal of Geotechnical Engineering*, 121(6), 513-518.

Fang, H-Y. (1991). *Foundation Engineering Handbook*, Kluwer Academic Publishers.

Feng, T.-W., and Lee, Y.-J. (2001). "Coefficient of consolidation from the linear segment of the $t^{1/2}$ curve." *Canadian Geotechnical Journal*, 38(4), 901-909.

Fox, E. N. (1948). "The mathematical solution for the early stages of consolidation." *Proceedings of the 2nd International Conference on Soil Mechanics and Foundation Engineering*, Rotterdam, 1, 41-42.

Gibson, R. E. (1958). "The progress of consolidation in a clay layer increasing in thickness with time." *Geotechnique*, 8(4), 171-182.

Guan, W. (2005). "Consolidation and arch formation of cohesive bulk solids in storage bins." *2005 ASAE Annual International Meeting*.

Hanna, D., Sivakugan, N. and Lovisa, J. (2011). "A simple approach to consolidation due to constant rate loading in clays." *International Journal of Geomechanics ASCE* (accepted and in production).

Harr M.E. (1966). *Foundations of Theoretical Soil Mechanics*. McGraw-Hill, New York.

Helinski, M., Fahey, M., and Fourie, A. (2011). “Behavior of cemented paste backfill in two mine stopes: measurements and modeling.” *Journal of Geotechnical and Geoenvironmental Engineering ASCE*, 137(2), 171-182.

Helwany, S. (2007). *Applied Soil Mechanics: with ABAQUS Applications*. Wiley, New Jersey.

Holtz, R.D., and Kovacs, W.D. (1981). *An introduction to geotechnical engineering*, Prentice-Hall.

Hsu, T-W., and Lu, S-C. (2006) “Behaviour of One Dimensional Consolidation under Time-Dependent Loading,” *The Journal of Engineering Mechanics*, 132(4), 457-462.

Jaky, J. (1948). “Earth pressure in silos.” *Proceedings of the 2nd International Conference on Soil Mechanics and Foundation Engineering*, 1, 103-107.

Janbu, N., Bjerrum, L., and Kjaernsli, B. (1956). “Veiledning ved losning av fundamentering sappgaver.” *Norwegian Geotechnical Institute*, 16.

Jumikis, A. R. (1962). *Soil mechanics*, Van Nostrand, New York, 415-418.

Kaniraj S. R. (1988). *Design aids in Soil Mechanics and Foundation Engineering*. McGraw-Hill, New Dehli.

Kim, T., Kim, N. K., Tumay, M. T. And Lee, W. (2007). “Spatial Distribution of Excess Pore-Water Pressure due to Piezocone Penetration in Overconsolidated Clay.” *Journal of Geotechnical and Geoenvironmental Engineering ASCE*, 133(6), 674-683.

Ladd, C. C., Whittle, A. J., and Legaspi, D. E. (1994). “Stress-deformation behavior of an embankment on Boston Blue Clay.” *Proceedings of Settlement '94, Geotechnical Special Publication*, 40(2), 1730-1759.

Lancellotta, R. (2009). *Geotechnical Engineering*, Taylor and Francis, Oxon, 2nd edn.

- Leonards, G. A. (1962). *Foundation Engineering*, McGraw-Hill.
- Leonards, G. A., and Altschaeffl, A. G. (1964). "Compressibility of clays." *Journal of Soil Mechanics and Foundation Engineering Division ASCE*, 90(SM5), 133-155.
- Marston, A. (1930). *The theory of external loads on closed conduits in the light of latest experiments*. Bulletin No. 96, Iowa Engineering Experiment Station, Ames, Iowa.
- McCarthy, D. F. (2007). *Essentials of Soil Mechanics and Foundations: Basic Geotechnics*. Prentice-Hall, 7th edn.
- Mesri, G. (1973). "Coefficient of secondary compression." *Journal of Geotechnical Engineering*, 99(SM1), 123-137.
- Mesri, G., and Godlewski, P.M. (1977). "Time and stress compressibility interrelationship." *Journal of the Geotechnical Engineering Division ASCE*, 103(GT5), 417-430.
- Mesri, G., Feng, T. W., Ali, S., and Hyat, T. M. (1994). "Permeability characteristics of soft clays." *Proceedings of the 13th International Conference on Soil Mechanics and Foundation Engineering*, Balkema, Rotterdam, The Netherlands, 2, 187-192.
- Mesri, G., Feng, T. W. and Shahien, M. (1999a). "Coefficient of consolidation by the inflection point method." *Journal of Geotechnical and Geoenvironmental Engineering ASCE*, 125(3), 716-718.
- Mesri, G., Stark, T. D., Ajlouni, M. A., and Chen, C. S. (1999b). "Closure on secondary compression of peat with and without surcharging." *Journal of the Soil Mechanics and Foundation Engineering Division ASCE*, 103(3), 417-430.
- Mikasa, M., and Takada, N. (1986). "Determination of coefficient of consolidation (C_v) for large strain and variable c_v values." *Consolidation of soil, testing and evaluation ASTM*, STP(892), 526-547.
- Nguyen, H. Q. (2007). *Reanalysis of the settlement of a levee on soft bay mud*. Master's Thesis, Massachusetts Institute of Technology.
- Olson, R.E. (1977) "Consolidation under Time-Dependent Loading," *Journal of the*

Geotechnical Engineering Division ASCE, 103(1), 55-60.

Olson, R. E. (1986). "State of the art: Consolidation Testing." *Consolidation of soil, testing and evaluation ASTM*, STP(892), 7-70.

Pandian, N. S., Sridharan, A., and Kumar, K. S. (1994). "Improved velocity method for the determination of coefficient of consolidation." *ASTM Geotechnical Testing Journal*, 17(1), 113-118.

Parkin, A. K. (1978). "Coefficient of consolidation by the velocity method." *Geotechnique*, 28(4), 472-474.

Perloff, W. H., and Baron, W. (1976). *Soil mechanics, principles and application*, Ronald, New York, 327-330.

Perloff, W. H., Nair, K., and Smith, J. G. (1965). "Effect of measuring system on pore water pressures in the consolidation test." *Proceedings of the 6th International Conference on Soil Mechanics and Foundation Engineering*, Montreal, 1, 338-341.

Powrie, W. (1997). *Soil Mechanics: Concepts and Applications*, E & FN Spon, London.

Prasad, Y.V.S.N., and Rao, S.N. (1995). "A new two point method of obtaining c_v from a consolidation test." *Canadian Geotechnical Journal*, 32(4), 741-746.

Raju, P. S. R. N., and Pandian, N. S., and Nagaraj, T. S. (1995). "Analysis and estimation of the coefficient of consolidation." *ASTM Geotechnical Testing Journal*, 18(2), 252-258.

Randolph, M. F., Leong, E. C., and Houlsby, G. T. (1991). "One-dimensional analysis of soil plugs in pipe piles." *Geotechnique*, 41(4), 587-598.

Ranjan, G. and Rao, A. S. R. (1991). *Basic and Applied Soil Mechanics*, Wiley Eastern.

Robinson, R. G. (1999). "Consolidation analysis with pore water pressure measurements." *Geotechnique*, 49(1), 127-132.

Schiffman, R. L. and Stein, J. R. (1970). "One-dimensional consolidation of layered systems," *Journal of the Soil Mechanics and Foundations Division ASCE*, 96(SM4), 1499-

1504.

Scott, R. F. (1961). "New method of consolidation-coefficient evaluation." *Journal of the Soil Mechanics and Foundation Engineering Division ASCE*, 87(SM1), 29-39.

Scott, R. F. (1963). *Principles of Soil Mechanics*, Addison-Wesley, USA.

Shukla, S.K., Sivakugan, N. and Das, B.M. (2009). "Methods of determination of the coefficient of consolidation and the time-rate of settlement – an overview." *International Journal of Geomechanics and Engineering*, 3(1), 89-108.

Singh, S. K. (2005). "Estimating consolidation coefficient and final settlement: triangular excess pore-water pressure." *Journal of Geotechnical and Geological Engineering ASCE*, 131(8), 1050-1055.

Singh S. K. (2007). "Diagnostic curve methods for consolidation coefficient." *International Journal of Geomechanics ASCE*, 7(1), 75–79.

Singh S. K. (2008). "Identifying consolidation coefficient: Linear excess pore-water pressure." *Journal of Geotechnical and Geoenvironmental Engineering*, 134(8), 1205-1209.

Singh, S. K., and Swamee, P. K. (2008). "Approximate simple invertible equations for consolidation curves under triangular excess pore-water pressures." *Geotechnical and Geological Engineering*, 26(3), 251-257.

Sivakugan, N. and Das, B.M. (2010). *Geotechnical Engineering: A Practical Problem Solving Approach*, J Ross Publishing, USA.

Sivaram, B., and Swamee, P. K. (1977). "A computational method for consolidation coefficient." *Soils and Foundations*, 17(2), 48-52.

Smith, I. (2006). *Smith's Elements of Soil Mechanics*. Blackwell, Oxford, 8th edn.

Sowers, G. F. (1979). *Soil Mechanics and Foundations: Geotechnical Engineering*, Macmillan Publishing, New York, 4th edn.

Sridharan, A., and Rao, A. S. (1981). "Rectangular hyperbola method for one-dimensional consolidation." *ASTM Geotechnical Testing Journal*, 37(3), 355-368.

Sridharan, A., Murthy, N. S., and Prakash, K. (1987). "Rectangular hyperbola method of consolidation analysis." *Geotechnique*, 37(3), 355-368.

Sridharan, A., and Prakash, K. (1995). "Critical appraisal of laboratory determination of c_v ." *International Symposium on Compression and Consolidation of Clayey Soil*, Hiroshima, Japan, Balkema Publishers, 567-572.

Sridharan, A., Prakash, K., and Asha, S. R. (1995). "Consolidation behavior of soils." *ASTM Geotechnical Testing Journal*, 18(1), 58-68.

Taylor, D. W. (1948). *Fundamentals of Soil Mechanics*. Wiley, New York.

Terzaghi, K. (1925). *Erdbaumechanik auf bodenphysikalischer Grundlage*, F. Devtike, Vienna.

Terzaghi, K. (1943). *Theoretical Soil Mechanics*, Wiley, New York.

Terzaghi, K., and Frohlich, O. K. (1936). *Theorie der Setzung von Tonschichten*, Leipzig and Wein, Franz Deuticka, Vienna, Austria.

Terzaghi, K., Peck, R. B., and Mesri, G. (1996). *Soil Mechanics in Engineering Practice*, Wiley, 3rd edn.

Ting, C. H., Shukla, S. K., and Sivakugan, N. (2010). "Arching in soils applied to inclined mine stopes." *International Journal of Geomechanics*, 11(1), 29-35.

Whitman, R. V., Richardson, A. M., and Healy, K. A. (1961). "Time-lags in pore pressure measurements." *Proceedings of the 5th International Conference on Soil Mechanics and Foundation Engineering*, 1, 407-411.

Winterkorn H. F., and Fang H.-Y. (1990). *Foundation Engineering Handbook*, Van Nostrand, 2nd edn.

Zhu, G. and Yin, J-H. (1998) "Consolidation of Soil under Depth-Dependent Ramp Load," *Canadian Journal of Geotechnical Engineering*, 35(2), 344-350.

Zhu, G., and Yin, J.-H. (2005). "Consolidation of a soil layer subsequent to cessation of deposition." *Canadian Geotechnical Journal*, 42(2), 678-682.